RNA-binding proteins regulate influenza virus infection

By

Mitchell P. Ledwith

A dissertation submitted in partial fulfillment of
the requirements for the degree of

Doctor of Philosophy
(Cellular and Molecular Biology)

at the
UNIVERSITY OF WISCONSIN-MADISON
2022

Date of final oral examination: 01/25/2022

The dissertation is approved by the following members of the Final Oral Committee:

Andrew Mehle, PhD, Associate Professor, Medical Microbiology and Immunology
Robert Kalejta, PhD, Professor, Molecular Virology and Oncology
Catherine A. Fox, PhD, Professor, Biomolecular Chemistry
Bill Sugden, PhD, Professor, Oncology
John-Demian Sauer, Associate Professor, Medical Microbiology and Immunology

Dedication

I dedicate this thesis to my brothers,

Nicholas Ledwith, Zachary Ledwith, and Andrew Ledwith.

I am so proud of all of you.

Acknowledgements

I would like to express gratitude to all those who have helped me in my training and completion of this degree. I firmly believe my successes have been and will continue to be the product of the people that surround me.

First, I would like the thank my thesis advisor Dr. Andrew (Andy) Mehle. Thank you for the opportunity to train and spend the last six years with you. I came to your lab when I was 21. Since then, I have grown immensely as a person, scientist, and leader. The culture of science you built is fundamental to all of our successes. I hope to carry that with me throughout my career.

Thank you to my thesis committee members Dr. Robert Kalejta, Dr. Catherine Fox, Dr. Bill Sugden, and Dr. JD Sauer for your guidance and continued support.

I would like to thank my early mentors Dr. Russ Feirer and Dr. Vera Terakanova who fostered my growth as a young researcher.

I am grateful for the post-doctoral scientists of the Mehle lab. Thank you Dr. Vy Tran, Dr. Steven Baker, Dr. Kaitlin Davis, and Dr. Cason King for not only providing everyday guidance, but also lifelong friendships.

I am thankful for members of the Mehle lab. We have spent more time together than we would all care to admit. Science can sometimes feel like a singular endeavor. Thank you for ensuring that is not the case, whether that be in the lab or on a patio. I am extremely fortunate to have met and learned from all of you.

I would like to thank the University of Wisconsin-Madison Cellular Molecular Biology program and members.

I am beyond thankful for my partner, Bridget Dorsey. Thank you for your love, patience, and support throughout graduate school.

Finally, I am thankful for my family. Thank you to my Grandpa, Wallace Rettler, for reminding me that I do not know everything. Thank you to Nicholas, Zachary, and Andrew Ledwith for your support. It has been so rewarding to watch you grow through my time in graduate school. Finally, thank you to my parents, Anne and Steve Ledwith. Your support and willingness to let my curiosity wander surely lead me to research. Thank you for supporting me and loving me every step of the way.

Table of Contents

List of Figures and Tables

List of Abbreviations (non conclusive)

3'UTR	Three-prime untranslated region
5'UTR	Three-prime untranslated region
ADAR	Adenosine deaminase RNA specific
ARE	AU-rich element
ASO	Anti-sense oligonucleotide
BPM	Bins per million
CARD	Caspase activation and recruitment domain
CDS	Coding sequence
CLIP	Cross-linking immunoprecipitation
CPM	Counts per million
DIRNA	Defective-interfering RNA
DUSP11	Dual-use specificity phosphatase 11
eIF	Eukaryotic initiation factor
HA	Hemagglutinin
IAV	Influenza A virus
IFIT	Interferon-induced protein with tetratricopeptide repeats
IFN	Interferon
ISG	Interferon-stimulated Gene
ISRE	Interferon-stimulated response element
lncRNA	long non-coding RNA
M2	Matrix Protein 2
m7G	7-methyl guanosine
MAVS	Mitochondrial antiviral signaling protein
MePCE	methylphosphate capping enzyme
miRNA	microRNA
mvRNA	mini viral RNA
NA	Neuraminidase
NEP	Nuclear export protein
NLS	Nuclear Localization Signal
NP	Nucleoprotein
NS1	Non-structural protein 1
nt	Nucleotide
NXF1	Nuclear export factor 1
OAS	Oligo-adenylate synthase
PA	Polymerase Basic 1
PABP	PolyA-binding Protein
PAMP	Pathogen-associated molecular pattern
PASTN	PA-swap-T2A-N
PB1	Polymerase basic 1
PB2	Polymerase basic 2
PIC	Pre-initiation complex
polyA	Poly-adenosine

PRR	Pattern recognition receptor
RBD	RNA-binding domain
RdRP	RNA-dependent RNA polymerase
RIG-I	Retinoic acid-inducible gene I
RIP	RNA immunoprecipitation
RLR	RIG-I like receptor
RNA pol I	RNA polymerase I
RNA pol II	RNA polymerase II
RPF	Ribosome protected footprint
rRNAs	Ribosomal RNAs
SMInput	Size-matched input
snoRNAs	Small nucleolar RNAs
snRNA	small nuclear RNA
snRNP	small nuclear ribonucleoprotein
SR	Serine and arginine rich
TPR	Tetratricopeptide repeat
TRIM25	Tripartite motif containing 25
U2AF	U2-auxiliary Factor
UMAP	Uniform manifold approximation and projection
UMI	Unique molecular identifier
vRNP	Viral ribonucleoprotein
VSV	Vesicular Stomatitis Virus
vtRNA	vault RNA
ZAP	Zinc finger antiviral protein

Abstract

Viruses are obligate intracellular parasites that depend on host resources and macromolecular machinery to selfishly replicate and spread genetic material. This genetic material can exist in multiple forms, with viruses utilizing RNA, DNA, and diverse combinations thereof to stably transmit between hosts. These diverse strategies require diverse replication schemes, e.g., DNA viruses must either encode or co-opt host DNA-dependent DNA polymerases to replicate a genome, and negative sense RNA viruses must encode and package RNA-dependent RNA polymerases in virons in order to replicate an RNA genome in the next host. Regardless of scheme, all viruses converge and are absolutely reliant on RNA, and more specifically the host ability to translate RNA molecules into proteins. Thus, both viruses and hosts have devoted significant coding capital in regulating RNA, with emphasis on the evolutionary struggle that exists at this nexus. The over-arching theme of this thesis is to illuminate how and why influenza viruses co-opt, manipulate, and embrace RNA regulation strategies of human hosts.

In the first chapter of this thesis, we profiled the RNA-binding characteristics of IFIT2, a canonically anti-viral and interferon-induced host protein, which influenza virus utilizes in a pro-viral manner. Through genome-wide cross-linking immunopreciptation sequencing (CLIP-seq) experiments, we found that IFIT2 binds mRNAs including those of influenza virus. We validated IFIT2 as an mRNA-binding protein, and found that IFIT2 specifically binds AU-rich regions in human RNAs with a preference for binding the mRNAs of other interferon-induced proteins. To accomplish a broadly anti-viral and selectively pro-viral function, we found that IFIT2 binds mRNAs to enhance their translation. Polysome and ribosome-profiling revealed that IFIT2-bound RNAs are poorly translated in the absence of IFIT2, including influenza virus mRNAs. This links the RNA-binding ability of IFIT2 to a functional role in translation, potentially explaining the

contradiction between the previously observed anti-viral phenotypic role for IFIT2 and the mechanistically observed pro-viral role for IFIT2 in the context of influenza virus. Altogether, these data describe a new node for the regulation of translation during interferon responses and highlight the regulatory volatility that exists at the mRNA interface during infection.

In the second chapter of this thesis, we sought to understand the non-specific RNA-binding capability of the influenza virus nucleoprotein, which binds and protects the negative-sense RNA genome to facilitate gene expression and genome replication. Despite this well-established role, the incongruity of the specificity of NP for the viral genome and known biochemical promiscuity of NP is not reconciled. To address this, we perfomed cross-linking immunoprecipitation sequencing to unbiasedly determine the identity of NP-bound RNAs during infection. NP binds the viral genome and anti-genome, but also engages with a number of discrete classes of host small non-coding RNAs. Many of these RNAs have been shown to be host-derived RIG-I agonists during DNA virus infections, or structurally resemble validated RIG-I agonists. We profiled the RNAs bound by RIG-I during infection with quantitative CLIP-seq and found that host RNAs are bound and sampled by RIG-I, and NP likely interferes with the ability of RIG-I to sample endogenous and exogenous agonists. These data show that NP not only acts as a structural component of the influenza gene expression and replication machinery, but also acts as a viral countermeasure for innate sensing of immunogenic RNAs.

As a whole, this thesis describes two dissimilar instances by which influenza manipulates host RNA regulation. While the context of these host protein:viral mRNA and viral protein:host non-coding RNA interactions are different, they collectively suggest that RNA regulation during the host innate response to viral infection is an essential and commonplace strategy, but often leaves the host exposed to quickly adapting viral pathogens.

CHAPTER 1
Introduction

Introduction

0.1 Viruses and cells

Viruses are intracellular pathogens that rely upon host cells to replicate genetic material. While viruses can self-assemble, they rely almost entirely upon the host for macromolecular synthesis. This dependence on the host necessitates direct and indirect interactions between viral and host processes in order to successfully replicate and continue to spread genetic material[1,2].

To this end, there are discrete and common steps that viruses must take in order to complete a replication cycle. In brief, viruses existing outside of a cell must attach and enter a cell, express viral genes to stimulate viral genome synthesis and generate viral structural proteins, replicate genomes, assemble progeny genomes with viral structural proteins, and eventually exit the cell to continue the next replication cycle. Throughout this process, the host cell attempts to directly detect replicating viruses or byproducts of viral replication and block discrete steps of the replication cycle. Unfortunately for the host, this is made difficult by the diversity of viral taxa.

All viruses broadly follow this procedure for replication, but viruses carry and replicate their genomic material with different strategies each posing a unique challenge for host identification and thwarting of the viral replication cycle. For example, viral genomes are composed of DNA, RNA or DNA/RNA hybrids, they are single- or double-stranded, and they are in positive- or negative-sense orientations (e.g. coding or anti-coding)[3]. DNA viruses generally replicate their genomes in the nucleus while RNA viruses replicate in the cytoplasm. However, poxviruses replicate their DNA genomes entirely in the cytosol, while influenza viruses uniquely replicate their RNA genomes within the nucleus of infected cells[4,5]. These are only two examples of the notable diversity that exists in viral replication schemes. While viruses

possess incredible diversity in the method by which they carry and replicate genetic material, they universally converge at RNA, and more specifically at the step of mRNA translation[6–8]. A defining feature of viruses is their complete or partial reliance on host ribosomes and translational apparati of the host. Narnaviruses are little more than an mRNA encoding a self-replicating RNA-dependent RNA-polymerase[9]. Conversely, in an example of partial reliance, large DNA viruses such as mimiviruses encode one or more ribosomal proteins that may interface with host translational machinery[10]. Regardless of the method by which they carry genetic material, all viruses traverse at least one RNA intermediate during their lifecycle. Thus, RNA regulation is a prominent feature of both viral replication schemes and the host defense against viruses.

1.1 Influenza viruses

Influenza viruses are the etiological agent of the respiratory disease influenza[11]. As a seasonally recurring disease with potential for annually epidemics and sporadic pandemics, influenza infections pose a constant threat to human health[12]. Influenza viruses belong to the family *Orthomyxoviridae*, broadly defined by their segmented negative-sense RNA genomes and tripartite RNA-dependent RNA polymerases (RdRPs)[13]. The family includes the prototypical members influenza A virus and influenza B virus – best studied because of their relevance to human health and disease – and diverse genera such as influenza C viruses, influenza D viruses, the tick-borne *Thogotoviruses*, the salmon-infecting *Isaviruses*, and arthropod-borne *Quaranjaviruses*[13].

Influenza virions consist of a host-derived lipid membrane irregularly studded with the viral glycoproteins hemagglutinin (HA) and neuraminidase (NA) that mediate the processes of viral attachment and exit[14]. The viral ion channel, matrix protein 2 (M2), traverses the membrane

and mediates viral uncoating[15]. Contralateral to the glycoproteins, the matrix protein, M1, adorns the inside of the virion membrane and facilitates viral budding and incorporation of genomic RNAs into virions[16,17]. Contained within the lumen of the virion are limiting amounts of the viral non-structural proteins, non-structural protein 1 (NS1) and nuclear export protein (NEP)[18], which play roles in host modulation[19] and viral genome packaging[20], respectively. Finally, the eight genomic segments are packaged in a bundled configuration poised for deposition into a host cell[21].

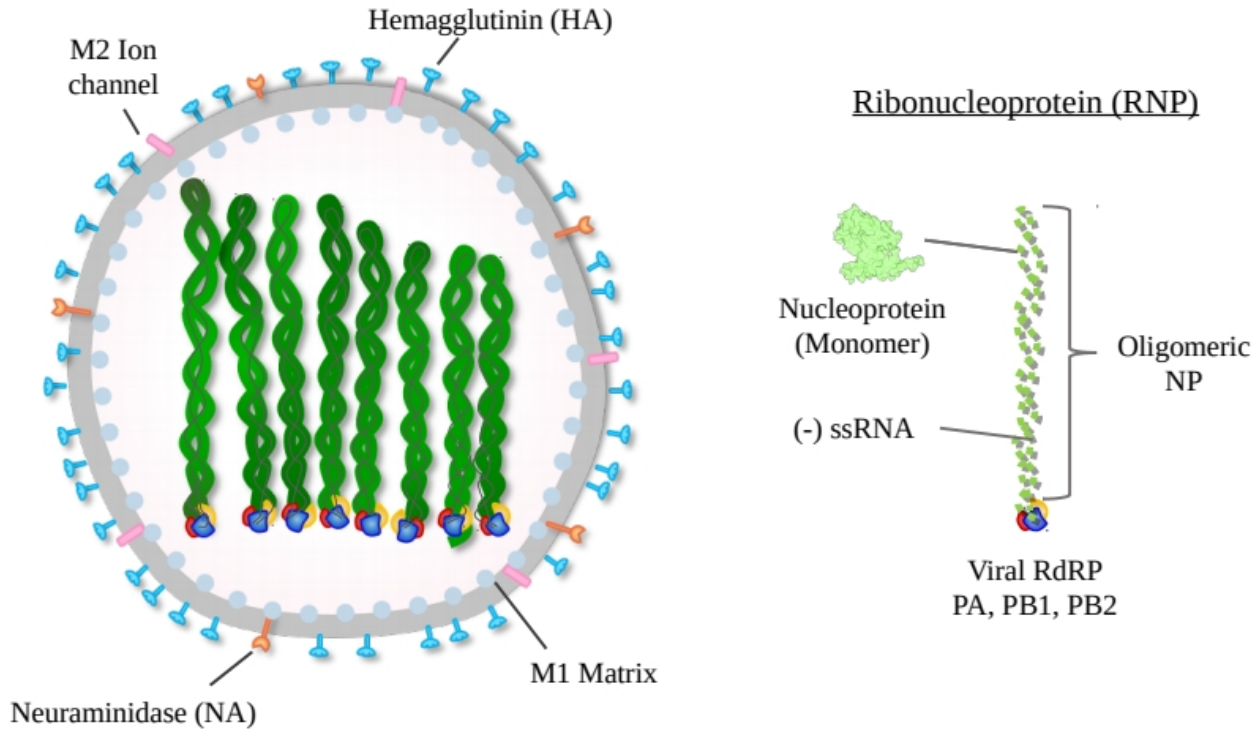

Figure 1. Structure of the influenza virion. (Left) Influenza virion coated in hemagglutinin and neuraminidase. The M2 ion channel spans the viral envelope and M1 coats the interior of the membrane. Inside, eight segments of negative-sense RNA genome are bundled. (Right) The influenza RNP structure. Negative sense viral RNA is bound on both ends by the trimeric RNA-dependent RNA polymerase (RdRP) comprised of PA, PB1, and PB2. Oligomeric nucleoprotein coats the entirety of the RNA to form a pseudo-helical structure.

The ~13.5 kilobase (kb) negative-sense genome of influenza A virus is subdivided into eight segments ranging from 865-2136 nucleotides (nt) in length[13]. These segments exist in the virion and during infection of a host cells as viral ribonucleoprotein (vRNP) particles. vRNPs are

comprised of the negative-sense genomic RNA secured into a pseudo-helical configuration by an oligomeric coating of nucleoprotein (NP)[22,23]. As a pseudo-helix, the 5'- and 3'- termini of the genomic RNA are in close proximity to each other and form the viral promoter, resembling a double-stranded panhandle structure. The viral promoter is recognized and bound by the viral RdRP, a heterotrimer of polymerase basic 2 (PB2), polymerase basic 1 (PB1), and polymerase acidic (PA)[24]. PB1 and PA are enzymes, exhibiting polymerase and endonuclease roles, respectively, while PB2 exhibits a structural role in binding cap-structures at the 5' end of mRNAs[25–27]. Altogether, these RNAs and proteins form the vRNPs packaged into influenza virus virions modeled in Figure 1.

1.2 Influenza virus replication

After HA recognizes and binds sialic acid on the surface of a new host cell, the incoming virion is internalized via receptor-mediated endocytosis[4]. Normal maturation of the endosome containing the viral particle results in acidification of the lumen of the virion via the ion channel M2, concomitantly disrupting the M1-NP interface and freeing the incoming vRNPs from their envelope. The drop in pH also induces wholesale structural changes in HA[4,28,29]. This structural reconfiguration fuses the viral envelope with the endosome membrane, releasing the freed vRNPs into the cytosol where they are actively chaperoned into the nucleus via host importin proteins. As most RNA viruses replicate exclusively in the cytosol, this is a facet of influenza virus infection that is almost exclusive to the *Orthomyxoviridae* family[4].

1.2.1 Influenza transcription

Once in the nucleus, parental vRNPs immediately begin transcription to produce viral mRNAs. The C-terminus of PA binds the C-terminal heptad repeats of RNA polymerase II (RNA pol II) to directly tether the viral RdRP to elongating transcription units[30,31]. In a process known

as “cap-snatching”, nascent 7-methyl guanosine (m7G) capped products of RNA pol II are captured by the cap-binding domain of PB2 and cleaved from the nascent host message 10-17 nt downstream from the cap at a guanosine residue by the endonuclease domain of PA[25,32]. These capped primers are likely produced from highly active RNA pol II promoters, including the spliceosomal small-nuclear RNAs U1 and U2, and cap-snatching from highly expressed protein coding promoters is thought to contribute to virally-induced shutoff of host gene expression[33–35]. The capped primer is threaded into the active site of PB1 and primes transcription from the 3’-end of the vRNA[36]. While the RdRP traverses the vRNP polymerizing the positive sense mRNA, NP molecules are displaced and relocated to the expelled template as it is threaded through the active site of the polymerase. Importantly, the RdRP remains bound to the 5’ and 3’ genome termini throughout the entire transcription cycle. On the 5’-end of the vRNA, a short stretch of encoded uridines induces stuttering to add a poly-adenosine (polyA) tail to the mRNA molecule[37]. After completion of the stuttering process, the mRNA is released. These viral mRNAs are exported to the cytosol via the nuclear export factor 1 (NXF1) pathway, a canonical mRNA export pathway consisting of a network of RNA-binding proteins that shuttle mRNAs to nuclear pores[38,39]. In addition, some viral mRNAs are recognized by RNA-binding proteins that mark and transit mRNAs through nuclear speckles to be spliced, to create mRNAs for M2, NEP, and several minor variant influenza proteins[40]. Altogether, influenza absolutely relies on this network of host transcriptional, splicing, and mRNA export pathways to synthesize viral mRNAs.

1.2.2 Influenza mRNA translation

In the cytosol, influenza mRNAs are translated into viral proteins consistent with canonical eukaryotic cap-dependent translation. In brief, the eukaryotic initiation factor (eIF)

eIF4E binds the mRNA cap in a rate-limiting step[41]. EIF4E is a member of the larger eIF4F complex that recruits the eIF3G complex with the 40S ribosomal subunit, initiator tRNA bound to eIF2, and translation initiation factors to form the 43S pre-initation complex (PIC). PIC scans and progresses through the 5' untranslated region (5'-UTR) of the mRNA until the start codon is encountered, after which the 60S ribosomal subunit is recruited to complete an 80S ribosome and polypeptide synthesis begins. Synthesis continues until a stop codon is encountered and the 80S ribosome is disassembled. PolyA-binding proteins (PABPs) bind the mRNA polyA tail and eIF4F and position the disassembling ribosome in close proximity to the 5'-UTR to allow for efficient recycling of ribosomes[42]. Influenza mRNAs are absolutely reliant on the host for translation and are subject to the same cis- and trans-acting factors that regulate host mRNA translation.

1.2.3 Influenza genome replication

With sufficient accumulation of newly synthesized NP, PB2, PB1, and PA, viral genome replication can occur. While much of the viral transcription likely occurs proximal to RNA pol II promoters in euchromatin, viral genome replication and progeny RNP assembly is thought to occur in the nucleolus, where RNA polymerase I (RNA pol I), small nucleolar RNAs (snoRNAs), and a suite of RNA-binding proteins synthesize and process 28S, 18S, and 5.8S ribosomal RNAs (rRNAs)[43]. vRNPs transit within the nucleus with the host protein clustered mitochondria protein homolog (CLUH), but how this is spatiotemporally accomplished is unknown, except that NP encodes a bipartite nuclear localization signal (NLS) between residues 198 and 216 that mediates localization to the nucleolus[44,45].

Genome replication requires both the resident polymerase on vRNPs and a second newly synthesized RdRP. To initiate genome replication, the newly synthesized RdRP forms a dimeric complex with the vRNP-resident RdRP bridged by ANP32A, a nuclear host protein

indispensable for viral genome replication[46]. The newly synthesized RdRP captures the nascent 5'-end of the cRNA, and free NP molecules encapsidate the growing antigenome. The process of cRNA to vRNA conversion occurs similarly, except that it uniquely requires a third trans-activating RdRP[47]. The exact mechanism by which ANP32A proteins facilitate genome replication, and specifically what steps require ANP32A proteins remains unclear[48–50]. The process of RNP assembly is tightly regulated. NP oligomerization occurs by insertion of a peptide tail on a free NP molecule into a groove on an encapsidated NP molecule, linking and providing rigidity to the RNP[23,51,52]. While the exact mechanism by which free NP is shepherded into a growing RNP is not clear, several host proteins including PKCδ, UAP56, and GCN5 play roles in regulating the free pool of NP via direct binding or post-translational modifications[53–55]. Outside of the local environment surrounding a replicating RNP, free NP is also spatiotemporally regulated, as NP accumulates in the nucleus early in infection and is exported to the cytosol late in infection[44,56]. After progeny vRNPs are synthesized, they undergo additional rounds of transcription and genome replication, or are exported from the nucleus via the CRM1-nuclear export pathway to be shuttled to sites of assembly at the surface of the cell enriched in M1, M2, HA, and NA[57,58].

As highlighted above, influenza utilizes or co-opts host RNA pol II transcription, host RNA splicing, NXF1 and CRM1-dependent nuclear export, cap-dependent translation, and rRNA maturation to synthesize mRNAs, splice mRNAs, export mRNA and RNPs, translate viral proteins, and replicate genetic material, respectively. These phenomenon are depicted in Figure 2. This is not an exhaustive list of RNA processes co-opted by influenza virus (e.g. influenza virus manipulates host RNA exosome components to promote replication)[59]. Extensive use of host RNA processing is not distinctive of influenza viruses, but rather is a unifying characteristic

among viruses[60–62]. The degree by which influenza is fully invested in host RNA regulation and processing provides a unique model system to study how viruses exploit their RNA environments.

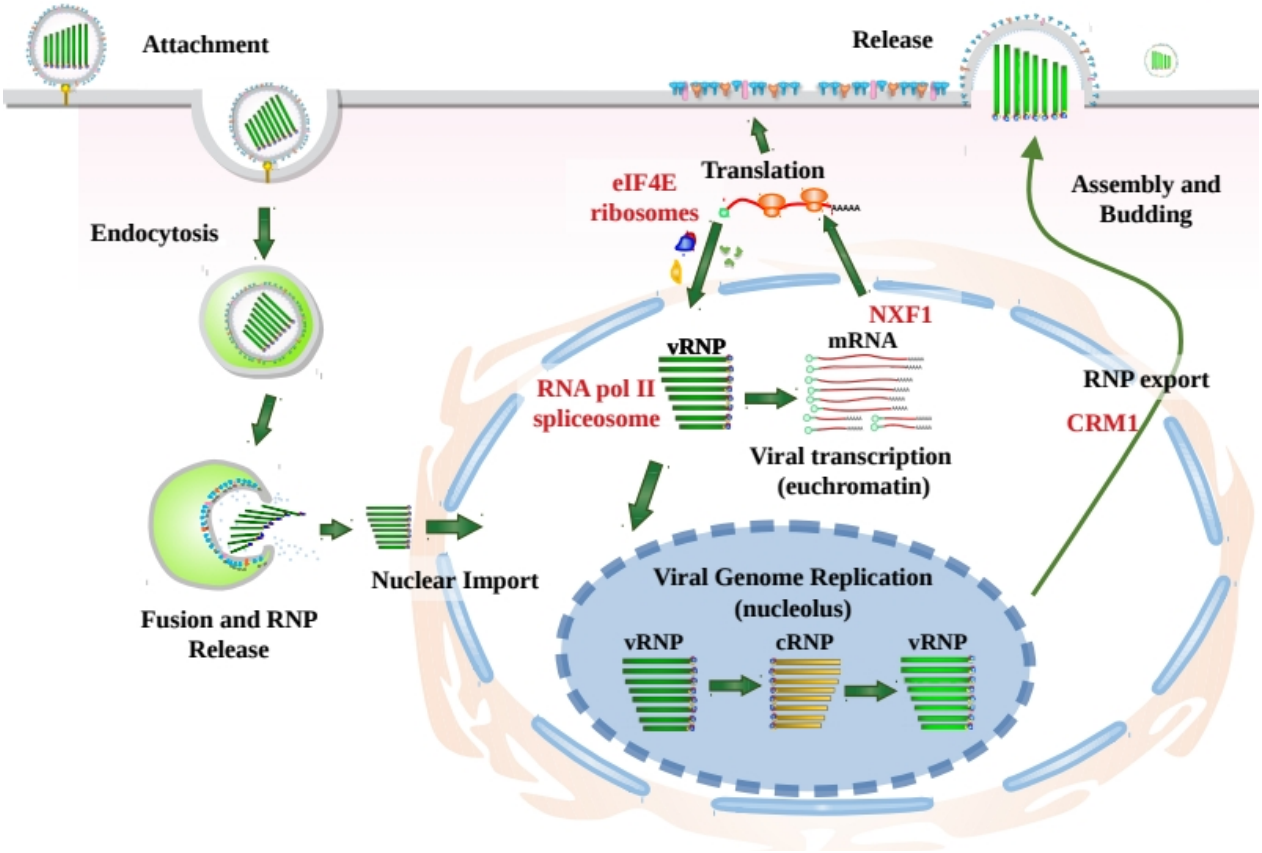

Figure 2. The influenza virus lifecycle and major RNA processes. Schematic of the viral lifecycle, highlighting key RNA processes, pathways, or proteins co-opted by influenza virus in red.

2.1 Host and viral RNAs

RNA is a diverse macromolecule that can encode protein products, provide structure or scaffolding for other RNAs or proteins, regulate the expression of other RNAs, act as signaling molecules, enzymatically modify itself or other RNAs, and fulfill other diverse tasks[63–65]. This is accomplished while spanning orders of magnitude in length and occupying a fraction of sequence space relative to proteins. Viruses and hosts regulate gene expression post-transcriptionally to contextually tune protein expression levels without necessarily changing the

transcriptional landscape. Outside of protein-coding RNAs, many host and virus-derived non-coding RNAs have emerged as critical positive or negative regulators of viral infection.

2.1.1 Co- and post-transcriptional regulation of viral and host mRNAs

After transcription, an mRNA is subject to the local regulation of splicing, nuclear export, translation, and RNA decay pathways. Prototypical mRNAs consist of a 5' m7G cap structure attached via a 5'- 5' linkage to the first mRNA base[66]. As one of the first steps of eukaryotic mRNA synthesis, the capping enzyme machinery contains a guanylyl-transferase activity that adds the terminal guanosine followed by methyl-transferase activity that modifies to base to a m7G cap to create nascent messages with a so-called cap0 structure. In higher eukaryotes, this is followed by 2'O-methylation of the ribose moieties on the first and second bases to create the cap1 and cap2 structures, respectively[67]. While many RNA viruses encode the enzymes to produce cap1 and cap2 viral mRNAs, the host caps stolen by influenza virus contain these marks, superseding the requirement for capping and methylation enzymes[66,68]. Cap structures allow for efficient translation of viral messages as outlined in section 1.2.2.

The processes of host mRNA splicing, polyadenylation, and nuclear export are kinetically linked to each other and RNA pol II transcription[69]. Serine- and arginine-rich (SR) RNA-binding proteins recognize sequences within 5'-splice sites and coordinate the assembly of the U1 subunit of the spliceosome, while distinct SR proteins and U2-auxiliary factor (U2AF) coordinate the assembly of the U2 subunit of the spliceosome on the 3'-splice site[65]. The Lsm8 small nuclear ribonucleoprotein (snRNP) containing U4, U5, and U6 small nuclear RNAs (snRNAs) finishes the assembly of the spliceosome and allows for the progression of the splicing reaction. A number of auxiliary proteins mediate alternative-splicing decisions. Influenza virus both exploits host RNA-binding proteins to regulate expression of spliced viral transcripts, and

disrupts host alternative-splicing to alter the outcome of infection[70–72]. While this phenomenon is common among DNA viruses that extensively utilize host splicing, the vast majority of RNA viruses avoid this process entirely.

Polyadenylation completes mRNA maturation and prepares mRNAs for export to the cytosol. The polyadenylation reaction of host transcripts is initiated by recognition of an "AAUAAA" motif in mRNAs by the cleavage and polyadenylation specificity factor (CPSF) complex[73]. The CPSF complex only contains the CPSF73, CPSF100, CPSF30, and CPSF160 proteins, but recruits >15 other RNA-binding and structural proteins that facilitate the addition of polyA tails to the 3'-end of mRNAs by polyA-polymerases. Nuclear export of spliced and polyadenylated mRNAs typically occurs via the NXF1-pathway as introduced in 1.2.1, where a network of export proteins recognize bound splicing and polyadenylation factors to efficiently export mature messages. RNA viruses commonly disrupt nuclear export of cellular mRNAs to promote synthesis of viral proteins, but influenza virus relies on this process for export of viral messages[38,39]. Instead, some strains of influenza virus NS1 inhibit polyadenylation by directly binding CPSF30, thus inhibiting host gene expression at the level of mRNA maturation but leaving mRNA export pathways intact, as influenza virus does not use the host to polyadenylate viral messages[37,74].

After maturation and export, mRNAs serve their primary role in templating protein synthesis. Section 1.2.2 describes a basic overview of cap-dependent translation. Translation can be regulated by cis-acting elements, trans-acting factors, and combinations thereof to regulate two principle steps in protein synthesis. The first step, translation initiation, is regulated by recognition of the cap by eIF4E, recruitment of translation initiation factors and initiator tRNAs bound to GTP-bound eIF2, and scanning the 5'-UTR for start codons[41]. Repressive RNA

structures in the 5’-UTR, regulation of eIF2 to preclude GDP-recycling, and binding of microRNAs (miRNAs) and RNA-binding proteins to the 3’-UTR that remodel mRNAs to prevent ribosome recycling all result in decreased levels of translation initiation. The translation factor eIF2A is a common target for initiation regulation. Phosphorylation of eIF2 by the kinases PKR, GCN2, or PERK prevents recycling of GDP and repression of translation. These kinases are activated by detection of viral replication, amino acid starvation, or ER-stress induction, respectively[75].

The second step, translation elongation, is regulated by the speed at which ribosomes read an mRNA template and polymerize amino acids. Similar to initiation regulation, elongation can be regulated by cis-acting and trans-acting factors[76]. Intuitively, relative differences in tRNA abundance can affect reading of cognate codons by an elongating ribosome[77]. During infection, there is evidence that the pool of free tRNAs changes to accommodate expression of antiviral genes, suggesting that the codon composition of mRNAs can differentially affect protein synthesis rates dependent on host-regulated tRNA abundances[78]. Pauses in ribosome elongation also accompany normal protein folding, where structurally complex regions in nascent polypeptides prevent the continued polymerization of amino acids until properly folded, or where 7SL RNA and the signal recognition particle pause the translation of membrane-bound proteins so the ribosome can transit to signal receptors and translate directly into the lumen of the ER[79,80]. Outside of studies in *Sacchoromyces,* few trans-acting factors have been identified that discretely regulate ribosome elongation, despite the appreciated importance of ribosome pausing, highlighting a knowledge gap in ribosome biology.

Transcripts have discrete half-lives, and transcript stability is tightly coupled to translational regulation and trans-acting RNA-binding proteins. Ribosomes that are aberrantly

translating messages are recognized and both ribosomes and transcripts are removed from the mRNA pool via endonucleotic cleavage and exonucleases[81,82]. Under normal circumstances, cells utilize several pathways to capture and selectively degrade aging mRNAs from the transcript pool. Deadenylation, decapping, and/or endonucleolytic cleavage promote rapid degradation of transcripts[83]. The process of transcript destabilization can be mediated by a number of RNA-binding proteins which recognize sequence motifs, often rich with adenosines and uridines (AU-rich elements or AREs), that directly recruit mRNA decay proteins to transcripts[84–86]. Conversely, other RNA-binding proteins recognize similar AU-rich sequences and promote transcript stability, competing with the destabilizing protein. For example, when expressed abundantly, HuR binds labile ARE-containing mRNAs and prevents their destabilization via AUF1 and KSRP, conveniently also maintaining protein synthesis from these mRNAs[87,88]. Thus, overlapping regulatory hubs between mRNA export, translation, and degradation pathways collectively determine the fate of messages.

Altogether, viruses must adhere to or subvert the rules that govern cellular mRNA regulation. Regulation of mRNA production, export, synthesis, and decay is complex, with each step connected and regulated by overlapping and competing sets of RNA-binding proteins[89]. Regulatory information in mRNAs is embedded within primary sequences or structures, either in the 5’-UTR, 3’-UTR, or coding sequences. While mammalian mRNAs often have the luxury of carrying expansive 3’-UTRs capable of uniquely encoding appropriate regulatory programs, many viral mRNAs are not afforded this space. For example, influenza mRNAs encode limited UTRs, requiring the adaptation of coding sequences to also serve to regulate mRNA fate[90].

2.1.2 Host non-coding RNAs

Although mRNAs play an essential coding role in cells, they are dwarfed in abundance by non-coding RNAs. Mature mRNAs likely represent only ~3-7% of the RNA population by mass in the average mammalian cell, and a fraction of that by total molecule number[91]. In contrast, rRNAs constitute >80% of the RNA mass and ~10% of the total molecule number, and tRNAs constitute ~10% of the total mass and >80% of the total RNA molecule number. Thus, discrete mRNAs occupy a nearly insignificant proportion of the RNA in the cell.

Host non-coding RNAs are broken into two classes based on an arbitrary length cutoff of 200 nucleotides, with RNAs larger than 200 nucleotides termed long non-coding RNAs (lncRNAs) regardless of function, and short RNAs coined according to their function as detailed in Table 1. Non-coding RNAs play diverse structural and enzymatic roles reflective of the diverse processes in RNA and protein synthesis described above. While 7SK, 7SL, small nucleolar RNAs (snoRNAs), and SINE RNAs are typically considered to be lncRNAs, they play distinct structural roles, and will be considered separately here from RNA pol II-transcribed lncRNAs that often function as scaffolds for RNA-binding proteins.

As briefly described in section 1.2.3, RNA pol I solely transcribes three of four ribosomal RNAs as part of the 45S pre-rRNA, a transcriptional array that contains rRNA sequences embedded within spacer sequences[92]. Once transcribed, the U3, U8, and U14 snoRNAs recognize and facilitate the separation of 5.8S, 18S, and 28S rRNA from spacer sequences and each other. Throughout rRNA maturation, >80 RNA-binding proteins, numerous snoRNAs, and 5S rRNA assemble and modify rRNAs to result in the mature 40S and 60S ribosomes. After maturation, 5.8S, 18S, and 28S are each capped by a single 5’-monophosphate.

Name/Biotype	Length††	RNA pol	Putative 5'-end structure*	Primary function
28S rRNA	~4000-5000 nt	I	monophosphate	Protein synthesis
18S rRNA	~1700-1900 nt	I	monophosphate	Protein synthesis
5.8S rRNA	~150 nt	I	monophosphate	Protein synthesis
5S rRNA	~150 nt	III	triphosphate	Protein synthesis
tRNA	~70-100 nt	III	monophosphate	Protein synthesis
7SK RNA	~340 nt	III	γ-methyl triphosphate	RNA pol II activation
7SL SRP RNA	~300 nt	III	triphosphate	Membrane protein translation
U1 snRNA	~164 nt	II	2,2,7-trimethyl cap	mRNA splicing
U2 snRNA	~188 nt	II	2,2,7-trimethyl cap	mRNA splicing
U4 snRNA	~144 nt	II	2,2,7-trimethyl cap	mRNA splicing
U5 snRNA	~117 nt	II	2,2,7-trimethyl cap	mRNA splicing
U6 snRNA	~106 nt	III	γ-methyl triphosphate	mRNA splicing
C/D snoRNAs	~60-300 nt	II†	monophosphate	RNA 2'O methylation
H/ACA snoRNAs	~60-300 nt	II†	monophosphate	RNA pseudouridylation
miRNAs	~22 nt	II	monophosphate	mRNA regulation
YRNAs	~84-112 nt	III	triphosphate	DNA replication initiation
vtRNAs	~86-141 nt	III	triphosphate	N/A
lncRNAs	~200-10000 nt	II	m7G cap	N/A
LINE RNAs	~6000 nt	II	m7G cap	N/A
SINE RNAs	~100-300 nt	III	triphosphate	N/A

Table 1. Abundant human non-coding RNAs. Human non-coding RNAs sorted roughly by cellular function. This list is not inclusive of many of the less-abundant or variant ncRNAs. *=RNAs containing 5'-end modification that occur co-transcriptionally or immediately following transcription. †=Some snoRNAs are transcribed by RNA pol III. N/A=diverse, unknown, or poorly defined functionality. ††=Nucleotide lengths taken as an aggregate of those reported in the NCBI Nucleotide database.

Although not transcribed by RNA pol I, the RNA pol III-transcribed tRNAs are also adorned by a single 5'-phosphate as a result of RNaseP-mediated excision of the tRNA leader sequence[93]. Some tRNA α-phosphates are further modified by methylphosphate transferases like BCDIN3D to form dimethyl α-phosphates[94]. Unlike tRNAs, RNA pol III transcribes 5S rRNA, but 5S rRNA is thought to retain a 5'-triphosphate[95].

RNA pol II transcribes several of the snRNAs that assemble to form the RNA components of the spliceosome, as detailed in section 2.1.1. The U1, U2, U4 and U5 RNAs are co-transcriptionally capped, followed by a unique 2,2,7-methyl addition to the guanosine cap catalyzed by trimethylguanosine synthase[67]. RNA pol II is also responsible for transcription of lncRNAs, LINE RNAs, miRNAs, and snoRNAs[96,97]. Many lncRNAs structurally resemble mRNAs, but lack coding regions[63]. miRNAs and snoRNAs are often processed out of pre-mRNAs as introns, and thus contain 5'-monophosphates as a result of this processing. snRNAs, snoRNAs, and miRNAs each assemble with RNA-binding proteins to form their structural or enzymatic RNPs.

Finally, RNA pol III not only transcribes tRNAs and 5S rRNAs, but is also responsible for transcribing the majority of the small non-coding RNAs, including 7SL, 7SK, U6, Y, vault, and SINE RNAs[98]. The 7SL, Y, vault (vt), and SINE RNAs are similar to 5S rRNAs and retain their 5'-triphosphate after transcription[95]. While 7SK and U6 snRNAs also retain a 5'-triphosphate, the methylphosphate capping enzyme (MePCE) catalyzes the addition of a methyl group on the γ-phosphate immediately following transcription[99]. This mark is thought to protect and stabilize these RNAs as they assemble into their respective RNP complexes.

While most of the non-coding RNAs described here have well described cellular roles as detailed in section 2.1.1, the functions of Y, vault, and SINE RNAs is less clear.. Y RNAs are thought to play a minor role in DNA replication initiation and RNA-misfolding, while vtRNAs have some demonstrated roles in drug-resistance and initiation of autophagy[100,101]. The SINE RNAs described here refer almost exclusively to Alu RNAs, which are parasitic transposons of primate genomes, and likely play few major functional roles in cells[91].

Like mRNAs, much of the processing, maturation, and eventual activity of non-coding RNAs is mediated by other non-coding RNAs and RNA-binding proteins, including those that are responsible for the manufacturing of non-coding RNAs. Non-coding RNA biogenesis pathways contain diverse processing, modification, and maturation steps that can be variable and subject to regulation. For example, dual-use specificity phosphate 11 (DUSP11) trims the 5'-triphosphates of non-coding RNAs to 5'-monophosphates, and the previously described BCDIN3D adds phosphate groups to the 5'-monophosphate of some tRNA species[94,102]. Less appreciated than steps in mRNA regulation, viruses implicitly utilize host non-coding RNAs to express viral genes and replicate, but the degree to which viruses manipulate host non-coding RNAs directly is not well understood.

2.1.2 Viral non-coding RNAs

The viral genome and antigenome give rise to several classes of non-coding RNAs that can augment or hinder viral replication at several steps. The svRNAs are short abortive replication products resembling 22-27 nt of the 5'-end of the genomic RNA. They bind the RdRP and are proposed to facilitate the switch from transcription to replication[103]. Defective-interfering (DI) RNAs and mini-viral (mv) RNAs differ in that they contain both ends of the viral genome and play antagonistic roles during viral replication[104,105]. DI RNAs were named according to their ability to be packaged into virions and interfere with subsequent rounds of infection, whereas the much shorter mvRNAs lack the viral packaging signals necessary for virion incorporation[104,106,107]. Both species are produced via a similar mechanism where a replicating RdRP disengages and then re-engages the template RNA downstream to yield short viral RNAs with internal deletions[104,108]. Consequently, these species are thought to out compete synthesis of full-length genomes, and both have been implicated as stimulators of host innate-immunity[109,110].

Name	Length	RNA sense	Function
vRNA	~900-2300 nt	(-)	Genomic RNA, templates transcription/replication
cRNA	~900-2300 nt	(+)	Antigenomic RNA, templates replication
DI RNAs	~300-500 nt	(+/-)	Erroneous replication defects, parasitize infection
mvRNAs	~30-80 nt	(+/-)	Erroneous replication defects, stimulate immunity
svRNA	~22-27 nt	(-)	RNP transcription to replication switch

Table 2. Influenza virus non-coding RNAs. Non-coding RNAs that accumulate in infected cells.

Other viruses produce more diverse and explicitly functional non-coding RNAs. Adenoviruses express two RNA pol III driven transcripts, virus-associated RNA I and II, that bind the kinase and host sensor of viral dsRNA, PKR, and inhibit its activation[111]. Kaposi's sarcoma-related herpesvirus expresses the lncRNA PAN that represent the majority of viral RNA in infected cells and sponges RNA-binding proteins to promote late viral gene expression[112]. Given their expanded coding capacity, there are many examples of DNA viruses expressing functional non-coding RNAs[113]. In RNA viruses, flaviviruses express sfRNA, a byproduct of digestion by exoribonuclease I (XRN1). This non-coding RNA tightly binds XRN1 and prevents its activity, inhibiting cellular RNA decay pathways[114]. Thus, viral non-coding RNAs can exist as byproducts of replication and RNA-processing, as specifically expressed functional RNAs with proviral functions, or both.

The diversity in form and function of host and viral non-coding RNAs is staggering, and they likely play additional minor roles not described here. Thousands of variant non-coding RNAs exist in the human genome that can perform functions different from their parental sequences[91,115]. Regardless, non-coding RNA constitutes the bulk of the RNA mass and molecules in a cell and performs important and specific roles in cellular homeostasis and viral replication.

3.1 Innate Immunity and RNA-binding proteins

Every intracellular viral process is performed at the expense of the host. Accordingly, hosts have developed extensive antiviral gene programs and surveillance mechanisms to attempt to detect replicating viruses[116]. Interferon stimulated genes (ISGs) are potently activated transcriptionally following detection of an invading virus. ISG protein products target and prevent nearly every step of the viral replication cycle[117,118]. In direct opposition to this pressure, viruses that avoid or subvert these host defenses by any means are able to persist and replicate. Eventually this evolutionary back-and-forth allows viruses to exist in niches that remain hostile to naive pathogens[119–122]. Therefore, viral evasion of host defenses exists as a combination of adaptation and exaptation, resulting in unexpected and counter intuitive countermeasures to host innate immunity.

3.1.1 Host sensors of RNA viruses

Vertebrate hosts express a suite of pattern recognition receptors (PRRs) or sensors poised to detect viral genomic material, which acts as a pathogen-associated molecular pattern (PAMP)[116,123]. Sensing viral genomic material can activate type I interferon production, a paracrine signaling pathway that systemically primes cells for invading pathogens, and promote production of interferon-stimulated genes to attempt to block viral replication intrinsically[117,118]. DNA sensors are employed by the host to detect DNA viruses. They are active in the cytoplasm, where cellular DNA should not exist, and are often sensitive to any DNA encountered[124]. In stark contrast, RNA sensors must disambiguate the origin of encountered RNAs in the cytosol, where numerous host RNAs exist. Given the diversity of RNA that exists in a cell, this task often requires fine molecular sensing of single moieties or structures on or in RNA, as described in

Table 3, with many of the exact moieties required for activation still unknown or ambiguously defined[125].

Sensor	Family	RNA-binding domain	Ligand
RIG-I	RLR	hel2/CTD	Short, 5’-triphosphate containing dsRNA
MDA5			Long, >500 nt duplex RNA
LGP2			N/A
PKR	PKR	dsRBD	>33 nt duplex RNA
OAS1	OAS	NTase	>15 nt duplex RNA with 3’-uridine overhang
OAS2			>35-40 nt duplex, ssRNA
OAS3			>50 nt duplex RNA
OASL			mRNA 5’UTR (IRF7)
IFIT1	IFIT	TPR	cap0 mRNA
IFIT2			N/A
IFIT3			N/A
IFIT5			5’-triphosphate, often tRNA

Table 3. Endogenous RNA sensors of viral infection. Host proteins that patrol the cytosol for viral RNAs or other PAMPs. N/A=Poorly defined preferences for discrete RNA targets.

The interferon-induced proteins with tetratricopeptide repeats (IFITs) are a family of four proteins that uniquely recognize RNA via tetratricopeptide repeats (TPRs), previously thought to only mediate protein-protein interactions[126]. While all four IFIT proteins are heavily synthesized during infection and have demonstrated antiviral roles, the molecular mechanism of this restriction has only been mapped for IFIT1 and IFIT5[127]. They each recognize discrete molecular signatures of viral RNAs, where IFIT1 recognizes cap0 structures common on many viral mRNAs, and IFIT5 recognizes 5’-triphosphate structures common to viral genomes[128–130]. IFIT2 has been proposed to bind AU-rich sequences *in vitro*, but this specificity has never been demonstrated *in vivo*[126]. The best characterized member, IFIT1, binds cap0 viral mRNAs and prevents recognition of the mRNA cap by translational machinery, effectively removing IFIT1-bound mRNAs from the translation pool[129,131]. In addition, it has been proposed that IFIT2

exhibits functional effects on translation by binding eIF3 and preventing translation initiation *in vitro*[132]. The high abundance of all IFIT proteins during infection, their potent antiviral nature, and recognition of discrete RNA species emphasize their importance during RNA virus infection.

Humans encode four members of the 2'-5' oligo-adenylate synthetase family (OAS) of RNA-binding proteins, with three of four exhibiting catalytic activity[133]. The catalytic members are activated by binding double-stranded RNA and synthesize 2'-5' oligoadenylate that activates RNaseL, a highly active non-specific nuclease that globally inhibits translation by degrading RNA[134]. OAS1, OAS2, and OAS3 have 1, 2, and 3 NTase domains, respectively, which gives rise to the increasing RNA duplex length required for activation between OAS family members[134–137]. While these enzymes have noted anti-viral roles during infection, the exact molecular determinants for activation and avoidance of self-sensing of host RNAs is unknown.

The kinase domain of PKR is activated following binding to dsRNA via a double-stranded RNA-binding domain (RBD). Oligomerization of two or more PKR proteins leads to phosphorylation of neighboring molecules and full activation of the kinase[138,139]. The primary target for PKR phosphorylation is eIF2, which prevents recycling of eIF2-GDP complexes and stalls cellular translation[6,75]. PKR displays no sequence preference for target RNAs, and has known tolerance for RNAs with minimal structures[140]. This includes some species of host-derived snoRNAs and intron-derived dsRNAs that are exposed to PKR under cellular stress or mitosis[141,142]. Like OAS proteins, the mechanism by which PKR avoids wide-spread activation by sensing cytosolic host RNAs is unclear.

The RIG-I like receptor family of RNA helicases have well defined roles in restricting RNA viruses, and also restrict some DNA viruses[143]. Of the RNA-binding proteins described here, the characteristics of the RNA targets engaged by RLRs are defined in greatest molecular

detail. Despite evolutionary relatedness of the RLR proteins, they have unique RNA-binding preferences. As a regulator of RIG-I and MDA5, LGP2 does not have well a defined preference for RNA, although it does carry a helicase (hel2) and C-terminal domain (CTD) related to the other RLRs[144–146].

MDA5 displays a preference for long dsRNAs (>500-1000 nt), thought to originate from the replicative products of positive-sense RNA viruses[147,148]. Long double-stranded RNAs can also form from complementary regions in host mRNAs. These double-stranded regions are tempered via A-I editing by Adenosine Deaminase RNA Specific (ADAR) to introduce bulges in the RNA duplex and disrupt MDA5 binding[149]. While MDA5 binds long double-stranded RNA, RIG-I prefers to bind short double-stranded hairpins[150]. The specificity of RIG-I is regulated by both the CTD and the hel2 domain. The CTD cradles the 5’-triphosphate with basic residues while the hel2 domain recognizes and threads onto the blunt ended base-pairing of the 5’- and 3’-ends[151–153]. This specificity for 5’-triphosphate is postulated to allow RIG-I to selectively bind viral RNAs that often retain unmodified 5’-ends, although many host RNAs are also transcribed with 5’-triphosphates (see Table 1). In influenza virus infection, RIG-I is activated by mvRNA and DI RNAs[104,110,154]. Outside of the context of RNA viruses, RIG-I can paradoxically play anti-viral roles during herpes virus and retrovirus infections, and it was recently demonstrated that RIG-I recognizes host phosphorylated RNAs to mediate this restriction. Through either unmasking of RNAs basally shielded by RNA-binding proteins or downregulation of the RNA phosphatase DUSP11, the host 5S-pseudogene141 RNA, vtRNAs, and Y RNAs were found to affect the replication of herpes simplex virus, Kasposi’s sarcoma-related herpesvirus, and human immunodeficiency virus, respectively[155–157]. While host RNAs activate RIG-I in these isolated examples, it is not well understood how RIG-I avoids activation given the high abundance of tri-

phosphorylated RNAs typically present in uninfected cells, or how RIG-I may discriminate against binding the diverse 5’-end structures present on eukaryotic non-coding RNAs.

3.1.2 Activation of RLRs and interferon stimulated genes

All of the aforementioned RNA-binding proteins are important in recognizing endogenous viral infections, but RIG-I and MDA5 play the greatest role in directly activating the type I interferon pathway[143]. These RLRs are tasked with surveying RNA molecules for viral RNA and inducing signaling cascades by multimerizing on RNA substrates and activating the mitochondrial antiviral signaling protein (MAVS), as depicted for RIG-I in Figure 3. Both sensors utilize RNA-binding domains to recognize RNA targets and engage helicases with the termini of bound targets[151,153,158]. MDA5 displays slow association kinetics with RNA, and ATP promotes the activity of the helicase to kinetically discriminate between short and long RNA duplexes. That is, hydrolysis and translocation of the helicase away from the bound end of the RNA is efficient and necessary for multimerization and induction of signaling[159,160]. Short RNA templates result in fast recycling of MDA5 molecules where they can encounter other RNA duplexes, whereas lengthy RNA molecules result in longer dwell times and greater probability that they oligomerize with other MDA5 molecules. In contrast, RIG-I displays fast association kinetics and relatively slow ATP hydrolysis[160,161]. This allows RIG-I to sample RNAs quickly and dwell for an extended period of time relative to MDA5, which is necessary given the shorter RNA templates recognized by RIG-I. In both instances, kinetic discrimination underlies the ability of RIG-I to recognize 5’-triphosphate ends and MDA5 to accumulate on long duplex RNAs.

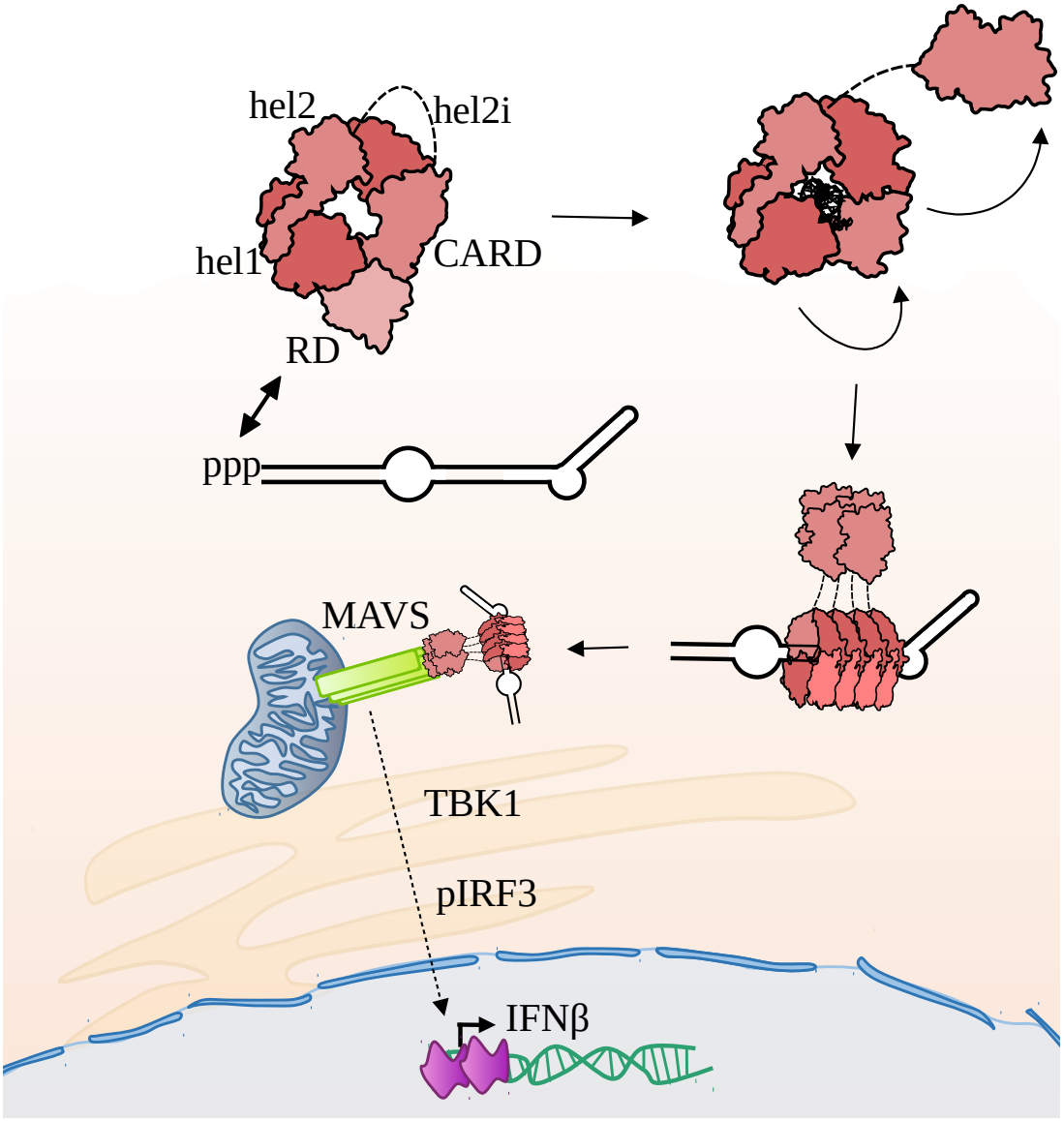

Figure 3. Activation of MAVS by RIG-I. (top left) RIG-I CARD bound to hel2i domain in autoinhibited state before binding 5'-triphosphate RNA. (top right) Ligand binding induces structural change where regulatory domain (RD) binds 5'-triphosphate and frees CARD, threading the RNA into the helicase. (bottom right) Successive binding reactions form RIG-I oligomers on RNA, completing a CARD tetramer. (bottom left) CARD tetramer binds and induces MAVS oligomerization, activating TBK1. TBK1 phosphorylates IRF3 which dimerizes and translocates into the nucleus to promote transcription of interferons and interferon-stimulated genes.

In the absence of activating RNA, RIG-I and MDA5 exist in an auto-inhibited state where the caspase activation and recruitment domains (CARDs) involved in MAVS signaling are

bound to the helicase domain[143]. Threading of the helicase domain onto the end of an RNA substrate frees the CARD domain[162]. Freed CARDs homo-oligomerize with at least three adjacent RLRs to form CARD tetramers, the minimal unit required for signaling through the CARDs of MAVs[153,163]. Tripartite motif containing 25 (TRIM25) mediates K63-linked ubiquitination of RIG-I CARDS and stabilizes the tetramer, promoting activation of MAVS[164]. Activated MAVS auto-aggregate and promote the phosphorylation of IRF3 and IκBα by TBK1 and IKKα/β, facilitating the nuclear translocation of the transcription factors IRF3 and NF-κB[143].

After activation and nuclear translocation, IRF3 and NF-κB are responsible for the transcriptional activation of hundreds of ISGs and multiple subtypes of type I interferon[165]. IRF3 and NF-κB recognize degenerate sequence elements in the promoters of these genes and recruit transcriptional machinery to rapidly produce antiviral mRNAs[166,167]. While the signaling cascade that leads to the production of interferon and ISG mRNAs is thoroughly elucidated, the factors regulating the post-transcriptional fate and eventual removal of these mRNA species from the translational pool is less well understood[168]. Many ISG and inflammatory mRNAs have AREs in their 3'-UTRs[85,169,170], subjecting them to rapid turnover by RNA-binding proteins. Similarly, Zinc Finger Antiviral Protein (ZAP) is expressed as short and long isoforms that mediate the degradation of interferon and viral mRNAs, respectively[171,172]. The protein products of ISG mRNAs are often toxic when expressed for extended timeframes, necessitating their transient expression and rapid removal from the translational pool[118]. Nevertheless, expression of these proteins is important for an antiviral response, and the cis- and trans-acting factors that interact to balance proper expression of these proteins need further exploration.

3.2 Influenza modulation of host RNA sensors

To counteract the recognition of viral RNA, viruses employ diverse tactics aimed at preventing the activation, sensing, signal transduction, and effector activities of RNA sensors of viral infection. NS1 is the canonical innate immune antagonist, complemented by several influenza proteins that play auxiliary roles in dampening the innate response to viral infection[19,173]. Indeed, all of the influenza virus genes have been implicated in antagonizing innate immunity to some degree[174]. In fact, single-cell RNA-sequencing experiments revealed that influenza virus efficiently prevents innate immune activation, even in infected cells that lack NS1[175]. Given that RNA-sensors and their RNA ligands are the impetus of innate immunity to RNA viruses, many of the antagonistic measures exercised by influenza virus target RNA or RNA processing.

Some members of the IFIT family of proteins can bind and recognize 5'-triphosphates[128,176]. Upon its characterization, IFIT1 was thought to bind 5'-triphosphates of viral RNAs[128,177], but it has more recently been demonstrated to strongly favor cap0 RNA[129–131]. In a similar line of experimentation, it was shown that IFIT1 binds and restricts influenza A virus[177], but this has since been thoroughly corrected in the literature[178]. In fact, given the nearly exclusive cytoplasmic localization of IFIT1, the tight association between the termini of the influenza genome and the RdRP, and the nuclear localization of replicating flu genomes, it is unlikely that IFIT1 would ever encounter an influenza 5'-triphosphate in a way that prevents viral replication. Nevertheless, influenza may modulate IFIT1 and IFIT5 in unconventional or indirect ways. Until recently, the *in vivo* RNA ligands of IFIT2 and IFIT3 and the effect of these IFITs on influenza virus replication were unknown. In chapter 2 of this thesis, we describe the co-option of IFIT2 and IFIT3 by influenza virus and demonstrate that IFIT2 has functionally diverged from the sensor roles of the paralogous IFIT proteins. These data suggest that viruses can not only

antagonize host RNA-binding proteins to prevent sensing, but can also utilize antiviral host RNA-binding proteins for their benefit.

NS1 plays a mult-functional role in dampening the cellular response to influenza virus, including the deactivation of OAS and PKR[179,180]. NS1 is structurally demarcated into a C-terminal RNA-binding domain and an N-terminal effector domain. The effector domain is responsible for binding host proteins, and the C-terminal RNA-binding domain is thought to bind double-stranded RNAs to prevent activation of innate immunity[19]. NS1 has been shown to prevent OAS-dependent innate immune activation, and the RNA-binding domain of NS1 was implicated as the mediator of this restriction[179]. Products of the OAS/RNaseL pathway can activate RIG-I, which is also modulated by NS1 (discussed below), making it difficult to ascertain where NS1 is truly acting[181]. Similarly, NS1 has been shown to disrupt auto-activation of PKR, and it was posited that NS1 out-competes PKR for RNA substrates[180]. More recently, it was demonstrated that NS1 inhibits PKR independently of RNA by a direct protein-protein interface[182]. Furthermore, formaldehyde RIP-seq of NS1 during viral infection suggest that NS1 primarily binds pre-mRNAs, consistent with a role in inhibiting pre-mRNA maturation[183]. Thus, while NS1 clearly plays a role in antagonizing PKR and OAS proteins, these restrictions may be mediated by indirect effects or protein-protein interfaces, and not by prevention of RNA sensing.

Finally, influenza encodes multiple antagonists of the RLR pathway. NS1 plays the most prominent role, but PB2, PA , M2, and a minor variant of PB1 expressed out of a separate frame, PB1-F2, have demonstrated activities in antagonizing activation of RLRs. PB2 and PB1-F2 can localize to the mitochondria to disrupt RLR signaling via disruption of MAVS[184,185]. PB2 interacts directly with MAVS to prevent signaling, whereas PB1-F2 also interacts with MAVS, but abrogates RLR signaling by disrupting the mitochondrial membrane potential, a requisite for

efficient signaling. M2 plays a similar role, where a fraction of the viral ion channel localizes to the mitochondrial membrane and depolarizes mitochondria[186]. In contrast, PA binds and prevents nuclear translocation of activated IRF3, thus stopping the RLR pathway before transcriptional activation[187]. NS1 is the best characterized antagonist of RLRs, where NS1 directly binds RIG-I to prevent the activation of MAVS[188,189]. As was the case for PKR and OAS, the RNA-binding activities of NS1 were thought to compete with RIG-I for substrates, but NS1 can bind and prevent signaling of a constitutively active RIG-I that lacks RNA-binding actively altogether[188]. NS1 can also directly inhibit MAVS, and has a role in blocking the TRIM25 mediated ubiquitination of RIG-I CARD[190,191]. RNA enhances the interaction between RIG-I and NS1, suggesting that the majority of RIG-I antagonism probably occurs after RIG-I binds RNA, potentially at the interface between RIG-I and MAVS[192]. Along with the primarily nuclear localization of RNPs and the observation that RNA encapsidated by NP likely prevents sensing by RIG-I, these data indicate that multiple viral mechanisms of RLR evasion combinatorially contribute to elusion of RNA-sensing. Indeed, in chapter 3 of this thesis, we describe a mechanism by which NP prevents the kinetic proofreading activity of RIG-I, adding to the growing list of host evasion strategies employed by viruses.

4.1 Summary

Viruses are subject to the host context in which they are replicating. This includes not only host proteins, but also the RNA environment and RNA-binding proteins that regulate this pool. This thesis describes two mechanisms by which influenza manipulates host RNA pathways to subvert the cellular response to infection; co-opting the normal function of IFIT2 to stimulate translation of viral mRNAs (Chapter 2) and binding of viral NP to cellular non-coding RNAs to disrupt RIG-I activation (Chapter 3).

References

1. Long, J. S., Mistry, B., Haslam, S. M. & Barclay, W. S. Host and viral determinants of influenza A virus species specificity. *Nat. Rev. Microbiol.* **17**, 67–81 (2019).
2. Kirui, J., Tran, V. & Mehle, A. Host factors regulating the influenza virus replication machinery. in *Influ Curr Res.* 77–100 (2016).
3. International Committee on Taxonomy of Viruses. *Taxonomy* **10**, (2019).
4. Dou, D., Revol, R., Östbye, H., Wang, H. & Daniels, R. Influenza A virus cell entry, replication, virion assembly and movement. *Front. Immunol.* **9**, 1–17 (2018).
5. Schramm, B. & Locker, J. K. Cytoplasmic organization of POXvirus DNA replication. *Traffic* **6**, 839–846 (2005).
6. Walsh, D., Mathews, M. B. & Mohr, I. Tinkering with translation: Protein synthesis in virus-infected cells. *Cold Spring Harb. Perspect. Biol.* **5**, 1–28 (2013).
7. Stern-Ginossar, N., Thompson, S. R., Mathews, M. B. & Mohr, I. Translational control in virus-infected cells. *Cold Spring Harb. Perspect. Biol.* **11**, (2019).
8. Gale, M., Tan, S.-L. & Katze, M. G. Translational Control of Viral Gene Expression in Eukaryotes. *Microbiol. Mol. Biol. Rev.* **64**, 239–280 (2000).
9. Hillman, B. I. & Cai, G. *The Family Narnaviridae. Simplest of RNA Viruses. Advances in Virus Research* vol. 86 (Copyright © 2013, Elsevier Inc. All Rights Reserved., 2013).
10. Brandes, N. & Linial, M. Giant Viruses—Big Surprises. 1–12 (2019).
11. Krammer, F. *et al.* Influenza. *Nat. Rev. Dis. Prim.* **4**, 1–21 (2018).
12. Taubenberger, J. K. & Morens, D. M. The Patology of Influenza Infections. *Annu Rev Pathol* **3**, 499–522 (2008).
13. Palese, P. & Shaw, M. *Orthomyxoviridae: The Viruses and Their Replication. Fields Virology, Volume 2*. (2001).
14. Murti, K. G. & Webster, R. G. Distribution of hemagglutinin and neuraminidase on influenza virions as revealed by immunoelectron microscopy. *Virology* **149**, 36–43 (1986).
15. Wharton, S. A., Belshe, R. B., Skehel, J. J. & Hay, A. J. Role of virion M2 protein in influenza virus uncoating: Specific reduction in the rate of membrane fusion between virus and liposomes by amantadine. *J. Gen. Virol.* **75**, 945–948 (1994).
16. Hilsch, M. *et al.* Influenza a matrix protein m1 multimerizes upon binding to lipid membranes. *Biophys. J.* **107**, 912–923 (2014).

17. Noton, S. L. *et al.* Identification of the domains of the influenza A virus M1 matrix protein required for NP binding, oligomerization and incorporation into virions. *J. Gen. Virol.* **88**, 2280–2290 (2007).

18. Hutchinson, E. & Fodor, E. Purification of influenza virions by haemadsorption and ultracentrifugation. *Protoc. Exch.* 1–7 (2014) doi:10.1038/protex.2014.027.

19. Hale, B. G., Randall, R. E., Ortin, J. & Jackson, D. The multifunctional NS1 protein of influenza A viruses. *J. Gen. Virol.* **89**, 2359–2376 (2008).

20. O'Neill, R. E., Talon, J. & Palese, P. The influenza virus NEP (NS2 protein) mediates the nuclear export of viral ribonucleoproteins. *EMBO J.* **17**, 288–296 (1998).

21. Noda, T. *et al.* Three-dimensional analysis of ribonucleoprotein complexes in influenza A virus. *Nat. Commun.* **3**, (2012).

22. Arranz, R. *et al.* The Structure of Native Influenza Virion Ribonucleoproteins. *Science (80-.).* **338**, 1634–1638 (2012).

23. Moeller, A., Kirchdoerfer, R. N., Potter, C. S., Carragher, B. & Wilson, I. A. Organization of the influenza virus replication machinery. *Science (80-.).* **338**, 1631–1634 (2012).

24. Klumpp, K., Ruigrok, R. W. H. & Baudin, F. Roles of the influenza virus polymerase and nucleoprotein in forming a functional RNP structure. *EMBO J.* **16**, 1248–1257 (1997).

25. Dias, A. *et al.* The cap-snatching endonuclease of influenza virus polymerase resides in the PA subunit. *Nature* **458**, 914–918 (2009).

26. Guilligay, D. *et al.* The structural basis for cap binding by influenza virus polymerase subunit PB2. *Nat. Struct. Mol. Biol.* **15**, 500–506 (2008).

27. Kobayashi, M., Toyoda, T. & Ishihama, A. Influenza virus PB1 protein is the minimal and essential subunit of RNA polymerase. *Arch. Virol.* 525–539 (1996).

28. Stegmann, T. Membrane fusion mechanisms: The influenza hemagglutinin paradigm and its implications for intracellular fusion. *Traffic* **1**, 598–604 (2000).

29. Eisfeld, A. J., Neumann, G. & Kawaoka, Y. At the centre: Influenza A virus ribonucleoproteins. *Nat. Rev. Microbiol.* **13**, 28–41 (2015).

30. Lukarska, M. *et al.* Structural basis of an essential interaction between influenza polymerase and Pol II CTD. *Nature* **541**, 117–121 (2017).

31. Engelhardt, O. G., Smith, M. & Fodor, E. Association of the Influenza A Virus RNA-Dependent RNA Polymerase with Cellular RNA Polymerase II. *J. Virol.* **79**, 5812–5818 (2005).

32. Plotch, S. J., Bouloy, M. & Krug, R. M. Transfer of 5’-terminal cap of globin mRNA to influenza viral complementary RNA during transcription in vitro. **76**, 1618–1622 (1979).

33. Gu, W. *et al.* Influenza A virus preferentially snatches noncoding RNA caps. *Rna* **21**, 2067–2075 (2015).

34. Sikora, D., Rocheleau, L., Brown, E. G. & Pelchat, M. Influenza A virus cap-snatches host RNAs based on their abundance early after infection. *Virology* **509**, 167–177 (2017).

35. Walker, A. P. & Fodor, E. Interplay between Influenza Virus and the Host RNA Polymerase II Transcriptional Machinery. *Trends Microbiol.* **27**, 398–407 (2019).

36. Wandzik, J. M. *et al.* A Structure-Based Model for the Complete Transcription Cycle of Influenza Polymerase. *Cell* **181**, 877-893.e21 (2020).

37. Poon, L. L. M., Pritlove, D. C., Fodor, E. & Brownlee, G. G. Direct Evidence that the Poly(A) Tail of Influenza A Virus mRNA Is Synthesized by Reiterative Copying of a U Track in the Virion RNA Template. *J. Virol.* **73**, 3473–3476 (1999).

38. Read, E. K. C. & Digard, P. Individual influenza A virus mRNAs show differential dependence on cellular NXF1/TAP for their nuclear export. *J. Gen. Virol.* **91**, 1290–1301 (2010).

39. Gales, J. P., Kubina, J., Geldreich, A. & Dimitrova, M. Strength in Diversity: Nuclear Export of Viral RNAs. *Viruses* **12**, (2020).

40. Mor, A. *et al.* Influenza virus mRNA trafficking through host nuclear speckles. *Nat. Microbiol.* **1**, (2016).

41. Jackson, R. J., Hellen, C. U. T. & Pestova, T. V. The mechanism of eukaryotic translation initiation and principles of its regulation. *Nat. Rev. Mol. Cell Biol.* **11**, 113–127 (2010).

42. Mangus, D. A., Evans, M. C. & Jacobson, A. Poly(A)-binding proteins: Multifunctional scaffolds for the post-transcriptional control of gene expression. *Genome Biol.* **4**, 1–14 (2003).

43. Miyamoto, S. *et al.* Migration of In fl uenza Virus Nucleoprotein into the Nucleolus Is Essential for Ribonucleoprotein Complex Formation.

44. Ozawa, M. *et al.* Contributions of Two Nuclear Localization Signals of Influenza A Virus Nucleoprotein to Viral Replication. *J. Virol.* **81**, 30–41 (2007).

45. Ando, T. *et al.* The host protein CLUH participates in the subnuclear transport of influenza virus ribonucleoprotein complexes. *Nat. Microbiol.* **1**, (2016).

46. Carrique, L. *et al.* Host ANP32A mediates the assembly of the influenza virus replicase. *Nature* **587**, 638–643 (2020).

47. Jorba, N., Coloma, R. & Ortín, J. Genetic trans-complementation establishes a new model for influenza virus RNA transcription and replication. *PLoS Pathog.* **5**, (2009).

48. Nilsson-Payant, B. E., tenOever, B. R. & te Velthuis, A. J. W. The host factor ANP32A is required for influenza A virus vRNA and cRNA synthesis. *J. Virol.* (2021) doi:10.1128/jvi.02092-21.

49. Baker, S. F., Ledwith, M. P. & Mehle, A. Differential Splicing of ANP32A in Birds Alters Its Ability to Stimulate RNA Synthesis by Restricted Influenza Polymerase. *Cell Rep.* **24**, 2581-2588.e4 (2018).

50. Mistryhtt, B. *et al.* Elucidating the Interactions between Influenza Virus Polymerase and Host Factor ANP32A. *J. Virol.* (2020).

51. Ye, Q., Krug, R. M. & Tao, Y. J. The mechanism by which influenza A virus nucleoprotein forms oligomers and binds RNA. *Nature* **444**, 1078–1082 (2006).

52. Turrell, L., Lyall, J. W., Tiley, L. S., Fodor, E. & Vreede, F. T. The role and assembly mechanism of nucleoprotein in influenza A virus ribonucleoprotein complexes. *Nat. Commun.* **4**, 1–11 (2013).

53. Hu, Y., Gor, V., Morikawa, K., Nagata, K. & Kawaguchi, A. Cellular splicing factor UAP56 stimulates trimeric NP formation for assembly of functional influenza viral ribonucleoprotein complexes. *Sci. Rep.* **7**, 4–10 (2017).

54. Hatakeyama, D. *et al.* Influenza A virus nucleoprotein is acetylated by histone acetyltransferases PCAF and GCN5. *J. Biol. Chem.* **293**, 7126–7138 (2018).

55. Mondal, A. *et al.* Influenza virus recruits host protein kinase C to control assembly and activity of its replication machinery. *Elife* **6**, 1–23 (2017).

56. Bui, M., Myers, J. E. & Whittaker, G. R. Nucleo-cytoplasmic localization of influenza virus nucleoprotein depends on cell density and phosphorylation. *Virus Res.* **84**, 37–44 (2002).

57. Digard, P., Elton, D., Simpson-Holley, M. & Medcalf, E. Interaction of the influenza virus nucleoprotein with F-actin. *Int. Congr. Ser.* **1219**, 503–512 (2001).

58. Li, J., Yu, M., Zheng, W. & Liu, W. Nucleocytoplasmic shuttling of influenza a virus proteins. *Viruses* **7**, 2668–2682 (2015).

59. Rialdi, A. *et al.* The RNA Exosome Syncs IAV-RNAPII Transcription to Promote Viral Ribogenesis and Infectivity. *Cell* **169**, 679-692.e14 (2017).

60. Chauhan, K., Kalam, H., Dutt, R. & Kumar, D. RNA Splicing: A New Paradigm in Host–Pathogen Interactions. *J. Mol. Biol.* **431**, 1565–1575 (2019).

61. Nagy, P. D. & Pogany, J. The dependence of viral RNA replication on co-opted host factors. *Nat. Rev. Microbiol.* **10**, 137–149 (2012).

62. Iselin, L. *et al.* Uncovering viral RNA–host cell interactions on a proteome-wide scale. *Trends Biochem. Sci.* **47**, 23–38 (2022).

63. Geisler, S. & Coller, J. RNA in unexpected places: Long non-coding RNA functions in diverse cellular contexts. *Nat. Rev. Mol. Cell Biol.* **14**, 699–712 (2013).

64. Lässer, C. Mapping Extracellular RNA Sheds Lights on Distinct Carriers. *Cell* **177**, 228–230 (2019).

65. Matera, A. G. & Wang, Z. A day in the life of the spliceosome. *Nat. Rev. Mol. Cell Biol.* **15**, 108–121 (2014).

66. Decroly, E., Ferron, F., Lescar, J. & Canard, B. Conventional and unconventional mechanisms for capping viral mRNA. *Nat. Rev. Microbiol.* **10**, 51–65 (2012).

67. Ghosh, A. & Lima, C. D. Enzymology of RNA cap synthesis. *Wiley Interdiscip. Rev. RNA* **1**, 152–172 (2010).

68. Hyde, J. L. & Diamond, M. S. Innate immune restriction and antagonism of viral RNA lacking 2'-O methylation. *Virology* 66–74 (2015).

69. Hocine, S., Singer, R. H. & Grünwald, D. RNA processing and export. *Cold Spring Harb. Perspect. Biol.* **2**, 1–20 (2010).

70. Huang, X. *et al.* An NS-segment exonic splicing enhancer regulates influenza A virus replication in mammalian cells. *Nat. Commun.* **8**, (2017).

71. Dubois, J., Terrier, O. & Rosa-Calatrava, M. Influenza viruses and mRNA splicing: Doing more with less. *MBio* **5**, (2014).

72. Thompson, M. G. *et al.* Viral-induced alternative splicing of host genes promotes influenza replication. *Elife* **9**, 1–20 (2020).

73. Colgan, D. F. & Manley, J. L. Mechanism and regulation of mRNA polyadenylation. *Genes Dev.* **11**, 2755–2766 (1997).

74. Nemeroff, M. E., Barabino, S. M. L., Li, Y., Keller, W. & Krug, R. M. Influenza virus NS1 protein interacts with the cellular 30 kDa subunit of CPSF and inhibits 3′ end formation of cellular pre-mRNAs. *Mol. Cell* **1**, 991–1000 (1998).

75. Adomavicius, T. *et al.* The structural basis of translational control by eIF2 phosphorylation. *Nat. Commun.* **10**, (2019).

76. Gebauer, F. & Hentze, M. W. Molecular mechanisms of translational control. *Nat. Rev. Mol. Cell Biol.* **5**, 827–835 (2004).

77. Gobet, C. *et al.* Robust landscapes of ribosome dwell times and aminoacyl-tRNAs in response to nutrient stress in liver. *Proc. Natl. Acad. Sci. U. S. A.* **117**, 9630–9641 (2020).

78. Smith, B. L., Chen, G., Wilke, C. O. & Krug, R. M. Avian influenza virus PB1 gene in H3N2 viruses evolved in humans to reduce interferon inhibition by skewing codon usage toward interferon-altered tRNA pools. *MBio* **9**, 1–14 (2018).

79. Collart, M. A. & Weiss, B. Ribosome pausing, a dangerous necessity for co-translational events. *Nucleic Acids Res.* **48**, 1043–1055 (2021).

80. Kellogg, M. K., Miller, S. C., Tikhonova, E. B. & Karamyshev, A. L. Srpassing co-translational targeting: The role of the signal recognition particle in protein targeting and mrna protection. *Int. J. Mol. Sci.* **22**, (2021).

81. Doma, M. K. & Parker, R. Endonucleolytic cleavage of eukaryotic mRNAs with stalls in translation elongation. *Nature* **440**, 561–564 (2006).

82. Juszkiewicz, S. & Hegde, R. S. Initiation of Quality Control during Poly(A) Translation Requires Site-Specific Ribosome Ubiquitination. *Mol. Cell* **65**, 743-750.e4 (2017).

83. Garneau, N. L., Wilusz, J. & Wilusz, C. J. The highways and byways of mRNA decay. *Nat. Rev. Mol. Cell Biol.* **8**, 113–126 (2007).

84. Sarkar, B., Xi, Q., He, C. & Schneider, R. J. Selective Degradation of AU-Rich mRNAs Promoted by the p37 AUF1 Protein Isoform. *Mol. Cell. Biol.* **23**, 6685–6693 (2003).

85. Khabar, K. S. A. Post-transcriptional control during chronic inflammation and cancer: A focus on AU-rich elements. *Cell. Mol. Life Sci.* **67**, 2937–2955 (2010).

86. Winzen, R. *et al.* Functional Analysis of KSRP Interaction with the AU-Rich Element of Interleukin-8 and Identification of Inflammatory mRNA Targets. *Mol. Cell. Biol.* **27**, 8388–8400 (2007).

87. Lal, A. *et al.* Concurrent versus individual binding of HuR and AUF1 to common labile target mRNAs. *EMBO J.* **23**, 3092–3102 (2004).

88. Ma, W. J., Chung, S. & Furneaux, H. The Elav-like proteins bind to AU-rich elements and to the poly(A) tail of mRNA. *Nucleic Acids Res.* **25**, 3564–3569 (1997).

89. Singh, G., Pratt, G., Yeo, G. W. & Moore, M. J. The clothes make the mRNA: Past and present trends in mRNP fashion. *Annu. Rev. Biochem.* **84**, 325–354 (2015).

90. Ferhadian, D. *et al.* Structural and functional motifs in influenza virus RNAs. *Front. Microbiol.* **9**, 1–11 (2018).

91. Palazzo, A. F. & Lee, E. S. Non-coding RNA: What is functional and what is junk? *Front. Genet.* **5**, 1–11 (2015).

92. Nazar, R. N. Ribosomal RNA processing and ribosome biogenesis in eukaryotes. *IUBMB Life* **56**, 457–465 (2004).

93. Hopper, A. K. & Phizicky, E. M. tRNA transfers to the limelight. *Genes Dev.* **17**, 162–180 (2003).

94. Tomita, K. & Liu, Y. Human BCDIN3D is a cytoplasmic tRNAHis-specific 5'-monophosphate methyltransferase. *Front. Genet.* **9**, 1–6 (2018).

95. Busch, H., Ramachandra, R., Rothblum, L. & YC, C. SnRNAs, SnRNPs, and RNA processing. *Annu. Rev. Biochem.* (1982).

96. Kufel, J. & Grzechnik, P. Small Nucleolar RNAs Tell a Different Tale. *Trends Genet.* **35**, 104–117 (2019).

97. Shukla, G. C., Singh, J. & Barik, S. MicroRNAs: Processing, maturation, target recognition and regulatory functions. *Mol. Cell. Pharmacol.* **3**, 83–92 (2011).

98. Kulaberoglu, Y. *et al.* RNA Polymerase III, Ageing and Longevity. *Front. Genet.* **12**, 1–7 (2021).

99. Jeronimo, C. *et al.* Systematic Analysis of the Protein Interaction Network for the Human Transcription Machinery Reveals the Identity of the 7SK Capping Enzyme. *Mol. Cell* **27**, 262–274 (2007).

100. Kowalski, M. P. & Krude, T. Functional roles of non-coding Y RNAs. *Int. J. Biochem. Cell Biol.* **66**, 20–29 (2015).

101. Hahne, J. C., Lampis, A. & Valeri, N. Vault RNAs: hidden gems in RNA and protein regulation. *Cell. Mol. Life Sci.* **78**, 1487–1499 (2021).

102. Choi, J. H. & Sullivan, C. S. DUSP11 and triphosphate RNA balance during virus infection. *PLoS Pathog.* **17**, 1–7 (2021).

103. Perez, J. T. *et al.* Influenza A virus-generated small RNAs regulate the switch from transcription to replication. *Proc. Natl. Acad. Sci. U. S. A.* **107**, 11525–11530 (2010).

104. te Velthuis, A. J. W. *et al.* Mini viral RNAs act as innate immune agonists during influenza virus infection. *Nat. Microbiol.* **3**, 1234–1242 (2018).

105. Dimmock, N. J. & Easton, A. J. Defective Interfering Influenza Virus RNAs: Time To Reevaluate Their Clinical Potential as Broad-Spectrum Antivirals? *J. Virol.* **88**, 5217–5227 (2014).

106. Hutchinson, E. C., von Kirchbach, J. C., Gog, J. R. & Digard, P. Genome packaging in influenza A virus. *J. Gen. Virol.* **91**, 313–328 (2010).

107. von Magnus, P. Incomplete Forms of Influenza Virus. *Adv. Virus Res.* **2**, 59–79 (1954).

108. Genoyer, E. & López, C. B. The Impact of Defective Viruses on Infection and Immunity. *Annu. Rev. Virol.* **6**, 547–566 (2019).

109. Mendes, M. & Russell, A. B. *Library-based analysis reveals segment and length dependent characteristics of defective influenza genomes*. *PLOS Pathogens* vol. 17 (2021).

110. Elshina, E. & te Velthuis, A. J. W. The influenza virus RNA polymerase as an innate immune agonist and antagonist. *Cell. Mol. Life Sci.* **78**, 7237–7256 (2021).

111. Vachon, V. K. & Conn, G. L. Adenovirus VA RNA: An essential pro-viral non-coding RNA. *Virus Res.* **212**, 39–52 (2016).

112. Rossetto, C. C. & Pari, G. S. PAN's labyrinth: Molecular biology of kaposi's sarcoma-associated herpesvirus (KSHV) PAN RNA, a multifunctional long noncoding RNA. *Viruses* **6**, 4212–4226 (2014).

113. Withers, J. B. *et al.* Idiosyncrasies of Viral Noncoding RNAs Provide Insights into Host Cell Biology. *Annu. Rev. Virol.* **6**, 297–317 (2019).

114. Chapman, E. G., Moon, S. L., Wilusz, J. & Kieft, J. S. RNA structures that resist degradation by Xrn1 produce a pathogenic dengue virus RNA. *Elife* **2014**, 1–25 (2014).

115. Lee, H., Zhang, Z. & Krause, H. M. Long Noncoding RNAs and Repetitive Elements: Junk or Intimate Evolutionary Partners? *Trends Genet.* **35**, 892–902 (2019).

116. Jensen, S. & Thomsen, A. R. Sensing of RNA Viruses: a Review of Innate Immune Receptors Involved in Recognizing RNA Virus Invasion. *J. Virol.* **86**, 2900–2910 (2012).

117. Schoggins, J. W. Interferon-Stimulated Genes: What Do They All Do? *Annu. Rev. Virol.* **6**, 567–584 (2019).

118. Schoggins, J. W. & Rice, C. M. Interferon-stimulated genes and their antiviral effector functions. *Curr. Opin. Virol.* **1**, 519–25 (2011).

119. Simmonds, P., Aiewsakun, P. & Katzourakis, A. Prisoners of war — host adaptation and its constraints on virus evolution. *Nat. Rev. Microbiol.* **17**, 321–328 (2019).

120. Bitzegeio, J., Sampias, M., Bieniasz, P. D. & Hatziioannou, T. Adaptation to the Interferon-Induced Antiviral State by Human and Simian Immunodeficiency Viruses. *J. Virol.* **87**, 3549–3560 (2013).

121. Mitchell, P. S. *et al.* Evolution-guided identification of antiviral specificity determinants in the broadly acting interferon-induced innate immunity factor MxA. *Cell Host Microbe* **12**, 598–604 (2012).

122. Leeks, A., West, S. A. & Ghoul, M. The evolution of cheating in viruses. *Nat. Commun.* **12**, 1–14 (2021).

123. Hansen, J. D., Vojtech, L. N. & Laing, K. J. Sensing disease and danger: A survey of vertebrate PRRs and their origins. *Dev. Comp. Immunol.* **35**, 886–897 (2011).

124. Dempsey, A. & Bowie, A. G. Innate immune recognition of DNA: A recent history. *Virology* **479**–**480**, 146–152 (2015).

125. Liu, G. Q. & Gack, M. U. Distinct and Orchestrated Functions of RNA Sensors in Innate Immunity. *Immunity* **53**, 26–42 (2020).

126. Yang, Z. *et al.* Crystal structure of ISG54 reveals a novel RNA binding structure and potential functional mechanisms. *Cell Res.* **22**, 1328–1338 (2012).

127. Diamond, M. S. & Farzan, M. The broad-spectrum antiviral functions of IFIT and IFITM proteins. *Nat. Rev. Immunol.* **13**, 46–57 (2012).

128. Katibah, G. E. *et al.* Broad and adaptable RNA structure recognition by the human interferon-induced tetratricopeptide repeat protein IFIT5. *Proc. Natl. Acad. Sci. U. S. A.* **111**, 12025–30 (2014).

129. Abbas, Y. M., Theres, B., Martínez-montero, S., Cencic, R. & Habjan, M. Structure of human IFIT1 with capped RNA reveals adaptable mRNA binding and mechanisms for. (2017) doi:10.1073/pnas.1612444114.

130. Hyde, J. L. & Diamond, M. S. Innate immune restriction and antagonism of viral RNA lacking 2 ’ -O methylation. *Virology* **479**–**480**, 66–74 (2015).

131. Habjan, M. *et al.* Sequestration by IFIT1 Impairs Translation of 2 9 O-unmethylated Capped RNA. **9**, (2013).

132. Terenzi, F., Hui, D. J., Merrick, W. C. & Sen, G. C. Distinct Induction Patterns and Functions of Two Closely Related Interferon-inducible Human Genes , ISG54 and ISG56 *. **281**, 34064–34071 (2006).

133. Choi, U. Y. un., Kang, J. S., Hwang, Y. S. ahn. & Kim, Y. J. Oligoadenylate synthase-like (OASL) proteins: dual functions and associations with diseases. *Exp. Mol. Med.* **47**, e144 (2015).

134. Muazzam Nasrullah 2018. RNA regulation of the antiviral protein 2’−5’-oligoadenylate synthetase (OAS). *Physiol. Behav.* **176**, 139–148 (2016).

135. Schwartz, S. L. *et al.* Human OAS1 activation is highly dependent on both RNA sequence and context of activating RNA motifs. *Nucleic Acids Res.* **48**, 7520–7531 (2020).

136. Koul, A. *et al.* Impact of double-stranded RNA characteristics on the activation of human 2'–5'-oligoadenylate synthetase 2 (OAS2). *Biochem. Cell Biol.* **98**, 70–82 (2020).

137. Donovan, J., Whitney, G., Rath, S. & Korennykh, A. Structural mechanism of sensing long dsRNA via a noncatalytic domain in human oligoadenylate synthetase 3. *Proc. Natl. Acad. Sci. U. S. A.* **112**, 3949–3954 (2015).

138. Zhang, F. *et al.* Binding of Double-stranded RNA to Protein Kinase PKR is Required for Dimerization and Promotes Critical Autophosphorylation Events in the Activation Loop. *J. Biol. Chem.* **276**, 24946–24958 (2001).

139. Lemaire, P. A., Anderson, E., Lary, J. & Cole, J. L. Mechanism of PKR Activation by dsRNA. doi:10.1016/j.jmb.2008.05.056.

140. Mayo, C. B. & Cole, J. L. Interaction of PKR with single-stranded RNA. *Sci. Rep.* **7**, 1–9 (2017).

141. Kim, Y. *et al.* PKR is activated by cellular dsRNAs during mitosis and acts as a mitotic regulator. *Genes Dev.* **28**, 1310–1322 (2014).

142. Osama, A. Y. *et al.* Potential role for snoRNAs in PKR activation during metabolic stress. *Proc. Natl. Acad. Sci. U. S. A.* **112**, 5023–5028 (2015).

143. Rehwinkel, J. & Gack, M. U. RIG-I-like receptors: their regulation and roles in RNA sensing. *Nat. Rev. Immunol.* **20**, 537–551 (2020).

144. Bruns, A. M., Leser, G. P., Lamb, R. A. & Horvath, C. M. The Innate Immune Sensor LGP2 Activates Antiviral Signaling by Regulating MDA5-RNA Interaction and Filament Assembly. *Mol. Cell* **55**, 771–781 (2014).

145. Satoh, T. *et al.* LGP2 is a positive regulator of RIG-I- and MDA5-mediated antiviral responses. *Proc. Natl. Acad. Sci. U. S. A.* **107**, 1512–1517 (2010).

146. Uchikawa, E. *et al.* Structural Analysis of dsRNA Binding to Anti-viral Pattern Recognition Receptors LGP2 and MDA5. *Mol. Cell* **62**, 586–602 (2016).

147. Kato, H. *et al.* Length-dependent recognition of double-stranded ribonucleic acids by retinoic acid-inducible gene-I and melanoma differentiation-associated gene 5. *J. Exp. Med.* **205**, 1601–1610 (2008).

148. Feng, Q. *et al.* MDA5 Detects the Double-Stranded RNA Replicative Form in Picornavirus-Infected Cells. *Cell Rep.* **2**, 1187–1196 (2012).

149. Liddicoat, B. J. *et al.* RNA editing by ADAR1 prevents MDA5 sensing of endogenous dsRNA as nonself. *Science (80-.).* **349**, 1115–1120 (2015).

150. Schlee, M. *et al.* Recognition of 5′ Triphosphate by RIG-I Helicase Requires Short Blunt Double-Stranded RNA as Contained in Panhandle of Negative-Strand Virus. *Immunity* **31**, 25–34 (2009).

151. Luo, D. *et al.* Structural insights into RNA recognition by RIG-I. *Cell* **147**, 409–422 (2011).

152. Kowalinski, E. *et al.* Structural basis for the activation of innate immune pattern-recognition receptor RIG-I by viral RNA. *Cell* **147**, 423–435 (2011).

153. Jiang, F. *et al.* Structural basis of RNA recognition and activation by innate immune receptor RIG-I. *Nature* **479**, 423–427 (2011).

154. Baum, A., Sachidanandam, R. & García-Sastre, A. Preference of RIG-I for short viral RNA molecules in infected cells revealed by next-generation sequencing. *Proc. Natl. Acad. Sci. U. S. A.* **108**, 3092 (2011).

155. Chiang, J. J. *et al.* Viral unmasking of cellular 5S rRNA pseudogene transcripts induces RIG-I-mediated immunity article. *Nat. Immunol.* **19**, 53–62 (2018).

156. Zhao, Y., Ye, X., Dunker, W., Song, Y. & Karijolich, J. RIG-I like receptor sensing of host RNAs facilitates the cell-intrinsic immune response to KSHV infection. *Nat. Commun.* **9**, 1–14 (2018).

157. Vabret, N. *et al.* Y-RNAs lead an endogenous program of RIG-I agonism mobilized upon RNA virus infection and targeted by HIV. *bioRxiv* (2019) doi:10.1101/773820.

158. Wu, B. *et al.* Structural basis for dsRNA recognition, filament formation, and antiviral signal activation by MDA5. *Cell* **152**, 276–289 (2013).

159. Peisley, A. *et al.* Kinetic mechanism for viral dsRNA length discrimination by MDA5 filaments. *Proc. Natl. Acad. Sci. U. S. A.* **109**, (2012).

160. Louber, J., Brunel, J., Uchikawa, E., Cusack, S. & Gerlier, D. Kinetic discrimination of self/non-self RNA by the ATPase activity of RIG-I and MDA5. *BMC Biol.* **13**, 11–14 (2015).

161. Devarkar, S. C., Schweibenz, B., Wang, C., Marcotrigiano, J. & Patel, S. S. RIG-I Uses an ATPase-Powered Translocation-Throttling Mechanism for Kinetic Proofreading of RNAs and Oligomerization. *Mol. Cell* **72**, 355-368.e4 (2018).

162. Kolakofsky, D., Kowalinski, E. & Cusack, S. A structure-based model of RIG-I activation. *Rna* **18**, 2118–2127 (2012).

163. Peisley, A., Wu, B., Xu, H., Chen, Z. J. & Hur, S. Structural basis for ubiquitin-mediated antiviral signal activation by RIG-I. *Nature* **508**, 110–114 (2014).

164. Gack, M. U. *et al.* TRIM25 RING-finger E3 ubiquitin ligase is essential for RIG-I-mediated antiviral activity. *Nature* **446**, 916–920 (2007).

165. Iwanaszko, M. & Kimmel, M. NF-KB and IRF pathways: Cross-regulation on target genes promoter level. *BMC Genomics* **16**, 1–8 (2015).

166. Andrilenas, K. K. *et al.* DNA-binding landscape of IRF3, IRF5 and IRF7 dimers: Implications for dimer-specific gene regulation. *Nucleic Acids Res.* **46**, 2509–2520 (2018).

167. Mulero, M. C., Wang, V. Y. F., Huxford, T. & Ghosh, G. Genome reading by the NF-κB transcription factors. *Nucleic Acids Res.* **47**, 9967–9989 (2019).

168. Savan, R. Post-transcriptional regulation of interferons and their signaling pathways. *J. Interf. Cytokine Res.* **34**, 318–329 (2014).

169. Rothamel, K. *et al.* ELAVL1 primarily couples mRNA stability with the 3′ UTRs of interferon-stimulated genes. *Cell Rep.* **35**, 109178 (2021).

170. Gillis, P. & Malter, J. S. The adenosine-uridine binding factor recognizes the AU-rich elements of cytokine, lymphokine, and oncogene mRNAs. *J. Biol. Chem.* **266**, 3172–3177 (1991).

171. Takata, M. A. *et al.* CG dinucleotide suppression enables antiviral defence targeting non-self RNA. *Nature* **550**, 124–127 (2017).

172. Schwerk, J. *et al.* RNA-binding protein isoforms ZAP-S and ZAP-L have distinct antiviral and immune resolution functions. *Nat. Immunol.* **20**, 1610–1620 (2019).

173. Hsu, A. C. Y. Influenza virus: A master tactician in innate immune evasion and novel therapeutic interventions. *Front. Immunol.* **9**, 1–11 (2018).

174. Du, Y. *et al.* Genome-wide identification of interferon-sensitive mutations enables influenza vaccine design. *Science (80-.).* **359**, 290–296 (2018).

175. Russell, A. B., Trapnell, C. & Bloom, J. D. Extreme heterogeneity of influenza virus infection in single cells. *Elife* **7**, 1–26 (2018).

176. Abbas, Y. M., Pichlmair, A., Górna, M. W., Superti-Furga, G. & Nagar, B. Structural basis for viral 5′-PPP-RNA recognition by human IFIT proteins. *Nature* **494**, 60–64 (2013).

177. Pichlmair, A. *et al.* IFIT1 is an antiviral protein that recognizes 5 ′ -triphosphate RNA. *Nat. Publ. Gr.* **12**, 624–630 (2011).

178. Pinto, A. K. *et al.* Human and Murine IFIT1 Proteins Do Not Restrict Infection of Negative-Sense RNA Viruses of the Orthomyxoviridae, Bunyaviridae, and Filoviridae Families. *J. Virol.* **89**, 9465–9476 (2015).

179. Min, J. Y. & Krug, R. M. The primary function of RNA binding by the influenza A virus NS1 protein in infected cells: Inhibiting the 2′-5′ oligo (A) synthetase/RNase L pathway. *Proc. Natl. Acad. Sci. U. S. A.* **103**, 7100–7105 (2006).

180. Bergmann, M. *et al.* Influenza Virus NS1 Protein Counteracts PKR-Mediated Inhibition of Replication. *J. Virol.* **74**, 6203–6206 (2000).

181. Malathi, K., Dong, B., Gale, M. & Silverman, R. H. Small self-RNA generated by RNase L amplifies antiviral innate immunity. *Nature* **448**, 816–819 (2007).

182. Min, J. Y., Li, S., Sen, G. C. & Krug, R. M. A site on the influenza A virus NS1 protein mediates both inhibition of PKR activation and temporal regulation of viral RNA synthesis. *Virology* **363**, 236–243 (2007).

183. Zhang, L. *et al.* Influenza Virus NS1 Protein-RNA Interactome Reveals Intron Targeting. *J. Virol.* **92**, 1–16 (2018).

184. Varga, Z. T., Grant, A., Manicassamy, B. & Palese, P. Influenza Virus Protein PB1-F2 Inhibits the Induction of Type I Interferon by Binding to MAVS and Decreasing Mitochondrial Membrane Potential. *J. Virol.* **86**, 8359–8366 (2012).

185. Graef, K. M. *et al.* The PB2 Subunit of the Influenza Virus RNA Polymerase Affects Virulence by Interacting with the Mitochondrial Antiviral Signaling Protein and Inhibiting Expression of Beta Interferon. *J. Virol.* **84**, 8433–8445 (2010).

186. Wang, R. *et al.* Influenza M2 protein regulates MAVS-mediated signaling pathway through interacting with MAVS and increasing ROS production. *Autophagy* **15**, 1163–1181 (2019).

187. Yi, C. *et al.* Influenza A virus PA antagonizes interferon-β by interacting with interferon regulatory factor 3. *Front. Immunol.* **8**, (2017).

188. Mibayashi, M. *et al.* Inhibition of Retinoic Acid-Inducible Gene I-Mediated Induction of Beta Interferon by the NS1 Protein of Influenza A Virus. *J. Virol.* **81**, 514–524 (2007).

189. Jureka, A. S., Kleinpeter, A. B., Tipper, J. L., Harrod, K. S. & Petit, C. M. The influenza NS1 protein modulates RIG-I activation via a strain-specific direct interaction with the second CARD of RIG-I. *J. Biol. Chem.* **295**, 1153–1164 (2020).

190. Gack, M. U. *et al.* Influenza A Virus NS1 Targets the Ubiquitin Ligase TRIM25 to Evade Recognition by the Host Viral RNA Sensor RIG-I. *Cell Host Microbe* **5**, 439–449 (2009).

191. Tseng, Y. Y. *et al.* Interaction between ns1 and cellular mavs contributes to ns1 mitochondria targeting. *Viruses* **13**, (2021).

192. Pichlmair, A. *et al.* RIG-I-mediated antiviral responses to single-stranded RNA bearing 5′-phosphates. *Science (80-.).* **314**, 997–1001 (2006).

CHAPTER 2
Influenza virus repurposes the antiviral protein IFIT2 to promote translation of viral mRNAs

Published as:
Vy Tran[1]*, Mitchell P. Ledwith[1]*, Thiprampai Thamamongood[2,3,4,5], Christina A. Higgins[1], Shashank Tripathi[6,7], Max W. Chang[8], Christopher Benner[8], Adolfo García-Sastre[6,7,9], Martin Schwemmle[2,3], Adrianus C. M. Boon[10], Michael S. Diamond[10] & Andrew Mehle[1] Influenza virus repurposes the antiviral protein IFIT2 to promote translation of viral mRNAs. Nat Microbiol 5, 1490–1503 (2020). https://doi.org/10.1038/s41564-020-0778-x

*these author contributed equally

1. Medical Microbiology and Immunology, University of Wisconsin Madison, Madison, WI, USA.
2. Institute of Virology, Medical Center, University of Freiburg, Freiburg, Germany.
3. Faculty of Medicine, University of Freiburg, Freiburg, Germany.
4. Spemann Graduate School of Biology and Medicine, University of Freiburg, Freiburg, Germany.
5. Faculty of Biology, University of Freiburg, Freiburg, Germany.
6. Department of Microbiology, Icahn School of Medicine at Mount Sinai, New York, NY, USA.
7. Global Health and Emerging Pathogens Institute, Icahn School of Medicine at Mount Sinai, New York, NY, USA.
8. Department of Medicine, University of California, San Diego, San Diego, CA, USA.
9. Department of Medicine, Division of Infectious Diseases, Icahn School of Medicine at Mount Sinai, New York, NY, USA.
10. Departments of Medicine, Molecular Microbiology, and Pathology & Immunology, Washington University School of Medicine, St. Louis, MO, USA.

Author Contributions:
M.P.L generated:
Figures 3A-E, 4, 5A-E, Ext.2D-E, Ext.4, Ext.5A-B, Ext.6A-D, Ext.7, S.Tables3-6
A.M. wrote the manuscript with editing and drafting by V.T. and M.P.L.

ABSTRACT

Cells infected by influenza virus mount a large-scale antiviral response and most cells ultimately initiate cell-death pathways in an attempt to suppress viral replication. We performed a CRISPR/Cas9-knockout selection designed to identify host factors required for replication following viral entry. We identified a large class of presumptive antiviral factors that unexpectedly act as important pro-viral enhancers during influenza virus infection. One of these, IFIT2, is an interferon-stimulated gene with well-established antiviral activity but limited mechanistic understanding. As opposed to suppressing infection, we show here that IFIT2 is instead repurposed by influenza virus to promote viral gene expression. CLIP seq demonstrated that IFIT2 binds directly to viral and cellular mRNAs in AU rich regions, with bound cellular transcripts enriched in interferon stimulated mRNAs. Polysome and ribosome profiling revealed that IFIT2 prevents ribosome pausing on bound mRNAs. Together, the data link IFIT2 binding to enhanced translational efficiency for viral and cellular mRNAs and ultimately viral replication. Our findings establish a model for the normal function of IFIT2 as a protein that increases translation of cellular mRNAs to support antiviral responses and explain how influenza virus uses this same activity to redirect a classically antiviral protein into a pro-viral effector.

Introduction

Cells express factors that selectively target and inhibit proteins and nucleic acids from invading pathogens[1,2]. Simultaneously, pathogens neutralize these inhibitors and co-opt other cellular factors for their own replication. The balance between these opposing forces influences the outcome of an infection and the course of disease.

Influenza virus is a serious public health threat causing significant morbidity and mortality. Humans are under continual assault by seasonal influenza virus outbreaks as well as sporadic pandemics with the potential for widespread infection and disease[3,4]. Like all viruses, influenza virus exploits, and in some cases subverts, cellular proteins and pathways to promote replication. These physical and genetic interactions have significant impacts on virus replication, innate antiviral responses and pathology. Moreover, the ability of influenza virus to productively engage the intracellular environment determines its host range and potential to transmit and cause disease in humans[5].

Genome-wide knockout screens have provided a global view of the interface between influenza virus and its host[6–10]. Despite the success of these approaches, technical and biological limitations have created a strong bias toward steps involved in viral entry. Here we perform a screen to specifically query the post-entry role of pro-viral host factors during influenza virus infection. Counter to expectation, our screen revealed that several innate anti-viral factors, especially IFIT2, enhanced influenza virus replication. Mechanistic studies showed that IFIT2 binds viral and host mRNAs and prevents ribosome pausing. This increases the translational efficiency of IFIT2-bound mRNAs, enhancing viral gene expression and replication. The combination of unbiased screening and mechanistic studies identified the process by which influenza virus hijacks IFIT2 to maximize replication, while also revealing how IFIT2 functions as part of the innate immune response.z

RESULTS

To identify cellular regulators of viral replication, we performed a genome-wide CRISPR-knockout selection (Fig. 1A, Extended Data Fig. 1A-C). Pooled gene-edited human A549 lung cells were challenged with influenza A virus (IAV) and surviving cells were isolated through sequential rounds of selection. Results from prior virus:host interaction screens identified key cellular co-factors, but also demonstrated a bias towards the entry process[6–9]. We therefore performed our selection with a IAV-G, a replication-competent influenza virus based on the A/WSN/1933 strain (H1N1; WSN) that is stably pseudotyped with the vesicular stomatitis virus glycoprotein (VSV-G) that bypasses this technical bottleneck[11]. Surviving cells were either re-challenged with IAV-G or were counter-selected with *bona fide* influenza virus. Both selection schemes enriched for cells with mutations in the genes coding for IFIT2 (interferon-induced protein with tetratricopeptide repeats 2) and IFIT3 (Fig. 1B, Supplementary Table 1). A separate selection was performed with an independently generated gene-edited pool of A549 cells. Cells were challenged with a different strain of IAV encoding GFP based on A/seal/Massachusetts/1-SC35M/1980 (SC35M Flu-GFP). IFIT2 and IFIT3 gene-edited cells were again among the most enriched cells in this selection (Fig. 1C, Supplementary Table 2). Thus, independent selections using different viruses showed that surviving cells were highly enriched for mutations in IFIT2 and IFIT3 (Extended Data Fig. 1D-G).

IFITs are a family of proteins in humans (e.g. IFIT1, 2, 3 and 5) that are induced following type I interferon (IFN) treatment or pattern recognition receptor activation[12,13]. IFITs exert antiviral activity against a diverse collection of RNA and DNA viruses, although this activity varies depending on the virus, IFIT paralog, and the species of origin[14–22]; the molecular functions of IFIT2 are largely undefined. Thus, it was unexpected that our selection, which was designed to identify cellular factors necessary for influenza virus replication, instead identified

IFN-stimulated genes (ISGs) with established antiviral activity for other viruses.

To validate the results of our selection, we evaluated the effects of IFIT2 on IAV replication. Multi-step IAV (WSN) replication was reduced by 1- to 2-$\log_{10}$ in two independently generated human *IFIT2* knockout cell lines (Fig. 1D, Extended Data Fig. 2A). Similar results were obtained in mouse *Ifit2* knockout embryo fibroblasts. Consistent with its role as an ISG, IFIT2 was largely undetectable in uninfected cells and upregulated upon infection. Knockout of IFIT2 or Ifit2 also conferred survival to cells challenged by diverse influenza viruses, including multiple IAV primary isolates, IAV-G, and influenza B virus (IBV) (Fig. 1E, Extended Data Fig. 2B). This phenotype was not a generic response, as knockout cells remained sensitive to infection and virally mediated cell death when infected with VSV (Fig. 1E). Additionally, we validated the role IFIT3 during IAV infection. Loss of IFIT3 also reduced IAV replication, although the magnitude was less than with loss of IFIT2 (Extended Data Fig. 2F-H). By contrast, loss of IFIT1 does not affect influenza virus replication[21]. The appearance of *IFIT1* as a lower-confidence candidate in our screens could result from the ability of IFIT1, 2 and 3 to form hetero-oligomers and modulate each other's activities[15,23–25].

Cells lacking IFIT2 survive challenge by viruses encoding native HA or pseudotyped with VSV-G, suggesting that the phenotype is independent of the influenza entry process (Fig. 1B and 1E). Given that IFIT2 is rapidly induced upon IAV infection (Extended Data Fig. 2C and [26]), we used highly sensitive reporter viruses to query primary transcription at early times post-inoculation and subsequent gene expression throughout infection[27,28]. Human A549 and 293 *IFIT2*$^{-/-}$ cell lines displayed ~50% decrease in viral gene expression beginning 2 hpi and continuing through 24 hpi (Fig. 2A, Extended Data Fig. 2D).

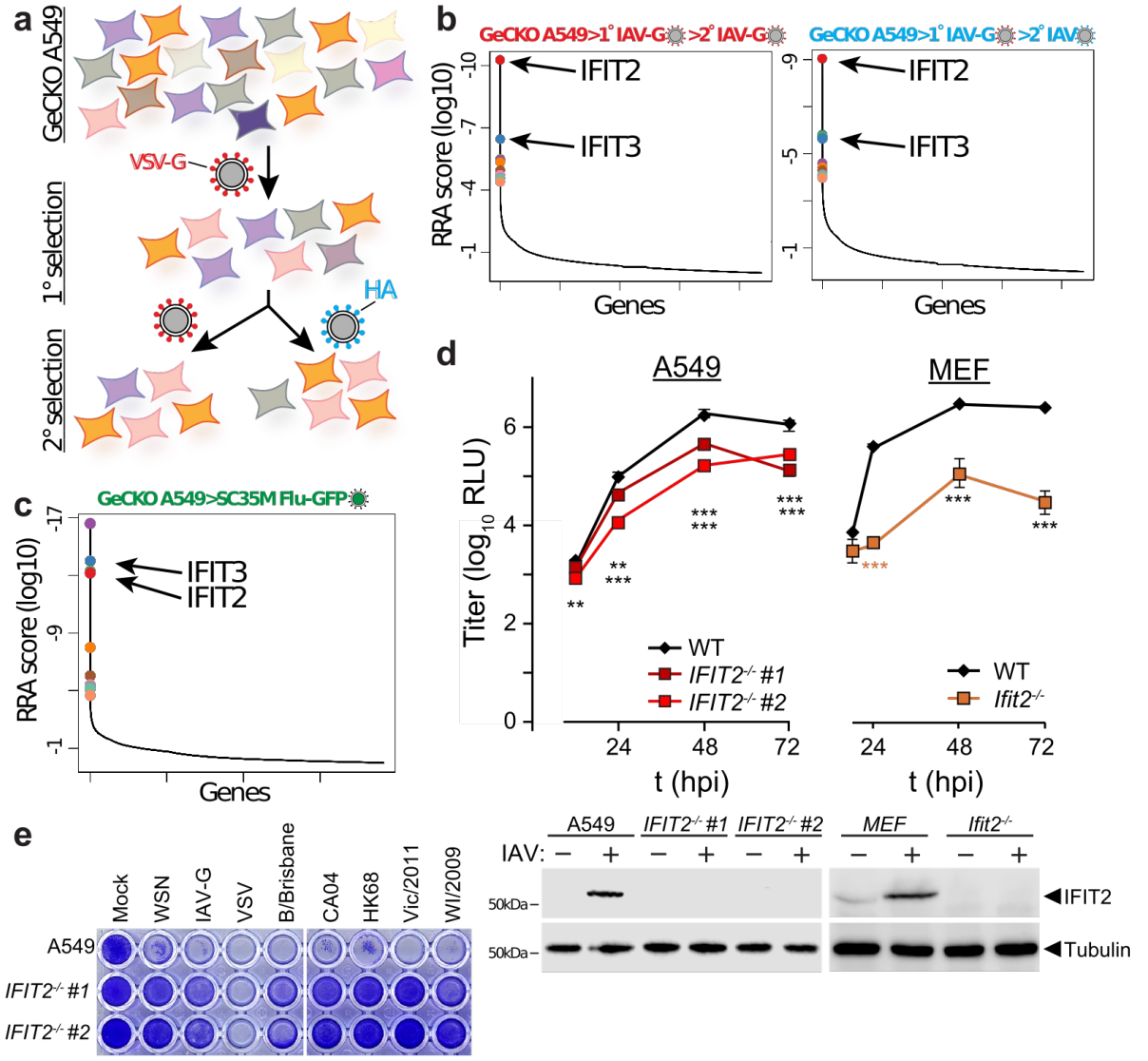

Figure 1. A CRISPR knockout screen identifies the antiviral roteins IFIT2 and IFIT3 as pro-viral regulators of influenza virus infection. **a,** Schematic of the genome-scale CRISPR knock-out (GeCKO) screen designed to specifically query host factors important for influenza virus infection after viral entry. **b-c,** MAGeCK (Model-based genome wide knock out)[52] analysis for selection schemes involving sequential IAV-G selections (b**,** left), IAV-G followed by WSN (**b,** right), or seven rounds with SC35M Flu-GFP (c). **d,** Multicycle replication kinetics of WSN in wild-type or knockout cells. Western blotting confirmed loss of IFIT2 in two independent clonal human A549 cell lines and loss of Ifit2 in mouse embryo fibroblasts. Data are mean of n = 3 independent infections ± sd. (** $p < 0.01$, *** $p < 0.001$ when compared to WT; one-way ANOVA with *post hoc* Tukey's HSD for multiple comparisons or a two-tailed Student's t-test). **e**, Viability of parental or *IFIT2* knockout A549 cells following challenge with diverse primary influenza isolates and VSV. VSV-G; vesicular stomatitis virus glycoprotein. IAV; influenza A virus. IAV-G; IAV stably encoding VSV-G. SC35M; A/seal/Mass/1-SC35M/1980. WSN; A/WSN/1933. B/Brisbane; B/Brisbane/60/2008. CA04; A/California/04/2009. HK68; A/Hong Kong/1/1968. Vic/2011; A/Victoria/361/2011. WI/2009; A/Wisconsin/15/2009.

Similar trends were obtained in mouse *Ifit2*$^{-/-}$ cells infected with reporter viruses based on WSN, the primary IAV isolate from the 2009 pandemic (CA04), or a primary IBV isolate (B/Brisbane) (Fig. 2B). *IFIT3*$^{-/-}$ cell lines also exhibit defects in gene expression (Extended Data Fig. 2I).

Defects in viral gene expression in seven independently generated knockout lines from three different cell types strongly implicate mutations in the *IFIT2* or *Ifit2* loci as opposed to background effects or off-target edits (Fig. 2A-B, Extended Data Fig. 2D). To confirm the pro-viral role of IFIT2, we transiently complemented knockout cells. Ectopic expression of IFIT2 in MEFs or 293 cells more than doubled viral gene expression in the knockout cells, but exhibited modest enhancement in WT cells (Fig. 2C, Extended Data Fig. 2E). IFIT2 binds model RNAs *in vitro*[29], although the RNAs bound by IFIT2 in cells are not known. To determine if RNA binding was important for the pro-viral function of IFIT2, cells were complemented with an RNA-binding IFIT2 mutant (R292E/K410E, IFIT2ΔRNA)[29]. The enhanced gene expression detected in cells complemented with IFIT2 was lost in cells complemented with IFIT2ΔRNA (Fig. 2C), suggesting a role for RNA binding by IFIT2 in promoting viral gene expression. Collectively, these data confirm that IFIT2 and IFIT3 have pro-viral activities and regulate expression of viral proteins during IAV infection. IFIT2 plays a role in inducing apoptosis via the intrinsic mitochondrial pathway and the proteins Bak and Bax[23]. Whereas apoptosis is a primary mechanism of cell death during IAV infection, it is also a key cellular process required for appropriate progression of the viral life cycle[30–32]. We therefore assessed whether changes in viral gene expression were related to IFIT2-induced apoptosis. Loss of IFIT2 reduced apoptosis and increased cell viability at later stages of infection (Extended data Fig. 3A-C). Lower viral replication in IFIT2-lacking cells may have contributed to reduced apoptosis.

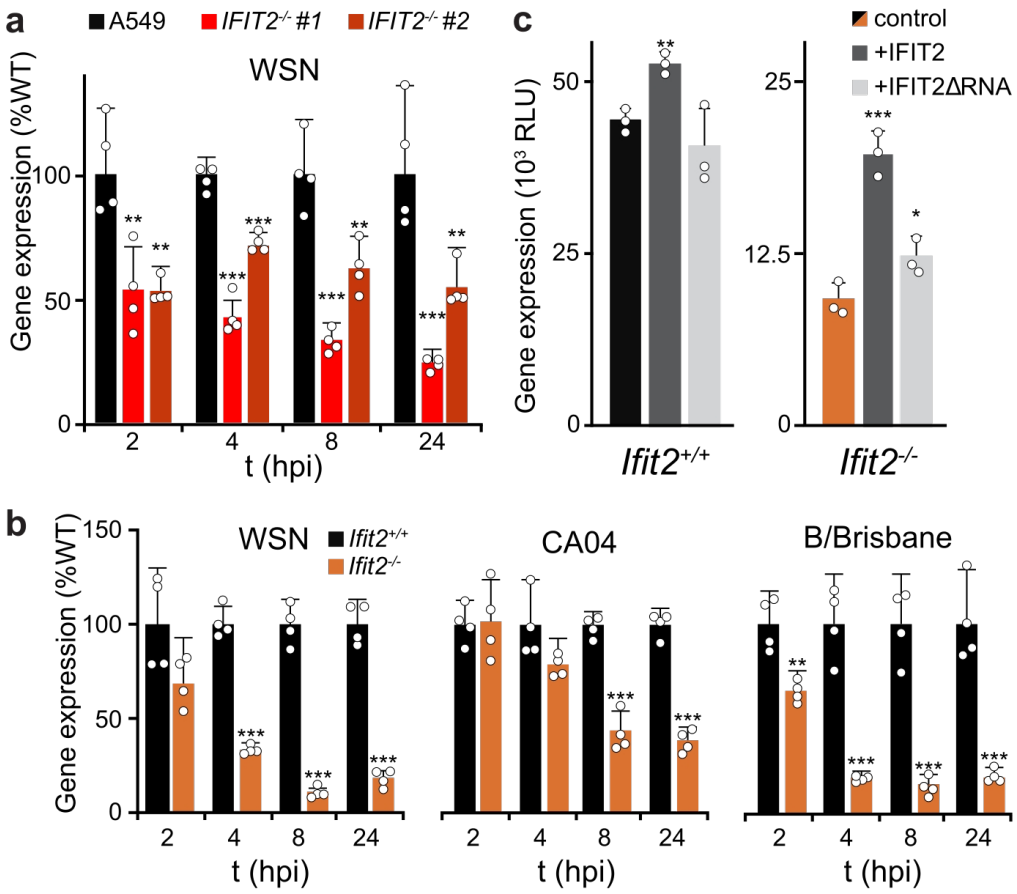

Figure 2. IFIT2 promotes IAV gene expression and progression through the viral life cycle. a-b, Viral gene expression measured in parental and *IFIT2* (**a**) or *Ifit2* (**b**) knockout cells infected with IAV or IBV reporter viruses (MOI = 0.05). **c**, WSN viral gene expression was measured 12 hr after infection of MEFs transiently complemented with IFIT2 or the RNA-binding mutant IFIT2ΔRNA. For all panels, reporter activity is a proxy for gene expression and data are shown as mean of n = 3-4 independent infections + sd (*p < 0.05, **p < 0.01; *** p < 0.001 when compared to WT or control conditions; Two-tailed Student's t-test for pairwise comparisons between control and knockout cells (b) or one-way ANOVA with *post hoc* Tukey's HSD for multiple comparisons to control conditions (a and c).

Interestingly, *Bak*$^{-/-}$/*Bax*$^{-/-}$ cells phenocopied *Ifit2*$^{-/-}$ cells in multi-step replication assays, but showed minimal changes in gene expression early during infection, unlike the significant defects in gene expression in cells lacking Ifit2 (Extended data Fig. 3D-E). Moreover, expression of IFIT2 in *Bak*$^{-/-}$/*Bax*$^{-/-}$ cells, but not IFIT2ΔRNA, enhanced viral gene expression during infection (Extended data Fig. 3F). Thus, IFIT2 still stimulates viral gene expression independent of its ability to stimulate apoptosis, indicating that these are separable functions.

RNA binding by IFIT2 was important for enhanced viral gene expression. We therefore performed UV crosslinking and immuno-precipitation followed by sequencing (CLIP-Seq) to identify all RNAs bound by IFIT2 during infection. IFIT2 preferentially binds protein-coding RNAs, with 1804 specific binding sites in 1247 mRNAs (Fig. 3A, Extended Data Fig. 4A-C, Supplemental Table 3). Meta-analysis mapped most IFIT2 binding sites to the 3' UTR of cellular mRNAs, although abundant binding in the coding sequence was also detected. Binding was not solely dependent on RNA levels as both abundant and lowly expressed transcripts were bound (Extended Data Fig. 4D). Motif discovery algorithms failed to find a strict sequence that defines IFIT2 binding sites. However, IFIT2-bound sites showed a clear skew in their nucleotide content and are AU rich, with ~20% of the sites containing the degenerate UAGnnUAU motif (Fig. 3B, Extended Data Fig. 4E-F). Gene ontology analysis revealed that IFIT2-bound mRNAs are highly enriched for genes involved in viral processes (Supplemental Table 3). ISGs were significantly enriched in the bound fraction (χ^2 $p<10^{-23}$), including potent regulators of viral infection like DDX58 (RIG-I), OAS, STAT1 and IRF1; IFIT2 even bound its own message as well as that of IFIT1 and IFIT3 (Fig. 3C, Supplemental Table 3). Remarkably, IFIT2 bound transcripts from all 8 influenza virus genes, but did not bind genomic minus-sense vRNA (Fig. 3D, Extended Data Fig. 5A).

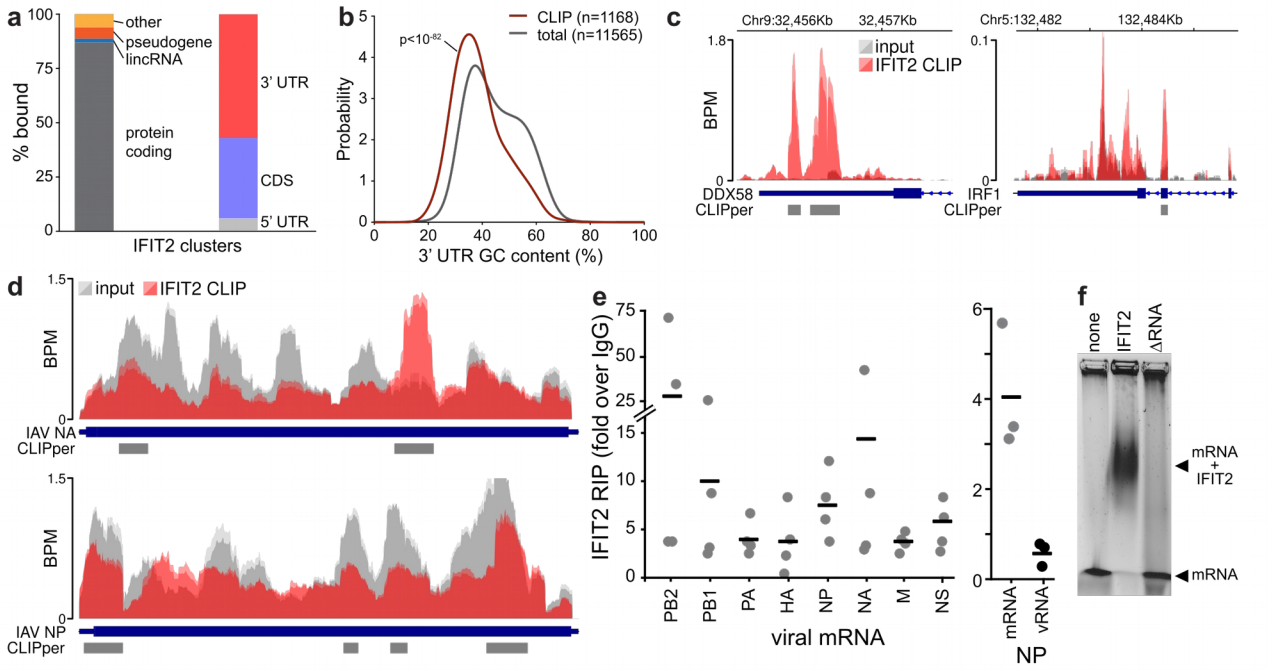

Figure 3. IFIT2 selectively binds AU-rich regions in viral and host mRNAs. CLIP was performed to identify RNAs directly bound by IFIT2 during IAV WSN infection. **a**, RNA biotypes bound by IFIT2 and binding locations within protein-coding transcripts were determined. **b,** Meta-analysis of GC content for peaks identified in the 3' UTR of bound mRNAs. IFIT2-bound sites were compared to all expressed 3' UTRs by a Mann-Whitney U-test. **c-d,** Relative CLIP intensity for IFIT2-bound and size-matched input control RNAs for host (c) and viral (d) transcripts. Data from replicate experiments are plotted as mean and standard deviation using dark and light shades of the same color, respectively. CLIPper-identified peaks are shown below. BPM = bins per million. **e**, qRT-PCR of viral mRNAs or genomic vRNA in IFIT2 RNA-immunoprecipitation (RIP) samples from infected cells. All replicates are shown (n = 4) along with a bar indicating the mean. **f**, Electromobility shift assay of viral NP mRNA with recombinant IFIT2 or IFIT2ΔRNA.

The number of called peaks on viral mRNAs was limited due to high background levels of viral sequence in the input control. This is due to the fact that influenza virus NP, whose function is to bind viral RNAs, co-migrates with IFIT2 during gel electrophoresis. This causes an artificial enrichment of viral RNAs in the size-matched input control used to establish baseline RNA levels in CLIP-Seq. Hence, the peak calling here is likely an under-estimation of the intensity of IFIT2 binding to viral RNAs. To confirm interactions with viral RNAs, we performed RNA immunoprecipitations (RIPs) coupled with RT-qPCR. Again, IFIT2 selectively bound RNA from all influenza virus genes, showing ~3- to 25-fold enrichment over IgG controls (Fig. 3E, left, Extended Data Fig. 5B). IFIT2 RNA binding was specific for plus-sense RNA as genomic vRNA was not enriched by IFIT2 RIP (Fig. 3E, right). Electromobility shift assays using recombinant IFIT2 and *in vitro* transcribed NP mRNA demonstrated that IFIT2 directly binds viral mRNAs, further confirming the CLIP-Seq data (Fig. 3F, Extended Data Fig. 5C). This binding was lost with recombinant IFIT2ΔRNA. These data show that IFIT2 binds AU-rich regions on viral and host mRNAs during infection.

We next sought to establish a mechanism by which IFIT2 enhances viral gene expression. IFIT2 preferentially bound mRNAs, therefore we asked whether IFIT2 associated with mRNAs undergoing translation. Capillary electrophoresis of RNAs present in IFIT2 RIPs from infected cells demonstrated strong enrichment of ribosomal RNAs (rRNAs), including 28S, 18S and 5/5.8S (Fig. 4A). Parallel immunoprecipitations of IFIT2 showed specific co-precipitation of the ribosome, as measured by blotting for the large subunit protein Rpl10. IFIT2-mRNA interactions were further characterized by performing polysome pelleting to isolate actively translating ribosomes (Fig. 4B). IFIT2 co-pelleted with ribosomes from infected cell lysate. EDTA treatment

dissociated polysomes, which dramatically reduced the amount of pelleted Rpl10 and completely eliminated co-pelleting IFIT2.

Polysome profiling was then performed to gain more resolution on the ribosome complexes with which IFIT2 interacts (Fig. 4C). IFIT2 co-migrated with initiating ribosomes and with the polysome fraction, indicating that IFIT2 is present with highly translated mRNAs containing multiple ribosomes. EDTA disrupted polysomes and IFIT2 no longer sedimented in the gradient. The abundance of 40S, 60S and 80S peaks as well as the polysome profiles were indistinguishable between WT and both *IFIT2*$^{-/-}$ A549 cell lines (Fig. 4D). Thus, knockout of IFIT2 did not cause global changes in translation during infection. The distribution of viral mRNAs in the polysome profile was then measured. Approximately 60% of total NP mRNA from infected cells was present in heavy polysome fractions, which represents highly translated messages with more than five ribosomes per mRNA. The abundance of viral NP mRNA amongst highly translated messages was reduced by approximately one third in the *IFIT2*$^{-/-}$ cell lines (Fig. 4D), and these mRNA were redistributed to fractions containing less efficiently translated messages (Extended Data Fig. 6A-C). The distribution of β-actin mRNA, a transcript that is not bound by IFIT2, was unchanged in its absence (Fig. 4D and Extended Fig. 6B). These findings were confirmed with a different separation strategy, measuring NP mRNA levels in polysome pellets from WT and *IFIT2*$^{-/-}$ cells lines (Fig. 4E). The proportion of total NP mRNA present in the polysome pellet was significantly decreased in both *IFIT2*$^{-/-}$ lines as compared to the WT control. To specifically assess changes in translation to all IFIT2-bound mRNAs, we performed ribosome profiling of infected cells. Translational efficiency was measured as the number of ribosome protected fragments (RPFs) for an mRNA relative to its abundance in the cell[33].

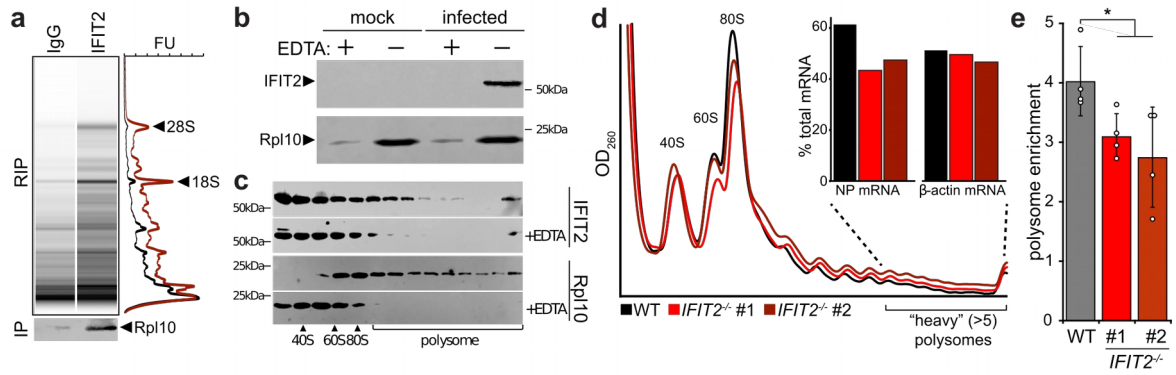

Figure 4. IFIT2 associates with active ribosomes and increases the translational efficiency of viral mRNAs. a, Capillary electrophoresis traces for RNAs that co-precipitate with IFIT2 or an IgG control from WSN-infected cell lysate. Ribosomal RNAs were identified by their size and are indicated. Simulated gels and paired chromatographs quantified by fluorescence units (FU) are shown. In a separate IFIT2 immuno-precipitation, co-precipitating ribosomal protein (Rpl10) was detected by western blot. **b-c,** Translationally active ribosomes were separated from infected or mock cell lysate by polysome pelleting (**b**) or profiling (**c**). Ribosome were dissociated with EDTA where indicated. Proteins in polysome pellets or fractions were detected by western blot. **d**, Polysome profiles from WT and *IFIT2*$^{-/-}$ A549 cells infected with IAV WSN. mRNA abundance amongst highly translated messages (>5 ribosomes/mRNA) was determined by qRT-PCR (inset). **e**, Enrichment of NP mRNA in the polysome relative to total RNA was determined by qRT-PCR for samples from WT and *IFIT2*$^{-/-}$ cells infected with IAV. Data are mean of n = 4 biologically independent samples +/- sd. (* $p < 0.05$, one-way ANOVA with *post hoc* Tukey's HSD for multiple comparisons to control conditions).

The translational efficiencies of IFIT2-bound viral mRNAs, cellular mRNAs, and ISG mRNAs were all reduced in *IFIT2*$^{-/-}$ cells compared to WT, whereas translation of most unbound mRNAs was largely unchanged (Fig. 5A-B, Extended Data Fig. 7A, Supplemental Table 4). Viral mRNA levels increased ~2-4 fold in *IFIT2*$^{-/-}$ cells, possibly due to decreased translation of ISGs under these conditions. Whereas translation efficiency decreased for viral mRNAs in *IFIT2*$^{-/-}$ cells compared to WT, the number of RPFs, used as a proxy for absolute translation levels, was largely unchanged. Nonetheless, western blotting revealed viral NP levels were lower in infected *IFIT2*$^{-/-}$ cells and restored upon ectopic IFIT2 expression (Extended Data Fig. 6D). This agrees with prior results showing defects in viral gene expression in cells lacking IFIT2/Ifit2 (Fig. 2, Extended Data Fig. 2D-E). To understand this apparent disconnect, RPFs were mapped to their respective transcripts (Fig. 5C, Extended Data Fig. 7B). Ribosome footprint density was distributed across the coding sequence in viral mRNAs during infection of WT cells, with minor local variations, reflecting efficiently translated messages[33]. In contrast, strong peaks of ribosome density selectively appeared on viral mRNAs during infection of *IFIT2*$^{-/-}$ cells. Many of the peaks spanned ~28-32 nt, the predicted footprint of a single ribosome[34]. The appearance of highly aligned footprints in the absence of IFIT2 is indicative of extensive ribosome pausing on viral mRNAs[33]. Thus, many of the RPFs on viral mRNAs in *IFIT2*$^{-/-}$ cells may result from non-productive pauses, explaining the decrease in protein production without a corresponding reduction in RPFs.

However, pausing was consistently increased in *IFIT2*$^{-/-}$ cells for cellular mRNAs, ISG mRNAs and viral mRNAs that are normally bound by IFIT2 (Fig 5E, Extended Data 7D-E). Pausing increased at many sites on viral mRNAs and at more limited positions in IFIT2-bound cellular transcripts (Fig. 5C-D).

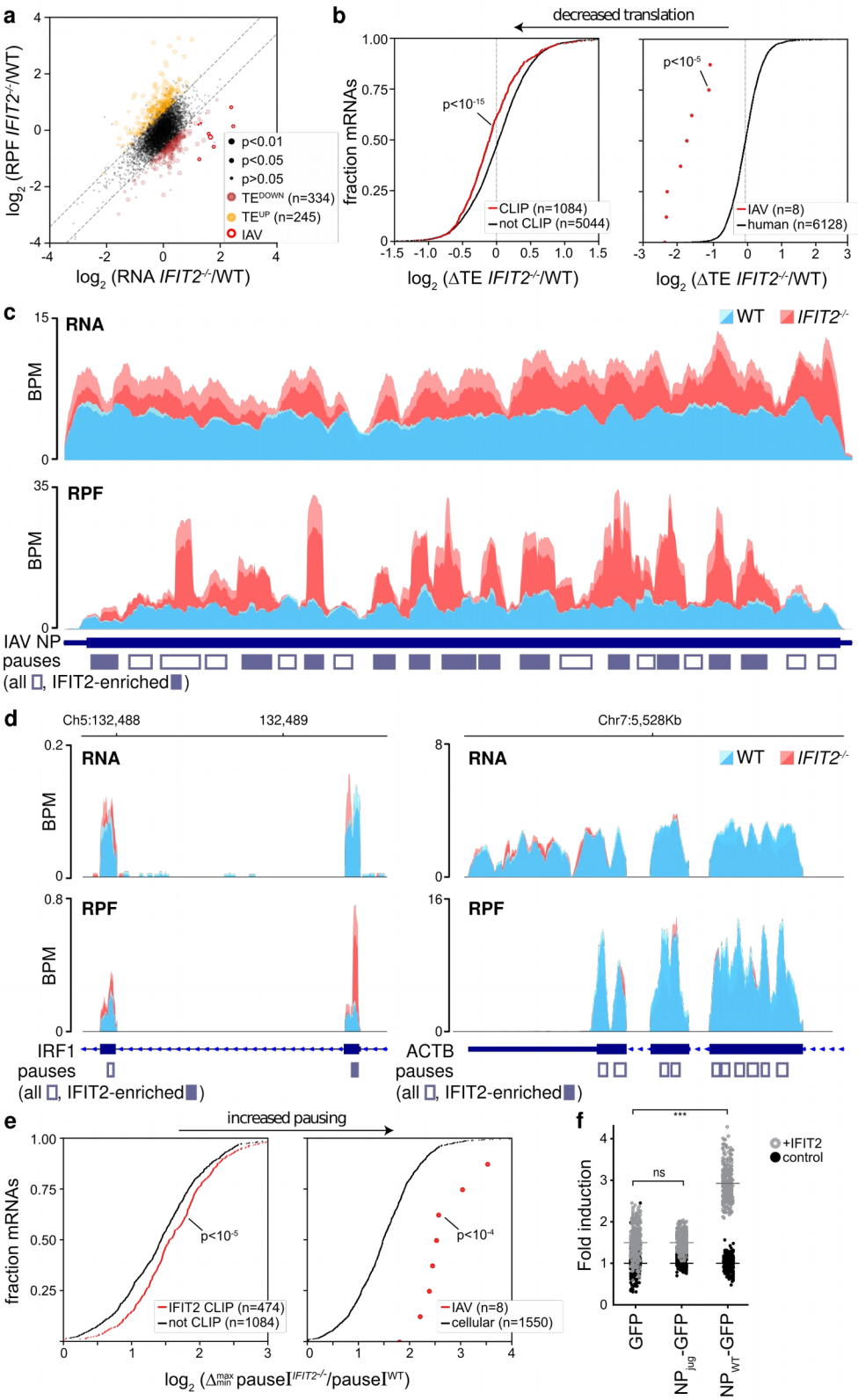

Figure 5. IFIT2 modulates translational efficiency by preventing ribosome pausing. Differentially translated mRNAs were identified by ribosome profiling of IAV WSN-infected WT and *IFIT2*$^{-/-}$ A549 cells. **a,** The relative contribution of transcription and translational were assessed by plotting fold changes

between *IFIT2*$^{-/-}$ and WT cells for input RNA versus ribosome protected fragments (RPF) from each transcript. Dotted lines represent a 1.5-fold ($\log_2$ 0.58) threshold. Transcripts that are differentially translated in *IFIT2*$^{-/-}$ cells have been colored, with IAV mRNAs highlighted. p values derived from a two-sided F-test (see Supplemental Table 4). **b,** The translational efficiency of all IFIT2-bound mRNAs (left) or viral mRNAs (right) is decreased in the absence of IFIT2. Bound transcripts were compared to unbound transcripts via a Mann-Whitney U-test. **c-d**, Accumulation of paused ribosomes in the absence of IFIT2. Normalized read density for total RNA (top) and RPFs (bottom) mapping to IFIT2-bound NP (c) and IRF1 (d, left) or unbound b-actin (d, right) mRNAs in infected WT and *IFIT2*$^{-/-}$ cells. Data from replicate experiments are plotted as mean and standard deviation using dark and light shades of the same color, respectively. Pause sites are shown below. Pause sites enriched in *IFIT2*$^{-/-}$ cells >1.5-fold are filled in. BPM = bins per million. **e,** Ribosome pausing increases during infection of *IFIT2*$^{-/-}$ cell. Changes in pause intensity (pauseI) at the maximum and minimum pauseI sites on each transcript were calculated during infection of WT and *IFIT2*$^{-/-}$ cells. All IFIT2-bound mRNAs (left) or viral mRNAs (right) were compared to remaining transcripts via a two-sided Mann-Whitney U-test. **f,** Sequence-dependent enhancement of NP translation in the presence of IFIT2 or control. NP was encoded as a GFP polyprotein using WT or juggled codons. Expression was quantified by fluorescence imaging of live cells. n = 2 biological replicates quantifying 177 fields of view each. IFIT2 induction of NP-GFP variants was compared to the GFP-only control using a one-way ANOVA with *post hoc* Tukey's HSD (*** $p < 0.001$).

Changes in pause intensity at these sites were not the result of global changes in ribosome processivity, as polysome profiles were indistinguishable in WT and *IFIT2*$^{-/-}$ cells and unbound control transcripts like ACTB and GAPDH showed no differential pausing (Fig. 4D, 5D, Extended Data Fig. 7C).

These data suggest that decreased translational efficiency for viral mRNA and cellular IFIT2-bound mRNAs may be due to ribosome pausing that occurs when IFIT2 is absent. We tested this possibility by correlating IFIT2-dependent changes in pause intensity and translational efficiency. IFIT2-bound viral mRNAs, cellular mRNAs, and ISG mRNA all showed a stronger correlation than unbound transcripts (Extended Data Fig. 7F). Finally, we used a functional assay to connect IFIT2 binding to changes in translation. IFIT2 was co-expressed in cells with an influenza virus NP-GFP polyprotein where NP was encoded by the native transcript, or one where silent mutations juggled the RNA sequence without changing the coding potential (NP_{jug}) (Extended Data Fig. 8A). NP and NP_{jug} contain a similar overall AU content, but the codon juggling eliminated clustered AU-rich regions found in the native NP mRNA. Changing the coding sequence did not alter expression of NP or NP_{jug} when they were expressed on their own (Fig. 5F). IFIT2 co-expression caused a ~3-fold increase in natively coded NP, following patterns observed in infection. By contrast, IFIT2 caused background-level changes in NP_{jug} expression that mirrored the GFP control. Similar results were obtained when blotting NP itself (Extended Data 8B). Combined, these data support a model where IFIT2 binds to and enhances the translational efficiency of host mRNAs by suppressing ribosome pausing.

Discussion

Viruses must overcome cellular defense to enable successful replication, often by evading detection or deploying viral countermeasures. Data presented here show that influenza virus

utilizes an additional strategy – exploiting cellular defenses to stimulate viral gene expression and replication. IFIT2 binds AU-rich mRNAs and increases their translational efficiency by decreasing ribosome pausing. Many of the transcripts bound by IFIT2 are important for antiviral responses, perhaps explaining the broad antiviral activity of IFIT2[12,13]. However, influenza virus co-opts this strategy, where viral mRNAs are also bound by IFIT2 resulting in increased production of viral gene products and ultimately tipping the balance to higher levels of viral replication (Extended Data Fig. 9).

The strategy of repurposing antiviral functions to support infection may be part of a more common tactic exploited by viruses: the entry of multiple enveloped viruses is enhanced by LY6E, the product of an ISG[35]; human cytomegalovirus virus has usurped the antiviral viperin and IFN-induced transmembrane (IFITM) proteins to facilitate infection[36,37]; and, HIV and BK virus may exploit the mutator function of APOBEC3 to acquire beneficial changes that accelerate escape from immune pressure or drug treatment[38–40]. Thus, the potent innate immune response creates strong pressures driving viruses to adopt multiple strategies to counteract these defenses, including converting antiviral proteins into pro-viral effectors.

Materials and Methods

Cells

Human alveolar epithelial (A549), Madin-Darby canine kidney (MDCK), Madin-Darby bovine kidney (MDBK), baby hamster kidney (BHK), and HEK293T cells were acquired from ATCC cultured in Dulbecco's modified Eagle's medium (DMEM) supplemented with 10% fetal bovine serum (FBS), 1% Penicillin/Streptomycin, and Corning GlutaGro supplement (Mediatech). Line were authenticated by the supplier. Murine embryonic fibroblasts (MEFs) derived from wildtype (WT), *Ifit2*$^{-/-}$ C57BL/6 embryos[41], *Bax*$^{-/-}$/*Bak*$^{-/-}$ double knockout embryos (a

gift from Chi Li, University of Louisville) were maintained in DMEM supplemented with 10% FBS and nonessential amino acids. Transduced A549 cells were selected and maintained in cell growth medium containing 0.5 µg/ml Puromycin (GenDepot). All cells were grown at 37°C in 5% CO_2. Cells are routinely tested for mycoplasma contamination using MycoAlert (Lonza).

Plasmids

The human LentiCRISPR Genome-wide CRISPR Knock Out (GeCKO) v2 (#1000000048) and Brunello (#73178) libraries were obtained from Addgene and prepared according to published protocols[42–44]. Briefly, each library was electroporated into *E. cloni* 10G Elite electrocompetent cells (Lucigen) in quadruplicate. After recovery, cells were plated and grown at 30°C for 14 h. Colonies were harvested by scraping plates. GeCKOv2 plasmid libraries were isolated using the QIAFilter Maxi Kit (Qiagen). Plasmids expressing the viral polymerase proteins, viral NP, and a genomic reporter vRNA have been described[45]. Plasmids encoding V5-tagged human IFIT2 and IFIT3 were a kind gift from N. Reich (Stony Brook University)[23]. The IFIT2 RNA binding mutant DM2 R292E/K410E (IFIT2ΔRNA)[29] was generated by sequential inverse PCR and confirmed by sequencing. Primers to generate the RNA binding mutant are listed below:

hIFIT2 R292E For: GTGCTGCTATgagGCAAAAGTCTTC
hIFIT2 R292E Rev: CCAATTTGGCAATGCAGG
hIFIT2 K410E For: GGAGAAAGAAgagATGAAAGACAAAC
hIFIT2 K410E Rev: CTTGATTTCTGGTTTATTTTTACAC

For bacterial expression, both WT and IFIT2ΔRNA were cloned into pENTR and moved into pHGGWA by Gateway recombination (Invitrogen).

The coding sequence of NP was altered with synonymous changes using GeneDesign to exchange the original codons with random selections from the same family[46], while avoiding rare codons and maintaining a similar overall codon adaptation index. Juggled NP sequence is:

>NP_juggle
ATGGCAACTAAGGGTACTAAGAGGAGCTATGAGCAAATGGAAACCGACGGCGAGCGTCAAAA
CGCTACAGAGATAAGGGCCAGTGTGGGCAAGATGATCGACGGGATCGGGCGGTTTTATATACAG
ATGTGTACTGAGTTGAAGCTTTCTGACTACGAAGGGAGACTAATCCAAAATAGTTTGACCATTG
AACGTATGGTACTATCGGCGTTCGATGAACGGCGCAACAAGTACCTCGAAGAGCACCCTTCTGC
CGGAAAGGACCCAAAAAAGACAGGTGGCCCGATTTATCGCCGCGTGGACGGTAAATGGCGTCG
TGAGCTTATTTTGTACGATAAGGAGGAGATCCGTAGGATATGGCGTCAGGCAAACAACGGCGAT
GACGCGACCGCCGGACTCACCCATATGATGATATGGCATTCGAACCTGAACGACGCGACGTATC
AACGAACTAGAGCACTGGTACGTACTGGTATGGACCCACGGATGTGTTCCTTGATGCAAGGATC
TACACTACCACGACGTAGTGGAGCAGCCGGCGCGGCGGTAAAGGGTGTCGGGACTATGGTAAT
GGAGCTGATAAGGATGATAAAGCGGGGCATAAACGACAGAAATTTTTGGCGTGGCGAAAACGG
GAGACGGACCCGCATAGCATACGAGCGTATGTGTAATATACTGAAGGGTAAGTTCCAGACCGCG
GCCCAGCGCACGATGGTTGACCAGGTAAGGGAATCGAGGAACCCGGGCAACGCGGAATTTGA
GGACCTGATTTTCCTTGCGAGATCGGCTCTAATTCTCCGGGGTTCCGTCGCACATAAAAGCTGT
CTCCCAGCTTGCGTTTACGGTTCGGCTGTTGCAAGCGGGTATGATTTCGAGCGCGAAGGTTATT
CACTCGTAGGGATCGATCCCTTTCGCTTACTGCAGAATTCCCAGGTCTATTCGCTCATTCGTCCT
AACGAAAACCCGGCCCATAAATCTCAGTTGGTTTGGATGGCTTGTCACTCAGCGGCGTTCGAG
GACCTCCGAGTCTCCTCCTTTATTCGAGGAACAAAGGTTGTACCGCGGGGCAAACTGTCTACCC
GGGGCGTCCAGATAGCGTCAAACGAGAATATGGAAACCATGGAGTCGTCAACGTTAGAGTTGC
GCTCACGGTATTGGGCAATCCGAACTCGTTCGGGTGGCAATACAAACCAGCAACGCGCCTCTTC
CGGACAGATATCTATTCAGCCCACTTTTTCTGTGCAACGGAACTTGCCCTTCGATCGGCCCACGA
TCATGGCGGCGTTTACAGGCAACACTGAAGGACGAACCTCCGATATGCGTACTGAGATTATCCG
CCTTATGGAGTCTGCTCGGCCTGAGGACGTCAGTTTTCAAGGACGCGGCGTTTTTGAACTAAGC
GATGAGAAAGCTACCTCTCCCATAGTTCCGTCGTTCGATATGTCCAACGAGGGTTCGTACTTTTT
TGGCGATAACGCGGAAGAATATGATAACTAA

The global GC content of the native and juggled NP are 47% and 52%, respectively. The gene was synthesized (GenScript) and cloned to created pCDNA3-jugNP. WT and juggled NP were also cloned into pCDNA3 as fusion proteins with a C-terminal GFP separated by 2A peptide from porcine teschovirus-1 polyprotein to create pCDNA3-NP-2A-GFP or pCDNA3-jugNP-2A-GFP. All plasmids were verified by sequencing.

Viruses and multicycle replication

Viral infections were performed using A/WSN/1933 (WSN), WSN stably encoding the VSV G glycoprotein (VSV-G) and GFP (IAV-G)[11], WSN encoding PB2-FLAG[47], A/California/04/2009 (CA04), and primary isolates obtained from BEI Resources: A/Hong Kong/1/1968 (H3N2) (HK68; Cat# NR-28620), A/Victoria/361/2011 (H3N2) (Vic/2011; Cat# NR-44022), and A/Wisconsin/15/2009 (H3N2) (WI/2009; Cat# NR-42007). Reporter viruses encoding the NanoLuc (Nluc) reporter gene as a polyprotein with PA have been previously described for the WSN (PASTN) and A/California/04/2009 (H1N1) strains (CA04-PASTN)[27,48].

A similar strategy was used to produce the influenza B reporter virus in the B/Brisbane/60/2008 background (B-PASTN). Replication kinetics of PASTN-B and the parental recombinant virus are shown (Extended Data Fig. 10). Recombinant SC35M NS1-2A-GFP-2A-NEP (SC35M Flu-GFP) is based on A/Seal/Massachusetts/1-SC35M/80 (H7N7) and was prepared as previously described plasmids[49]. VSV-GFP was generously provided by P. Bates (University of Pennsylvania). Viruses were propagated in MDCK or MDBK cells in virus growth medium (VGM; DMEM, 0.3% bovine serum albumin, 25 mM HEPES, and 0-0.5 μg/ml of L-1-tosylamido-2-phenylethyl chloromethyl ketone [TPCK] trypsin) or in 9-11 day old embryonated chicken eggs. Viral stocks were titered on MDCK cells. VSV and FVG-G viruses were titered on BHK cells.

Multicycle replication experiments were performed in triplicate and infected at multiplicities of 0.01-0.1. For infections of MEFs, viruses were diluted and grown in DMEM containing 1% FBS and Penicillin/Streptomycin. All other infections were performed in VGM. Aliquots were removed at the indicated time points and titers were determined by plaque assay or by NanoGlo Titer Assay[28].

Viral gene expression assays

Viral gene expression was measured using PASTN-based reporter following previous protocols[27,28]. This virus encodes the *NanoLuc (NLuc)* reporter in a polycistronic version of the PA gene. Briefly, cells were grown to confluence in a white 96-well plate and infected at MOI = 0.01 at least in triplicate. Cells were washed after 1 hr to remove the inoculum and any residual NLuc from the viral stocks. Infections were allowed to proceed for the indicated times and NLuc activity was quantified as a proxy for viral gene expression. NLuc activity was measured *in situ* using the Nano-Glo assay system (Promega) and a plate reader.

GeCKOv2 lentivirus library packaging and A549 transduction

For lentiviral packaging, 293T cells (2.4 x 10^8 cells) were grown in 15 cm dishes to 40% confluence. Cells were transfected with equivalent concentrations of psPAX2, pVSV-G, and LentiCRISPRv2 library A and B using Transit-2020 (Mirus). After 6 h, the medium was replaced with DMEM containing 10% FBS and 1% BSA. After 60 h post transfection, the supernatant was harvested, pooled, centrifuged for 10 min at 4°C, and filtered through a 0.45 μm low protein binding membrane. Lentiviral libraries were then concentrated using ultracentrifugation and resuspended in DMEM containing 10% FBS and 1% BSA. The LentiCRISPRv2 lentivirus library was then titered by transducing A549 cells and counting puromycin-resistant colonies three weeks post-selection and by determining percent transduction by counting viable cells following 4 days of puromycin selection. To generate the GeCKO A549 knockout library, 10^8 early passage A549 cells were transduced in the presence of 8 μg/ml polybrene at a multiplicity of 0.3 for ~287-fold library coverage for selection with IAV-G and WSN. A separate GeCKO A549 knockout library was prepared for selection with SC35M Flu-GFP using an independently generated lentiviral library. Cells were selected with puromycin containing media (0.5 μg/ml) 24-48 h post-transduction. Transduced cells were frozen 10-11 days following antibiotic selection or used immediately.

Genome-wide GeCKO selection with IAV-G and WSN and sequencing

IAV-G and WSN selections: The experimental workflow is diagrammed in Fig. 1 and Extended Data Fig. 1. GeCKO-A549 cells were created with the GeCKO genome-wide sgRNA library[43] and plated at a presumed 530X library coverage. GeCKO-A549 cells were infected at an MOI of 0.3 with IAV-G[50], which was determined to be the minimal multiplicity of infection necessary for complete killing of non-transduced A549 cells. Infected cells were incubated for

20-21 days with media changes every 3-4 days. Following the primary IAV-G selection, surviving cells were re-plated and a fraction was frozen. Re-plated cells were subject to a secondary challenge with IAV-G or WSN to enrich for resistant cells. Surviving cells were expanded for an additional 20-21 days. Even though this approach contained multiple rounds of selection and a counter-screen, we consider it a single biological replicate as the selection began with a single pool of GeCKO-A549 cells. A completely independent selection was performed using a uniquely generated knockout cell pool and IAV-SC35M (see below).

Deep sequencing and data analysis of selected gRNAs: Genomic DNA was extracted from frozen cell pellets using the Blood & Cell Culture Midi kit (Qiagen). To ensure sufficient coverage of the library, genomic DNA was extracted from $3x10^7$ cells from the GeCKO-A549 parental library and selected cells from the primary selections. For each sample, sgRNA sequences were amplified by nested PCR in 3-13 separate reactions containing 10 µg of genomic DNA in each reaction. Previously published primers were used to amplify the LentiCRISPRv2 sgRNAs[42]:

v2Adaptor_F: AATGGACTATCATATGCTTACCGTAACTTGAAAGTATTTCG
v2Adaptor_R: TCTACTATTCTTTCCCCTGCACTGTtgtgggcgatgtgcgctctg
F01:
AATGATACGGCGACCACCGAGATCTACACTCTTTCCCTACACGACGCTCTTCCGATCTtAAGTAG
AGtcttgtggaaaggacgaaacaccg
F02:
AATGATACGGCGACCACCGAGATCTACACTCTTTCCCTACACGACGCTCTTCCGATCTatACACG
ATCtcttgtggaaaggacgaaacaccg
F03:
AATGATACGGCGACCACCGAGATCTACACTCTTTCCCTACACGACGCTCTTCCGATCTgatCGCGC
GGTtcttgtggaaaggacgaaacaccg
F04:
AATGATACGGCGACCACCGAGATCTACACTCTTTCCCTACACGACGCTCTTCCGATCTcgatCATG
ATCGtcttgtggaaaggacgaaacaccg
F05:
AATGATACGGCGACCACCGAGATCTACACTCTTTCCCTACACGACGCTCTTCCGATCTtcgatCGTT
ACCAtcttgtggaaaggacgaaacaccg
F06:
AATGATACGGCGACCACCGAGATCTACACTCTTTCCCTACACGACGCTCTTCCGATCTatcgatTCC
TTGGTtcttgtggaaaggacgaaacaccg

F07:
AATGATACGGCGACCACCGAGATCTACACTCTTTCCCTACACGACGCTCTTCCGATCTgatcgatAACGCATTtcttgtggaaaggacgaaacaccg
F08:
AATGATACGGCGACCACCGAGATCTACACTCTTTCCCTACACGACGCTCTTCCGATCTcgatcgatACAGGTATtcttgtggaaaggacgaaacaccg

Resulting amplicons were gel-quantified and equimolar amounts were pooled, gel extracted using the MinElute gel extraction kit (Qiagen), and sequenced using a HiSeq 2500 (Illumina). Raw FASTQ files were demultiplexed and trimmed using the FASTX-Toolkit in Galaxy and then processed by Galaxy to contain only the unique sgRNA sequence[51]. MAGeCK was then used to align the reads to the GeCKO library, calculate the number of aligned reads for each sequence, and identify positively selected hits[52] (Supplemental Table 1).

Genome-wide Brunello selection with SC35M Flu-GFP and sequencing

SC35M Flu-GFP selections: Brunello A549 knockout library cells were created using the two-vector Brunello system by transducing A549-Cas9 cells with the sgRNA library[44]. Cells were plated at a presumed 1000-fold coverage and infected with SC35M Flu-GFP at an MOI of 0.1. In parallel, mock-infected cells were harvested. Surviving cells were expanded and re-infected with SC35M Flu-GFP under the same conditions for 7 rounds of selection and harvested on day 63 post infection. The SC35M Glu-GFP selection was performed as a single biological replicate. A completely independent selection was performed using a uniquely generated knockout cell library and IAV-WSN (see above).

Deep sequencing and data analysis of selected gRNAs: Genomic DNA (gDNA) of cell pellets was isolated using Quick-DNA™ Miniprep Plus Kit (Zymo Research). PCR was performed on gDNA to construct Illumina sequencing libraries with each containing 5 µg gDNA following the Broad Institute protocol PCR of sgRNAs for Illumina sequencing. Briefly, gDNA was aliquoted into PCR tubes in a 50 µl total volume. A PCR mastermix containing Extaq DNA

polymerase (Clontech), ExTaq buffer, dNTP, P5 stagger primers (see below) and water were prepared. 40 µl of PCR mixture and 10 µl of a barcode P7 primer (see below) were added to each tube containing 50 µl of gDNA. Primers used for Brunello amplicons are:

P5-0:
AATGATACGGCGACCACCGAGATCTACACTCTTTCCCTACACGACGCTCTTCCGATCTTTGTGG
AAAGGACGAAACACCG
P5-1:
AATGATACGGCGACCACCGAGATCTACACTCTTTCCCTACACGACGCTCTTCCGATCTCTTGTGG
AAAGGACGAAACACCG
P5-2:
AATGATACGGCGACCACCGAGATCTACACTCTTTCCCTACACGACGCTCTTCCGATCTGCTTGTG
GAAAGGACGAAACACCG
P5-3:
AATGATACGGCGACCACCGAGATCTACACTCTTTCCCTACACGACGCTCTTCCGATCTAGCTTGT
GGAAAGGACGAAACACCG
P5-4:
AATGATACGGCGACCACCGAGATCTACACTCTTTCCCTACACGACGCTCTTCCGATCTCAACTT
GTGGAAAGGACGAAACACCG
P5-6:
AATGATACGGCGACCACCGAGATCTACACTCTTTCCCTACACGACGCTCTTCCGATCTTGCACCT
TGTGGAAAGGACGAAACACCG
P5-7:
AATGATACGGCGACCACCGAGATCTACACTCTTTCCCTACACGACGCTCTTCCGATCTACGCAA
CTTGTGGAAAGGACGAAACACCG
P5-8:
AATGATACGGCGACCACCGAGATCTACACTCTTTCCCTACACGACGCTCTTCCGATCTGAAGAC
CCTTGTGGAAAGGACGAAACACCG
P7-A01:
CAAGCAGAAGACGGCATACGAGATCGGTTCAAGTGACTGGAGTTCAGACGTGTGCTCTTCCGA
TCTTCTACTATTCTTTCCCCTGCACTGT
P7-A02:
CAAGCAGAAGACGGCATACGAGATGCTGGATTGTGACTGGAGTTCAGACGTGTGCTCTTCCGA
TCTTCTACTATTCTTTCCCCTGCACTGT

PCR samples were amplified as follows: 95°C for 1 min, followed by 28 cycles of 95 °C for 30 s, 53 °C for 30 s, 72 °C for 30 s with a final 10 min. at 72 °C. The PCR products were then purified from 2% agarose gels using a gel extraction kit (Zymo Research). PCR amplicons were purified via double size-selection with Sera-Mag SpeedBeads (GE). Cleanup was verified by visualizing samples on 2% agarose gels. Concentrations of each sample were determined using a Qubit fluorometer with dsDNA high-sensitivity assay reagents. Samples were then sequenced on an Illumina NextSeq 500. The resulting sequencing reads were trimmed to 20-nt

potential sgRNA sequences using cutadapt[53]. The MAGeCK software suite was used to assign these sequences to targets and genes[52]. Comparisons between survivor and control samples were carried out using MAGeCK's robust rank aggregation method for significance testing (Supplemental Table 2).

Knockout clone generation and genotyping by Indel Detection by Amplicon Analysis

IFIT2 and IFIT3 knockout A549 cells were generated by cloning sgRNA oligos into pLentiCRISPRv2 at the BsmBI site. The oligo sequences are:

IFIT2.1 sgRNA For: caccgAGAACGCCATTGACCCTCTG
IFIT2.1 sgRNA Rev: aaacCAGAGGGTCAATGGCGTTCTc
IFIT2.2 sgRNA For: caccgGGCCAGTAGGTTGCACATTG
IFIT2.2 sgRNA Rev: aaacCAATGTGCAACCTACTGGCCc
IFIT3.1 sgRNA For: caccgCACTGCGGAGGACATCTGTT
IFIT3.1 sgRNA Rev: aaacAACAGATGTCCTCCGCAGTGc

Lentivirus particles were produced and used to transduce A549 cells as above. Following 11-14 days of antibiotic selection, transduced cells were sorted into 96-well plates to generate clonal cell lines. Each 96-well plate was incubated for 3-4 weeks and colonies were amplified. Indel Detection by Amplicon Analysis was used as described to genotype the edited clones[54]. Briefly, genomic DNA was isolated in each 96-well plate and A549 control cells. Amplicons were fluorophore labelled by tri-primer PCR using a universal 6-FAM M13 5'-labelled primer and primers flanking the sgRNA target site in the genomic DNA with the sense primer containing a M13 extension. Primers are listed below:

6-FAM M13 Uni: GTAAAACGACGGCCAGTG
IFIT2.1 IDAA M13 For: GTAAAACGACGGCCAGTGgtccctatagaattgagagtccag
IFIT2.1 IDAA Rev: GAACATCTGTTACACCTGGGG
IFIT2.2 IDAA M13 For: GTAAAACGACGGCCAGTGgaattccttggagagcagcctac
IFIT2.2 IDAA Rev: CAGGCATAGTTTCCCCAGGTG
IFIT3.1 IDAA M13 For: GTAAAACGACGGCCAGTGgccttgtagcagcacccaatc
IFIT3.1 IDAA Rev: CTGGACTGGCAATTGCGATGTAC

PCRs were diluted 1:5, mixed with the Geneflo Rox-625 size standard (ABI/Life Technology), and analyzed by capillary gel electrophoresis. Data were analyzed using Peak Scanner Software V2.0 (ABI/Life Technology). Positive clones were selected by both IDAA and confirmed by western blotting.

Knockout 293 cells were generated by Synthego. Homozygous knockouts clones were created by limiting dilution, identified by western blotting lysate from infected or IFN-treated cells, and verified by Sanger sequencing across the edited site.

Viral clearance assay

To compare resistance of cells to different viruses, A549 or edited cells were seeded in a 96-well plate at 40,000 cells per well and treated with different concentrations of viruses that were the lowest infectious dose shown to produce extensive cytopathic effects in pilot experiments (~1 TCID50). Approximately seven days after treatment, cells were rinsed with phosphate-buffered saline (PBS), fixed with ethanol, and stained with crystal violet.

Western blotting

Cells were harvested and lysed in RIPA buffer containing protease inhibitor cocktail (Roche Life Science). Protein concentration was measured by Bradford Assay. Lysates were separated on 10-15% PAGE gel and transferred to a PVDF membrane for blocking and antibody incubation. The antibodies used were as follows: anti-IFIT2 (1:300, Proteintech 126041AP), anti-RNP (1:1000, BEI Resources Repository, NR-3133), anti-V5-HRP (1:10,000, Sigma, V2260), anti-Tubulin (1:5000, Sigma, T6199), anti-Rpl10 (1:500, Santa Cruz sc-768), PARP-1 (1:1000, Cell Signaling Technologies, 9542S), M2 anti-FLAG (1:1000, Sigma F1804), anti-NP (1µg/ml, clone H16-L10-4R5[55]) and a custom mouse anti-IFIT3 monoclonal (1:5 of hybridoma supernatant).

Complementation assay

WT and *Ifit2*$^{-/-}$ MEFs were complemented with IFIT2, IFIT2ΔRNA, or empty vector control by nucleofection. 2x10^{6} MEFs were nucleofected with 5 µg total DNA using the MEF nuclefector kit 1 (Lonza VPD-1004) and setting T-020 in the Nucleofector 2b device. Cells were plated allowed to recover prior to inoculation with PASTN at an MOI of 0.01. Viral gene expression was measured 12 hpi using the Nano-Glo assay system (Promega).

Knock-in of epitope tag at *IFIT2* locus in A549 cells

CRISPR/Cas9-mediated knock-in of a V5 epitope tag was performed by the Genome Engineering & iPSC Center at Washington University School of Medicine. An sgRNA compatible with S. pyogenes Cas9 was designed to target TTCAGCATCAAGCTGGAATG at the 3' end of the *IFIT2* open reading frame. Donor DNA was synthesized encoding a linker sequence followed by the V5-6xHis epitope tag, blocking mutations to prevent re-cutting, and 150 bp homology arms on both sides.

>Donor DNA
AAATGCGACTTTCTAAAAATGGAGCAGATTCTGAGGCTTTGCATGTCTTGGCATTCCTTCAGGA
GCTGAATGAAAAAATGCAACAAGCAGATGAAGACTCTGAGAGGGGTTTGGAGTCTGGAAGCC
TCATCCCTTCAGCATCAAGCTGGAACGGTGAAGGATCCACTAGTCCAGTGTGGTGGAATTCTGC
AGATATCCAGCACAGTGGCGGCCGCTCGAGTCTAGAGGGCCCGCGGTTCGAAGGTAAGCCTAT
CCCTAACCCTCTCCTCGGTCTCGATTCTACGCGTACCGGTCATCATCACCATCACCATTGAAGAA
TAGAGATGTGGTGCCCACTAGGCTACTGCTGAAAGGGAGCTGAAATTCCTCCACCAAGTTGGTA
TTCAAAATATGTAATGACTGGTATGGCAAAAGATTGGACTAAGACACTGGCCATACCACTGGAC
AGGGTTATGTTAACACCT

A549 cells were edited with Cas9/sgRNA in the presence of donor DNA to favor homology directed repair. The pool of edited cells was single cell cloned and homozygous knock-in clones were identified by high-throughput sequencing.

IFIT2 eCLIP

IFIT2 eCLIP protocol was adapted from previously published work[56–58] and performed on two independent biological replicates for each experimental condition. Briefly, 10^{7} A549-IFIT2

knock-in cells were plated the day prior to infection for 24 hr (MOI = 0.02 WSN). To form RNA:protein adducts, cells were washed in PBS, placed on ice for UV crosslinking with 254 nm light at 400 mJ/cm^2, exposed again at 200 mJ/cm^2, collected by scraping, pelleted and snap frozen in liquid nitrogen. Cells were thawed on ice, lysed in CLIP lysis buffer (50 mM HEPES [pH 7.5], 150 mM KCl, 2 mM EDTA, 0.5% [v/v] NP-40, 1 mM dithiothreitol [DTT], 0.5% DOC w/v, 1× EDTA-free protease inhibitor cocktail [Roche]), and clarified by centrifugation. RNase T1 (ThermoFisher) was added to 0.1 units/µl and lysates were incubated at room temperature for 10 min. Digestion was halted by placing samples on ice. Aliquots were removed for generation of the size-matched input control. IFIT2:RNA complexes were captured by adding Dynabeads protein A (Invitrogen) with pre-bound anti-V5 antibody and mixing for 3 hr at 4˚C. Beads were magnetically isolated and washed extensively in lysis buffer, followed by a high salt buffer (50 mM Tris pH [7.4], 1 M NaCl, 1 mM EDTA, 0.1% SDS, 0.5% Na-deoxycholate, 1% NP-40), and ultimately exchanged into a dephosphorylation buffer (50 mM Tris-HCl [pH 7.9], 100 mM NaCl, 10 mM MgCl2, 1 mM DTT). Samples were treated with calf intestinal phosphatase (NEB), washed with dephosphorylation buffer and exchanged into PNK buffer (50 mM Tris-HCl [pH 7.5], 50 mM NaCl, 10 mM MgCl2, 5 mM DTT). RNA was phosphorylated using [γ-^{32}P]-ATP and polynucleotide kinase (NEB). Samples were washed sequentially in PNK buffer, high salt buffer, and finally lysis buffer.

Purified IFIT2:RNA adducts were separated by SDS-PAGE, transferred to nitrocellulose and visualized by phosphor-imaging. Size-matched input controls were separated in parallel on the same gel. Standard western blotting on lysates was also performed separately to confirm the position of IFIT2. Regions corresponding to ~10-200 kDa larger than IFIT2 were cut from the RNA-bound membrane and processed into 2 mm strips. Membranes were placed in Eppendorf

tubes and RNA was released by treating samples with proteinase K (Dot Scientific) in digestion buffer (100 mM Tris pH 7.5, 10 mM EDTA, 50 mM NaCl, 1% SDS). An equal volume of phenol (pH 6.8):chloroform:isoamyl alcohol (250:49:1 ratio) was added and RNA extracted into the aqueous layer. RNA was purified on column (Zymo Research) and eluted in water.

RNAs were converted into sequencing libraries. The 3’ ends of RNA fragments were healed by treating with polynucleotide kinase in the absence of ATP and purified with Dynabeads MyOne silane (ThermoFisher). A pre-adenylated DNA adapter (NEB S1315) was ligated onto the 3’ end using a truncated T4 RNA ligase 2 (NEB). Ligation was terminated and free adapter was removed by purifying product with Dynabeads MyOne silane beads. Product was used for reverse transcription by SuperScript III (Invitrogen) in First Strand buffer using one of the following primers which contain indices to allow for multiplexing (index lowercase) and unique molecular identifies (UMI, N’s) to allow for accurate quantification:

1: 5’-NNaaccNNNNNAGATCGGAAGAGCGTCGTGGATCCCTGATTGATGGTGC-3’
2: 5’-NNacaaNNNNNAGATCGGAAGAGCGTCGTGGATCCCTGATTGATGGTGC-3’
3: 5’-NNgccaNNNNNAGATCGGAAGAGCGTCGTGGATCCCTGATTGATGGTGC-3’
4: 5’-NNgaccNNNNNAGATCGGAAGAGCGTCGTGGATCCCTGATTGATGGTGC-3’
5: 5’-NNtccgNNNNNAGATCGGAAGAGCGTCGTGGATCCCTGATTGATGGTGC-3’
6: 5’-NNtgccNNNNNAGATCGGAAGAGCGTCGTGGATCCCTGATTGATGGTGC-3’
7: 5’-NNccggNNNNNAGATCGGAAGAGCGTCGTGGATCCCTGATTGATGGTGC-3’
8: 5’-NNttaaNNNNNAGATCGGAAGAGCGTCGTGGATCCCTGATTGATGGTGC-3’
9: 5’-NNattgNNNNNAGATCGGAAGAGCGTCGTGGATCCCTGATTGATGGTGC-3’
10: 5’-NNaggtNNNNNAGATCGGAAGAGCGTCGTGGATCCCTGATTGATGGTGC-3’
11: 5’-NNcgccNNNNNAGATCGGAAGAGCGTCGTGGATCCCTGATTGATGGTGC-3’
12: 5’-NNctaaNNNNNAGATCGGAAGAGCGTCGTGGATCCCTGATTGATGGTGC-3’
13: 5’-NNcattNNNNNAGATCGGAAGAGCGTCGTGGATCCCTGATTGATGGTGC-3’
14: 5’-NNggttNNNNNAGATCGGAAGAGCGTCGTGGATCCCTGATTGATGGTGC-3’
15: 5’-NNgtggNNNNNAGATCGGAAGAGCGTCGTGGATCCCTGATTGATGGTGC-3’
16: 5’-NNtattNNNNNAGATCGGAAGAGCGTCGTGGATCCCTGATTGATGGTGC-3’

The reaction was terminated with ExoSap-IT (ThermoFisher), RNA was hydrolyzed with NaOH and neutralized with HCl. cDNA was purified with Dynabeads MyOne silane, 5’

phosphorylated with polynucleotide kinase, and purified once more with Dynabeads MyOne silane.

cDNA was circularized with CircLigase II (Lucigen) annealed to an oligo (5'-ATCAGGGATCCACGACGCTCTTCAAAA-3') and digested with BamHI. Linearized product was purified with Dynabeads MyOne silane. qPCR was performed to determine the appropriate cycle number for preparative amplification. Library was amplified with sequencing adapters using Q5 DNA polymerase (NEB) and the following primers:

p5: 5'-AATGATACGGCGACCACCGAGATCTACACTCTTTCCCTACACGACGCTCTTCCGATCT-3'
p3: 5'-CAAGCAGAAGACGGCATACGAGATCGGTCTCGGCATTCCTGATTGATGGTGCCTACAG-3'

PCR product was size-selected on an agarose gel and purified with on a gel extraction kit (Zymo Research). The library was quantified with the NEBNext Library Quant Kit for Illumina (NEB).

Each library was pooled and sequenced on an Illumina HiSeq4000 (Novogene). Summary statistics and accession numbers are in Supplementary Table 6. Data quality control filtering was done with FastQC v0.11.5, de-multiplexed, adapters were trimmed with BBMAP 37.56, and sequences were aligned using HISAT2 v2.0.5 to a custom hg38 concatenated to the influenza A virus genome (A/WSN/33). PCR duplicates were removed by collapsing reads based on UMIs to yield a unique number of RNAs mapping to each position. The results were used as input for CLIPPER 0.1.4 to identify CLIP peaks statistically enriched over the size-matched input controls. Correlation analysis showed a high degree of overlap between replicates (Extended Data Fig. 5B)**.** Data were analyzed with IDR 2.0.03 to measure peak reproducibility across replicates (Extended Data Fig. 5C). Bedtools v2.26.0 was used for genomic data manipulation and pyGenomeTracks 2.1 was used for bigwig visualization. Motif searching and logo

generation were performed on CLIP peaks with HOMER v4.11[59]. Detailed analytical pipeline is shown below.

1. Trim fastq with BBDuk in the BBMap suite[60].
    a. bbduk_runner_CLIP.py
2. Demultiplex and slice UMIs with custom python script.
    a. debarcode.py
3. Retrim with BBDuk.
    a. bbduk_runner2.py
4. Map to human and WSN genomes.
    a. hisat2_runner.py
5. Filter out unmapped reads.
    a. preparesamforpcrdedup.py
6. PCR-deduplicate with UMIs and read-starts using custom python script.
    a. PCR_dup_remover.py
7. Call peaks with CLIPper using human and WSN genomes[61].
    a. CLIPPER_runner.py
8. Concatenate adjacent and overlapping peaks with custom python script.
    a. merge_adjacent_peaks.py
9. Count reads in CLIP peaks and size-matched input using bedtools coverage[62].
10. Perform input normalization with a Chi^2 or Fisher's exact test (depending on number of counts) with custom python script.
    a. 9+10 wrapped together in one script, input_norm.py
    b. then, mergetranscriptpeaks.py
11. Perform IDR on rep1 and rep2 to filter out un-replicating peaks. Ranking based on p value from Chi^2 or Fisher's exact test. Set IDR cutoff at 540 (p value < 0.05).
    a. run_IDR_analysis.py, https://github.com/nboley/idr
12. Cluster biotype analysis with custom python script.
    a. Intersect bed with gene_biotype.bed derived from GRCh38 gtf
    b. count_CLIP_metabiotype_new.py
13. Filter on protein-coding genes with custom python script.
14. Filter on 2 log fold-change (CLIP/input) and relative proportion of dataset (>10^\-18 average coverage) with custom python script.
    a. plot_coverage_CLIPvexpression.py
15. Intersect and segregate clusters with protein coding mRNAs with custom python script.
    a. Intersect with bed file split on 5'UTR,3'UTR, and CDS derived from GRCh38 gtf
    b. split_CLIP_meta.py
16. Calculate FPKM of CLIP origin mRNAs compared to expressed mRNAs with custom python script.
    a. fpkm_distribution.py
17. Calculate GC-content of clusters compared to all corresponding sub-mRNA regions that are expressed with custom python script.
    a. fasta_peak_to_gc_kde.py
18. Calculate length of sub-mRNA regions on CLIPped transcripts and compare to the same regions in all expressed mRNAs with custom python script.
    a. bed12_bed6_length_kde.py
19. Perform saturation analysis with custom python script by testing peak recall on sub-sampled bams with CLIPper.
    a. Sub-sample 50% of bam, determine % of peaks that can be re-discovered with half of the input data.
20. Visualization with bedtools coverage, then normalization with custom python scripts and plotting with pyGenomeTracks[63].
21. GO analysis performed with ShinyGO[64]

Electromobility shift assays

His-GST-IFIT2 and His-GST- IFIT2ΔRNA were purified based on prior approaches[29]. Briefly, proteins were expressed in *E. coli* at 16 ˚C overnight. Bacteria was lysed by sonication in high salt buffer (20 mM HEPES pH 7.4, 1 M NaCl) supplemented with 0.5 mg/ml lysozyme and 0.2 mM PMSF. Lysates were clarified by centrifugation and applied to glutathione sepharose FF (GE Life Sciences). Resin was washed extensively with high salt buffer followed by low salt buffer (20 mM HEPES pH 7.4, 150 mM NaCl). Protein was eluted with low salt buffer containing 10 mM reduced glutathione. Protein was dialyzed against an excess of low salt buffer containing 10% glycerol. Proteins were quantified by Bradford assay, assessed by gel electrophoresis, aliquoted, flash frozen in liquid nitrogen and stored at -80 ˚C until use.

Capped and poly-adenylated NP mRNA was synthesized from a PCR-generated template using the HiScribe T7 ARCA (with tailing) kit as recommended (NEB E2060S). The template was designed to mimic virally synthesized mRNA by initiating transcription at the extreme 3’ end of NP vRNA and terminating at the poly-U tract. Products were verified by formaldehyde denaturing agarose gel electrophoresis.

Protein:RNA binding reactions were performed by assembling 20 µl reactions containing ~25 nM mRNA and 0 or 2.5 µM protein in 20 mM HEPES, 150 mM NaCl, 2.5 mM $MgCl_2$, 1 mM DTT and 4U RNasin. binding was performed at room temperature for 45 min. Samples were separated on a 0.8% agarose gel at 4 ˚C. The gel was prepared and run in 1x TBE with 5 mM $MgCl_2$. After separation, the gel was stained with Sybr Gold and RNA was visualized.

qRT-PCR

RNA was isolated using TRIzol (Thermo-Fisher) and reverse-transcribed essentially as described[65] with the following modifications. Influenza mRNAs were reverse-transcribed with

in-house produced MMLV-RT at 42˚C for one hour with a uniquely-tagged poly-dT primer (tag in bold, **CGCACCAGATCGTTCGAGTCG**TTTTTTTTTTTTTTTTTTTT). Influenza vRNAs were reverse-transcribed at 42˚C in independent reactions with uniquely-tagged primers specific for the NP segment (**GGCCGTCATGGTGGCGAAT**ACCATAATGACCGATGGCCCAAGT). For normalization, 18S rRNA was reverse-transcribed in the same reactions with the uniquely-tagged primer (**CGGTCATGGTGGCGAATAA**CCAAGATCCAACTACGAGCTT)[66]. Resulting cDNA was diluted 1:10 in water, and qPCR was performed in technical duplicate or triplicate with iTaq Universal SYBR Green Supermix (Bio-Rad) in a Step One Plus RT-PCR instrument (Applied Biosystems) using the following sets of forward primers and a reverse primer identical in sequence and direction to the bolded tags described in the reverse-transcription primers:

PB2_mRNAF: AGGAGATATGGACCAGCATTAAG
PB1_mRNAF: GTATGGTGGAGGCTATGGTTT
PA_mRNAF: GAACCTGGGACCTTTGATCTT
HA_mRNAF: GTATCAGATTCTGGCGATCTACTC
NP_mRNAF: AGACCAGAAGATGTGTCTTTCC
NA_mRNAF: CTGTATGAGGCCTTGCTTCT
M_mRNAF: CTCTCGTCATTGCAGCAAATATC
NS_mRNAF: GCGGGAACAATTAGGTCAGA
NA_vRNAF: ACATCACTTTGCCGGTATCAGGGT
NP_vRNAF: CTCAATATGAGTGCAGACCGTGCT
NA_cRNAF: TGAATAGTGATACTGTAGATTGGTCT
NP_cRNAF: CGATCGTGCCCTCCTTTG
18S_F: GGCCCTGTAATTGGAATGAGTC.

Specific forward and reverse primers were used for the amplification of GAPDH and β-Actin cDNA primed by the tagged poly-dT primer:

GAPDH_F: ACCGTCAAGGCTGAGAACGG
GAPDH_R: GTGGTGAAGACGCCAGTGGA
β-Actin_F: AGAGCTACGAGCTGCCTGAC
β -Actin_R: AGCACTGTGTTGGCGTACAG

IFIT2-RIP qRT-PCR and Bioanalyzer

A549 cells were infected with WSN (MOI = 0.02) for 24 h. Cells were lysed in co-immunoprecipitation buffer (50 mM Tris pH 7.5, 150 mM NaCl, 0.5% NP40, 1x protease inhibitor cocktail (Sigma), and 20U/mL RNasin (Promega)). Clarified lysates were precleared and incubated for 16 h with 3 µg of IFIT2 antibody or rabbit IgG (Cell Signaling Technologies 2729S) in the presence of 1mg/mL BSA. Immuno-complexes were captured with protein A agarose resin (Sigma) for one hour and washed 6 times with co-immunoprecipitation buffer. 10% of the resin was reserved for western blot analysis and RNA was extracted from the remainder with TRIzol, precipitated and resuspended in 10 µl of water. An equal volume of IFIT2-bound RNA and IgG-bound RNA was used for qRT-PCR analysis. RT was performed as above and the sample was subsequently split into 8 PCRs to separately measure each viral gene. IFIT2-bound samples were normalized to IgG-bound samples using the °Ct method. RNA was visualized on an Agilent 2100 Bioanalyzer with an RNA 6000 Pico Chip following the manufacturer's instructions.

IFIT2 reporter assays

The impact of IFIT2 on NP translation was measured using the NP-2A-GFP fusion proteins. 293T cells were transfected in triplicate with constructs expressing either NP-2A-GFP, jugNP-2A-GFP or GFP alone in the presence or absence of IFIT2. Cells were stained with Hoescht 33342 48 hr post-transfection and fluorescence was quantified using a Cytation 5 spectrophotometer (BioTek). GFP and Hoescht fluorescence were measured from a 15 x 15 point grid in each well. Fold induction was calculated relative to the IFIT2-minus controls and average across all replicates.

Ribosome Profiling

Ribosome profiling was based on previous protocols and performed on two independent biological replicates[67,68]. $5x10^6$ A549 cells were plated the day prior and subsequently infected for 24 hr (MOI = 0.02 WSN). Following treatment cells were rapidly frozen *in situ* in liquid nitrogen. Cells were thawed, lysed in buffer (10 mM HEPES [pH 7.5], 100 mM KCl, 5 mM $MgCl_2$, 0.5% NP-40, 0.5% deoxycholate, 4 mM DTT, 20 U/mL RNasin, 1x protease inhibitor without EDTA), and disrupted by passage through a 23 G needle. Lysates were clarified by centrifugation and a sample was removed for total RNA analysis. The remainder was digested with RNase I (ThermoFisher AM2294) at 0.5 U/µl for 30 m at 24˚C with mixing. Reaction was quenched with RNasin and layered onto pre-formed 10-50% sucrose gradient prepared in 20mM HEPES (pH 7.5), 75 mM KCl, 5 mM $MgCl_2$, 20 U/mL RNasin, 4 mM DTT and 1x protease inhibitor without EDTA. Gradients were centrifuged in a swinging bucket rotor at 150,000 x g for 2 hrs at 4˚C. Gradients were fractionated. Monosome-containing fractions were identified by western blot, pooled and concentrated by centrifugation on a 100,000 MWCO filter. Monosomes were disrupted into large and small subunits by dilution into buffer supplemented with 50mM EDTA. Samples were centrifuged again through a 100,000 MWCO filter, this time recovering ribosome-protected RNA fragments present in the flow through. RNA was extracted with an equal volume of phenol (pH 6.8):chloroform:isoamyl alcohol (250:49:1 ratio) and precipitated from the aqueous phase following resuspension in water.

Total RNA was extracted from cell lysates using Trizol and poly A selection was performed on 10µg total RNA using magnetic oligo-dT25 beads (NEB S1419). Poly A RNA was fragmented with Mg^{2+} by heating in First Strand buffer at 94˚C for 24 m. Fragments were precipitated and resuspended in water. Fragmented poly A RNA and the ribosome protected

fragments were separated on a 15% TBE-UREA gel using 0.5x TBE. Gels were stained with SYBR gold and RNA corresponding to 27-32 nt was excised from ribosome protected samples and 25-48 nt was excised from fragmented poly A RNA. RNA was eluted from the gel, extracted with Trizol and resuspended in water.

RNAs were converted into sequencing libraries following the same approach used in the eCLIP protocol above, except with 24 unique 5-nt barcodes.

1: 5'-NNTGTCTNNNNAGATCGGAAGAGCGTCGTGGATCCCTGATTGATGGTGC-3’
2: 5'-NNGACAGNNNNAGATCGGAAGAGCGTCGTGGATCCCTGATTGATGGTGC-3’
3: 5'-NNTTGGANNNNAGATCGGAAGAGCGTCGTGGATCCCTGATTGATGGTGC-3’
4: 5'-NNCCGTTNNNNAGATCGGAAGAGCGTCGTGGATCCCTGATTGATGGTGC-3’
5: 5'-NNAACGANNNNAGATCGGAAGAGCGTCGTGGATCCCTGATTGATGGTGC-3’
6: 5'-NNACTTCNNNNAGATCGGAAGAGCGTCGTGGATCCCTGATTGATGGTGC-3’
7: 5'-NNACTCGNNNNAGATCGGAAGAGCGTCGTGGATCCCTGATTGATGGTGC-3’
8: 5'-NNTGAGANNNNAGATCGGAAGAGCGTCGTGGATCCCTGATTGATGGTGC-3’
9: 5'-NNCTCAGNNNNAGATCGGAAGAGCGTCGTGGATCCCTGATTGATGGTGC-3’
10: 5'-NNGAGACNNNNAGATCGGAAGAGCGTCGTGGATCCCTGATTGATGGTGC-3’
11: 5'-NNCGATCNNNNAGATCGGAAGAGCGTCGTGGATCCCTGATTGATGGTGC-3’
12: 5'-NNGTACTNNNNAGATCGGAAGAGCGTCGTGGATCCCTGATTGATGGTGC-3’
13: 5'-NNAGAGGNNNNAGATCGGAAGAGCGTCGTGGATCCCTGATTGATGGTGC-3’
14: 5'-NNGCACANNNNAGATCGGAAGAGCGTCGTGGATCCCTGATTGATGGTGC-3’
15: 5'-NNTCTGGNNNNAGATCGGAAGAGCGTCGTGGATCCCTGATTGATGGTGC-3’
16: 5'-NNCTCTTNNNNAGATCGGAAGAGCGTCGTGGATCCCTGATTGATGGTGC-3’
17: 5'-NNCTGTANNNNAGATCGGAAGAGCGTCGTGGATCCCTGATTGATGGTGC-3’
18: 5'-NNCACATNNNNAGATCGGAAGAGCGTCGTGGATCCCTGATTGATGGTGC-3’
19: 5'-NNATCCANNNNAGATCGGAAGAGCGTCGTGGATCCCTGATTGATGGTGC-3’
20: 5'-NNTGTTCNNNNAGATCGGAAGAGCGTCGTGGATCCCTGATTGATGGTGC-3’
21: 5'-NNTGGACNNNNAGATCGGAAGAGCGTCGTGGATCCCTGATTGATGGTGC-3’
22: 5'-NNGATCCNNNNAGATCGGAAGAGCGTCGTGGATCCCTGATTGATGGTGC-3’
23: 5'-NNGCAAGNNNNAGATCGGAAGAGCGTCGTGGATCCCTGATTGATGGTGC-3’
24: 5'-NNAAGGTNNNNAGATCGGAAGAGCGTCGTGGATCCCTGATTGATGGTGC-3’

Each library was pooled and sequenced on an Illumina NextSeq500 (NUSeq Core, Northwestern University). Ribosome protected fragments from all conditions were ~32nt long, consistent with protection afforded by a monosome. Summary statistics and accession numbers are in Supplementary Table 6. Data were analyzed with the following pipeline.

<u>Ribosome profiling analysis</u>

1. Trim fastq with BBDuk[60].
    a. bbduk_runner_ribo.py
2. Demultiplex and slice UMIs with custom python script.

   a. debarcode_ribo.py
3. Retrim with BBDuk.
   a. bbduk_runner2.py
4. Map to human rRNA contig using HISAT2[69].
   a. hisat2_runner_rRNA.py
5. Filter and retain unmapped reads.
   a. rRNAalign_refastq.py
6. Map to human and WSN genomes with splice database.
   a. Generate splice database with hisat2_extract_splice_sites.py from GRCh38 gtf
   b. hisat2_runner.py
7. Filter out unmapped reads.
   a. preparesamforpcrdedup.py
8. PCR-deduplicate with UMIs and read-starts using custom python script.
   a. PCR_dup_remover.py
9. Phase ribosomes with non-overlapping ORFs using plastid[70].
10. Count RPFs and RNAs in coding sequences using featureCounts[71]. Filter out mitochondrial mRNAs and histones.
11. Run differential expression analysis on RNA and RPF using edgeR in R script[72].
    a. The design matrix was used to program the negative binomial general linear models in EdgeR to model WT and knockout cells as two different cell types (two-factor design).
    b. Model as a full factorial experiment, then contrast the difference between IFIT2KO infection/IFIT2KO mock vs WT infection/WT mock
    c. run_edgeR.R
12. Run analysis on RNA-normalized RPFs using custom R script. Analyze these data with edgeR, modeling data from WT and knockout cells as two different cell types.
    a. dispersion factors for each gene for RNA and RPF are modeled separately and then recombined, to better look at situations in which only RNA or only RPF change with treatment.
    b. data were modeled as a full factorial experiment similar to above. This allowed the comparison of IFIT2KO infection TE/ IFIT2KO mock TE vs WT infection TE/WT mock TE, i.e. normalizing for differences in cell type before looking at the effect of IFIT2 on infection.
13. Prepare cumulative distribution frequency curves with custom python scripts, using a log cpm cutoff to 5.
    a. all listed as cumulative_distribution_CLIP*.py
14. Visualization with bedtools coverage[62], then normalization with custom python scripts and plotting with pyGenomeTracks[63]

Pause site analysis:

Identification of pause peaks:

1. Extract coverage over all expressed CDS from all RPF files using bedtools coverage[62].
2. To prevent confounding effects of alternative splicing, filter out genes that have <75% of sequence covered in RPFs and those that have average RPF coverage < 8 (~roughly corresponds to RPKM of ~10 in our datasets).
3. Remove regions where there is 0 RPF coverage.
4. Median-normalize coverage on a per-gene basis
5. Calculate slope of read coverage on a 5-nt interval over CDS per sample and per gene
   a. following prior approaches[33], the first and last 17nt of the CDS are masked to avoid identifying pause sites known to occur at start and stop codons[34].
6. Calculate the maximum change in slope over a gapped interval representing boundaries consistent with a pause ribosome (50 nt interval blocking internal 28 nt). Ascending slope is positive (m_a), descending slope is negative (m_d), max_delta_slope (m_max) = m_a-m_d.
7. Call peaks using scipy.signal find_peaks algorithm[33]. Peaks are plateau-shaped and peaks are called in the middle of plateau.
8. Combine peaks from replicate samples. Re-center peaks that overlap.

9. Combine peaks from the same conditions. Re-center over-lapping peaks.
10. Extend peaks 17-nt either side to generate the pause site and record as bed12.

Quantify peaks:

1. Count reads overlapping each pause in all datasets with bedtools coverage[62].
2. Analyze differential expression analysis on peaks using edgeR and R script[72]. Libraries were re-scaled to the size of original RPF libraries – calculate the library size and normalization factor of RPF library and replace original in DGEList with these. Each pause was modeled as an independent mRNA.
3. To produce an adjusted log2 fold change for each pause, a custom offset matrix was used where each row of the original offset matrix (loge(library_size) from 2) was transformed by taking the base e exponential to restore untransformed library size. This was multiplied by a vector containing 1's (for non-IFIT2KOixn libraries) or the fold change from log2FC_IFIT2KO/WTinfection (for IFIT2KOixn libraries). This new matrix was loge transformed and replaced the offset matrix after dispersion estimation. This effectively scales the library size of the IFIT2KO infection libraries with log2FC of the RPF libraries, preventing changes in RPF density from being called as differential pausing.
    a. Same full factorial design as RPF analysis 11+12 above
    b. In addition, use an additional contrast in glmQLFTest as a second coefficient, KO/WT infection w/ o mock normalization (or model as the same cell type). This outputs a second log2FC (simply KO/ WT infection) and a p-value after testing for differential expression of the combined effects of both coefficients. This can be used as an additional filter when looking for differential pausing.
4. Catalog these log2 fold changes as pauseI and separate sub-populations based on the maximum, median and minimum intensity pause sites present on each transcript, using normalized log2 fold changes from 3a above.
5. Determine changes in pauseI during infection of WT and IFIT2$^{-/-}$ cells by measuring changes in intensity of the maximum and minimum pause sites on each transcript.
6. Conservative comparisons of changes in pauseI at each site in WT or IFIT2$^{-/-}$ cells were made using mock-normalized data, and more general changes in pauseI were assessed using only data from infected cells. Pause sites with log2 fold change of at least 0.58 under both comparisons were considered (Supplementary Table 5).

CLIP-ribo cross analysis via pause-TE index:

1. Calculate pause-TE index as pauseI/TE using the maximum pause site for each transcript.
2. Plot cumulative distribution frequency curves with custom python scripts, filtering on RPKM > 10 in RPF libraries.
    a. all cumulative_distribution_CLIP*.py files

Polysome Pelleting

Polysome pelleting was performed essentially as described[73] with the following modifications. A549 cells were mock-infected or infected with WSN at an MOI of 1 for 6 h. Before harvest, cells were treated with 100 ug/mL cycloheximide for 5 min at 37˚C. Cells were lysed in modified polysome extraction buffer (10 mM HEPES pH 7.5, 100 mM KCl, 5 mM $MgCl_2$, 4 mM DTT, 0.5% NP-40, 100 ug/mL cycloheximide, 20 U/mL RNasin, 10%[W/V] sucrose, and 1x protease inhibitor cocktail without EDTA). Clarified lysate was split in half and one half was treated with 30 mM EDTA to dissociate ribosomes.

Western blot of polysome: Polysomes were pelleted by layering lysate onto 2.5 mL of 25% (W/V) sucrose prepared with polysome cushion buffer (20 mM HEPES pH 7.5, 75 mM KCl, 5 mM $MgCl_2$, 4 mM DTT, 20 U/mL RNasin, 100 µg/mL cycloheximide, 1x protease inhibitor cocktail without EDTA, and +/- 30 mM EDTA) followed by centrifugation in an SW41 rotor at 150,000 x g (29,500 rpm) for 4 h at 4˚C. The supernatant was removed and the pelleted protein was dissolved in 1x SDS-PAGE sample buffer with gentle shaking at 60˚C for 30 mins. Samples were analyzed by western blot.

qRT-PCR of RNA from high molecular weight polysomes: A fraction of the cell lysate was reserved as an input control. High molecular weight polysomes were pelleted by layering cell lysates onto 2.5 mL of 37.5% (W/V) sucrose prepared with polysome cushion buffer followed by centrifugation a in an SW41 rotor at 150,000 x g (29,500 rpm) for 2 h at 4˚C. The supernatant was removed and RNA was extracted from pelleted polysomes and the corresponding input samples with TRIzol, pelleted and re-dissolved in water. The abundance of NP mRNA in the polysome pellet relative to total RNA was calculated using the °°Ct method with18S rRNA as reference control. Data were then presented as fold-enrichment in the polysome pellet.

Polysome profiling

Polysome profiling was based on published protocols[74,75]. A549 cells were mock-infected or infected with WSN at an MOI of 1 for 6 h. Cells were treated with 100 µg/mL cycloheximide for 5 min at 37˚C prior immediately prior to lysing in polysome extraction buffer. Clarified lysate was split in half and one half was treated with 30 mM EDTA to dissociate ribosomes. Lysate corresponding to a cell equivalent of ~10 OD_{260} was layered on 12.5 mL linear 10-50% (W/V)

sucrose gradients prepared with polysome cushion buffer. Samples were centrifuged in an SW41 rotor at 210,000 x *g* (35,000 rpm) for 2 h at 4˚C.

Gradients were separated on a Teledyne ISCO gradient fractionation system outfitted with a Foxy JR fraction collector. Sixteen equal fractions were collected using the “time” setting on the fraction collector while continuously monitoring absorbance of the gradient using a UA-5 detector and a Type-6 optical unit equipped with a 260 nm filter. The analog voltage output of the detector was converted to a digital signal and recorded every 10 milliseconds to plot an absorbance trace.

RNA was isolated from polysome profiles by extracting 200 µl of each fraction with TRIzol and dissolving the RNA in 20 µl of water. qRT-PCR analysis was performed for NP and β-actin mRNA using the percent-total normalization technique[76]. Western-blots were directly performed on all gradient fractions after addition of 5x SDS-PAGE sample buffer.

Caspase activation

Induction of apoptosis was quantified by measuring caspase 3 and caspase 7 activity with the Caspase-Glo 3/7 Assay (Promega). For virally induced apoptosis, WT or knockout MEFs were infected at an MOI of 0.01 and measured at the indicated times. For IFIT2-mediated apoptosis, IFIT2 was expressed in 293T cells for 72 h prior to measuring caspase activity. To measure virus production when caspase activity was inhibited, A549 cells were inoculated with WSN at an MOI of 0.3 and the infection was allowed to proceed for 24 h to establish robust replication. Media and any virus produced during the first 24 h were removed and replaced with fresh media containing increasing concentrations of Z-VAD-FMK (EMD Millipore) or the DMSO solvent. Cells were incubated for an additional 8 h. Caspase activity was measured and virus produced during this period was quantified by plaque assay.

Statistics and Reproducibility

Unless otherwise noted, data represent means ± standard deviations (n=3 or more technical replicates) and are representative of at least three independent biological replicates. Excel (16.15) and Prism 8 were used for graphing and statistical analyses. Pairwise comparisons were made using a Student's T test. Multiple comparison were performed by a one-way ANOVA with *post hoc* Tukey's HSD. Significance was defined as $P< 0.05$ and is indicated when necessary with an asterisk (*). Double (**) or triple (***) asterisks are denoted where $P <0.01$ or $P < 0.001$, respectively. Analyses used for eCLIP and ribosome profiling are indicated within their respective protocols. Cumulative distribution frequencies were compared using a Mann-Whitney U test.

Data availability

Data supporting the findings of this study are available within the paper and its Supplementary Information and Tables, with the exception of raw data for eCLIP and ribosome profiling which are accessible as BioProject PRJNA633047 containing BioSample accessions SAMN14931303- SAMN14931312 and SRA accession SRR11794832-SRR11794851 (Supplementary Table 6). All other data are available from the corresponding author upon reasonable request.

Code Availability

Existing code used for data analysis are described above. Custom code and pipelines are described above, available at https://github.com/mehlelab/ or from the corresponding author upon request.

Acknowledgements

This work was supported by the National Institutes of Health R21AI125897 and R01AI125271, the UW2020:WARF Discovery Initiative, and a Shaw scientist award to A.M., an NIH National Service Award T32 GM07215 to V.T., a National Science Foundation grant GRFP DGE-1747503 to M.P.L., R01AI104972 to M.S.D, a R01AI118938 to A.C.B. the German Research Foundation (DFG; SFB 1160, project 13) to M.S., the Excellence Initiative of the German Research Foundation (GSC-4, Spemann Graduate School) and the Ministry for Science, Research and Arts of the State of Baden-Wuerttemberg to T.T., U19AI106754 to C.B, and HHSN272201400008C - Center for Research on Influenza Pathogenesis (CRIP), a NIAID-funded Center of Excellence for Influenza Research and Surveillance (CEIRS), and U19AI135972 A.G-S. A.M. holds an Investigators in the Pathogenesis of Infectious Disease Award from the Burroughs Wellcome Fund. We thank D. Poole for technical assistance, members of the Mehle laboratory, M. Harrison, C. Fraser, S. Floor and J.D. Sauer for valuable input and C. Li, N. Reich, P. Friesen, Y. Kawaoka, L. Ristow, and R. Welch for sharing reagents.

Supplementary Tables

Supplementary Table 1. Top hits from genome-wide CRISPR-Cas9 screen following sequential challenge with IAV-G or IAV-G and IAV.

Supplementary Table 2. Top hits from genome-wide CRISPR-Cas9 screen following challenge with SC35M Flu-GFP.

Supplementary Table 3. IFIT2-bound transcripts. IFIT2 CLIP; GO biological processes; ShinyGO meta-analysis; ISG Chi^2; ISGs

Supplementary Table 4. Changes in ribosome occupancy in IFIT2-knockout cells. Infection ribosome profiling; ΔTE of CLIPped ISGs

Supplementary Table 5. IFIT2-dependent ribosomal pausing.

Supplementary Table 6. Sequencing statistics and Sequence Read Archive identifiers for CLIP and ribosomal profiling data.

All supplementary tables available with the online version of the published manuscript: https://doi.org/10.1038/s41564-020-0778-x

Extended Data

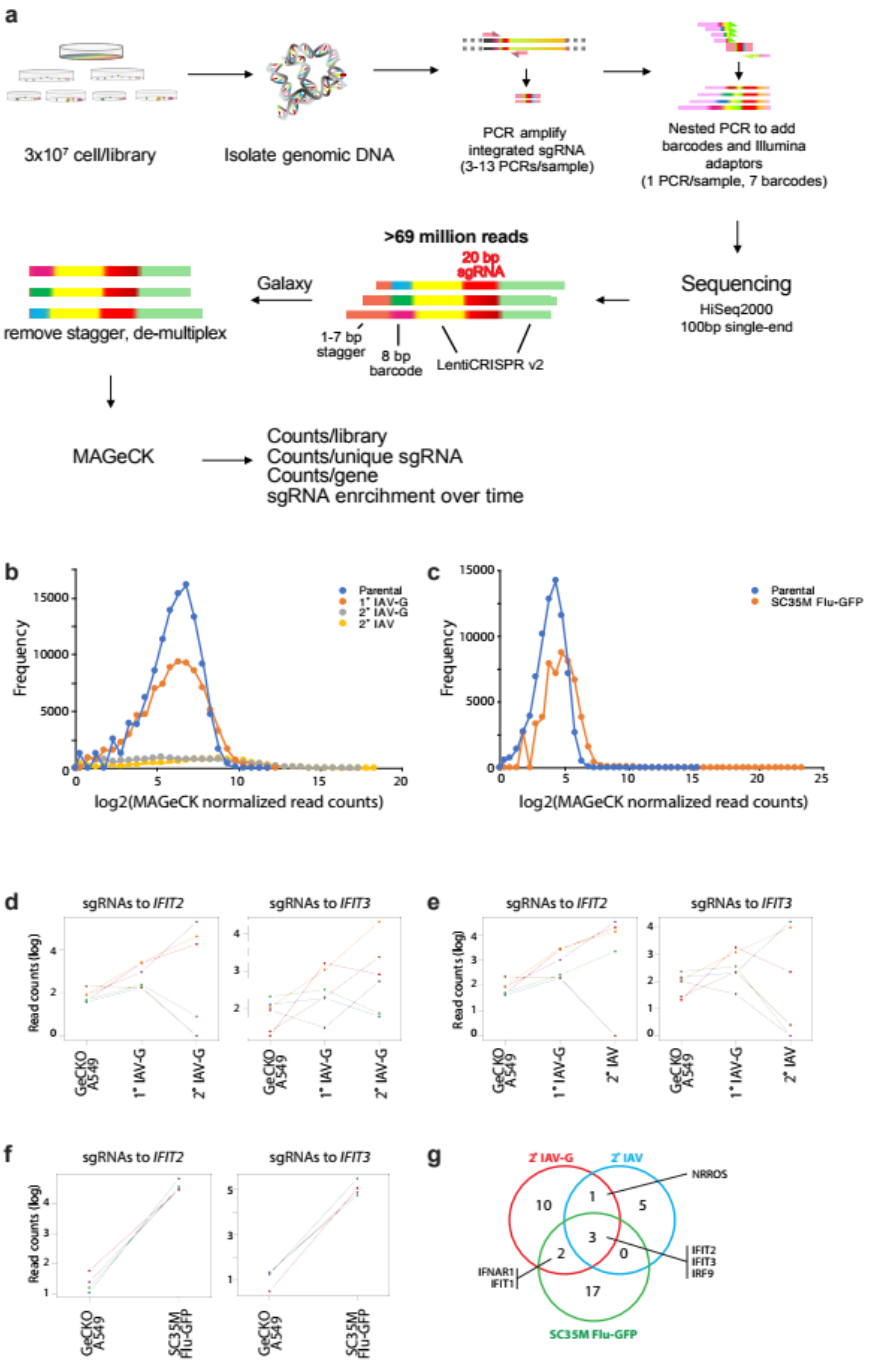

Extended Data Figure 1. Enrichment of IFIT2 and IFIT3 over sequential influenza virus selections. **a,** Schematic for hit analysis and selection. **b-c,** Frequency distribution of sgRNAs present in the parental libraries and those following selection with WSN (b) or SC35M Flu-GFP (c). **d-f,** sgRNA enrichment trajectories following (d) sequential IAV-G selections, (e) IAV-G followed by *bona fide* influenza virus (WSN) infection or (f) selection with SC35M Flu-GFP. The abundance of each sgRNA targeting the indicated gene is shown. **g**, Overlap between top hits from each screen. A conservative cut-off of RRA<10^5 was used to define top hits.

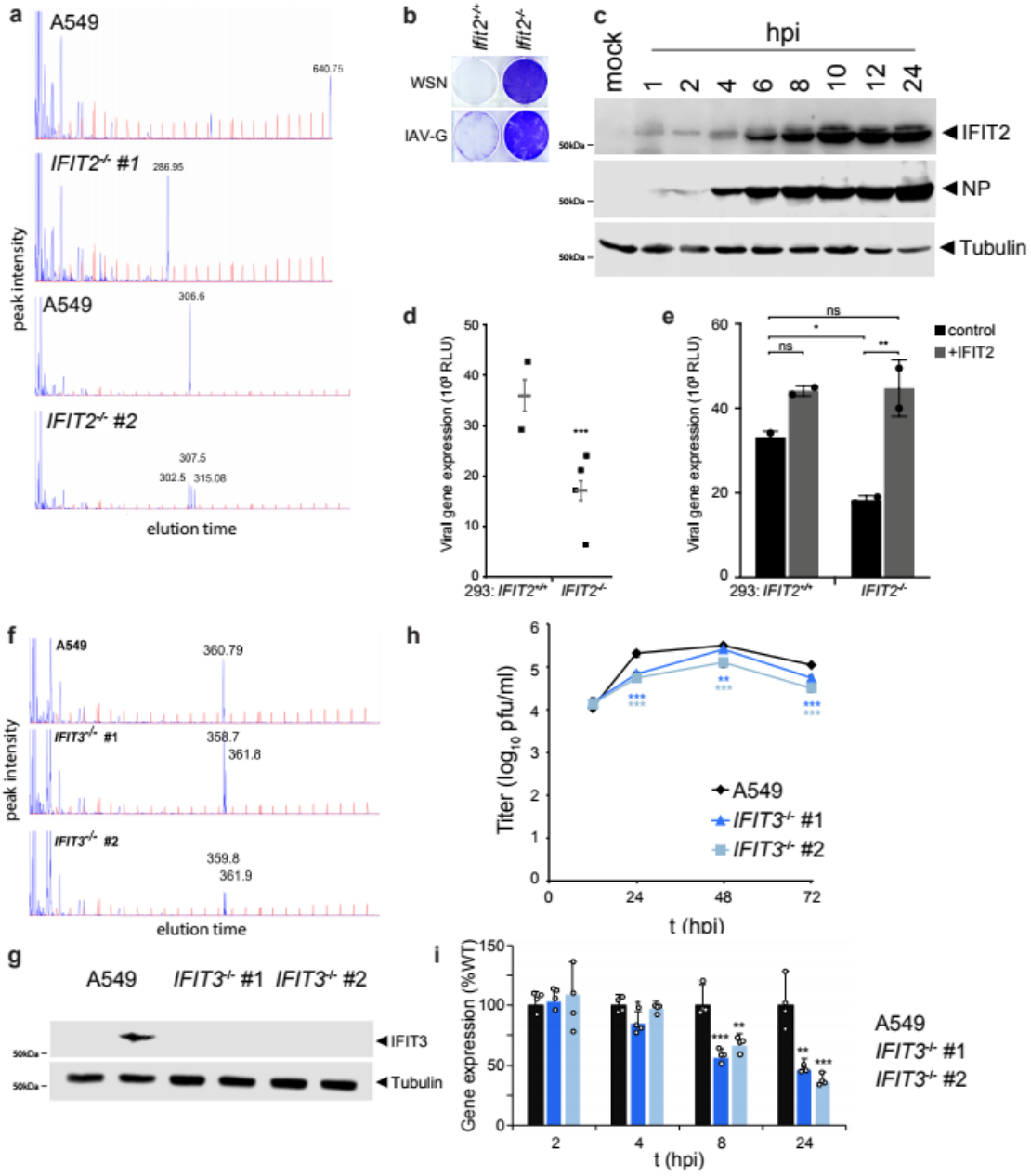

Extended Data Fig. 2 Characterization of replication and protein expression in the presence or absence of IFIT2 or IFIT3.a, Two IFIT2-/- clones were created in A549 cells by CRISPR/Cas9 mutagenesis using distinct sgRNAs. Homozygous knockouts were identified by IDAA (indel detection by amplicon analysis). Chromatographs are shown for WT and mutant amplicons from IFIT2 knockout line #1 targeting AGAACGCCATTGACCCTCTG and IFIT2 knockout line #2 targeting GGCCAGTAGGTTGCACATTG. Size standards appear in red and amplicon peaks are shown in blue with calculated sizes in nucleotides listed above each peak. **b**, Ifit2-/- MEFS survive infection. WT and knockout cells were challenged with WSN or IAV stably encoding VSV-G (IAV-G). Surviving cells were visualized by staining with crystal violet. **c**, Kinetics of IFIT2 and NP expression were determined by infecting A549 cells with WSN (MOI = 0.2) and measuring protein expression by western blotting samples acquired at the indicated times post-infection. **d**, Clonal WT or IFIT2-/- 293 cells were infected with an IAV (WSN) reporter virus at an MOI = 0.01 and viral gene expression was measured 8 hpi. Each

point represents mean gene expression (n = 4) from 4 independent clonal knockout lines. The mean of all lines is shown as a gray bar ± SEM. **e**, IFIT2 was expressed in WT 293 cells (clonal line 1B8) or IFIT2-/- knockout 293 cells (clonal line 3B9) for 12 hr followed by infection with an IAV (WSN) reporter virus (MOI = 0.1) for 8 hr. n = 2 independent infections. **f**, Two homozygous IFIT3-/- clones were identified by IDAA. Chromatographs are shown for WT and mutant amplicons from IFIT3 knockout lines #1 and #2 targeting CACTGCGGAGGACATCTGTT. Size standards appear in red and amplicon peaks are shown in blue with calculated sizes in nucleotides listed above each peak. **g**, Infection-induced IFIT3 expression was monitored in WT and IFIT3 knockout cells by western blotting. **h**, Multi-cycle replication of WSN in wildtype or IFIT3 knockout A549 human lung cells. Data represent mean ± standard deviation (n = 3 independent infections). **i**, Viral gene expression in wildtype or IFIT3 knockout cells infected with an influenza reporter virus for the indicated times. Data represent mean + sd (n = 4 independent infections). (*** $p < 0.001$; two-tailed Student's t-test for pairwise comparisons between control and knockout clonal lines in d; * $p < 0.05$; ** $p < 0.01$ one-way ANOVA with post hoc Tukey's HSD for e, h and i).

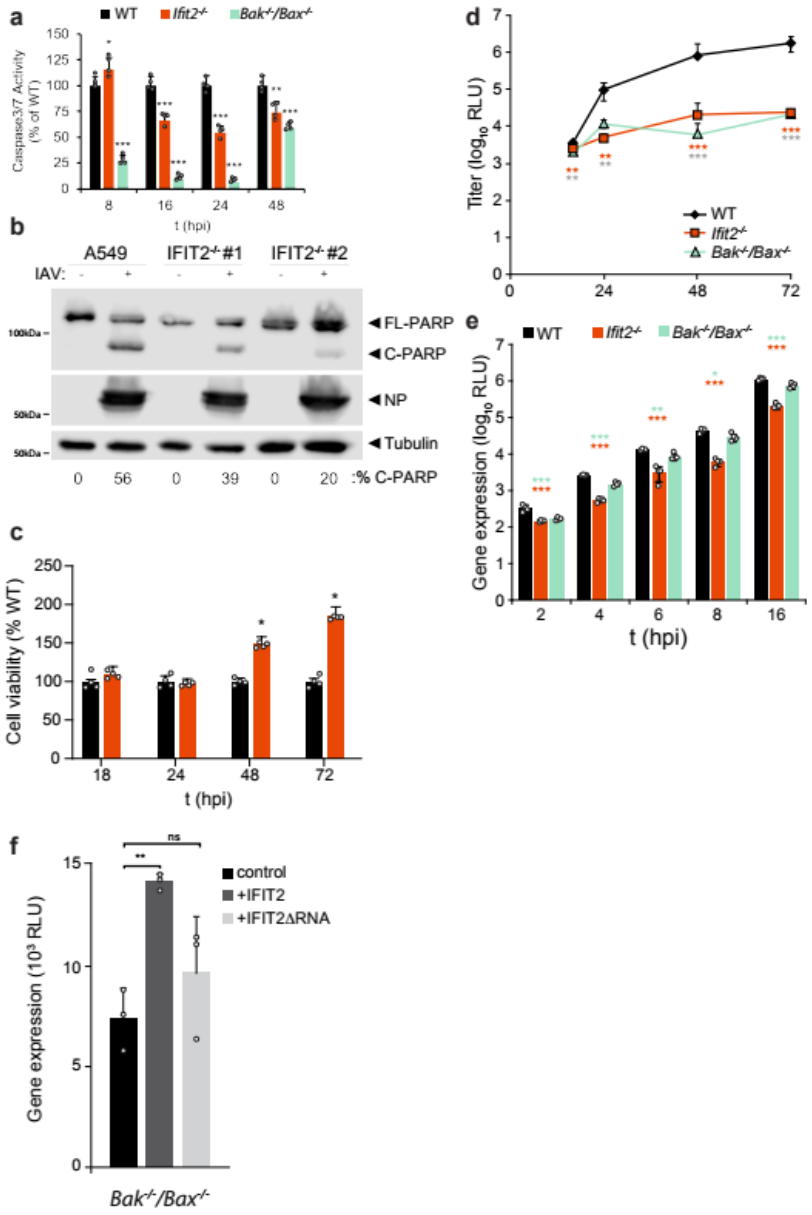

Extended Data Fig. 3 Human IFIT2 and murine Ifit2 promote virus-induced apoptosis. a, Caspase 3/7 activity was measured in wildtype, Ifit2-/-, and Bak/Bax-/- MEFs infected with WSN at an MOI of 0.01 for the indicated times. n = 4 independent infections ± standard deviation. **b**, Expression of cleaved (C-PARP) versus full-length (FL-PARP) PARP-1 in IAV infected A549 and IFIT2 knockout cell lines. Protein bands were quantified and the percent C-PARP of total PARP signal normalized to a tubulin loading control is indicated below. **c**, Viability of Ifit2-/- cells during infection with WSN assessed by CellTiter Glo Assay at the indicated time points. n = 4 independent infections ± standard deviation. **d**, Multicycle replication of WSN reporter virus in in WT, Ifit2-/-, and Bak/Bax-/- MEFs. n = 3 independent infections ± standard deviation. **e**, Single-cycle WSN reporter virus gene expression at early time points post-infection in WT, Ifit2-/-, and Bak/Bax-/- MEFs. n = 4 independent infections ± standard deviation. **f**, WSN reporter virus gene expression in Bak/Bax-/- cells ectopically expressing an empty vector, hIFIT2, or hIFIT2-ΔRNA. n = 3 independent infections ± standard deviation. *p < 0.05, **p < 0.01; *** p < 0.001; Two-tailed Student's T-test for pairwise comparisons (c) or one-way ANOVA with post hoc Tukey's HSD for multiple comparisons to WT cells (a, d, e and f). All data are plotted as mean ± sd.

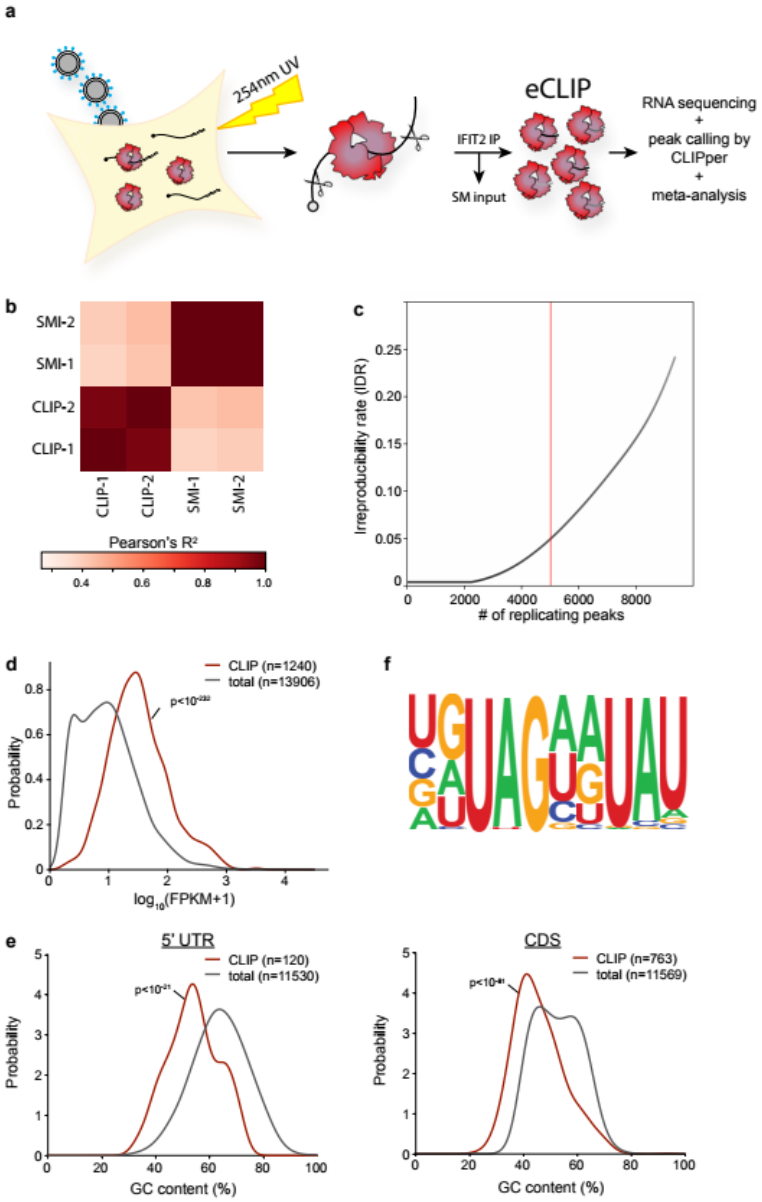

Extended Data Fig. 4 Analysis of IFIT2 CLIP-Seq data. a, Experimental workflow for eCLIP of IFIT2 from IAV WSN-infected A549 cells. RNA-protein adducts were formed in infected cells by UV cross-linking. Lysates were prepared and RNA was partially digested with RNase. A fraction of lysate was removed to serve as the size-matched input control (SM input). IFIT2 was immunopurified and bound RNAs were processed via eCLIP followed by sequencing and analysis. **b**, CLIP-Seq was performed in duplicate and compared for IFIT2 CLIP or size-matched input (SMI) controls. Pearson's correlation coefficient is shown as a heatmap. **c**, Concordance between ranked peaks in two independent biological replicates of IFIT2 CLIP-Seq was assessed by calculating an irreproducible discover rate (IDR). A conservative threshold of 5% was used to identify significant peaks. **d**, Abundance distribution in the size-matched input control for all transcripts and those with IFIT2 CLIP peaks. Populations were compared by a two-sided Mann-Whitney U-test. **e**, Meta-analysis of GC content for peaks identified in the 5' UTR and coding sequence (CDS) of bound transcripts. IFIT2-bound RNAs were compared to all expressed 5' UTRs or CDS via a two-sided Mann-Whitney U-test. **f**, A degenerate UAGnnUAU motif was found in ~20% of IFIT2 CLIP peaks ($p = 10^{-279}$ compared to background).

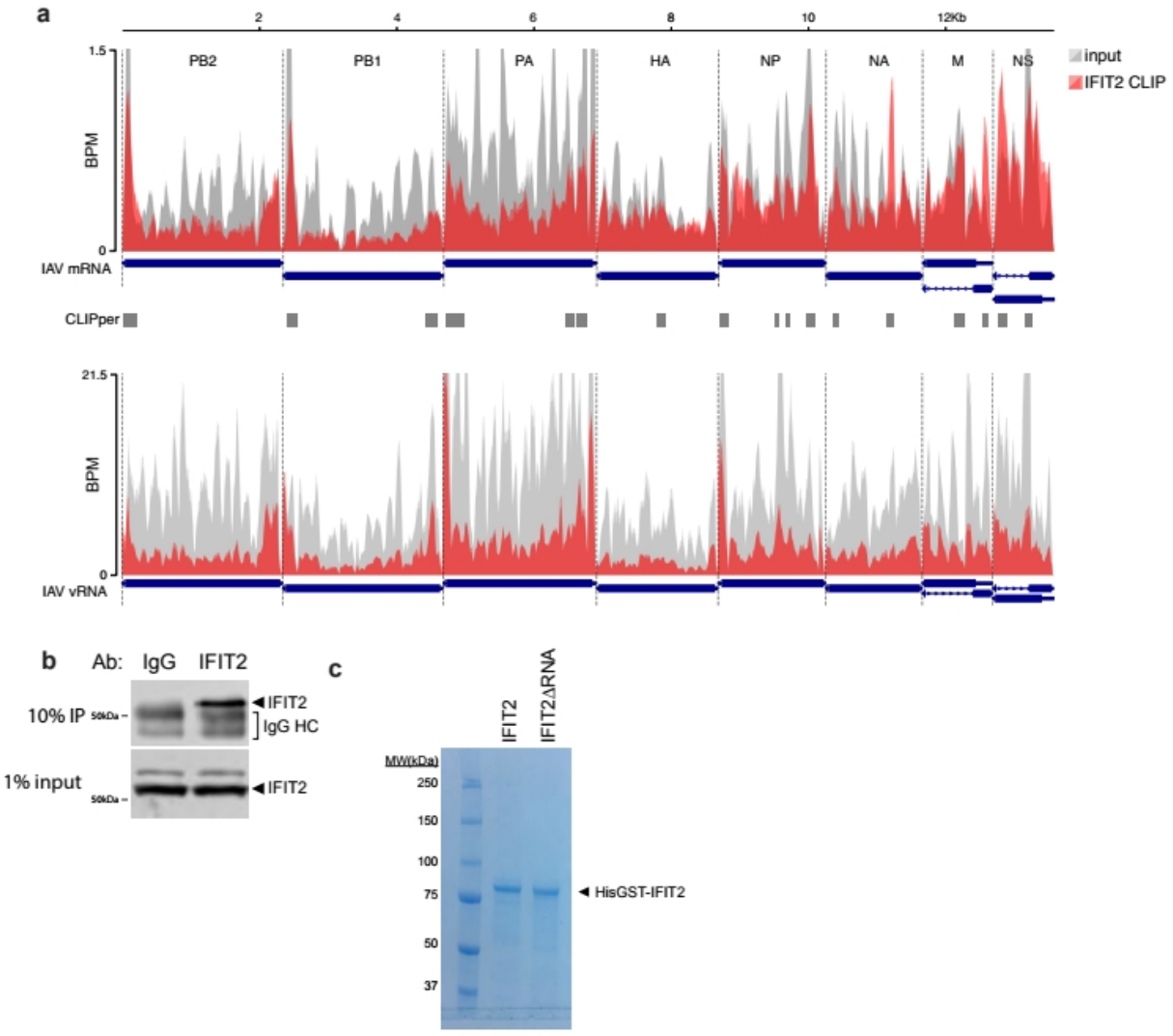

Extended Data Fig. 5 IFIT2 binds viral mRNA but not genomic vRNA. a, IFIT2 CLIP-Seq was performed on WSN infected cells. Reads were mapped to viral mRNA (top) or genomic vRNA (bottom) and analyzed with CLIPper. No CLIP peaks were identified on the genomic RNA. Data from biological duplicates of size-matched input controls or IFIT2 CLIP are plotted as mean and standard deviation using dark and light shades of the same color, respectively. BPM = bins per million. **b**, Western blot of immunoprecipitated IFIT2 or IgG controls used for RIP-qRT-PCR shown in Fig. 3e. **c**, Recombinant HisGST-IFIT2 used for EMSA analysis in Fig. 3f was expressed and purified from E. coli. Protein integrity and purity was verified by gel electrophoresis and Coomassie staining. IFIT2ΔRNA = R212E/K410E mutant.

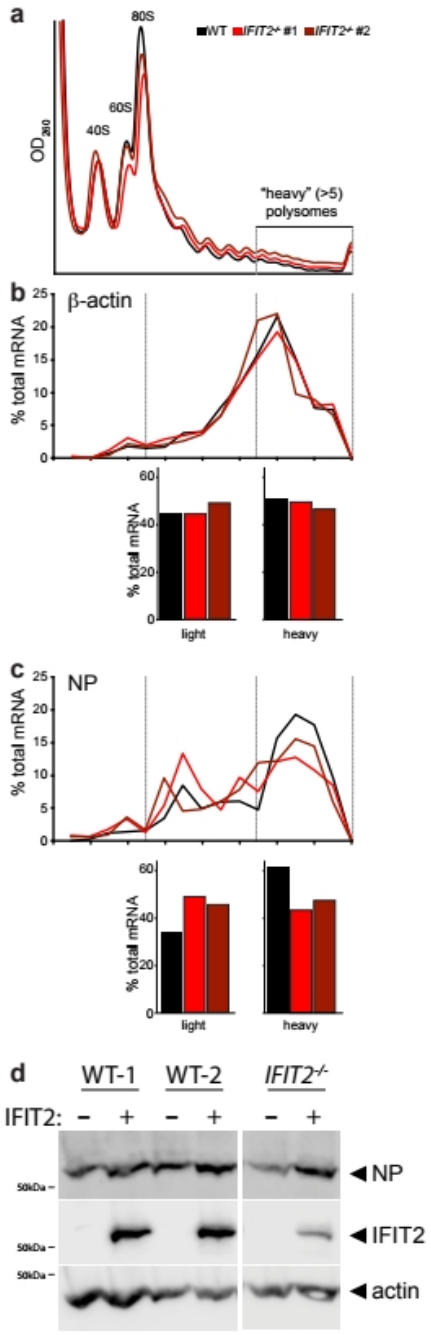

Extended Data Fig. 6 IFIT2 enhances the translational efficiency of influenza virus NP mRNA. a–c, Full dataset underlying results presented in Fig. 4d. Polysome profiling was performed on WT and IFIT2-/- A549 cells infected with WSN. a, The polysome profile is shown again for clarity. b, qRT-PCR quantification of β-actin or c, NP mRNA in each fraction. The sum of less efficiently translated mRNA present in "light" polysome fractions (5 or less ribosomes per message) or efficiently translated mRNA in "heavy" polysome fractions (>5 ribosomes per message) is shown under each trace. Loss of IFIT2 shifts NP mRNA towards the top of the gradient, indicating less efficient translation than in WT cells. **d,** IFIT2-/- 293 cells or two clones of WT cells were transfected with an IFIT2 expression vector or an empty vector control prior to infection with WSN. Proteins were detected by western blot.

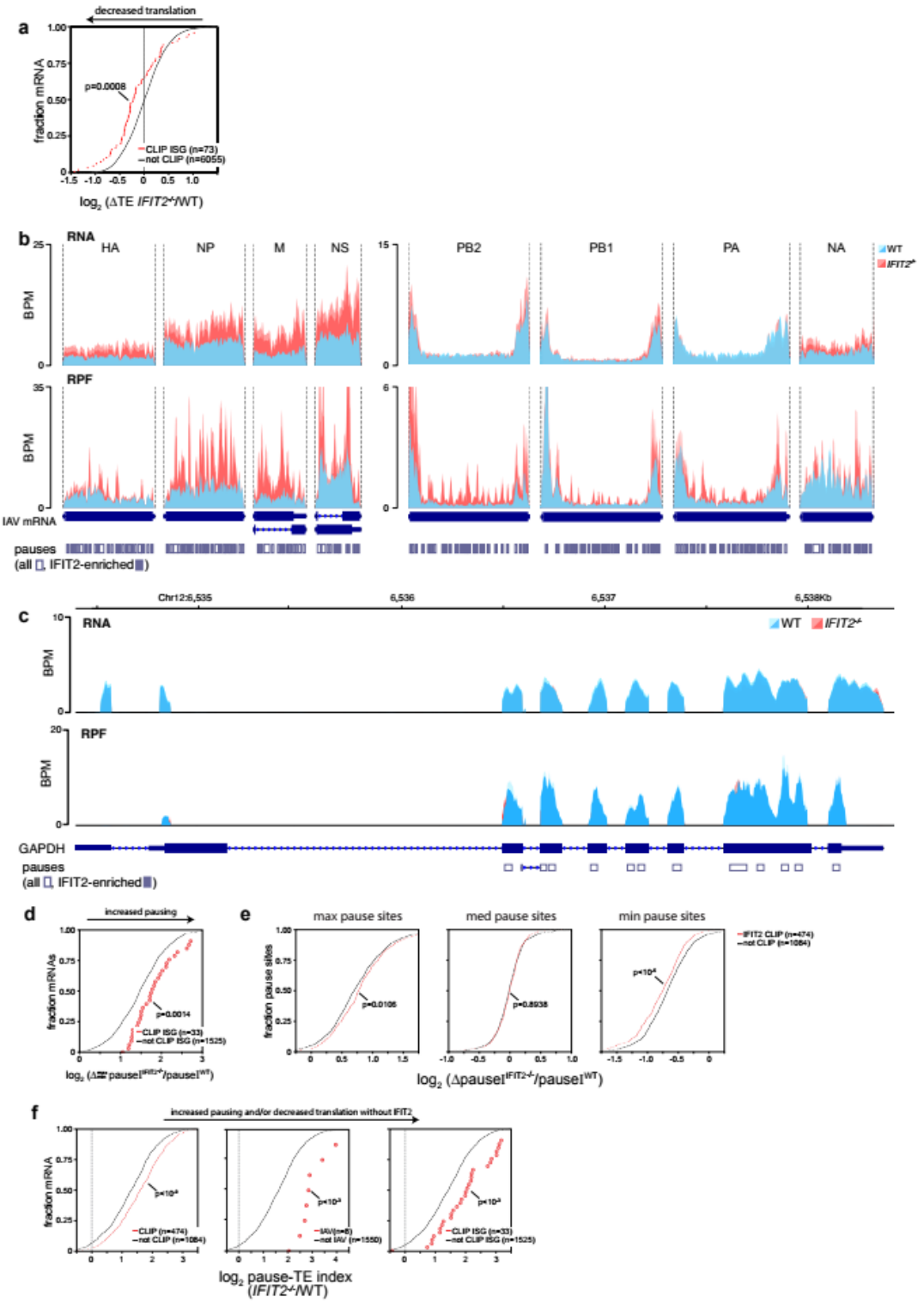

Extended Data Fig. 7 Loss of IFIT2 results in ribosomal pausing that decreases translation and increases pausing of IFIT2-bound mRNAs. Ribosome dynamics were monitored in cells infected with IAV WSN. **a**, The translational efficiency of IFIT2-bound ISG mRNAs is decreased in the absence of IFIT2. Bound transcripts were compared to unbound transcripts via a two-sided Mann-Whitney U-test. **b-c**, Accumulation of paused ribosomes in the absence of IFIT2. Normalized read density for total RNA

(top) and ribosome-protected fragments (RPFs) (bottom) mapping to IAV mRNAs (b) or GAPDH (c) in infected WT and IFIT2-/-cells. A close-up view of NP is shown in Fig. 5c. Data from replicate experiments are plotted as mean and standard deviation using dark and light shades of the same color, respectively. Pause sites are shown below. Pause sites enriched in IFIT2-/- cells >1.5-fold are filled in. High coverage at the 5' and 3' end of PB2, PB1 and PA is consistent with low levels of defective-interfering (DI) particles commonly found in laboratory viral stocks. Note that there are no IFIT2-dependent pause sites identified on GAPDH mRNA. BPM = bins per million. **d**, Ribosome pausing increases during infection of IFIT2-/- cells. Changes in pause intensity (pauseI) between the maximum and minimum pauseI sites on each transcript were calculated during infection of WT and IFIT2-/- cells. **e**, Transcripts contain multiple pause sites. The pause sites with the minimum, median and maximum pauseI were identified. The effect of IFIT2 on pausing for each of these classes was determined by comparing IFIT2-bound transcripts to unbound transcripts. In the absence of IFIT2, pauseI increases at the strongest pause sites (maximum) while it is reduced at the weakest pause sites (minimum). The median pause sites are unchanged. **f**, Increased pausing and decreased translation are correlated for IFIT2-bound mRNAs. The relationship between pausing and translation efficiency was assessed by calculating a pause-TE index (pauseImax/TE) for each transcript. Changes in the pause-TE index were assessed for IFIT2-bound mRNAs (left), IAV mRNAs (middle), and ISG mRNAs (right). Comparisons in (d–f) were performed via a two-sided Mann-Whitney U-test.

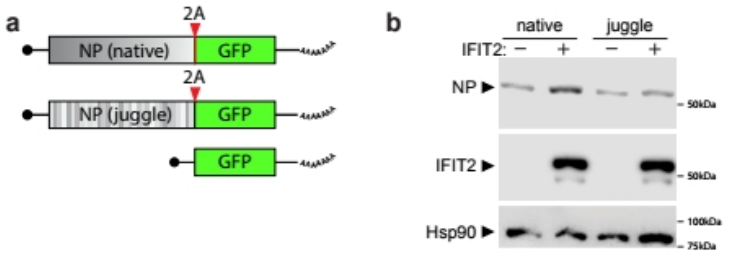

Extended Data Fig. 8 Sequence-dependent enhancement of NP translation in the presence of IFIT2. **a**, Diagram of NP-2A-GFP polyprotein. For cell-based assays in Fig. 5f, NP was expressed as a polyprotein where NP was separated from GFP by the 2A cleavage sequence from porcine teschovirus. NP is shaded to represent the codon juggling that introduced silent mutations to NPjug. See Methods for details. **b**, NP was expressed in 293T cells from a gene encoding WT or juggled codons for only NP, and not a polyprotein. IFIT2-V5 was co-expressed where indicated. Expression was detected by western blot, including Hsp90 as a loading control.

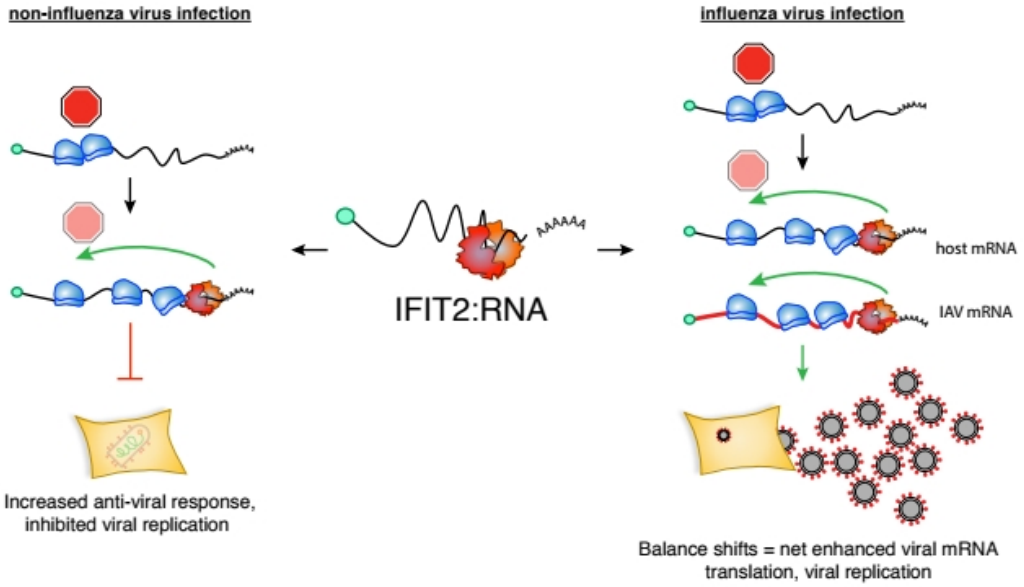

Extended Data Fig. 9 Classic "antiviral" proteins can be re-purposed during infection into pro-viral effectors. A model for the dichotomous functions of IFIT2. IFIT2 enhances translation of host mRNAs, including ISGs, to exert antiviral activity to diverse viruses. Yet, as shown here, IFIT2 is re-purposed during influenza virus infection to increase translation of viral mRNAs and shift the balance resulting in a net increase in viral mRNA translation and viral replication.

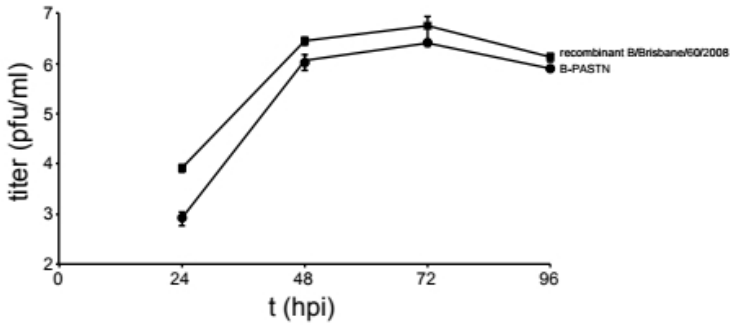

Extended Data Fig. 10 Replication kinetics of recombinant B/Brisbane/60/2008 and the reporter virus B/Brisbane/60/2008-PASTN. An influenza B reporter virus encoding NanoLuc in the PA gene segment (see Methods for details). Infections were performed in MDCK cells (MOI = 0.01) at 33 ˚C and viral titers were determined by plaque assay at the indicated time points. Data are mean of n = 3 independent infection ± standard deviation.

References

1. Iwasaki, A. & Pillai, P. S. Innate immunity to influenza virus infection. *Nat. Rev. Immunol.* **14**, 315–28 (2014).
2. Downey, J., Pernet, E., Coulombe, F. & Divangahi, M. Dissecting host cell death programs in the pathogenesis of influenza. *Microbes Infect.* (2018). doi:10.1016/J.MICINF.2018.03.005
3. Krammer, F. *et al.* Influenza. *Nat. Rev. Dis. Prim.* **4**, 3 (2018).
4. Wang, D., Zhu, W., Yang, L. & Shu, Y. The Epidemiology, Virology, and Pathogenicity of Human Infections with Avian Influenza Viruses. *Cold Spring Harb. Perspect. Med.* (2020). doi:10.1101/cshperspect.a038620
5. Long, J. S., Mistry, B., Haslam, S. M. & Barclay, W. S. Host and viral determinants of influenza A virus species specificity. *Nat. Rev. Microbiol.* **17**, 67–81 (2019).
6. Carette, J. E. E. *et al.* Haploid genetic screens in human cells identify host factors used by pathogens. *Science* **326**, 1231–5 (2009).
7. Heaton, B. E. *et al.* A CRISPR Activation Screen Identifies a Pan-avian Influenza Virus Inhibitory Host Factor. *Cell Rep.* **20**, 1503–1512 (2017).
8. Li, B. *et al.* Genome-wide CRISPR screen identifies host dependency factors for influenza A virus infection. *Nat. Commun.* **11**, 164 (2020).
9. Han, J. *et al.* Genome-Wide CRISPR/Cas9 Screen Identifies Novel Host Factors Essential for Influenza Virus Replication. *CellReports* **23**, 596–607 (2018).
10. Schaack, G. A. & Mehle, A. Experimental approaches to identify host factors important for influenza virus. in *Influenza: The Cutting Edge* (eds. Neumann, G. & Kawaoka, Y.) In Press (Cold Spring Harbor Laboratory Press, 2019). doi:10.1101/cshperspect.a038521
11. Hao, L. *et al.* Drosophila RNAi screen identifies host genes important for influenza virus replication. *Nature* **454**, 890–3 (2008).
12. Diamond, M. S. & Farzan, M. The broad-spectrum antiviral functions of IFIT and IFITM proteins. *Nat. Rev. Immunol.* **13**, 46–57 (2013).
13. Fensterl, V. & Sen, G. C. Interferon-Induced Ifit Proteins: Their Role in Viral Pathogenesis. *J. Virol.* **89**, 2462–2468 (2015).
14. Li, Y. *et al.* ISG56 is a negative-feedback regulator of virus-triggered signaling and cellular antiviral response. *Proc. Natl. Acad. Sci. U. S. A.* **106**, 7945–7950 (2009).
15. Pichlmair, A. *et al.* IFIT1 is an antiviral protein that recognizes 5’-triphosphate RNA. *Nat. Immunol.* **12**, 624–30 (2011).
16. Daffis, S. *et al.* 2’-O methylation of the viral mRNA cap evades host restriction by IFIT family members. *Nature* **468**, 452–456 (2010).
17. Schoggins, J. W. *et al.* Pan-viral specificity of IFN-induced genes reveals new roles for cGAS in innate immunity. *Nature* **505**, 691 (2014).
18. Szretter, K. J. *et al.* 2’-O methylation of the viral mRNA cap by West Nile virus evades

Ifit1-dependent and -independent mechanisms of host restriction in vivo. *PLoS Pathog.* **8**, (2012).

19. Terenzi, F., Saikia, P. & Sen, G. C. Interferon-inducible protein, P56, inhibits HPV DNA replication by binding to the viral protein E1. *EMBO J.* **27**, 3311–3321 (2008).
20. Fensterl, V. *et al.* Interferon-induced Ifit2/ISG54 protects mice from lethal VSV neuropathogenesis. *PLoS Pathog.* **8**, (2012).
21. Pinto, A. K. *et al.* Human and Murine IFIT1 Proteins Do Not Restrict Infection of Negative-Sense RNA Viruses of the Orthomyxoviridae, Bunyaviridae, and Filoviridae Families. *J. Virol.* **89**, 9465–76 (2015).
22. Daugherty, M. D., Schaller, A. M., Geballe, A. P. & Malik, H. S. Evolution-guided functional analyses reveal diverse antiviral specificities encoded by IFIT1 genes in mammals. *Elife* **5**, 1–22 (2016).
23. Stawowczyk, M., Van Scoy, S., Kumar, K. P. & Reich, N. C. The interferon stimulated gene 54 promotes apoptosis. *J. Biol. Chem.* **286**, 7257–7266 (2011).
24. Fleith, R. C. *et al.* IFIT3 and IFIT2/3 promote IFIT1-mediated translation inhibition by enhancing binding to non-self RNA. *Nucleic Acids Res.* **46**, 5269–5285 (2018).
25. Johnson, B. *et al.* Human IFIT3 Modulates IFIT1 RNA Binding Specificity and Protein Stability. *Immunity* **48**, 487–499 (2018).
26. Benitez, A. A. *et al.* In Vivo RNAi Screening Identifies MDA5 as a Significant Contributor to the Cellular Defense against Influenza A Virus. *Cell Rep* **11**, 1714–1726 (2015).
27. Tran, V., Moser, L. A., Poole, D. S. & Mehle, A. Highly sensitive real-time in vivo imaging of an influenza reporter virus reveals dynamics of replication and spread. *J. Virol.* **87**, 13321–13329 (2013).
28. Tran, V. *et al.* Multi-Modal Imaging with a Toolbox of Influenza A Reporter Viruses. *Viruses* **7**, 5319–5327 (2015).
29. Yang, Z. *et al.* Crystal structure of ISG54 reveals a novel RNA binding structure and potential functional mechanisms. *Cell Res.* **22**, 1328–1338 (2012).
30. Takizawa, T. *et al.* Induction of programmed cell death (apoptosis) by influenza virus infection in tissue culture cells. *J. Gen. Virol.* **74 (Pt 11**, 2347–55 (1993).
31. Mühlbauer, D. *et al.* Influenza Virus-Induced Caspase-Dependent Enlargement of Nuclear Pores Promotes Nuclear Export of Viral Ribonucleoprotein Complexes. *J. Virol.* **89**, JVI.03531-14 (2015).
32. Wurzer, W. J. *et al.* Caspase 3 activation is essential for efficient influenza virus propagation. *EMBO J.* **22**, 2717–28 (2003).
33. Ingolia, N. T., Lareau, L. F. & Weissman, J. S. Ribosome Profiling of Mouse Embryonic Stem Cells Reveals the Complexity and Dynamics of Mammalian Proteomes. *Cell* **147**, 789–802 (2011).
34. Wolin, S. L. & Walter, P. Ribosome pausing and stacking during translation of a

eukaryotic mRNA. *EMBO J.* **7**, 3559–3569 (1988).

35. Mar, K. B. *et al.* LY6E mediates an evolutionarily conserved enhancement of virus infection by targeting a late entry step. *Nat. Commun.* **9**, 3603 (2018).

36. Seo, J., Yaneva, R., Hinson, E. R. & Cresswell, P. Human cytomegalovirus directly induces the antiviral protein viperin to enhance infectivity. *Science (80-.).* **332**, 1097–1100 (2011).

37. Xie, M. *et al.* Human Cytomegalovirus Exploits Interferon-Induced Transmembrane Proteins To Facilitate Morphogenesis of the Virion Assembly Compartment. *J. Virol.* **89**, 3049–3061 (2015).

38. Peretti, A. *et al.* Characterization of BK Polyomaviruses from Kidney Transplant Recipients Suggests a Role for APOBEC3 in Driving In-Host Virus Evolution. *Cell Host Microbe* **23**, 628-635.e7 (2018).

39. Kim, E.-Y. *et al.* Human APOBEC3 induced mutation of human immunodeficiency virus type-1 contributes to adaptation and evolution in natural infection. *PLoS Pathog* **10**, e1004281 (2014).

40. Mulder, L. C. F., Harari, A. & Simon, V. Cytidine deamination induced HIV-1 drug resistance. *Proc. Natl. Acad. Sci. U. S. A.* **105**, 5501–5506 (2008).

41. Cho, H., Shrestha, B., Sen, G. C. & Diamond, M. S. A role for Ifit2 in restricting West Nile virus infection in the brain. *J. Virol.* **87**, 8363–71 (2013).

42. Sanjana, N. E., Shalem, O. & Zhang, F. Improved vectors and genome-wide libraries for CRISPR screening. *Nat. Methods* **11**, 783–784 (2014).

43. Shalem, O. *et al.* Genome-scale CRISPR-Cas9 knockout screening in human cells. *Science* **343**, 84–7 (2014).

44. Doench, J. G. *et al.* Optimized sgRNA design to maximize activity and minimize off-target effects of CRISPR-Cas9. *Nat. Biotechnol.* **34**, 184 (2016).

45. Mondal, A. *et al.* Influenza virus recruits host protein kinase C to control assembly and activity of its replication machinery. *Elife* **6**, e26910 (2017).

46. Richardson, S. M., Wheelan, S. J., Yarrington, R. M. & Boeke, J. D. GeneDesign: Rapid, automated design of multikilobase synthetic genes. *Genome Res.* **16**, 550–556 (2006).

47. Dos Santos Afonso, E., Escriou, N., Leclercq, I., van der Werf, S. & Naffakh, N. The generation of recombinant influenza A viruses expressing a PB2 fusion protein requires the conservation of a packaging signal overlapping the coding and noncoding regions at the 5’ end of the PB2 segment. *Virology* **341**, 34–46 (2005).

48. Karlsson, E. A. *et al.* Visualizing real-time influenza virus infection, transmission and protection in ferrets. *Nat. Commun.* **6**, 6378 (2015).

49. Reuther, P. *et al.* Generation of a variety of stable Influenza A reporter viruses by genetic engineering of the NS gene segment. *Sci. Rep.* **5**, 11346 (2015).

50. Watanabe, T., Watanabe, S., Noda, T., Fujii, Y. & Kawaoka, Y. Exploitation of nucleic acid packaging signals to generate a novel influenza virus-based vector stably expressing two

foreign genes. *J. Virol.* **77**, 10575–83 (2003).

51. Afgan, E. *et al.* The Galaxy platform for accessible, reproducible and collaborative biomedical analyses: 2016 update. *Nucleic Acids Res.* **ahead of p**, (2016).

52. Li, W. *et al.* MAGeCK enables robust identification of essential genes from genome-scale CRISPR/Cas9 knockout screens. *Genome Biol.* 1–12 (2014). doi:10.1186/s13059-014-0554-4

53. Martin, M. Cutadapt removes adapter sequences from high-throughput sequencing reads. *EMBnet.journal* **17**, 10 (2011).

54. Yang, Z. *et al.* Fast and sensitive detection of indels induced by precise gene targeting. *Nucleic Acids Res.* **43**, e59 (2015).

55. Yewdell, J. W. & Gerhard, W. Antigenic characterization of viruses by monoclonal antibodies. *Annu. Rev. Microbiol.* **35**, 185–206 (1981).

56. Huppertz, I. *et al.* iCLIP: Protein-RNA interactions at nucleotide resolution. *Methods* **65**, 274–287 (2014).

57. Van Nostrand, E. L. *et al.* Robust transcriptome-wide discovery of RNA-binding protein binding sites with enhanced CLIP (eCLIP). *Nat. Methods* **13**, 508–514 (2016).

58. Kutluay, S. B. *et al.* Global changes in the RNA binding specificity of HIV-1 gag regulate virion genesis. *Cell* **159**, 1096–1109 (2014).

59. Heinz, S. *et al.* Simple combinations of lineage-determining transcription factors prime cis-regulatory elements required for macrophage and B cell identities. *Mol. Cell* **38**, 576–589 (2010).

60. Bushnell, B. BBMap (version 37.75) [Software]. *Available at https://sourceforge.net/projects/bbmap/* (2015).

61. Lovci, M. T. *et al.* Rbfox proteins regulate alternative mRNA splicing through evolutionarily conserved RNA bridges. *Nat. Struct. Mol. Biol.* **20**, 1434–1442 (2013).

62. Quinlan, A. R. & Hall, I. M. BEDTools: a flexible suite of utilities for comparing genomic features. *Bioinformatics* **26**, 841–842 (2010).

63. Ramírez, F. *et al.* High-resolution TADs reveal DNA sequences underlying genome organization in flies. *Nat. Commun.* **9**, 189 (2018).

64. Ge, S. X., Jung, D. & Yao, R. ShinyGO: a graphical gene-set enrichment tool for animals and plants. *Bioinformatics* (2019). doi:10.1093/bioinformatics/btz931

65. Kawakami, E. *et al.* Strand-specific real-time RT-PCR for distinguishing influenza vRNA, cRNA, and mRNA. *J. Virol. Methods* **173**, 1–6 (2011).

66. Kiselak, E. A. *et al.* Transcriptional regulation of an axonemal central apparatus gene, sperm-associated antigen 6, by a SRY-related high mobility group transcription factor, S-SOX5. *J. Biol. Chem.* **285**, 30496–505 (2010).

67. Ingolia, N. T., Brar, G. A., Rouskin, S., McGeachy, A. M. & Weissman, J. S. The ribosome profiling strategy for monitoring translation in vivo by deep sequencing of ribosome-protected mRNA fragments. *Nat. Protoc.* **7**, 1534–1550 (2012).

68. Guo, H., Ingolia, N. T., Weissman, J. S. & Bartel, D. P. Mammalian microRNAs predominantly act to decrease target mRNA levels. *Nature* **466**, 835–840 (2010).

69. Kim, D., Langmead, B. & Salzberg, S. L. HISAT: A fast spliced aligner with low memory requirements. *Nat. Methods* **12**, 357–360 (2015).

70. Dunn, J. G. & Weissman, J. S. Plastid: nucleotide-resolution analysis of next-generation sequencing and genomics data. *BMC Genomics* **17**, 958 (2016).

71. Liao, Y., Smyth, G. K. & Shi, W. featureCounts: an efficient general purpose program for assigning sequence reads to genomic features. *Bioinformatics* **30**, 923–930 (2014).

72. Robinson, M. D., McCarthy, D. J. & Smyth, G. K. edgeR: a Bioconductor package for differential expression analysis of digital gene expression data. *Bioinformatics* **26**, 139–140 (2010).

73. Sheets, M. D., Fritz, B., Hartley, R. S. & Zhang, Y. Polyribosome analysis for investigating mRNA translation in Xenopus oocytes, eggs and embryos. *Methods* **51**, 152–156 (2010).

74. Mayeur, G. L., Fraser, C. S., Peiretti, F., Block, K. L. & Hershey, J. W. B. Characterization of eIF3k: a newly discovered subunit of mammalian translation initiation factor elF3. *Eur. J. Biochem.* **270**, 4133–9 (2003).

75. Gantt, K. R., Jain, R. G., Dudek, R. W. & Pekala, P. H. HuB localizes to polysomes and alters C/EBP-beta expression in 3T3-L1 adipocytes. *Biochem. Biophys. Res. Commun.* **313**, 619–22 (2004).

76. Panda, A. C., Martindale, J. L. & Gorospe, M. Polysome Fractionation to Analyze mRNA Distribution Profiles. *Bio-protocol* 7, (2017).

CHAPTER 3
Influenza virus nucleoprotein disrupts sensing of immunogenic RNAs by RIG-I

Mitchell P. Ledwith[1], Kaitlin A. Davis[1], & Andrew Mehle[1]
1. Medical Microbiology and Immunology, University of Wisconsin Madison, Madison, WI, USA.

Author Contributions:
M.P.L generated all data in the chapter with the exception of:
Cellular fractionation in Figures S1A-B (K.A.D.)
M.P.L. wrote the chapter with editing by A.M.

ABSTRACT

Negative-sense RNA viruses encapsidate their genomes as ribonucleoprotein complexes with sequence agnostic nucleoproteins to facilitate gene expression and genome replication. The processes governing ribonucleoprotein assembly necessitate the non-specific RNA-binding of nucleoproteins, but the nature of interactions between unencapsidated nucleoproteins and host RNA is not understood. We utilized eCLIP-seq to unbiasedly profile the viral and host RNAs bound by influenza A virus NP. In addition to viral genomic RNAs, we identified a suite of host non-coding RNAs that interact with NP. Binding to these non-coding RNAs is context-specific and likely regulated spatiotemporally, reinforcing the plasticity of NP-RNA interactions. Several of the RNAs are known, host-derived agonists of RIG-I, the pattern recognition receptor with specificity for blunt double-stranded RNA with 5'-triphosphates. We show that infection induces an immunogenic change in NP-bound RNAs that stimulates RIG-I. Unbiased profiling of RNAs bound by RIG-I revealed that RIG-I basally surveys many of the RNAs bound by NP, and we demonstrate that NP can compete with RIG-I to prevent sensing of immunogenic RNAs. Our findings establish the identity of a pool of host RNAs patrolled by RIG-I and highlight a role for NP in suppressing the infection-induced immunogenicity of host non-coding RNAs.

INTRODUCTION

Negative-sense RNA viruses package genomes into virions with RNA-dependent RNA polymerases (RdRPs) and an oligomeric coating of nucleocapsid (N) to form a ribonucleoprotein complex (RNP)[1]. N, also called nucleoprotein (NP) in some viruses, are non-specific RNA-binding proteins that protect the genomic RNA from extrinsic damage and facilitate the processes of gene expression and genome replication[2,3]. Upon infection of a host cell, the RdRPs transcribe viral mRNAs from the negative-sense viral genome[4]. After sufficient expression of new RNP components and with external influences from trans-acting host or viral proteins, the RNPs transition from transcription to genome replication, where the RdRP plays an active role in the ordered deposition of N/NP along the progeny genome. Following genome replication, the N/NP interact with membrane proteins at the site of budding to enable genome packaging and viral release. Thus, N/NPs are indispensable for the stability, gene expression, replication, and assembly of negative-strand RNA viruses.

The eight segments of the influenza A virus (IAV) genome are enscapsidated by oligomeric NP, and bound on both termini by a trimeric RdRP composed of the viral gene products PB2, PB1, and PA to form a double helical-like RNP structure[5–7]. The RNP is deposited into the cytoplasm after viral fusion and actively trafficked into the nucleus where viral transcription occurs[8]. Like all negative-sense RNA viruses, IAV NP is required for multiple steps in the viral lifecycle, but is best recognized for a role in genome replication. After accumulation of new RdRP and NP in the nucleus, genome replication is initiated by recruitment of a second polymerase to the template genome[9]. This newly synthesized polymerase captures the nascent end of the replication product, and oligomeric NP is deposited onto the growing RNA as the resident polymerase traverses the template genome[10–12]. The positive-sense intermediate is copied back into a negative-sense genome through a similar mechanism and either enters into

subsequent rounds of transcription and genome replication or traffics into the cytoplasm to sites of viral budding[13–15]. Genome replication is an orchestrated process where multiple host and viral factors regulate the capture and shepherding of free NP into progeny RNPs, but little is known of the regulation and dynamics of the free pool of NP[16–19].

NP binds RNA non-specifically, allowing it to coat the entirety of the viral genome[20–22]. Influenza virus NP is structurally demarcated into a head, body, and tail domain[12]. In iterative oligomerizations, the tail of a free NP molecule inserts into a groove located between the body and head domains of an adjacent molecule[11]. Proximal to the groove, RNA threads through a positively-charged RNA-binding channel shielded by a flexible loop. Recent structural data of NP crystallized with oligomers of RNA reveal that this positively-charged groove directly engages the phosphodiester backbone of the RNA oligomer[23]. The binding groove can physically accommodate both purines and pyrimidines, structurally confirming the apparent lack of observed sequence specificity. The extremely high expression levels of NP during the peak of infection, its dynamic localization throughout infection, and the lack of structurally-defined sequence specificity raised the possibility that NP interacts not only with viral RNA, but with host RNA, and that these NP:host RNA interactions may serve roles outside of spurious aggregates[19,24–29].

Here, we unbiasedly profiled the RNAs bound by NP during and outside of infection. As expected, NP primarily binds negative-sense genomic RNA during infection[30]. We also found that NP reproducibly and specifically binds discrete classes of human small non-coding RNAs. We demonstrate that binding of some host RNAs is likely dependent upon the sub-cellular localization of NP, but this spatial specificity occurs in the absence of any sequence specificity. We identified a new role for non-coding RNAs during influenza virus infection, where infection

induces immunogenic self-sensing of these RNAs by retinoic acid-inducible gene I (RIG-I), a cytoplasmic pattern recognition receptor that recognizes short double-stranded RNAs with triphosphorylated 5'-ends[31]. We further define a pool of non-coding RNAs that bind and are monitored by RIG-I. Furthermore, we find that NP competes for this pool of RIG-I ligands and likely prevents RIG-I from efficiently sampling both host and viral RNAs to suppress innate immune activation during infection. This study defines a new role for the NP from a negative-stranded RNA virus in dampening the cell-intrinsic response to infection and puts forth an obstruction model whereby a viral RNA-binding protein disrupts the ability of RIG-I to kinetically survey the RNA landscape in cells and efficiently activate innate immune responses.

RESULTS

Influenza nucleoprotein binds host RNA

Influenza NP binds viral genomic RNA to form RNPs in infected cells, and binds a broad array of nucleic acids *in vitro*[20,22,32]. To characterize the full spectrum of RNAs bound by (NP) during infection, we infected human A549 lung cells with IAV and performed RNA-immunoprecipitation with an NP-specific monoclonal antibody followed by sizing analysis. As expected, sizing traces demonstrated that NP purifications enrich for viral genomic RNAs (900-2100bp). In addition to these larger RNAs, immunoprecipitations also enrich smaller RNA species (100-300nt) that resemble the sizing of aberrant products of genome replication like defective-viral genomes[33,34], or potentially host-derived RNAs (Fig. 1A). To unbiasedly profile NP-bound RNAs, we employed enhanced-crosslinking and immunoprecipitation (eCLIP) which utilizes size-matched input samples (SMInput) and stringent purification steps to identify RNAs bound and enriched by RNA-binding proteins[35]. Short wavelength UV-light efficiently cross-linked NP to its natively bound substrates (Fig. S1A). High-throughput sequencing of these bound RNAs revealed that ~75% of bound sequences are derived from the viral genome, confirming our ability to detect known targets of NP (Fig. 1B). Similar to previous observations, NP binds the viral genome non-uniformly, with specific regions reproducibly covered and protected[36–38] (Fig. S1B). Surprisingly, ~25% of bound sequences are host-derived, suggesting that a significant portion of NP engages host RNAs during infection.

To probe whether these host RNAs are being recognized specifically, we utilized size-matched input samples and compared them to NP-eCLIP samples on a per gene basis. This gene-level analysis revealed specific enrichment of NP-bound RNAs and that many of the host RNAs belong to non-coding and repetitive RNA families. Non-coding RNAs can be encoded by 1000’s

of unique degenerate loci as pseudogenes, making them notoriously difficult to quantify and accurately map[39–41]. To address this, we designed a two-pass mapping, *de novo* transcriptome assembly, and re-mapping protocol to quantify these RNA populations (Fig. S2). Per gene differential enrichment analysis revealed that outside of the viral genome and anti-genome, non-coding and repetitive RNAs are enriched in the NP-eCLIP, especially U5, U6, and U6ATAC spliceosomal small nuclear RNAs (snRNAs), U3 or SNORD3 small nucleolar RNAs (snoRNAs), 7SK snRNA, 7SL signal recognition particle RNA, vault RNAs, Y RNAs, and Alu RNAs (Figs. 1C, 1D). No obvious sequence motifs were present in NP binding sites on host RNAs, similar to how NP binds the viral genome in a sequence-independent fashion. We further leveraged the single-nucleotide resolution of eCLIP and performed peak-calling with CLIPper, a CLIP-seq peak-calling algorithm, followed by normalization to the size-matched input, where we similarly identified ~1500 high-confidence CLIP peaks in the human genome with ~300 annotated as non-coding RNAs[42] (Fig. 1E). Despite representing only ~20% of the identified peaks, small non-coding RNAs contribute more than 70% of total reads to NP-eCLIP peaks (Fig. S1C). Collectively, these results indicate that influenza NP reproducibly and specifically engages with host non-coding RNAs during influenza infection.

RNA-binding proteins typically have a restricted binding repertoire of one or a few classes of RNAs[40,43]. For example, RNA-binding proteins with roles in splicing associate with introns and intron-exon boundaries or RNA-binding proteins with roles in post-transcriptional regulation associate with mRNA 3’-UTRs. Unlike many previously profiled RNA-binding proteins, NP enriched for RNAs spanning and localizing to several diverse classes and cellular compartments. To contextualize this unique RNA-binding activity, we compared the peaks identified during NP-eCLIP to the publicly available ENCORE database of eCLIP datasets[40].

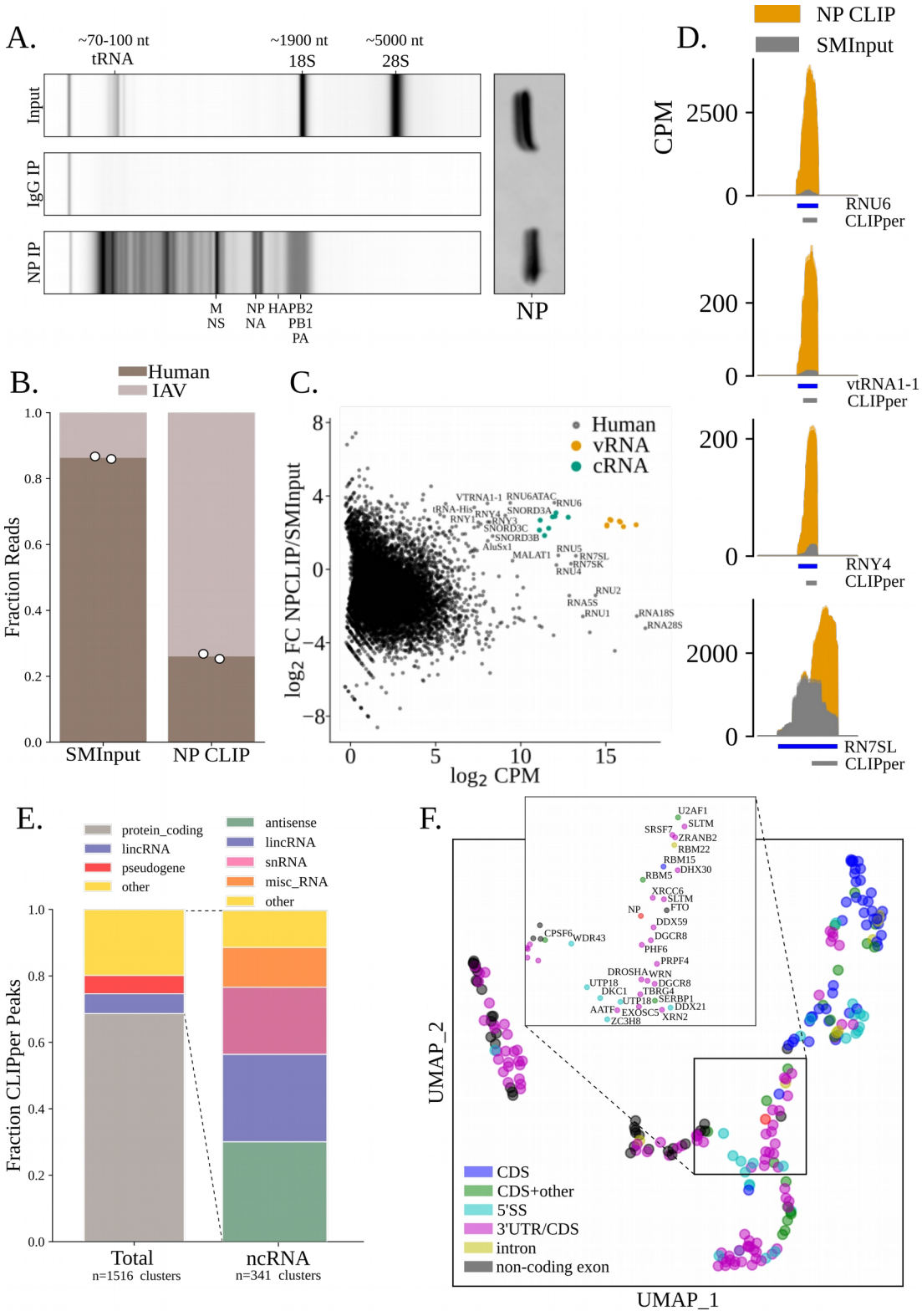

Figure 1. IAV NP associates with human non-coding RNAs during infection. (A) Bioanalyzer sizing analysis of eluate RNAs from an RNA-immunoprecipitation of NP (left) and western blots for NP from A549 cells infected for 24h with IAV (m.o.i. 0.02). (right). (B) Frequency of host- and IAV-derived reads in SMInput and NP eCLIP libraries from A549 cells infected with IAV for 24h (m.o.i. 0.02). (C) Log_2

fold-change enrichment of genes in the NP eCLIP plotted against average counts per million (CPM) in CLIP and SMInput. Yellow dots denote enrichment of influenza genomic RNA, and green dots denote enrichment of antigenomic RNA. (D) Read coverage in CPM of NP eCLIP libraries relative to SMInput over select non-coding RNAs. CLIPper-called peaks denoted under coverage track. Blue tracks depict RNAs. Solid colors represent replicate mean and shaded represent standard deviation of (n=2) biological replicates. (E) Human RNA-biotypes of CLIPper-called peaks (left) and further division of non-coding RNAs (ncRNA) into annotated biotypes (right). (F). Clustering of eCLIP datasets from ENCORE database with uniform manifold approximation based on their percent overlap to annotated biotypes. Dot color denoted by NP eCLIP library (red) or available hierarchical clustering of eCLIP libraries in the ENCORE database.

Dimensionality reduction and visualization with uniform manifold approximation and projection (UMAP) recapitulated known binding preferences of proteins in the ENCORE database[44] (Fig. 1F). NP clustered with RNA-binding proteins that lack a defined role in post-transcriptional mRNA regulation, consistent with its diverse RNA-binding profile. Proteins in this cluster act in the processing of non-coding RNAs, such as DCGR8, RMB5, and WDR43, which act in miRNA maturation, splicing, and ribosome biogenesis pathways, respectively[45–47]. These data, together with our inability to capture sequence motifs in NP-eCLIP peaks, demonstrate that NP promiscuously binds host RNA, especially non-coding RNAs, during infection.

Infection regulates RNA-binding repertoire of NP

While NP:host RNA complexes are abundant and reproducibly identifiable, they only represent ~30% of the total complexes, with viral RNA comprising the remainder. To determine if these complexes are formed intrinsically or if this is an infection-specific phenomenon, we again utilized eCLIP to profile NP-bound RNAs outside of the context of infection. To quantitatively assess and compare this condition to that of infection, we developed an eCLIP spike-in protocol to mitigate biases present in global analyses of immunoprecipitated samples[48] (Figs. S3A-B). Briefly, NP was expressed and cross-linked to RNA in *Drosophila* S2 cells. *Drosophila* samples were spiked into A549 CLIP lysates at equal ratios to assess immunoprecipitation efficiency across conditions, analogous to the Chip-rx technique used in ChIP-seq[49]. Sequence divergence between *Drosophila* and humans permits unique identification of RNAs derived from the common spike-in control. This strategy disambiguates >99.5% of sequencing reads (Fig. S3C), allowing for the accurate quantification and differential assessment of RNA-binding across sampls prepared in parallel.

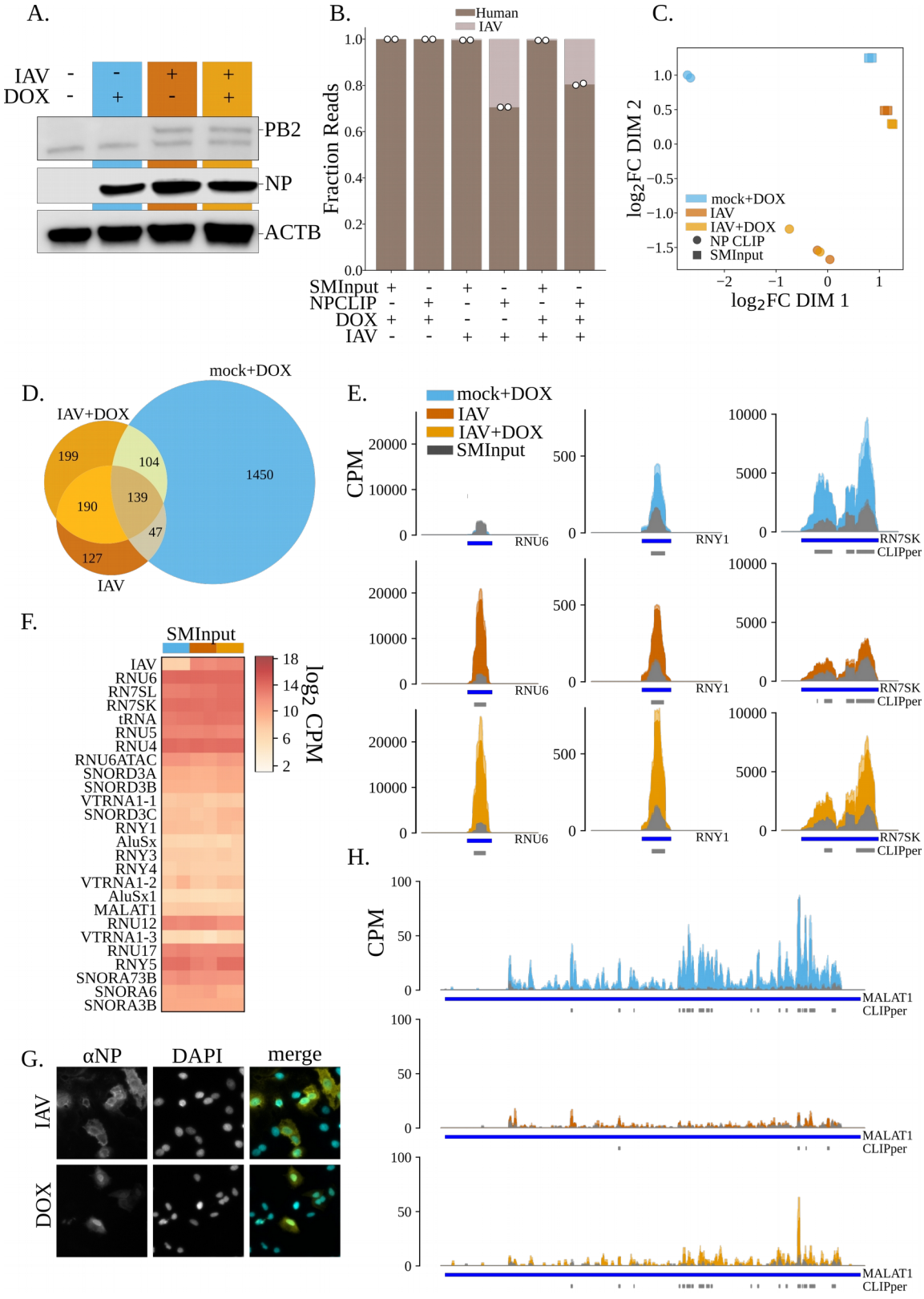

Figure 2. NP RNA-binding is dynamically controlled by infection. (A) Western blotting of NP and PB2 in tetNP-A549 cells treated with 2.5ug/mL doxycycline, infected with IAV (m.o.i. 0.01), or both for

24h. (B) Frequency of human- and IAV-derived reads from NP eCLIP and SMInput experiments performed as described in (a). (C) Principle coordinate analysis of *Drosophila* reference-normalized NP eCLIP and SMInput libraries described in (b). (D) Overlap of CLIPper-called peaks from eCLIP libraries. (E) Read coverage in counts per million (CPM) of NP eCLIP libraries relative to SMInput over select non-coding RNAs. CLIPper-called peaks denoted under coverage track. Blue tracks depict RNAs. Solid colors represent replicate mean and shaded represent standard deviation of (n=2) biological replicates. (F). Log_2 CPM of select non-coding RNAs in SMInput. (G) Immunofluorescense microscopy of tetNP-A549s stained for NP during infection (m.o.i. 0.01) or 1 ug/mL doxycycline treatment for 24h. (G) Read coverage as in (e) but over MALAT1 gene body.

To express NP outside of the context of infection, we generated an A549 cell line that inducibly expresses NP. tetNP-A549 cells were mock treated, induced, infected, or induced and infected for 24h followed by eCLIP-seq (Fig. 2A). Reads were mapped to a hybrid human/ D*rosophila*/influenza genome appended with *de novo* assembled repetitive elements and deconvoluted to retain reads mapping uniquely to one species. Upon infection, 30% of NP CLIP reads were influenza virus-derived in uninduced cells, whereas 20% of NP CLIP reads were influenza virus-derived when NP was pre-expressed before infection (Fig. 2B). Principle coordinate analysis revealed that NP binds a distinct collection of RNA when expressed alone compared to infection (Fig. 2C). To assess the disparate binding activities, we performed peak-calling and input normalization to identify the RNAs bound by NP across conditions. Over 40% of identified peaks overlapped between both infection conditions, but only ~13% overlapped between the mock infected and infection libraries, suggesting widespread changes in RNA-binding (Fig. 2D).

Gene-level analysis of the RNAs bound by NP demonstrate this differential binding. Of note, U6 snRNA, one of the most abundant RNAs bound by NP during infection does not interact with NP outside of infection (Fig. 1E, left). In contrast, NP induction enhances binding to 7SK RNA compared to infection alone (Fig. 2E, right). RNY1 displays no differential binding between conditions (Fig. 2E, middle). Altogether, >1400 eCLIP peaks are differentially bound between induced and infected samples, with ~1200 peaks enriched in the induced condition and ~250 peaks enriched in the infected condition (Fig. S4A, TableS1). Of the non-coding RNAs bound by NP, most are stably expressed across conditions, eliminating the possibility that binding discrepancies are a function of RNA abundance (Fig. 2F).

The localization of NP is dynamically regulated during infection. Early in infection, NP localizes to sites of viral genome replication in the nucleolus, and globally shift to the cytosol late in infection[28,50,51]. To test whether the localization of NP differs between induction and infection, we performed immunofluorescence staining. NP is distributed throughout the nucleus and cytoplasm in induced cells and is localized to the nuclear periphery and cytoplasm in infected cells (Fig. 2G). Induced cells have a higher abundance of nuclear NP. To test whether the subcellular localization dictates the availability of NP to RNA, we performed eCLIP using cytosolic and nuclear fractions from infected cells. Principle coordinate analysis of nuclear eCLIP reveal that it resembles eCLIP from NP-induced cells, whereas cytosolic eCLIP resemble NP-infected samples (Fig. S4B-C). Indeed, MALAT1, an exclusively nuclear-localized lncRNA, is differentially bound by induced NP[52] (Fig. 2H). These data suggest that which host RNAs are bound by NP is regulated in part by the subcellular localization of NP, although we cannot exclude other infection-induced factors, and that NP:RNA interactions may be dynamically regulated throughout the cycle of infection as NP localization changes.

NP-bound RNAs are immunogenic

Many of the host RNAs highly bound by NP during infection such as 7SL, Y RNAs, and vtRNAs have been implicated as host-derived agonists of RIG-I, the pattern recognition receptor that efficiently discriminates host RNAs from viral RNAs by recognizing short double-stranded RNAs with 5’-triphosphates[53–56]. Activation of RIG-I promotes the oligomerization of mitochondrial anti-viral signaling protein (MAVS) and the eventual induction of interferon stimulated genes[31]. Indeed, RNU6, RNY4, and vtRNA1-1 are all predicted to adopt short double-stranded RNA structures when folded in isolation (Fig. 3A). We sought to determine if these RNAs signal through RIG-I to activate type I interferon responses.

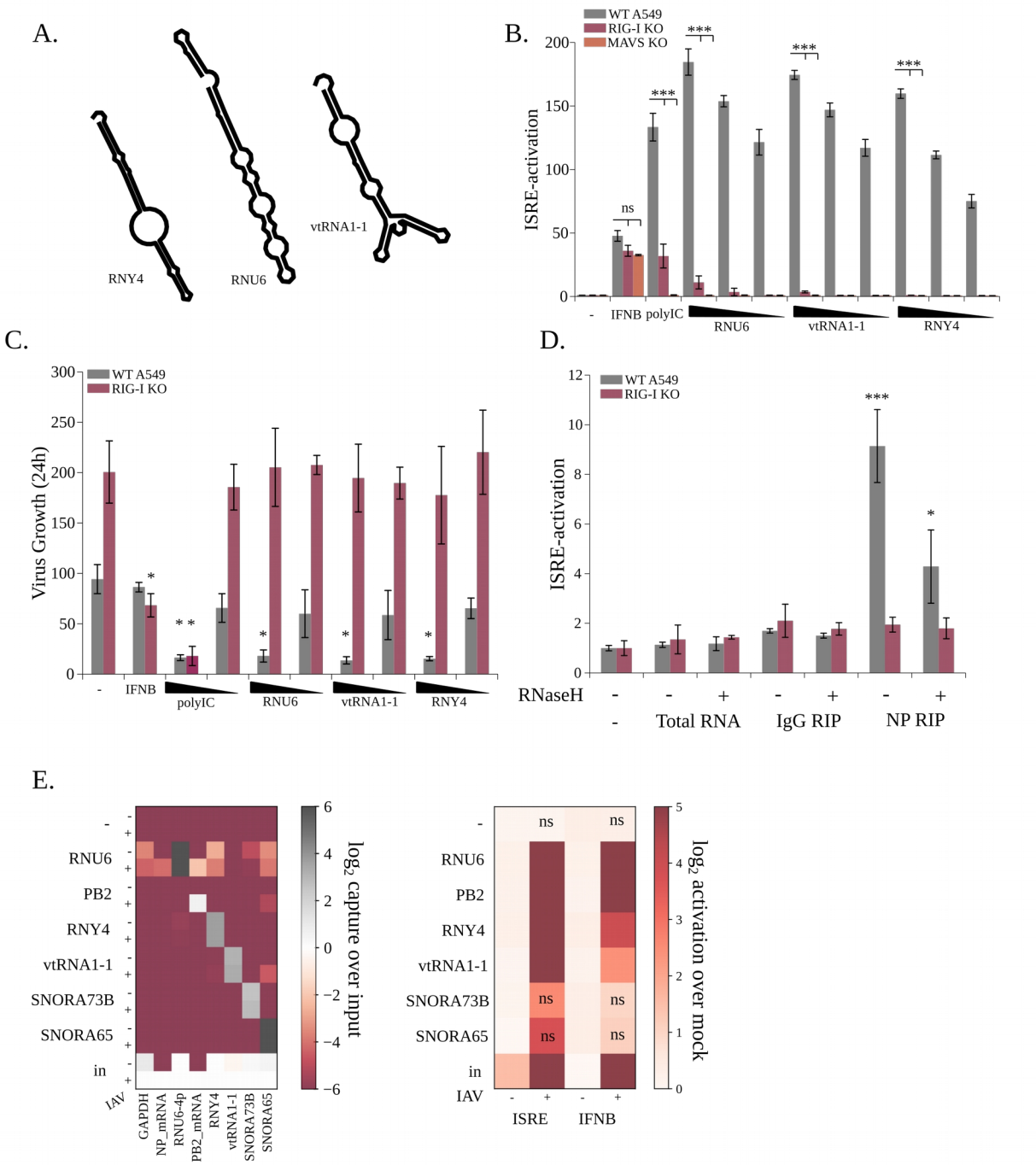

Figure 3. Non-coding RNAs signal through RIG-I. (A) Minimum free energy RNA secondary structures predicted using RNAFold for select non-coding RNAs. (B) Interferon-stimulated response element (ISRE) NanoLuc A549 reporter cells transfected with decreasing amounts of *in vitro* transcribed non-coding RNAs, mixed molecular weight polyIC, mock transfected, or treated with 100 U/mL IFNB for 24h and assayed for ISRE activation. Data are (n=2) and representative of 3 independent biological replicates. * $P < 0.001$ with ANOVA and *post-hoc* correction. Only first RNA concentration shown. (C) WT or RIG-I knockout A549 cells treated as in (b) were infected with PASTN for 24h. Supernatants were overlayed on MDCK cells and assayed for viral gene expression of the influenza reporter virus after 16h. Data are (n=3) and representative of 2 independent biological replicates. * $P < 0.05$ for comparison back to matched genotype mock with ANOVA and *post-hoc* correction. (D) Eluates of NP RNA-

immunoprecipitations from IAV infected A549 cells (m.o.i. 0.02, 24h) were treated with an RNaseH-based depletion targeting influenza RNA. Resultant RNAs were transfected into WT or RIG-I KO reporter cells and assayed for ISRE-promter induction. Data are (n=2) and representative of 3 independent biological replicates. * $P<0.05$, *** $P<0.001$ as determined by ANOVA with post hoc correction relative to mock. (E) Anti-sense oligonucleotide captures of indicated non-coding RNAs from mock- or IAV-infected (m.o.i. 0.02, 24h) A549 cells. Resultant RNAs were measured for enrichment relative to input by qRT-PCR (left) or transfected into report cells (right) and assayed for ISRE- or IFNB-promoter induction. Data are (n=2) and representative of at least 2 independent biological replicates. $P<0.001$ for all comparisons to mock unless noted as not significant (ns).

To test this, we utilized WT, RIG-I KO, and MAVS KO reporter cells harboring a luciferase gene under the control of the ISG54 promoter. RNAs were *in vitro* transcribed and transfected into reporter cells to assay for stimulation of innate immunity. All RNAs potently induced the ISG54 promoter, and this activation was almost entirely dependent on RIG-I, and by extension, MAVS (Fig. 3B). Removal of the 5'-triphosphate of *in vitro* transcribed RNAs with calf-intestinal phosphatase completely abrogated sensing of non-coding RNAs (Fig. S5). RIG-I activation normally establishes an anti-viral state. Influenza virus replication was significantly reduced in cells transfected with immunogenic RNAs. This effect was completely dependent on RIG-I, and the inhibitory phenotype was lost in RIG-I knockout cells, reinforcing the importance of the RIG-I pathway in host antagonism of viral infection, and prompting the possibility that these RNAs may play antiviral roles during infection (Fig. 3C).

To determine if the RNAs associated with NP during a *bona fide* infection are directly immunostimulatory, we immunoprecipitated NP and isolated the bound RNA. As we had previoulsy shown, NP bound both host non-coding RNAs and viral genome (Fig. S6A). NP-bound RNAs stimulated strong ISRE activation 10-fold over mock, total RNA or IgG controls (Fig. 4D). Influenza genomes are a demonstrated agonist of RIG-I, and this may contribute to ISRE activation caused by NP-bound RNAs and mask any contribution of host RNAs. We therefore utilized an RNaseH-based depletion protocol with utilized tiling oligos that specifically deplete influenza virus genomic RNA from immunoprecipitated samples. The depletion protocol efficiently removed all influenza segments from immunoprecipitated samples or *in vitro* transcribed viral genomes, and eliminated the ability of *in vitro* transcribed genomes to induce ISRE activation (Fig. S6B-C). In contrast, NP-immunoprecipitated samples depleted of viral

RNAs retain activity, inducing ISRE activation 4-fold. Thus, immunogenic, RNAs bound by NP directly stimulate innate immunity during infection (Fig. 3D).

Self RNAs are not normally immunogenic, yet host RNAs bound by NP during infection activate innate immune sensing. To selectivity test the immunogenicity of discrete ncRNAs, we used an anti-sense oligonucleotide (ASO) purification strategy to isolate target RNAs from heterogeneous populations. ASO purification specifically enriched for the RNAs of interest from mock or total RNA (Fig. 3E, left). From infected cells, we wanted to test if the immunogenecity of non-coding RNAs changed as a consequence of influenza infection, as demonstrated previously in HSV-1 and KSHV infections[53,55]. Captured RNAs were transfected into reporter cells lines to assay for activation of the ISG54 or type I interferon promoters. RNU6, RNY4, vtRNA1-1, and influenza genomic RNA captured from infected cells all potently stimulated the ISG54 and type I interferon promoters (Fig. 3E, right). To our surprise, despite efficient capture of RNAs from mock-treated cells, transfection of these RNAs caused little, if any, activation. We also ASO-purified SNORA65 and SNORA73B, two ncRNAs that are not bound by NP. In contrast to NP-bound RNAs, samples enriched for SNORA73B and SNORA65 show only modest activation during infection. These data suggest that the RNAs bound by NP are subject to infection-specific regulation to alter their immunogenicity and increase flux through the RIG-I pathway.

NP-bound self RNAs are bound by and signal through RIG-I

To investigate the increased immunogenicity of ncRNAs caused by infection, we assessed RNA binding by RIG-I. Accurate quantification and comparisons between immunoprecipitated libraries necessitate equivalent amounts of target protein in each sample. While RIG-I is a PRR responsible for the detection and activation of innate immunity, RIG-I

itself is interferon inducible, making comparisons between mock and infected samples impossible[31]. To avoid this confounding variable, we generated a cell line that constitutively expresses RIG-I. Infection of these cells with influenza and vesicular stomtatitis virus (VSV), another RIG-I-sensitive RNA virus, demonstrate that constitutive RIG-I expression restricts replication of both viruses[57] (Fig. 4A). We quantitatively assessed RIG-I RNA binding across conditions by performing RIG-I eCLIP with *Drosophila*-expressed RIG-I spike-ins. As expected, RIG-I binds and enriches for the termini of influenza genomic segments one, two, and three, coding for PB2, PB1 and PA, respectively[58]. This recapitulates prior RIG-I:RNA associations and confirms the known stimulatory effects of the 5'-triphosphate laden panhandle present in influenza genomes and defective interfering segments, providing confidence in our approach[33,58] (Fig. 4B).

While influenza virus-derived RNAs are the only foreign RNAs in these cells, they only constitute ~15% of the total RNAs bound by RIG-I (Fig. S7C). RIG-I eCLIP enriched for a discrete population of non-coding RNAs, namely the Y RNAs, vtRNAs, RNU6, RNA5.8S, and tRNAs, identifying several new RNAs bound by RIG-I endogenously (Fig 4C). Thus, host-derived RNAs are bound by RIG-I and may function as agonists during infection. To determine if RIG-I is differentially binding RNAs between mock and infection conditions, we performed principle coordinate analysis on RIG-I eCLIP and size-matched input samples. The first dimension cleanly separates RIG-I-bound RNAs from size-matched input controls, demonstrating the markedly restricted pool of RNAs actually bound by RIG-I (Fig 4D). The second dimension separates samples based on their experimental condition, but does not add further differentiation between mock and infected samples, suggesting similar binding patterns in these cells (Fig. 4D).

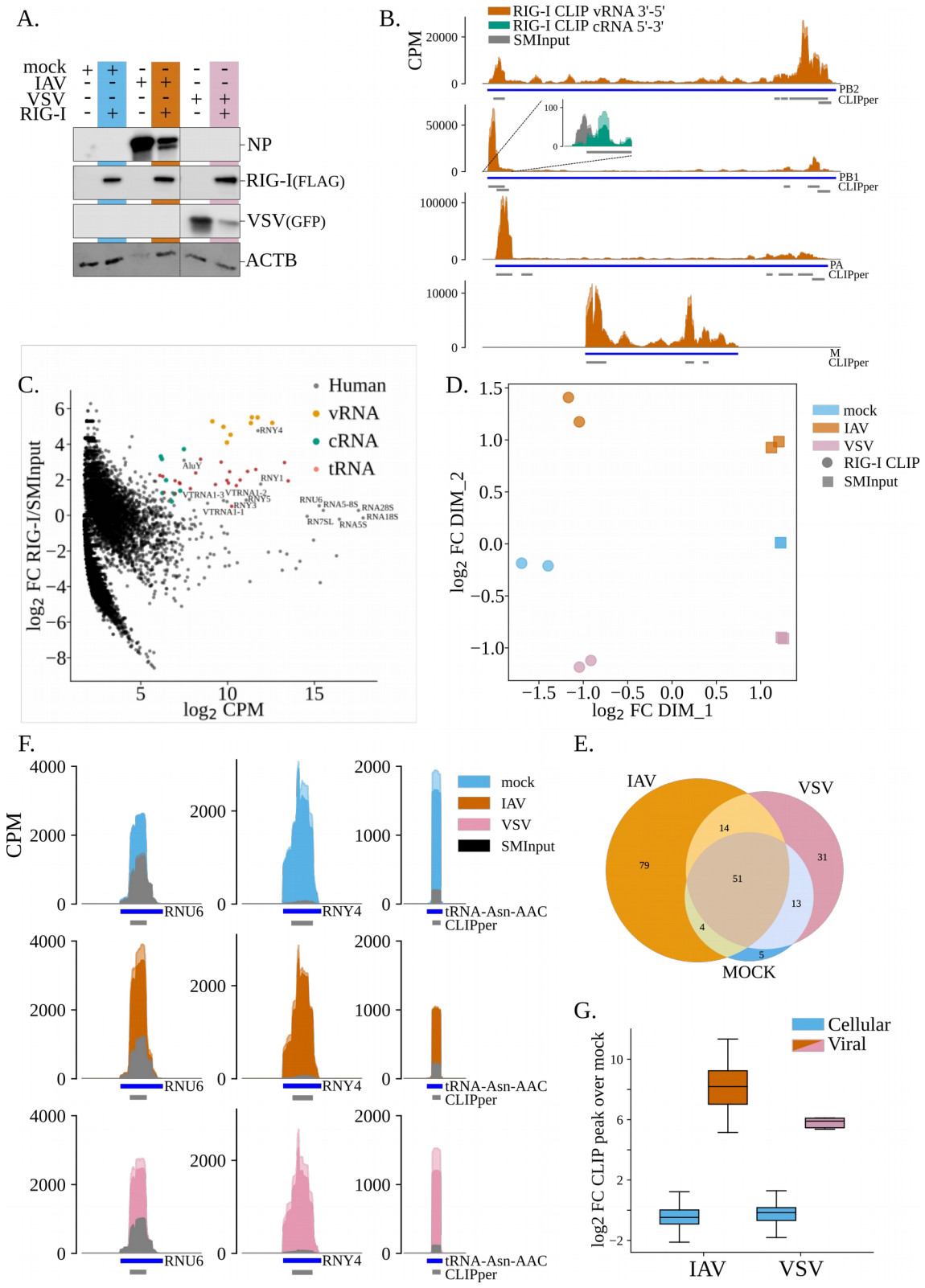

Figure 4. RIG-I surveys non-coding RNAs. (A) Western blotting of NP, RIG-I, and VSV-expressed GFP. WT or RIG-I stable A549s were mock-infected, infected with IAV (m.o.i.=0.01, 24h) , or infected with VSV-GFP (m.o.i.=0.001, 24h). (B) Read coverage in counts per million (CPM) of RIG-I eCLIP

libraries relative to SMInput over select influenza genomic RNAs or anti-genomic RNAs (inset). CLIPper-called peaks denoted under coverage track. Blue tracks depict RNAs. Solid colors represent replicate mean and shaded represent standard deviation of (n=2) biological replicates. (C) Log_2 fold-change enrichment of genes in the RIG-I eCLIP plotted against average counts per million (CPM) in CLIP and SMInput libraries. Yellow dots denote enrichment of influenza genome RNAs, green dots denote enrichment of influenza antigenome RNAs, and red dots denote enrichment of tRNAs. (D) Principle coordinate analysis of RIG-I eCLIP and SMInput libraries prepared as in (a). (E) Overlap of CLIPper-called peaks from mock, IAV-infected, and VSV-infected RIG-I eCLIP libraries. (F) Read coverage as in (b) over select non-coding RNAs, but for mock, IAV-infected, and VSV-infected RIG-I eCLIP libraries. (G) Log_2 FC of infection over mock RIG-I eCLIP in a combined set of all identified RIG-I eCLIP peaks separated by host- or virus-derived RNAs.

To assess binding at single-nucleotide resolution, we performed peak-calling with CLIPper followed by input normalization to identify RNAs differentially bound between mock and infected conditions. Nearly all (68/73) peaks identified as significantly bound in mock-infected cells were also identified in cells infected with influenza virus or VSV infection (Fig 4E, TableS2). Similarly, ~60% of peaks identified in VSV infection were also identified in IAV infection, with approximately half of the differentially called peaks absent from VSV-infected samples belonging to the influenza virus genome. This similarity is reflected in the read densities across RIG-I bound transcripts, where binding is consistent between mock, influenza virus, and VSV infected cells (Fig. 4F). Finally, we calculated fold-changes between mock and infected samples and compared differential binding of RIG-I to host or viral peaks. In both cases, cellular peaks display little change in binding, suggesting that RIG-I binds and surveils cellular RNAs independent of viral infection (Fig. 4G), even though these binding events do not result in RIG-I activation.

The lack of differential binding identified here fits well with kinetic models of RIG-I activity, where RIG-I samples RNAs with fast association and slow dissociation kinetics[59,60]. This suggests that the binding observed at baseline represents RIG-I actively surveying for 5'-triphosphorylated RNAs. To understand the interaction between RIG-I-surveyed and NP-bound RNAs, we compared overlap between peaks identified from RIG-I eCLIP and NP eCLIP during infection. Of the 197 peaks identified as being bound by RIG-I, 111 are also occupied by NP (Fig. 5A). To understand if NP-binding may modulate the kinetic proofreading activity of RIG-I, we leveraged the resolution afforded by eCLIP and compared normalized single-nucleotide resolution binding between mock RIG-I eCLIP, influenza virus infection RIG-I eCLIP, and infection NP eCLIP.

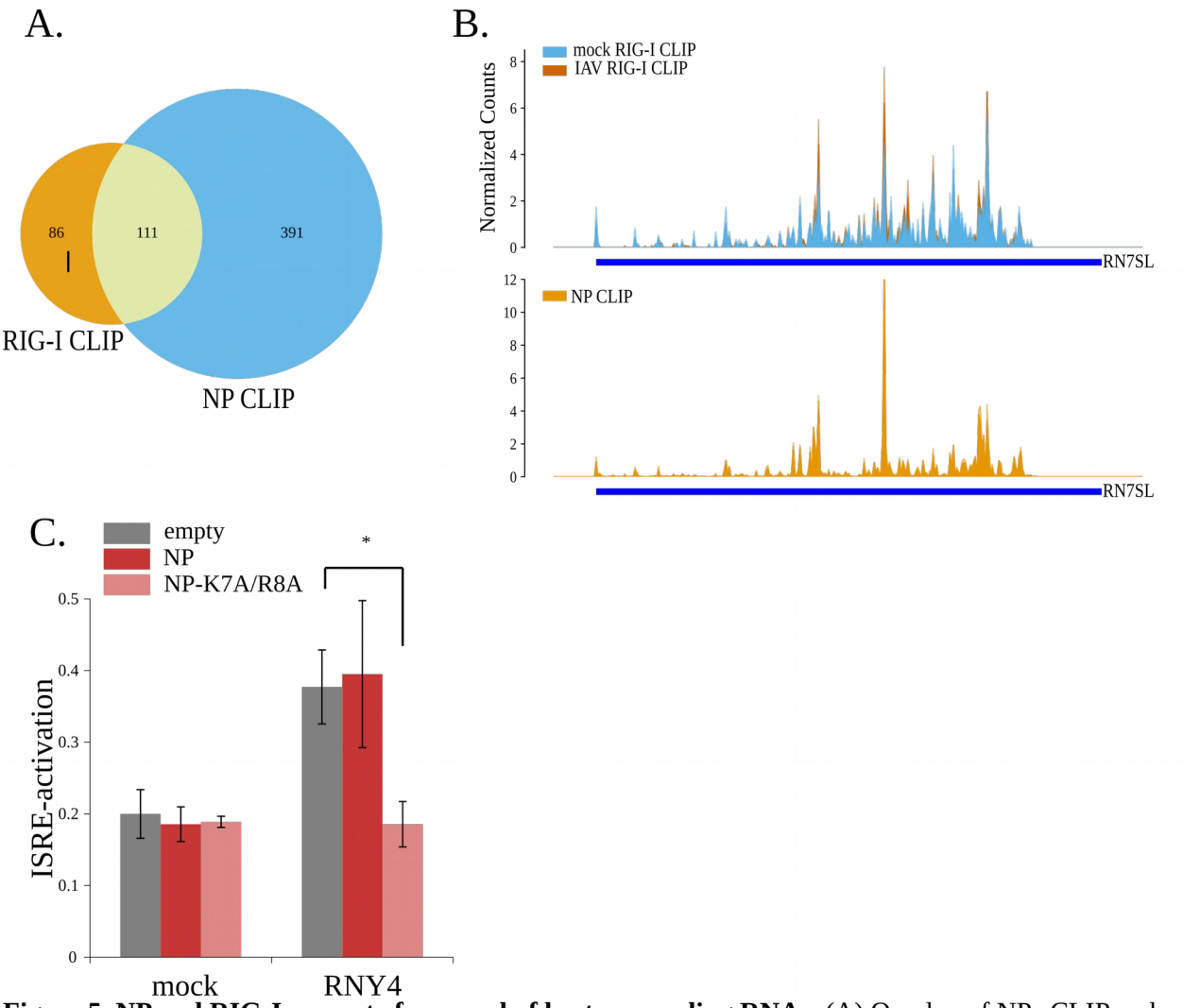

Figure 5. NP and RIG-I compete for a pool of host non-coding RNAs. (A) Overlap of NP eCLIP and RIG-I eCLIP peaks from IAV-infected samples. (B) Read coverage of the 5'-mapped base in RIG-I (top) and NP (bottom) eCLIP libraries on 7SL RNA. Coverage was normalized in each library to enable direct comparisons between cross-linking sites on the 7SL RNA. Solid colors represent replicate mean and shaded represent standard deviation of (n=2) biological replicates. (C) Interferon-stimulated response element (ISRE) reporter cells were transfected with a control plasmid, WT NP, or an NLS-mutant of NP. After 24h, cells were transfected with *in vitro* transcribed RNY4 or a mock control and assayed for ISRE-promoter activation. Data are (n=3) and representative of 3 independent biological replicates. * $P<0.05$ as determined by ANOVA with *post hoc* correction relative to empty.

Single nucleotide cross-linking events indicate that infected RIG-I has a greater propensity to cross-link at discrete basepairs along specific RNAs relative to mock RIG-I (Fig. 5B). These crosslinking sites are commonly occupied by NP during infection, and also occur most frequently at sites predicted to lack RNA secondary structure. While crosslinking efficiency is predicted to be poor between double-stranded RNA and RNA-binding proteins, these comparisons are being made across conditions relative to identical sites in different samples, mitigating this concern.

Given that crosslinking analysis suggest that NP may interfere with proper monitoring of the RNA pool, we sought to directly test whether NP interferes with RIG-I sensing. To ensure that RIG-I and NP are localized to the same subcellular localization, we introduced a mutation into one of two nuclear localization signals in NP (K7AR8A) to promote cytoplasmic retention and mimic the localization of NP during late stages of infection[25,27]. WT NP-GFP fusions localized primarily to the nucleus, while those harboring the K7A/R8A mutation displayed cytoplasmic localization (Fig. S8). WT or K7A/R8A NP was pre-expressed in ISRE-reporter cells prior to introduction of the immunogenic self-RNA RNY4. The presence of nuclear-localized NP did not affect ISRE activation, yielding activity similar to the empty vector control (Fig. 5C). However, cytoplasmic NP completely abrogated sensing, with ISRE expression remaining at levels in mock cells. Thus, cytoplasmic NP prevents the proper recognition and sensing of immunogenic self RNAs.

Discussion

The nucleoproteins of RNA viruses must retain flexible RNA-binding capabilities to accomplish their primary function as encapsidators of the viral genome[10–12]. Assembly of viral RNPs is tightly regulated to ensure monomeric, RNA-free N/NP is available to coat newly

synthesized genomes[1,9,17,61]. However, N/NP is often produced in vast excess and a subpopulation associates with other RNA, which has been assumed to create non-productive aggregates. We now reveal that these are not inconsequential by-products, but rather influenza virus NP directly engages specific host RNAs to suppress innate immune sensing during infection. The RNA-binding repertoire of NP is unique among known RNA-binding proteins, where ncRNAs with roles in transcription, splicing, ribosome biogenesis, and translation are all specifically bound by NP. The process of RNA-binding is likely dynamically regulated throughout the course of infection as NP transits from sites of viral replication in the nucleolus to site of viral budding at the plasma membrane. As infection progresses, NP encounters many of the host RNAs that are basally monitored by RIG-I. We demonstrate that these RNAs become immunogenic during infection and activate innate immunity via RIG-I, and that NP can bind and prevent the proper sensing of these immunogenic RNAs. Self-sensing is emerging as an important component of antiviral responses[53–55,62]. Our data reveal new roles for the non-specific RNA-binding capabilities of NP and highlight how viral expression of highly abundant non-specific RNA-binding proteins disrupts self-sensing of host RNAs.

RIG-I must efficiently discriminate between foreign and self RNA to avoid auto-inflammatory disease and interfonopathies[59,63,64]. Our findings provide new insights into the role for RIG-I in basally monitoring the RNA landscape in cells. Using quantitative eCLIP, we defined a small subset of RNAs continuously monitored by RIG-I. This pool includes many RNAs with largely undefined or poorly defined functions, such as the Y RNAs and vault RNAs. The biochemical kinetics of the association of RIG-I with RNA suggest that RIG-I encounters RNAs irrespective of their 5’-ends[59]. After association, RIG-I escapes unpreferred RNAs with an off rate for 5’-hydroxyl ends twice that of 5’-triphoshpate ends. ATP-binding promotes

promiscuity of RIG-I and loading of the helicase domain onto blunt ended substrates. Once loaded, RIG-I hydrolyzes ATP to engage the substrate and translocate into double-stranded RNA structure. Nevertheless, the difference in rate constants between favored and unfavored RNA is not great enough for perfect discrimination, and the prevailing model suggests that translocation is absolutely required for turnover of RIG-I improperly engaged with non-PAMP substrates. Our data show routine sampling of self RNAs by RIG-I without activation of innate immunity, supporting the kinetic discrimination model whereby a small pool of endogenous RNA substrates buffers RIG-I sampling and provides a set of substrates to be continually monitored, thereby preventing accidental oligomerization and activation of self-sensing by molecular crowding.

The continual sampling of RNA not only allows for efficient recycling of RIG-I, but also rapid recognition of PAMP RNAs when introduced into the system. RNU6, vtRNA1-1 and RNY4 all activated RIG-I sensing, but only when purified from infected cells. This suggests that the immunogenecity of small ncRNAs is differentially regulated during infection. Almost all of the RNAs bound by RIG-I are generated by RNA pol III, which transcribes non-coding RNAs with 5’-triphosphate ends[65]. Previous work has implicated the dual-specificity phosphatase 11 (DUSP11) as a regulator of the 5’-triphosphate status of non-coding RNAs. DUSP11 prunes phosphates off of 7SL, RNY4, and vtRNA1-1 to prevent activation of RIG-I[54–56]. Disturbing DUSP11 activity impacts innate immune activity. During infection by HIV or reactivation of KSHV, DUSP11 expression is impaired resulting in increased immunogenicity of self RNA. A similar process regulating the 5’-triphosphate status may also contribute to the differential immunogenicity observed during influenza infection.

Identification of new RIG-I ligands, namely RNU6 and tRNAs, add additional layers of complexity to self-sensing of host RNAs. U6 and 7SK RNAs are transcribed by RNA polIII and

immediately processed by methylphosphate capping enzyme (MECPE), capping the gamma-phosphate with a methyl group[66]. While triphosphates are the preferred substrate of RIG-I, the affinity for gamma-methyl triphosphate is unknown. Methyl-7-guanosine capped RNAs can be bound by RIG-I if they lack N1 and N2 2'O-methylation, a signature of host RNAs[67]. Thus, it is possible that RIG-I can efficiently bind gamma-methyl triphosphate. This would suggest that additional post-transcriptional marks normally shield U6 RNAs from RIG-I, that removal of the gamma-phosphate by some enzymatic means prevent sensing, or that RNA structure prevents efficient loading of RIG-I onto RNU6. In addition, tRNAs are processed out of pre-tRNAs by nucleases, resulting in monophosphate ends that can be further modified by methylases[68,69]. Altogether, these results suggest that RNA-processing and innate sensing of RNAs are intrinsically linked, and regulation and modification of host RNAs represent an underappreciated facet of innate immunity.

Many RNA viruses encode proteins that disable or prevent recognition of viral RNAs by RLRs[70]. This inhibition can be mediated by direct interaction with RLRs[71,72], disruption of co-factors that are required for RLR activation[73,74], interception of signaling cascades downstream of RLRs[75,76], or by directly binding viral RNA to prevent sensing[77]. While NS1 is the predominant RIG-I antagonist in influenza virus-infected cells, NP is also thought to prevent sensing of viral genomic material by encapsidating viral RNA in ribonucleoproteins[78]. Our data demonstrate a new role for NP, where binding of non-coding RNAs prevents surveillance and sensing of self RNAs by RIG-I, and suggests that non-specific viral RNA-binding proteins may broadly exert auxiliary effects in disrupting host sensing of immunogenic RNAs.

Materials and Methods

Cells

Human alveolar epithelial (A549), Madin-Darby canine kidney (MDCK), and HEK293T cells were purchased from the American Type Culture Collection (ATCC) and maintained in Dulbecco's modified Eagle's medium (DMEM) and 10% fetal bovine serum (FBS) at 37°C and 5% CO_2. *Drosophila* Schneider 2 (S2) cells were maintained in Schneider's *Drosophila* medium supplemented with 10% FBS and 1% antibiotic/antimicotic and grown at 25°C without CO_2. A549 wildtype, RIG-I$^{-/-}$, and MAVS$^{-/-}$ A549s were a gift from C. McCormick (Dalhousie University) and 293T wildtype and RIG-I$^{-/-}$ were a gift from S. Sarkar (University of Pittsburgh). Transduced A549 lines were selected and propagated in either 0.5 μg/mL puromycin or 6 μg/mL blasticidin. Transduced S2 cells were selected and maintained in 2 μg/mL puromycin. Cells were regularly verified to be mycoplasma negative using MycoAlert (Lonza).

Plasmids and *in vitro* transcribed RNAs

NP expression plasmids were generated by PCR-amplification of the previously described pCAGGs-NP and gibson assembly into pEF1-3xFLAG. The NLS-mutant, NP-K7AR8A, was generated by inverse PCR. Doxycycline-inducible NP plasmids were generated by PCR-amplification of pCAGGs-NP and gibson assembly into pSBtet-BP-NP (Addgene). The stable RIG-I expression plasmid pSB-RIG-I was generated by PCR-amplification of pEFBOS-RIG-I-2xFLAG, a gift from J. Patton (Indiana University), and gibson assembly into pSBtet-BP to replace BFP and create pSBtet-RIGIP. The copper-inducible *Drosophila* plasmids pMT-puro-NP and pMT-puro-RIG-I were generated by PCR-amplification of pCAGGs-NP and pEFBOS-RIG-I-2xFLAG and restriction cloning into pMT-puro (Addgene). The ISRE- and IFNβ-response element plasmids pSB-BB-ISRE-N2AG and pSBS-BB-IFNβ-N2AG used to create A549

reporter cells were generated by a three piece stitching reaction between PCR-amplicons derived from either pISRE-FFLuc or pIFNβ-FFLuc, NanoLuc, and GFP. The stitched products was used in a gibson assembly with pSBbi-BP. The ISRE-response element plasmid pLX304-ISRE-FFLuc used to create 293T reporter cells was generated by PCR-amplification of pISRE-FFLuc and gibson assembly into pLX304 (Addgene)

Non-coding RNAs were reverse-transcribed from total RNA with gene-specific primers and cloned via gibsosn assembly into a pNL backbone for maintenance (Promega). T7 RNA polymerase transcription templates were PCR-amplifed with gene-specific primers, purified, and 2 µg DNA template was *in vitro* transcribed in a 100 uL reaction with 40 mM Tris pH 7.9, 6 mM $MgCl_2$, 10 mM DTT, 2 mM spermidine, 2mM rNTP, 1 uL RNasin(+) (Promega), and 3 uL Hi-T7 RNA polymerase mix (NEB) for 2h at 37°C. RQ1 DNaseI (Promega) was added and the reaction was incubated for 30 minutes at 37°C. RNA was purified via phenol-chloroform or TRIzol extraction, and the resultant product checked for purity and size via TBE denaturing urea polyacrylamide gel electrophoresis and SYBR-gold (Invitrogen) to form the following products (DNA sequence noted).

RNY4: ggctggtccgatggtagtgggttatcagaacttattaacattagtgtcactaaagttggtatacaacccccactgctaaatttgactggcttttt
RNU6:
gtgctcgcttcggcagcacatatactaaaattggaacgatacagagaagattagcatggcccctgcgcaaggatgacacgcaaattcgtgaagcgttccat
attttt
vtRNA1-1:
ggctggctttagctcagcggttacttcgacagttctttaattgaaacaagcaacctgtctgggttgttcgagacccgcgggcgctctccagtccttttt

For 5'-triphosphate removal experiments, 2 µg of *in vitro* transcribed RNAs were mock-incubated or treated with calf-intestinal phosphatase (NEB) in a 20 µL reaction with NEB buffer 2 for 30 minutes. RNA was purified via RNA clean-and-concentrator kits (Zymo).

ISRE/IFN-B reporter assays

Cells were transfected with *in vitro* transcribed RNA, mixed-molecular weight polyIC, or mock transfected with Transit-X2 (Mirus). Cells were incubated for 24h, lysed in *Renilla*

Luciferase Assay buffer (Promega), and assayed for NanoLuc, Firefly Luciferase, and/or *Renilla* Luciferase, depending on the reporter system used.

For NP/RNA co-transfection assays, 293Ts were plated in 96-well plates and forward transfected using Transit-X2 with 90 ng control plasmid, pEF1-NP-3xFLAG, pEF1-NP-K7AR8A-3xFLAG, and 10 ng pRL-SV40 and incubated for 24 hours. Immunogenic RNA was introduced at 25 ng/well via transfection with Transit-X2. Cells were incubated for 24 h and assayed for Firefly Luciferase induction relative to *Renilla* Luciferase.

Generation of transduced cell lines

Fireflyfly luciferase ISRE reporter cells were generated by lentiviral transduction with pLX304-ISRE-FFLuc lentiviruses. Cells were allowed to recover and were selected in 6 μg/mL blasticidin. NanoLuc ISRE- and IFNβ- reporter cells were generated by transfection of A549s with equal amounts of pSB-ISRE-NLuc2AGFP/pSB-IFNβ-NLuc2AGFP and pCMV(CAT)T7-SB100, a plasmid expressing the sleeping beauty transposase (Addgene). Cells were allowed to recover and were selected in 6 μg/mL blasticidin. Doxycycline-inducible NP A549s and stable RIG-I expressing A549s were generated similarly, except pSBtet-BP-NP and pSB-RIG-I were transfected with the transposase and selected in 0.5 μg/mL puromycin. Copper inducible NP and RIG-I S2 cells were generated by transfection of pMT-puro-NP and pMT-puro-RIG-I with Transit-X2 (Mirus) and selection with 2 μg/mL puromycin for 2-4 weeks.

NP-RNA immunoprecipitation and qRT-PCR/bioanalyzer

A549 cells were infected with WSN (m.o.i.=0.02, 24h) and lysed in co-immunoprecipitation buffer (50 mM Tris pH 7,5, 150 mM NACl, 0.5% NP-40) supplemented with 20 U/mL RNasin (Promega) and 1xprotease inhibitor cocktail (Sigma). Lysates were clarified by centrifugation and pre-cleared with protein-A agarose (Santa Cruz) for 1h. Before

immunoprecipitation, 20 µL of input lysate was suspended in TRIzol. Lysates were incubated with the mouse monoclonal antibodies H16-L10 directed against NP or B-2 directed against GFP (Santa Cruz). Protein-RNA complexes were captured with protein A agarose (Sigma) for 1 h and washed 5-6 times with co-immunoprecipitation buffer. RNA was eluted off of the resin with TRIzol and resuspended in a volume of 10 µL. Equal volumes of RNA were utilized for qRT-PCR or sized on an Agilent 2100 Bioanalyzer RNA pico chip.

For qRT-PCR, equivalent volumes of RNA were reverse-transcribed with random-hexamer primed MMLV-RT. The resulting cDNA was diluted 1:10 and used for qPCR with the iTaq Universal SYBR Green Mastermix (Bio-rad) on a Step One Plus RT-PCR instrument (Applied Biosystems) using forward and reverse primers described below. Fold enrichment relative to the input was calculated with the ΔCt method. qPCR primers indicated below.

RNU6_F: GCTTCGGCAGCACATATACTAAAAT
RNU6_R: CGCTTCACGAATTTGCGTGTCAT
RNY4_F: GTCCGATGGTAGTGGGTTATC
RNY4_R: AAAGCCAGTCAAATTTAGCAGT
vtRNA1-1_F: CGACAGTTCTTTAATTGAAACAAGC
vtRNA1-1_R: AAGGACTGGAGAGCGCCC
IAV_NA_F: ACATCACTTTGCCGGTATCAGGGT
IAV_NA_R: ACCATAATGACCGATGGCCCAAGT

RNaseH vRNA depletion assay

RNaseH depletion of target RNAs was performed essentially as described, with slight modifications[79]. Briefly, 100 ng of *in vitro* transcribed influenza RNAs or equal volumes of RNAs from NP RNA-immunoprecipitations were combined with 0.5 mM dNTPs, 1.25 µM probe mixture listed below (containing gene-specific and universal primers targeting the conserved termini of the flu genome), and water to 10 µL. Samples were heated at 65°C for 5 minutes, and snap-cooled on ice to anneal the probe mixtures to the RNA. A 10 µL mixture containg 2x First Strand Buffer, 20 U RNasin(+), 10mM DTT, and 0.5 µL SuperScript III reverse

transcriptase (Thermo Fisher Scientific) was added to the RNA and incubated at room temperature for 5 minutes, 42°C for 30 minutes, and 50°C for 30 minutes.

To digest DNA:RNA hybrid products, 2.5 U RNaseH (Thermo Fisher Scientific) was added to the reverse transcription reaction with 2 uL First Strand Buffer in a 10 µL volume and allowed to incubate at 37°C for 30 minutes. This reaction was mixed with 2 µL RQ1 in buffer, and allowed to incubate at 37°C for 15 minutes. The reaction was terminated by addition of buffer RLT (Qiagen), and purified with a MyOne-silane bead (Thermo Fisher Scientific) based cleanup and eluted in a 5 µL volume of water. Successful depletion of RNA was checked via TBE denaturing urea polyacrylamide gel electrophoresis and staining with SYBR-gold (Invitrogen).

NS_minu_483-464: CTTCGGTGAAGGCCCTTAGT
NS_plus_440-459: TGACCGGCTGGAGACTCTAA
M_minu_514-495: CCTATGAGACCGATGCTGGG
M_plus_462-481: TGGTATGCGCAACCTGTGAA
NA_minu_1006-987: TCCGTTTGCTCCATCAGCAG
NA_minu_518-499: CACTTGCTGACCAAGCAACC
NA_plus_926-945: AGTGGGGTTTTCGGTGACAA
NA_plus_468-487: CTCCGTCCCCGTACAATTCA
NP_minu_1041-1022: TGCCATCCACACCAGTTGAC
NP_minu_528-509: GGGATCCATTCCTGTGCGAA
NP_plus_1091-1110: GGACGAAAGTGGTCCCAAGA
NP_plus_536-555: GCTCACTGATGCAGGGTTCA
HA_minu_1128-1167: TCATTCTGATGATGATAACC
HA_minu_642-623: GCTCATCACTGCTAGACGGG
HA_plus_530-549: GCTGACGAAGAAGGGGGATT
HA_plus_1153-1172: GATCAGGCTATGCAGCGGAT
PA_minu_516-497: ATCGAGAGTGTAGTCGGCCT
PA_minu_1152-1133: TGGTGCCATGTTCTCACCAA
PA_minu_1697-1678: GACACATGGCCTATGGCACT
PA_plus_1758-1777: GATGGAAATGAGGCGTTGCC
PA_plus_1225-1244: AGGTCGCTTGCAAGTTGGAT
PA_plus_660-679: CAAGCTTGCCGACCAAAGTC
PB1_minu_415-396: AGTCATAGGTCTGTCGGCCT
PB1_minu_848-829: CCTCCAACTGGCAATCCTGA
PB1_minu_1662-1643: CATTTGAGCGGTTGCTGGAC
PB1_plus_1562-1581: GGGTGTCTGGGATCAACGAG
PB1_plus_829-848: TCAGGATTGCCAGTTGGAGG
PB1_plus_375-394: ACGAGTGGACAAGCTGACAC
PB2_minu_2097-2078: AACTGCGGACTCAACTCCAG
PB2_minu_1217-1198: GCTTCGGCAATCGACTGTTC
PB2_minu_676-657: ATCTCGTTTTGCGGACCAGT
PB2_plus_1509-1528: AGTGGTGAGCATTGACCGTT

PB2_plus_1053-1072: AGAGGTGCTTACGGGCAATC
PB2_plus_533-552: CTAACGAAGTGGGAGCCAGG
uni13: AGTAGAAACAAGG
uni12deg: AGCRAAAGCAGG

Generation of biotin-labeled oligos

Enzymatic synthesis of biotin-labeled capture probes was performed essentially as described[80]. Briefly, RNA complementary to the designed probes was generated by *in vitro* transcription reactions with T7 RNA polymerase. These reactions were templated by PCR-amplification of non-coding RNA pNL plasmids with the primers:

capture_RNU6_F: TAATACGACTCACTATAGGgcccctgcgcaaggatga
capture_RNU6_R: ACCAGATCGTTCGAGTCGgaacgcttcacgaatttgcg
capture_RNY4_F: TAATACGACTCACTATAGGgtcactaaagttggtatacaa
capture_RNY4_R: ACCAGATCGTTCGAGTCgaaGcaaatttagcagtgg
capture_vtRNA1-1_F: TAATACGACTCACTATAGGGAAACAAGCAACCTGTCTGGGT
capture_vtRNA1-1_R: ACCAGATCGTTCGAGTCGGCCCGCGGGTCTCGAACAA
capture_PB2_F: TAATACGACTCACTATAGGGTCTGGCTGTCAGTAAGTATGCT
capture_PB2_R: ACCAGATCGTTCGAGTCGAACGGAAACGGAACTCTAGC
capture_SNORA73B_F: TAATACGACTCACTATAGGgcttcccagagtcctgtgga
capture_SNORA73B_R: ACCAGATCGTTCGAGTCGgtttgtctccccagtcattgt
capture_SNORA65_F: TAATACGACTCACTATAGGGTTGTTCTTCATGTGGATGACTC
capture_SNORA65_R: ACCAGATCGTTCGAGTCGCCCATGCTTTCGGCACAG

The resultant RNA was purified by phenol chloroform extraction and 10 µg was used in a reverse transcription reaction with MMLV and a biotin-tagged reverse transcription primer: biotin-ACCAGATCGTTCGAGTCG. The reaction was terminated after 3 h by hydrolysis of the RNA via addition of 1N NaOH for 15 minutes at 72°C, neutralization of the NaOH by addition of 1N HCl, and purified with a column-based cleanup (Zymo). The resulting cDNA was checked for size and purity via TBE denaturing urea polyacrylamide gel electrophoresis with SYBR-gold staining and resulted in the probe sequences:

RNU6: biotin-ACCAGATCGTTCGAGTCGgaacgcttcacgaatttgcgtgtcatccttgcgcagggg
RNY4: biotin-ACCAGATCGTTCGAGTCGAAgcaaatttagcagtgggggttgtataccaactttagtgac
vtRNA1-1: biotin-ACCAGATCGTTCGAGTCGgcccgcgggtctcgaacaacccagacaggttgcttgtttc
PB2: biotin-ACCAGATCGTTCGAGTCGaacggaaacggaactctagcatacttactgacagccagac
SNORA73B: biotin-ACCAGATCGTTCGAGTCGgtttgtctccccagtcattgtccacaggactctgggaagc
SNORA65: biotin-ACCAGATCGTTCGAGTCGcccatgctttcggcacagagtcatccacatgaagaacaac

Anti-sense oligonucleotide RNA capture

RNA samples for anti-sense oligonucleotide captures (ASOs) were generated by mock-infecting or infecting A549s with WSN (m.o.i. = 0.02, 24 h) and extracting total RNA with TRIzol. Ten µg total RNA was mixed with 100 ng DNA probe in binding buffer (10 mM HEPES pH 7.5, 500 mM LiCl, 1 mM EDTA) and incubated at 65°C for 5 minutes, and then let bind 15 minutes at room temperature. Five µL of Streptavidin C1 beads (Thermo Fisher Scientific) were mixed with oligonucleotide-bound RNAs and incubated with shaking at 25°C for 30 minutes. The beads were magnetically separated three times and washed with low-salt wash buffer (20 mM Tris pH 7.5, 200 mM LiCl, 1 mM EDTA) , dried, and resuspended in elution buffer (20 mM Tris pH7.5, 1 mM EDTA). Elution was carried out by heating at 95°C for 1.5 minutes and quickly separating the beads from the supernatant.

eCLIP-sequencing

The NP enhanced CLIP (eCLIP) protocol was previously adapted from published work and performed as described for eCLIP demonstrated in Figure 1[35,81,82]. Briefly, 10^7 A549 cells were infected with WSN (m.o.i. = 0.02, 24 h) and washed with PBS immediately before UV-crosslinking with 400 mJ/cm^2, then 200 mJ/cm^2 254 nM UV light after which cells were scraped, collected, and flash frozen. Cells were lysed in CLIP lysis buffer (50 mM HEPES pH 7.5, 150 mM KCl, 2 mM EDTA, 0.5% v/v NP-40, 1 mM DTT, 0.5% DOC w/v, and 1x EDTA-free protease inhibitor (Roche)). Lysates were digested with 0.1 U/µL RNaseT1 (Thermo Fisher Scientific) for 10 minutes at room temperature. Size-matched inputs were taken and NP was immunopurified by adding Dynabeads protein A (Invitrogen) pre-bound with monoclonal NP H16-L10 to the lysates and incubated for 3 h at 4°C. Beads were washed twice in lysis buffer, twice in high-salt buffer (50 mM Tris pH 7.4, 1 M NaCl, 1 mM EDTA, 0.1% SDS, 0.5% DOC,

1% NP-40) and twice in lysis buffer followed by labeling the RNA with γ32P-ATP. Labeled complexes were separated via SDS-PAGE, transferred to a nitrocellulose membrane, and digested off the membrane with proteinase K (Dot Scientific). RNA was captured by column purification (Zymo) and processed for ligation with a pre-adenylated DNA adapter (New England Biolabs) to generate eCLIP libraries as described.

Preparation of S2 cell lines for eCLIP spike-in was accomplished similarly. 60^7 copper-inducible NP or RIG-I S2 cells were plated and treated with 500 μM $CuCl_2$ for 48 h. Cells were collected, cross-linked, and lysed before digestion with 0.05 U/uL RNaseI (Ambion) for 10 minutes at room temperature. Lysates were aliquoted and flash frozen.

Preparation of A549 eCLIP libraries in Figure 2 and Figure 4 were similarly processed. For A549-tetNP cells, 10^7 cells were treated with 2.5 μg/mL doxycycline, infected with WSN (m.o.i. = 0.01, 24 h), or both infected and treated. For A549-RIG-I cells, 10^7 cells were infected with WSN (m.o.i. = 0.01, 24 h), infected with VSV (m.o.i. = 0.001, 24 h), or mock-infected. Cells were washed, cross-linked, and flash frozen. Lysates were processed as described previously, with the following exceptions. Lysates were treated with 0.05 U/uL RNaseI (Ambion) for 10 minutes at room temperature, quenched by transfer to ice, and *Drosophila* lysates were added in equivalent volumes at ~1:1 A260 and 1:5 volume ratio to A549 lysates. Lysates were immunoprecipitated with monoclonal NP H16-L10 bound to protein A dynabeads or monoclonal M2 (Sigma), dependent on the target RNA-binding protein. Beads were incubated and washed twice with lysis buffer, twice with high salt buffer, and twice with lysis buffer before separation via SDS-PAGE. RNA samples were processed as described, except samples were ligated with the pre-adenylated DNAlinker: AppAGATCGGAAGAGCACACGTCTG-C3 (IDT) and reverse transcribed with the following indexed primers.

1: NNaaccNNNNNAGATCGGAAGAGCGTCGTGgatcCAGACGTGTGCTCTTC
2: NNacaaNNNNNAGATCGGAAGAGCGTCGTGgatcCAGACGTGTGCTCTTC
3: NNattgNNNNNAGATCGGAAGAGCGTCGTGgatcCAGACGTGTGCTCTTC
4: NNaggtNNNNNAGATCGGAAGAGCGTCGTGgatcCAGACGTGTGCTCTTC
5: NNcgccNNNNNAGATCGGAAGAGCGTCGTGgatcCAGACGTGTGCTCTTC
6: NNccggNNNNNAGATCGGAAGAGCGTCGTGgatcCAGACGTGTGCTCTTC
7: NNctaaNNNNNAGATCGGAAGAGCGTCGTGgatcCAGACGTGTGCTCTTC
8: NNcattNNNNNAGATCGGAAGAGCGTCGTGgatcCAGACGTGTGCTCTTC
9: NNgccaNNNNNAGATCGGAAGAGCGTCGTGgatcCAGACGTGTGCTCTTC
10: NNgaccNNNNNAGATCGGAAGAGCGTCGTGgatcCAGACGTGTGCTCTTC
11: NNggttNNNNNAGATCGGAAGAGCGTCGTGgatcCAGACGTGTGCTCTTC
12: NNgtggNNNNNAGATCGGAAGAGCGTCGTGgatcCAGACGTGTGCTCTTC
13: NNtccgNNNNNAGATCGGAAGAGCGTCGTGgatcCAGACGTGTGCTCTTC
14: NNtgccNNNNNAGATCGGAAGAGCGTCGTGgatcCAGACGTGTGCTCTTC
15: NntattNNNNNAGATCGGAAGAGCGTCGTGgatcCAGACGTGTGCTCTTC
16: NNttaaNNNNNAGATCGGAAGAGCGTCGTGgatcCAGACGTGTGCTCTTC

Resulting cDNAs were circularized and linearized, followed by amplification with the following primers and indexing with unique dual indices (IDT).

Read_1: ACACTCTTTCCCTACACGACGCTCTTCCGATCT
Read_2: GTGACTGGAGTTCAGACGTGTGCTCTTCCGATCT

Libraries were processed as previously described with the modifications described in Figures S2 and S3. Breifly, Each library was pooled and sequenced on an Illumina HiSeq4000 (Fig. 1, Novogene) or Illumina NovaSeq6000 (Figs. 2,4, UW-Madison Biotechnology Center). Summary statistics and accession numbers are in Supplementary Table X. Data quality control filtering was done with FastQC v0.11.5, de-multiplexed, adapters were trimmed with BBMAP 37.56, and sequences were aligned using HISAT2 v2.2.1 to custom hg38/dm6/WSN/VSV indices or Bowtie2.4.5 to repetitive elements[83–85]. Trinity was used for RNA-seq *de novo* assembly[86]. PCR duplicates were removed by collapsing reads based on UMIs to yield a unique number of RNAs mapping to each position. The results were used as input for CLIPPER 2.0.1 to identify CLIP peaks statistically enriched over the size-matched input controls[42]. Data were analyzed with IDR 2.0.03 to measure peak reproducibility across replicates. Bedtools v2.26.0 was used for genomic data manipulation, and edgeR was used for comparing across libraries[87,88]. Custom scripts and workflows are available at: https://github.com/mehlelab/

Multicycle viral growth

Prior to infection, cells were transfected with immunostimulatory RNAs as described above. Viral infections were performed with a reporter virus expressing NanoLuc as polyprotein with PA in viral growth medium (DMEM, 0.3% bovine serum albumin, 25 mM HEPES, 1x penicillin-streptomycin, and 0.25 µg/mL TPCK-treated trypsin) at a multiplicity of infection of 0.05. Infections were allowed to progress for 24 hours at which point the supernatants were harvested and overlayed on MDCK cells. Viral gene expression was measured 16 h later by lysing in *Renilla* Luciferase Assay buffer and assaying for NanoLuc expression.

Immunofluorescence

tetNP-A549 cells were plated in an 8-well glass bottomed slide (Ibidi) and treated with doxycycline or infected with WSN. Cells were allowed to incubate for 24h, washed in PBS, and crosslinked with 4% paraformaldehyde in PBS. Crosslinked cells were permeabilized with 0.2% Triton-100 in PBS, blocked in 50 mM NH_4Cl with 4% BSA, and incubated for 1h with 1:1000 dilution anti-RNP (BEI Resources Repository). After washing, cells were incubated with 1:1000 donkey anti-goat alexa 568 (Thermo Fisher Scientific) and imaged with an EVOS cell imaging system (Thermo Fisher Scientific).

Western-blotting

Cells were lysed in co-immunoprecipitation buffer supplemented with 0.5% w/v sodium deoxycholate and 1x protease inhibitor cocktail and clarified by centrifugation. Clarified lysates were separated via polyacrylamide gel electrophoresis on 10% concentration gels and transferred to nitrocellulose membranes for blotting. Antibodies were diluted at the following concentrations: anti-RNP (1:1000, BEI Resources Repository), anti-tubulin (1:3000, Sigma), anti-Bactin (1:3000, Proteintech), anti-lamin A/C (Cell Signaling Technologies), or M2 anti-flag

(1:1000, Sigma). Membranes were imaged with chemiluminescent (Sigma) or infrared secondary antibodies (Licor).

Statistics and Reproducibility

Unless noted in figure legend, data represent means ± standard deviations (n=3 or more technical replicates) and are representative of at least three independent biological replicates. Statsmodels, Scipy, and/or matplotlib were used for graphing and statistical analyses. Pairwise comparisons were made using a Student's T test and multiple comparisons were made using a one-way ANOVA with *post hoc* Tukey's HSD. Significance was defined as $P<0.05$ with an asterisk (*) and $P<0.001$ with a triple asterisk (***). Analyses used for eCLIP are indicated in their respective methods.

Acknowledgements

This work was supported by the National Institutes of Health R21AI125897 and R01AI125271, the UW2020:WARF Discovery Initiative, and a Shaw scientist award to A.M. and a National Science Foundation grant GRFP DGE-1747503 to M.P.L. We thank members of the Mehle laboratory for valuable input and M. Harrison, C. McCormick, and S. Sarkar for gifts of reagents.

Supplementary Tables available upon request:

TableS1: edgeR calculated logFC and logCPM between mock+DOX and ixn NP eCLIP libraries.

TableS2: edgeR calculated logFC and logCPM between RIG-I eCLIP libraries.

TableS3: Sequencing statistics for eCLIP libraries.

Supplementary Data

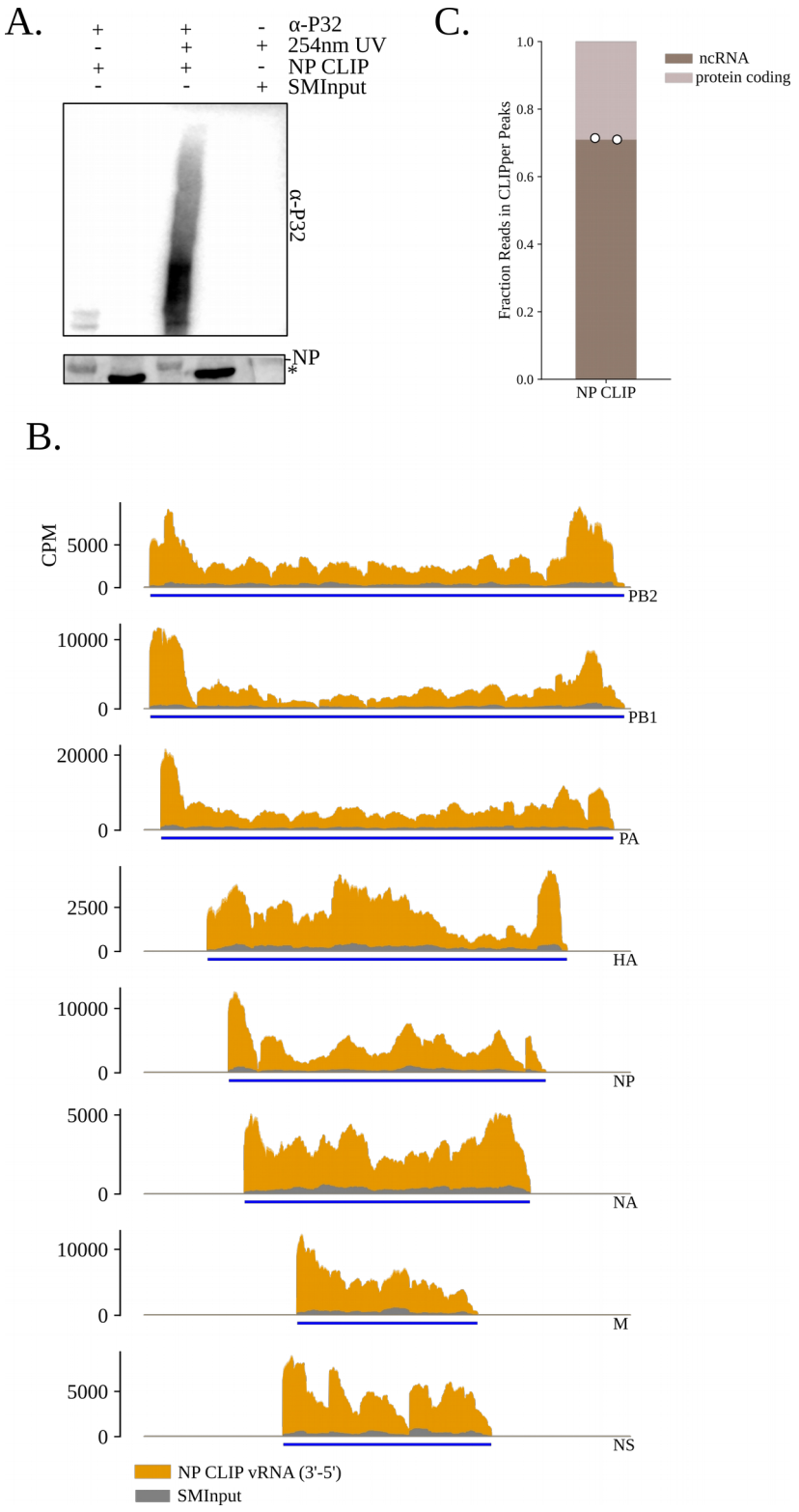

Figure S1. (Related to Figure 4). NP eCLIP recovers crosslinked viral RNA. (A) Autoradiograph of ^{32}P-labeled NP eCLIP RNAs bound to nitrocellulose membrane with and without 254 nM UV cross-

linking (top) and western blot for NP (bottom). (B) Read coverage for NP eCLIP libraries in counts per million (CPM) over the negative-sense genomic RNAs (left) or the positive-sense antigenomic RNAs (right) demonstrating uneven coverage across genome. CLIPper-called peaks are denoted along bottom of read track. (C) Fraction of host-derived reads aligning in CLIPper-called peaks separated by protein-coding or non-coding/repetitive RNAs as defined by their RNA biotype.

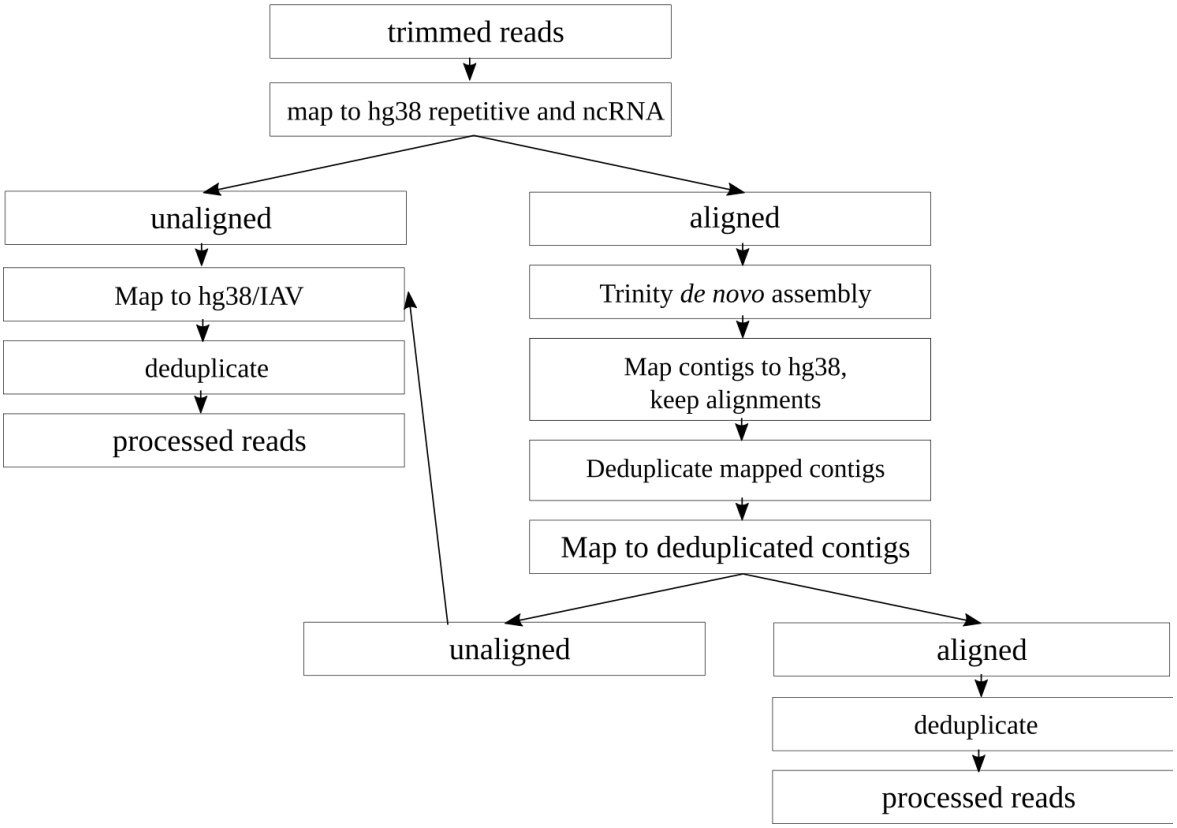

Figure S2. (Related to Figure 1). Mapping scheme utilized for accurate PCR-deduplication of non-coding RNAs.

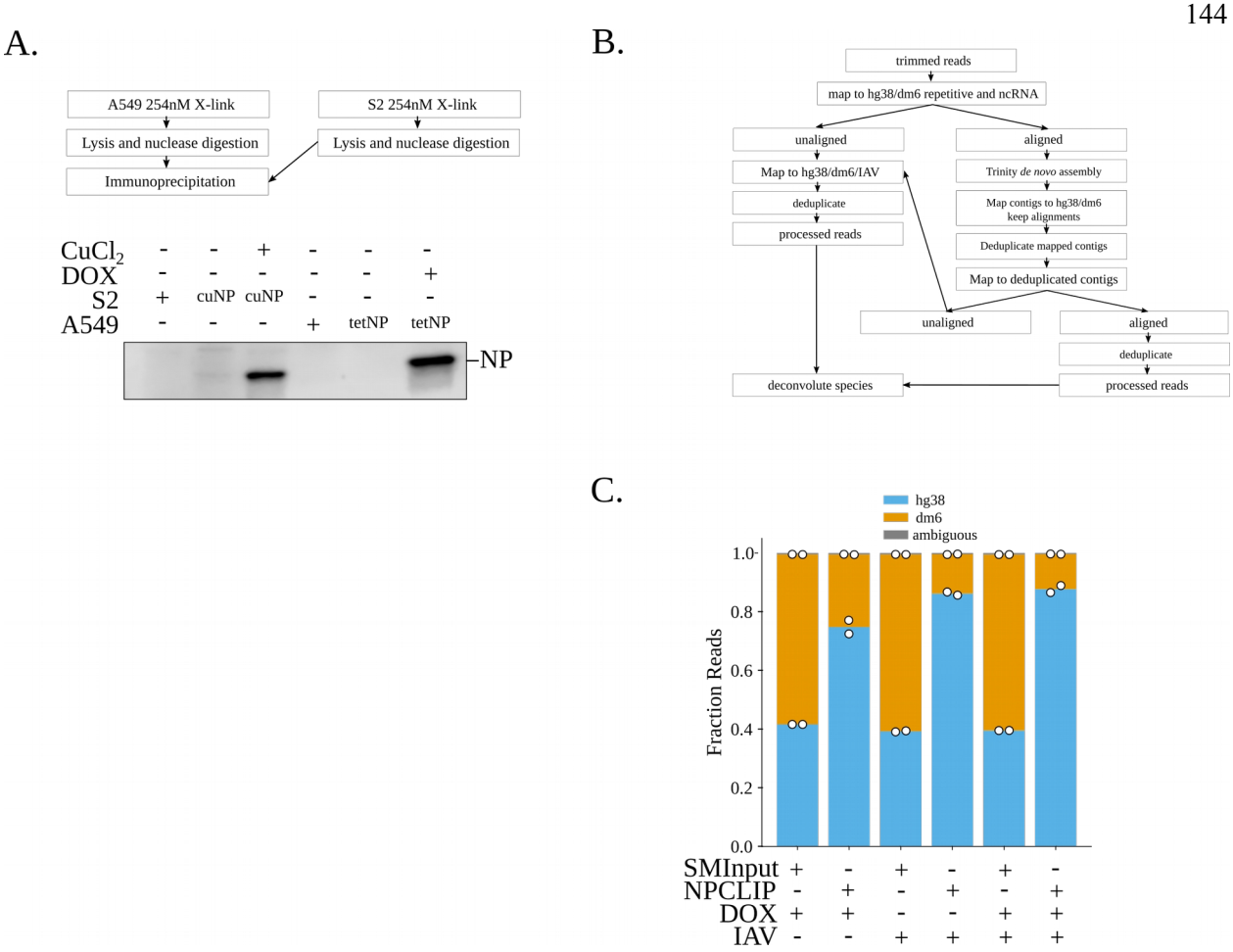

Figure S3. (Related to Figure 2). eCLIP spike-ins allow for quantitative recovery of cross-linked RNA. (A) Experimental layout of eCLIP spike-in scheme. eCLIP lysates are processed identically until size-matched inputs are taken, at which point *Drosophila* and A549 lysates are combined (top). NP western blot of NP induction in *Drosophila* cuNP-S2 and tetNP-A549cells by addition of 500 uM $CuCl_2$ or 2.5 ug/mL doxycycline for 48h or 24h, respectively (bottom). (B) Bioinformatic mapping and read deconvolution scheme. Reads are processed identically as in Fig. S2A, except that reads are mapped to a combined dm6/hg38/viral genome and deconvoluted into their respective species after PCR-deduplication. (C) Frequency uniquely mapping to dm6 or hg38 genomes indicate >99% proper read assignment.

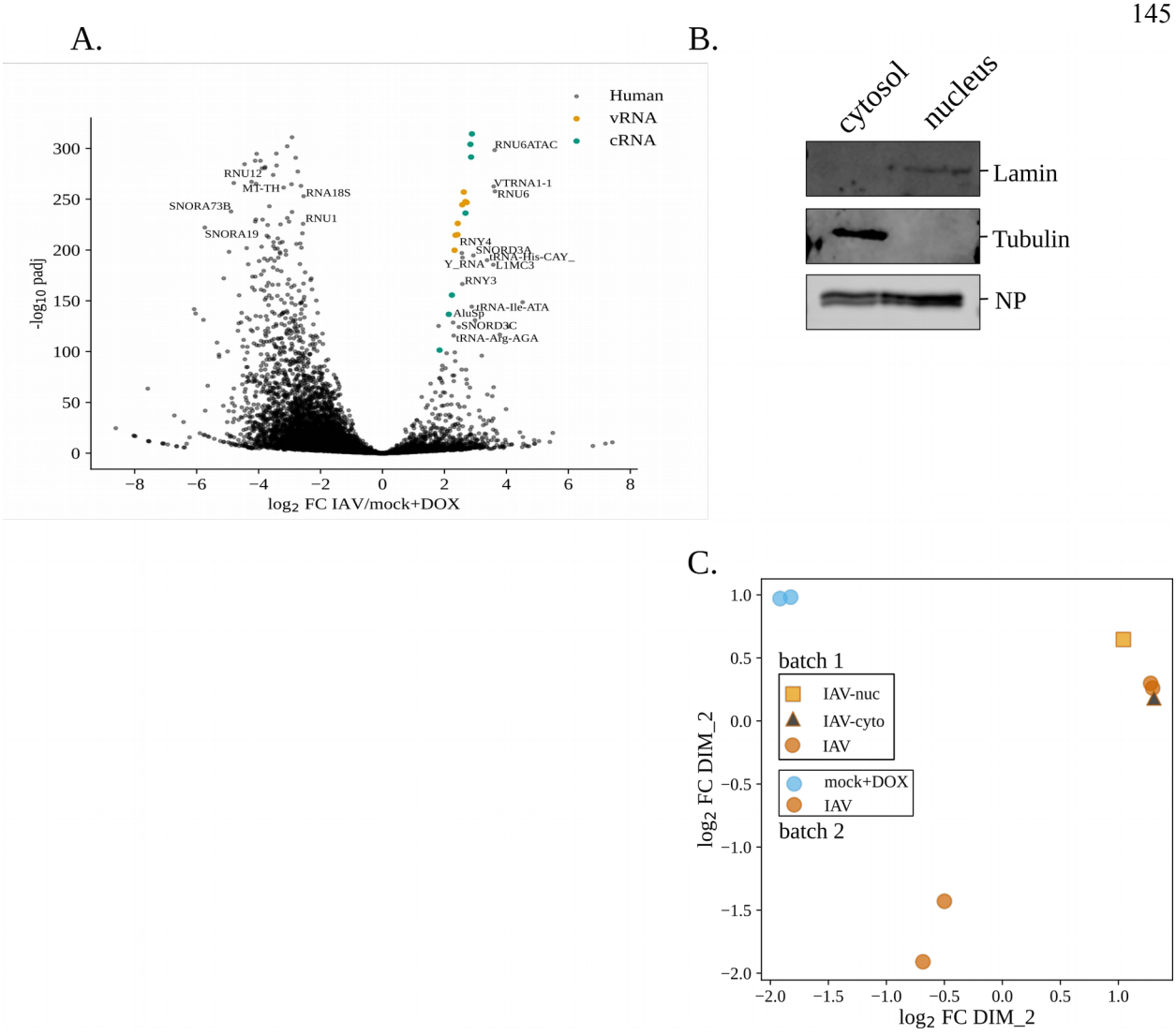

Figure S4. (Related to Figure 2) NP eCLIP of NP-induced cells mimic nuclear NP eCLIP. (A) Log_2 fold-change in read density in CLIPper called peaks between NP-eCLIP from infection and doxycycline induction plotted against -log_{10} adjusted p-value of differential enrichment. Yellow dots denote enrichment of influenza genomic RNA, and green dots denote enrichment of antigenomic RNA, with peaks on select non-coding RNAs labeled. (B) Western blots demonstrating enrichment of cytosolic (tubulin) and nuclear (lamin) fractions of infected A549s lysates before preparation of eCLIP libraries. (C) Principal coordinate analysis of nuclear-cytoplasmic NP eCLIP libraries. Dimension 1 separates batch-effects from two sets of library preparations, while dimension 2 groups NP-induced libraries (mock+DOX) with nuclear NP eCLIP.

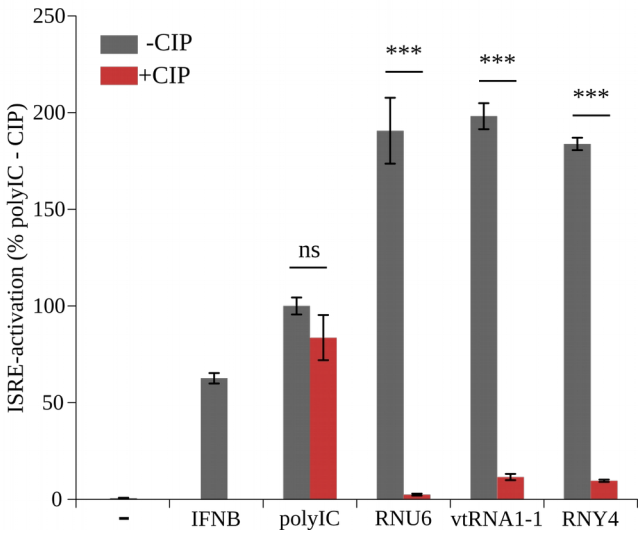

Figure S5. (Related to Figure 3) 5'-triphosphate is required sensing of non-coding RNAs. Mixed molecular-weight polyIC or 100 ng *in vitro* transcribed non-coding RNAs were treated with calf-intestinal phosphatase (CIP) or mock treated and transfected into ISRE-reporter cells. IFNβ at 100 U/mL was used as a control. Cells were assayed for ISRE-induction 24 h after treatment. * P<0.001 as determined by ANOVA with *post hoc* correction relative to -CIP.

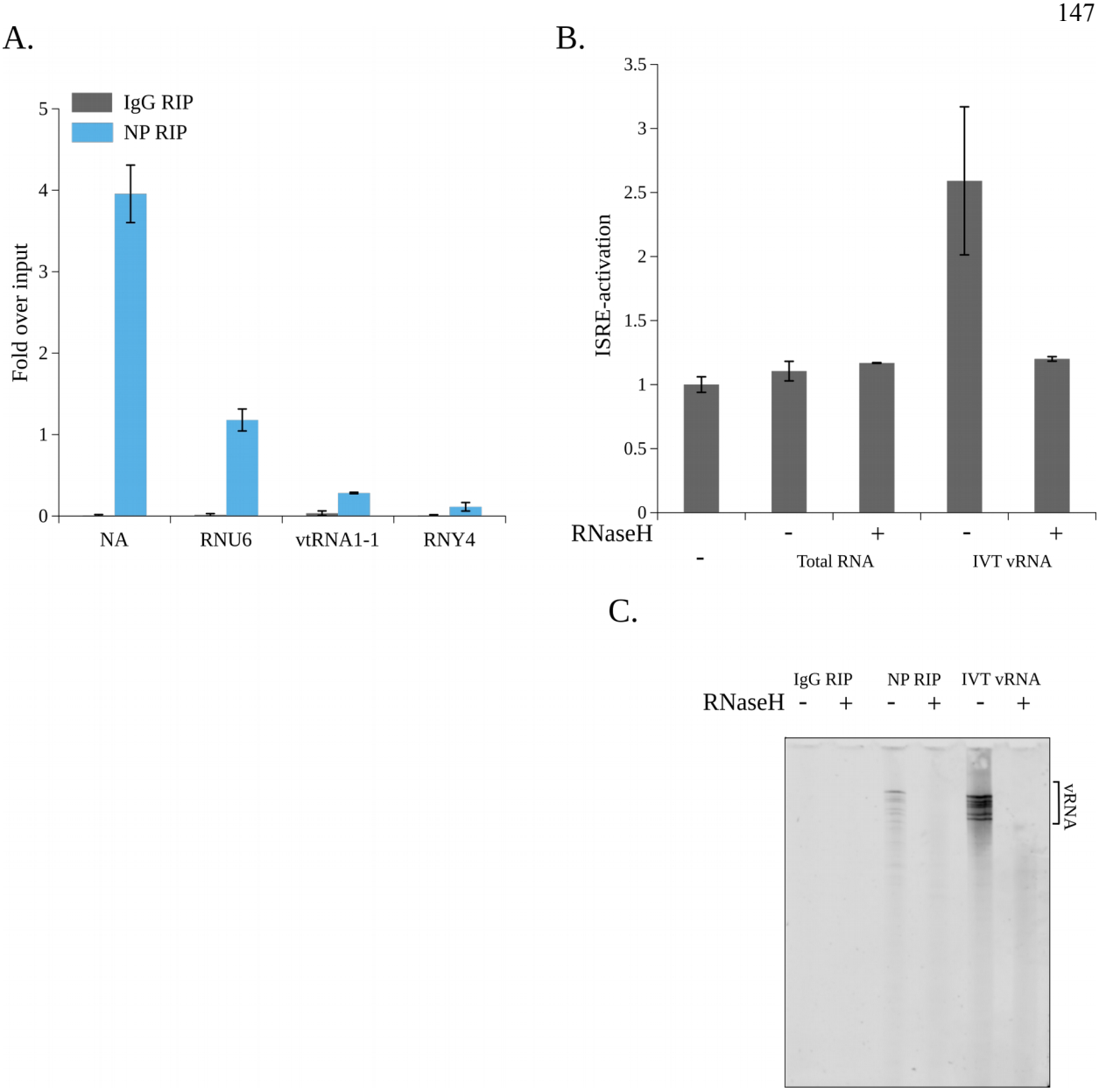

Figure S6 (Related to Figure 3) RNase-H depletion of immunostimulatory influenza genomic RNAs. (A) Total eukaryotic RNA or *in vitro* transcribed influenza genomic RNAs were treated with an RNase-H based depletion protocol targeting influenza genomic RNAs. Resultant RNAs were transfected into ISRE-reporter cells and assay for ISRE stimulation. Probe depletion completely removes immunogenic species. Data are (n=2) and representative of 3 independent biological replicates. (B) Non-coding RNA or influenza NA RNA were quantified in NP RNA-immunoprecipitations from IAV-infected A549s (m.o.o=0.02, 24h) via qRT-PCR. Enrichement was calculated relative to input RNAs, and compared to IgG control. Data are (n=2) and representative of at least 3 independent biological replicates. (C) Eluates fo NP RNA-immunoprecipitations from IAV infected A549s (m.o.i. = 0.02, 24h) or *in vitro* transcribed influenza genomic RNAs were treated with the RNase-H based depletion protocol. RNA were separated via TBE urea polyacrylamide gel electrophoresis and imaged with SYBR-gold staining.

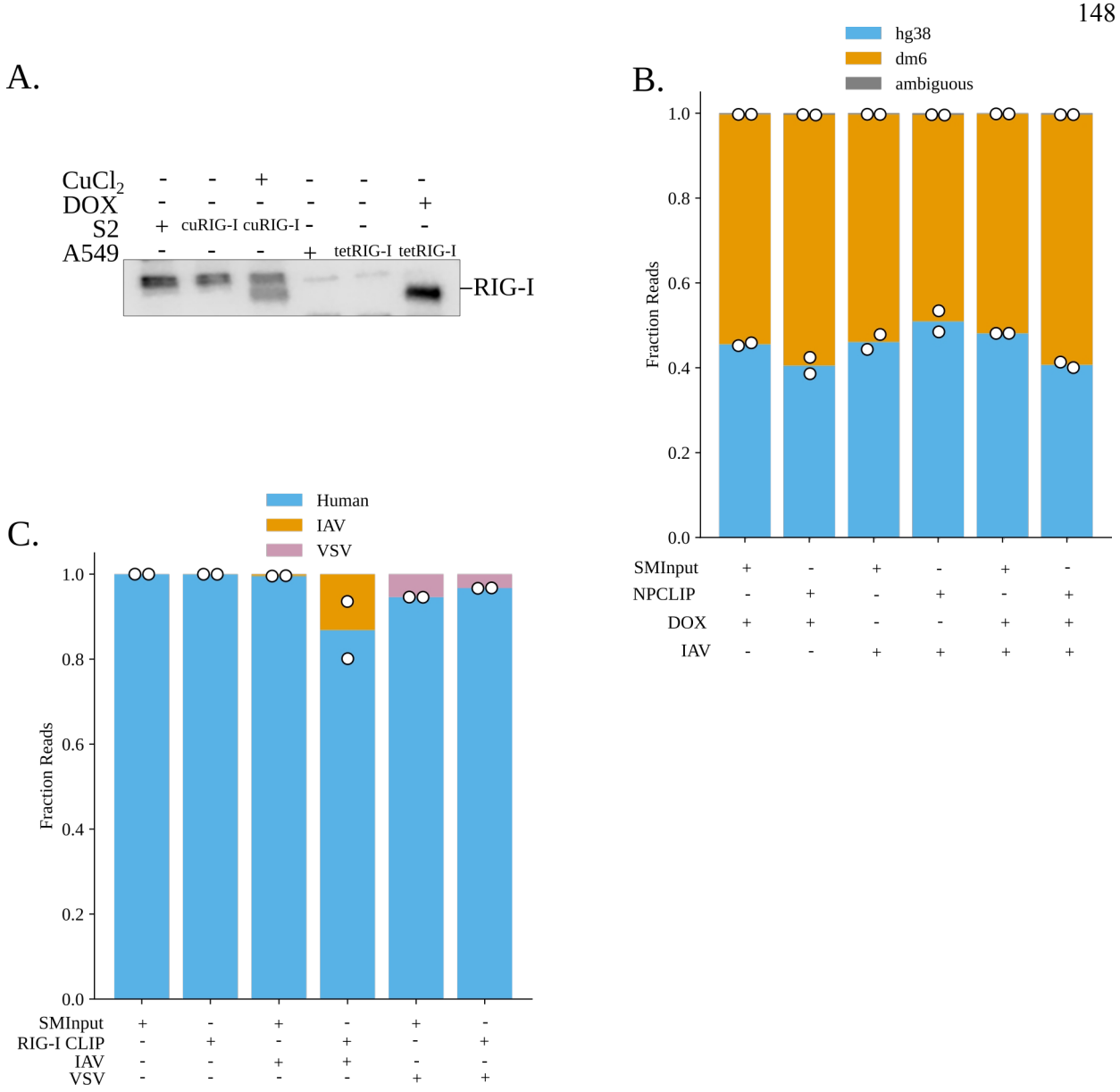

Figure S7. (Related to Figure 4). eCLIP spike-ins allow for quantitative assessment of RIG-I RNA-binding. (A) RIG-I western blot (FLAG) of RIG-I induction in *Drosophila* cuRIG-I-S2 and tetRIG-I-A549 cells by addition of 500 µM $CuCl_2$ or 2.5 µg/mL doxycycline for 48h or 24h, respectively. (B) Fraction read counts uniquely mapping to dm6 or hg38 genomes indicate >99% proper read assignment, allowing for quantitative analysis of RIG-I RNA-binding. (C) Fraction read counts of human-, IAV-, and VSV-derived reads from RIG-I eCLIP and SMInput experiments performed as described in Figure 4.

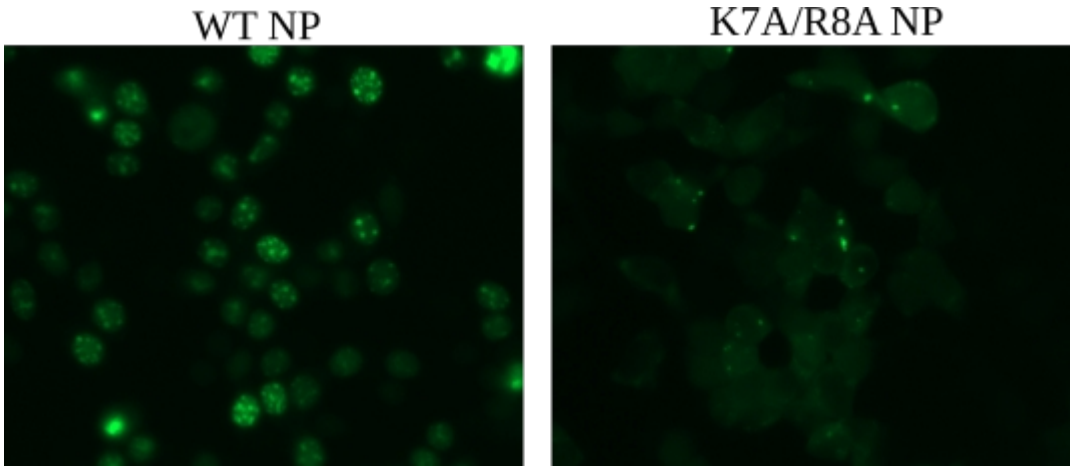

Figure S8 (Related to Figure 5). NLS-mutant of NP displays diffuse cellular localization. 293T cells were transfected with an eGFP fusion of wildtype NP (left) or K7AR8A NP (right) and imaged 24 hours post transfection via fluorescence microscopy. Wildtype NP displays puncta indicative of nucleolar localization.

References

1. Ortín, J. & Martín-Benito, J. The RNA synthesis machinery of negative-stranded RNA viruses. *Virology* **479**–**480**, 532–544 (2015).

2. Luo, M., Terrell, J. R. & Mcmanus, S. A. Nucleocapsid Structure of Negative Strand RNA Virus. *Viruses* **12**, (2020).

3. Ruigrok, R. W. H., Crépin, T. & Kolakofsky, D. Nucleoproteins and nucleocapsids of negative-strand RNA viruses. *Curr. Opin. Microbiol.* **14**, 504–510 (2011).

4. Compans, R. W. *et al. Biology of Negative Strand RNA Viruses: The Power of Reverse Genetics*. (2001).

5. Moeller, A., Kirchdoerfer, R. N., Potter, C. S., Carragher, B. & Wilson, I. A. Organization of the influenza virus replication machinery. *Science (80-.).* **338**, 1631–1634 (2012).

6. Arranz, R. *et al.* The Structure of Native Influenza Virion Ribonucleoproteins. *Science (80-.).* **338**, 1634–1638 (2012).

7. Klumpp, K., Ruigrok, R. W. H. & Baudin, F. Roles of the influenza virus polymerase and nucleoprotein in forming a functional RNP structure. *EMBO J.* **16**, 1248–1257 (1997).

8. Dou, D., Revol, R., Östbye, H., Wang, H. & Daniels, R. Influenza A virus cell entry, replication, virion assembly and movement. *Front. Immunol.* **9**, 1–17 (2018).

9. Fodor, E. & Velthuis, A. J. W. T. Structure and function of the influenza virus transcription and replication machinery. *Cold Spring Harb. Perspect. Med.* **10**, 1–14 (2020).

10. Vreede, F. T., Ng, A. K., Shaw, P. C. & Fodor, E. Stabilization of influenza virus replication intermediates is dependent on the RNA-binding but not the homo-oligomerization activity of the viral nucleoprotein. *J. Virol.* **85**, 12073–12078 (2011).

11. Turrell, L., Lyall, J. W., Tiley, L. S., Fodor, E. & Vreede, F. T. The role and assembly mechanism of nucleoprotein in influenza A virus ribonucleoprotein complexes. *Nat. Commun.* **4**, 1–11 (2013).

12. Ye, Q., Krug, R. M. & Tao, Y. J. The mechanism by which influenza A virus nucleoprotein forms oligomers and binds RNA. *Nature* **444**, 1078–1082 (2006).

13. Gales, J. P., Kubina, J., Geldreich, A. & Dimitrova, M. Strength in Diversity: Nuclear Export of Viral RNAs. *Viruses* **12**, (2020).

14. York, A., Hengrung, N., Vreede, F. T., Huiskonen, J. T. & Fodor, E. Isolation and characterization of the positive-sense replicative intermediate of a negative-strand RNA virus. *Proc. Natl. Acad. Sci. U. S. A.* **110**, 1–8 (2013).

15. Jorba, N., Coloma, R. & Ortín, J. Genetic trans-complementation establishes a new model for influenza virus RNA transcription and replication. *PLoS Pathog.* **5**, (2009).

16. Hatakeyama, D. *et al.* Influenza A virus nucleoprotein is acetylated by histone acetyltransferases PCAF and GCN5. *J. Biol. Chem.* **293**, 7126–7138 (2018).

17. Mondal, A. *et al.* Influenza virus recruits host protein kinase C to control assembly and activity of its replication machinery. *Elife* **6**, 1–23 (2017).

18. Hu, Y., Gor, V., Morikawa, K., Nagata, K. & Kawaguchi, A. Cellular splicing factor UAP56 stimulates trimeric NP formation for assembly of functional influenza viral ribonucleoprotein complexes. *Sci. Rep.* **7**, 4–10 (2017).

19. Chenavas, S. *et al.* Monomeric Nucleoprotein of Influenza A Virus. *PLoS Pathog.* **9**, (2013).

20. Baudin, F., Bach, C., Cusack, S. & Ruigrok, R. W. H. Structure of influenza virus RNP. I. Influenza virus nucleoprotein melts secondary structure in panhandle RNA and exposes the bases to the solvent. *EMBO J.* **13**, 3158–3165 (1994).

21. Kingsbury, D. W., Jones, I. M. & Murti, K. G. Assembly of influenza ribonucleoprotein in vitro using recombinant nucleoprotein. *Virology* **156**, 396–403 (1987).

22. Scholtissek, C. & Becht, H. Binding of ribonucleic acids to the RNP-antigen protein of influenza viruses. *J. Gen. Virol.* **10**, 11–16 (1971).

23. Jiang, F. *et al.* Structural basis of RNA recognition and activation by innate immune receptor RIG-I. *Nature* **479**, 423–427 (2011).

24. Bui, M., Myers, J. E. & Whittaker, G. R. Nucleo-cytoplasmic localization of influenza virus nucleoprotein depends on cell density and phosphorylation. *Virus Res.* **84**, 37–44 (2002).

25. Ozawa, M. *et al.* Contributions of Two Nuclear Localization Signals of Influenza A Virus Nucleoprotein to Viral Replication. *J. Virol.* **81**, 30–41 (2007).

26. Tang, Y. S., Xu, S., Chen, Y. W., Wang, J. H. & Shaw, P. C. Crystal structures of influenza nucleoprotein complexed with nucleic acid provide insights into the mechanism of RNA interaction. *Nucleic Acids Res.* **49**, 4144–4154 (2021).

27. Digard, P., Elton, D., Simpson-Holley, M. & Medcalf, E. Interaction of the influenza virus nucleoprotein with F-actin. *Int. Congr. Ser.* **1219**, 503–512 (2001).

28. Yu, M. *et al.* Identification and Characterization of Three Novel Nuclear Export Signals in the Influenza A Virus Nucleoprotein. *J. Virol.* **86**, 4970–4980 (2012).

29. Mullin, A. E., Dalton, R. M., Joao Amorim, M., Elton, D. & Digard, P. Increased amounts of the influenza virus nucleoprotein do not promote higher levels of viral genome replication. *J. Gen. Virol.* **85**, 3689–3698 (2004).

30. Palese, P. & Shaw, M. *Orthomyxoviridae: The Viruses and Their Replication. Fields Virology, Volume 2*. (2001).

31. Rehwinkel, J. & Gack, M. U. RIG-I-like receptors: their regulation and roles in RNA sensing. *Nat. Rev. Immunol.* **20**, 537–551 (2020).

32. Yamanaka, K., Ishihama, A. & Nagata, K. Reconstitution of influenza virus RNA-nucleoprotein complexes structurally resembling native viral ribonucleoprotein cores. *J. Biol. Chem.* **265**, 11151–11155 (1990).

33. te Velthuis, A. J. W. *et al.* Mini viral RNAs act as innate immune agonists during influenza virus infection. *Nat. Microbiol.* **3**, 1234–1242 (2018).

34. Dimmock, N. J. & Easton, A. J. Defective Interfering Influenza Virus RNAs: Time To Reevaluate Their Clinical Potential as Broad-Spectrum Antivirals? *J. Virol.* **88**, 5217–5227 (2014).

35. Van Nostrand, E. L. *et al.* Robust transcriptome-wide discovery of RNA-binding protein binding sites with enhanced CLIP (eCLIP). *Nat. Methods* **13**, 508–514 (2016).

36. Le Sage, V. *et al.* Non-uniform and non-random binding of nucleoprotein to influenza A and B viral RNA. *Viruses* **10**, 1–11 (2018).

37. Le Sage, V. *et al.* Mapping of Influenza Virus RNA-RNA Interactions Reveals a Flexible Network. *Cell Rep.* **31**, 107823 (2020).

38. Williams, G. D. *et al.* Nucleotide resolution mapping of influenza A virus nucleoprotein-RNA interactions reveals RNA features required for replication. *Nat. Commun.* **9**, 1–12 (2018).

39. Palazzo, A. F. & Lee, E. S. Non-coding RNA: What is functional and what is junk? *Front. Genet.* **5**, 1–11 (2015).

40. Van Nostrand, E. L. *et al.* A large-scale binding and functional map of human RNA-binding proteins. *Nature* **583**, 711–719 (2020).

41. Hoffmann, A. *et al.* Accurate mapping of tRNA reads. *Bioinformatics* **34**, 1116–1124 (2018).

42. Yeo, G. W. *et al.* An RNA code for the FOX2 splicing regulator revealed by mapping RNA-protein interactions in stem cells. *Nat. Struct. Mol. Biol.* **16**, 130–137 (2009).

43. Hentze, M. W., Castello, A., Schwarzl, T. & Preiss, T. A brave new world of RNA-binding proteins. *Nat. Rev. Mol. Cell Biol.* **19**, 327–341 (2018).

44. McInnes, L., Healy, J. & Melville, J. UMAP: Uniform Manifold Approximation and Projection for Dimension Reduction. (2018).

45. Bi, X. *et al.* RNA Targets Ribogenesis Factor WDR43 to Chromatin for Transcription and Pluripotency Control. *Mol. Cell* **75**, 102-116.e9 (2019).

46. Mourão, A. *et al.* Structural basis for the recognition of spliceosomal SmN/B/B' proteins by the RBM5 OCRE domain in splicing regulation. *Elife* **5**, 1–26 (2016).

47. Wang, Y., Medvid, R., Melton, C., Jaenisch, R. & Blelloch, R. DGCR8 is essential for microRNA biogenesis and silencing of embryonic stem cell self-renewal. *Nat. Genet.* **39**, 380–385 (2007).

48. Chen, K. *et al.* The Overlooked Fact: Fundamental Need for Spike-In Control for Virtually All Genome-Wide Analyses. *Mol. Cell. Biol.* **36**, 662–667 (2016).

49. Orlando, D. A. *et al.* Quantitative ChIP-Seq normalization reveals global modulation of the epigenome. *Cell Rep.* **9**, 1163–1170 (2014).

50. Miyamoto, S. *et al.* Migration of In fl uenza Virus Nucleoprotein into the Nucleolus Is Essential for Ribonucleoprotein Complex Formation.

51. Neumann, G., Castrucci, M. R. & Kawaoka, Y. Nuclear import and export of influenza virus nucleoprotein. *J. Virol.* **71**, 9690–9700 (1997).

52. Arun, G., Aggarwal, D. & Spector, D. L. MALAT1 long non-coding RNA: Functional implications. *Non-coding RNA* **6**, 1–17 (2020).

53. Chiang, J. J. *et al.* Viral unmasking of cellular 5S rRNA pseudogene transcripts induces RIG-I-mediated immunity article. *Nat. Immunol.* **19**, 53–62 (2018).

54. Vabret, N. *et al.* Y-RNAs lead an endogenous program of RIG-I agonism mobilized upon RNA virus infection and targeted by HIV. *bioRxiv* (2019) doi:10.1101/773820.

55. Zhao, Y., Ye, X., Dunker, W., Song, Y. & Karijolich, J. RIG-I like receptor sensing of host RNAs facilitates the cell-intrinsic immune response to KSHV infection. *Nat. Commun.* **9**, 1–14 (2018).

56. Choi, J. H. *et al.* DUSP11-mediated control of 5′-triphosphate RNA regulates RIG-I sensitivity. *Genes Dev.* **34**, 1697–1712 (2020).

57. Linder, A. *et al.* Defective Interfering Genomes and the Full-Length Viral Genome Trigger RIG-I After Infection With Vesicular Stomatitis Virus in a Replication Dependent Manner. *Front. Immunol.* **12**, 1–17 (2021).

58. Baum, A., Sachidanandam, R. & García-Sastre, A. Preference of RIG-I for short viral RNA molecules in infected cells revealed by next-generation sequencing. *Proc. Natl. Acad. Sci. U. S. A.* **108**, 3092 (2011).

59. Devarkar, S. C., Schweibenz, B., Wang, C., Marcotrigiano, J. & Patel, S. S. RIG-I Uses an ATPase-Powered Translocation-Throttling Mechanism for Kinetic Proofreading of RNAs and Oligomerization. *Mol. Cell* **72**, 355-368.e4 (2018).

60. Lässig, C. *et al.* ATP hydrolysis by the viral RNA sensor RIG-I prevents unintentional recognition of self-RNA. *Elife* **4**, 1–20 (2015).

61. Curran, J., Marq, J. B. & Kolakofsky, D. An N-terminal domain of the Sendai paramyxovirus P protein acts as a chaperone for the NP protein during the nascent chain assembly step of genome replication. *J. Virol.* **69**, 849–855 (1995).

62. Choi, J. H. & Sullivan, C. S. DUSP11 and triphosphate RNA balance during virus infection. *PLoS Pathog.* **17**, 1–7 (2021).

63. Kato, H., Oh, S. W. & Fujita, T. RIG-I-like receptors and type I interferonopathies. *J. Interf. Cytokine Res.* **37**, 207–213 (2017).

64. Louber, J., Brunel, J., Uchikawa, E., Cusack, S. & Gerlier, D. Kinetic discrimination of self/non-self RNA by the ATPase activity of RIG-I and MDA5. *BMC Biol.* **13**, 11–14 (2015).

65. Busch, H., Ramachandra, R., Rothblum, L. & YC, C. SnRNAs, SnRNPs, and RNA processing. *Annu. Rev. Biochem.* (1982).

66. Jeronimo, C. *et al.* Systematic Analysis of the Protein Interaction Network for the Human Transcription Machinery Reveals the Identity of the 7SK Capping Enzyme. *Mol. Cell* **27**, 262–274 (2007).

67. Devarkar, S. C. *et al.* Structural basis for m7G recognition and 2′-O-methyl discrimination in capped RNAs by the innate immune receptor RIG-I. *Proc. Natl. Acad. Sci. U. S. A.* **113**, 596–601 (2016).

68. Hopper, A. K. & Phizicky, E. M. tRNA transfers to the limelight. *Genes Dev.* **17**, 162–180 (2003).

69. Tomita, K. & Liu, Y. Human BCDIN3D is a cytoplasmic tRNAHis-specific 5'-monophosphate methyltransferase. *Front. Genet.* **9**, 1–6 (2018).

70. Leung, D. W., Basler, C. F. & Amarasinghe, G. K. Molecular mechanisms of viral inhibitors of RIG-I-like receptors Daisy. *Trends Microbiol.* **20**, 139–146 (2012).

71. Childs, K. S., Andrejeva, J., Randall, R. E. & Goodbourn, S. Mechanism of mda-5 Inhibition by Paramyxovirus V Proteins. *J. Virol.* **83**, 1465–1473 (2009).

72. Fan, L., Briese, T. & Lipkin, W. I. Z Proteins of New World Arenaviruses Bind RIG-I and Interfere with Type I Interferon Induction. *J. Virol.* **84**, 1785–1791 (2010).

73. Gack, M. U. *et al.* Influenza A Virus NS1 Targets the Ubiquitin Ligase TRIM25 to Evade Recognition by the Host Viral RNA Sensor RIG-I. *Cell Host Microbe* **5**, 439–449 (2009).

74. Brisse, M. & Ly, H. Viral inhibitions of PACT-induced RIG-I activation. *Oncotarget* **8**, 60725–60726 (2017).

75. Varga, Z. T., Grant, A., Manicassamy, B. & Palese, P. Influenza Virus Protein PB1-F2 Inhibits the Induction of Type I Interferon by Binding to MAVS and Decreasing Mitochondrial Membrane Potential. *J. Virol.* **86**, 8359–8366 (2012).

76. Prins, K. C., Cárdenas, W. B. & Basler, C. F. Ebola Virus Protein VP35 Impairs the Function of Interferon Regulatory Factor-Activating Kinases IKKε and TBK-1. *J. Virol.* **83**, 3069–3077 (2009).

77. Barik, S. What really rigs up RIG-I? *J. Innate Immun.* **8**, 429–436 (2016).

78. Baum, A. & García-Sastre, A. Differential recognition of viral RNA by RIG-I. *Virulence* **2**, 166–169 (2011).

79. Fauver, J. R. *et al.* A reverse-transcription/RNase H based protocol for depletion of mosquito ribosomal RNA facilitates viral intrahost evolution analysis, transcriptomics and pathogen discovery. *Virology* **528**, 181–197 (2019).

80. McHugh, C. A. *et al.* The Xist lncRNA interacts directly with SHARP to silence transcription through HDAC3. *Nature* **521**, 232–236 (2015).

81. Huppertz, I. *et al.* iCLIP: Protein-RNA interactions at nucleotide resolution. *Methods* **65**, 274–287 (2014).

82. Tran, V. *et al.* Influenza virus repurposes the antiviral protein IFIT2 to promote translation of viral mRNAs. *Nat. Microbiol.* **5**, 1490–1503 (2020).

83. Kim, D., Langmead, B. & Salzberg, S. L. HISAT: a fast spliced aligner with low memory requirements. *Nat. Methods* **12**, 357–360 (2015).

84. Langmead, B. & Salzberg, S. L. Fast gapped-read alignment with Bowtie 2. *Nat. Methods* **9**, 357–359 (2012).

85. Bushnell, B., Rood, J. & Singer, E. BBMerge – Accurate paired shotgun read merging via overlap. *PLoS One* **12**, 1–15 (2017).

86. Grabherr, M. G. ., Brian J. Haas, Moran Yassour Joshua Z. Levin, Dawn A. Thompson, Ido Amit, Xian Adiconis, Lin Fan, Raktima Raychowdhury, Qiandong Zeng, Zehua Chen, Evan Mauceli, Nir Hacohen, Andreas Gnirke, Nicholas Rhind, Federica di Palma, Bruce W., N. & Friedman, and A. R. Trinity: reconstructing a full-length transcriptome without a genome from RNA-Seq data. *Nat. Biotechnol.* **29**, 644–652 (2013).

87. Robinson, M. D., McCarthy, D. J. & Smyth, G. K. edgeR: A Bioconductor package for differential expression analysis of digital gene expression data. *Bioinformatics* **26**, 139–140 (2009).

88. Quinlan, A. R. & Hall, I. M. BEDTools: A flexible suite of utilities for comparing genomic features. *Bioinformatics* **26**, 841–842 (2010).

-

CHAPTER 4
Discussion

Author Contributions:
M.P.L generated all data in the chapter.

Summary

Viruses exist solely to selfishly spread genetic elements. To broadly accomplish this ultimate goal, viruses must insert themselves into their host environment and utilize pre-existing cellular pathways to their replicative advantage[1,2]. To combat this manipulation, hosts initiate innate immune pathways in an attempt to block nearly every step of the viral replication cycle. These selective pressures propagate viruses resistant to host countermeasures. Thus, viruses are subject to their immediate cellular environment, and their replication strategies reflect and embrace the hostile antiviral environment of the host.

Direct host/virus interactions underpin the successful replication of viruses. To explore these linkages, prior studies of host interactions with influenza virus have focused extensively on protein-protein interfaces regulating the viral lifecycle[3]. While informative and important for understanding influenza viruses, they largely ignore an underappreciated swathe of influenza biology that revolves around RNA-binding protein:RNA interactions. RNA regulation is central to normal cellular function and occupies a substantial branch of the innate response to viruses, especially for RNA viruses[4,5]. Studying RNA-binding proteins has historically presented challenges that limit the interpretation of global analyses, slowing the progression of the field, but recent advances in high-throughput RNA methodologies now allow for the rigorous dissection of RNA-binding proteins and the RNAs they regulate in infection[6,7].

In the first chapter of this thesis, we dissected the interaction between a host RNA-binding protein and the viral mRNAs that it regulates. We identified interferon-induced protein with tetratricopeptide repeats 2 (IFIT2) as a proviral regulator of influenza virus gene expression in a CRISPR-based screen. Given that IFIT2 is a demonstrated ISG and antiviral effector for multiple viruses, this proviral activity occurred because influenza virus exploited of an interferon-induced RNA-binding protein. High-throughput characterization of bound RNAs

revealed that IFIT2 primarily associates with host mRNA coding sequences and 3’ UTRs. IFIT2 also engages influenza mRNAs. IFIT2 RNA-binding activity was found to positively regulate the translation of bound messages by promoting ribosome processivity. Collectively, these studies elucidated the molecular mechanism by which IFIT2 functions and revealed how influenza virus usurps a canonically antiviral RNA-binding protein to enhance viral replication.

In the second chapter of this thesis, we characterized the interplay between the viral nucleoprotein (NP), the host transcriptome, and host RNA-binding proteins that regulate innate immune activation. NP is a structural component of the influenza virus ribonucleoprotein (RNP) complex and displays non-specific RNA-binding and oligomerization characteristics. Surprisingly, we found that NP also binds a discrete population of host RNAs during infection, comprised mostly of non-coding RNAs. We demonstrate that these RNAs become immunogenic during infection, and using quantitative high-throughput sequencing methodologies, that the RNA pattern recognition receptor RIG-I binds and monitors these RNAs. These data suggest that NP binds immunogenic RNAs and interferes with their activation of RIG-I, taming infection-induced self-sensing of RNAs that would otherwise suppress viral replication.

In summation, these unique instances of influenza virus mediated regulation, where a host RNA-binding protein engages viral RNAs and a viral RNA-binding protein sequesters host RNAs, emphasize the importance of and highlight the functional volatility that exist at the RNA interface in viral infection.

1.1 IFIT2 as a translational regulator

We identified IFIT2 in a genome-wide CRISPR-based screen for proviral influenza host factors, paradoxically in contrast to the known role for IFIT2 as an antiviral effector[8–11]. The IFIT proteins are vertebrate specific ISGs potently induced during type I interferon responses[5]. They

display marked species-specific adaptation, with human IFIT2 and murine Ifit2 sharing ~60% sequence identity, reinforcing the importance of this family in shaping the evolutionary history of vertebrate species. The IFIT proteins have demonstrated roles in restricting the replication of diverse viral families, often dependent on the host species and specific IFIT protein[12–14]. This restriction is best defined for IFIT1, where discrimination of 2'O-methylation allows IFIT1 to bind and inhibit the cap-dependent translation of viral Cap0 mRNAs[15]. It has been suggested that IFIT2 similarly displays a role in translation inhibition, but this effect is centered around binding and disrupting eIF3 function[16]. However, other work has been unable to repeat these observations and suggests that IFIT2 does not function during translation initiation[17,18]. A specific function for IFIT2 during initiation remains to be established. Despite the appreciated role in exercising RNA-mediated restriction of viruses, the *in vivo* RNA ligands of IFITs have not been well characterized. We formerly defined the bound RNA targets and characterized a molecular function for IFIT2. Our work demonstrates a starkly new role for IFIT proteins, where IFIT2 binds mRNAs to enhance their translation. Altogether, these data suggest IFIT2 functions as a post-transcriptional regulator of mRNA translation during type I inteferon responses.

1.2.Cellular function of IFIT2

In addition to the work presented in chapter 2, we sought to determine the role for IFIT2 in generalized type I interferon responses. In parallel with the samples generated during influenza infection, we performed eCLIP and Ribo-seq on cells treated with type I interferon. We detected a similar binding profiles during infection or a type I interferon response, suggesting that infection does not dramatically change the RNAs bound by IFIT2 (Fig. 1A). Similar to what was observed during influenza infection, cells lacking IFIT2 poorly translate IFIT2-bound RNAs, supporting a role for IFIT2 in regulating the translation of ISG mRNAs during type I

interferon responses (Fig. 1B). The cumulative effect is the increased production of a subset of ISGs and a generic enhancement of anti-pathogen responses. This activity is consistent with the normal antiviral role for IFIT2, and raises the possibility that restriction of viruses such as vesicular stomatitis virus and Sendai virus is mediated entirely by the indirect effects of ISG stimulation exerted by IFIT2[8,99]. Indeed, cells lacking IFIT2 poorly express a subset of ISGs and likely make less protein from the IFIT2-target transcripts that are present (Fig. 1C). While IFIT2 does associate with ~25% of known ISGs, some of the differentially expressed genes identified here are not directly regulated by IFIT2, suggesting that multiple networks of interferon regulatory genes act in concert to exert the antiviral functions of IFIT2. These data identify a post-transcriptional gene network potentially responsible for the efficient induction of innate responses to viral infection.

Cells lacking IFIT2 exhibited a unique translational phenomenon where bound mRNAs accumulated ribosomes at discrete locations, indicative of a ribosome processivity defect[19]. While it is clear that IFIT2 regulates the translation of bound messages, the cis- or trans-acting factors responsible for IFIT2-regulated ribosome processivity defects are not known. Processivity can be regulated by RNA secondary structure, highly structured regions of nascent polypeptides, oxidative damage to mRNAs, tRNA deprivation and starvation, or unique di-codon sequences[20,21]. These stressors prevent elongation of the ribosome and recruit ribosome quality control proteins to mediate the disassembly and destruction of the stalled ribosome and mRNA[22,23]. It is possible that IFIT2 recruits other trans-acting ribosome quality control factors such as ZNF598, RACK1, or EDF1 to help resolve stalled ribosomes on ISG mRNAs[23–27]. Regardless of the method by which IFIT2 alleviates ribosome processivity defects, this represents a new axis for the translational regulation of interferon responses. In addition to a role

in innate immunity, IFIT2 also promotes the induction of apoptosis and activation of caspases[28,29]. Our data suggest that the RNA-binding activity of IFIT2 can regulate apoptosis, and that this is partially responsible for influenza-induced cell death. Given the role for IFIT2 in regulating translation, it is possible that the apoptotic effects are regulated by IFIT2-mediated production of apoptosis-inducing proteins, connecting the translational role of IFIT2 to both innate immunity and intrinsically induced cell death pathways.

1.3 IFIT RNA-binding

IFIT tetratricopeptide repeats uniquely mediate the RNA-binding abilities of this family. IFIT1 and IFIT5 both discriminate the 5'-ends of RNA, and utilize tandem tetratricopeptide repeats to cradle the phosphodiester backbone of RNA in a positively charged binding tunnel[14,30,31]. This binding mode is independent of RNA sequence, and only discriminates the 5'-end of RNAs with hydrophobic residues existing at the bottom of the RNA tunnel. When IFIT2 was first characterized, it was proposed that IFIT2 binds double-stranded AU-rich RNA, representing a binding mode that potentially differs from the narrow binding channels present in IFIT1 and IFIT5[17].

Our genome-wide analysis suggests that IFIT2 does have specificity for AU-rich RNAs in cells, and recognizes a degenerate "UAGnnUAU" motif present in some target RNAs. The width of the binding channel, observation that IFIT2-binding occurs internally on RNAs, and sequence specificity of IFIT2 collectively propose a novel RNA-binding mechanism. IFIT2 was crystallized in a domain swapped dimer conformation, where helices 7-9 are swapped with a binding partner to generate an extensive binding interface of both electrostatic and hydrophobic interactions[17]. With a binding interface of >4000 angstroms, this likely represent a highly stable structure.

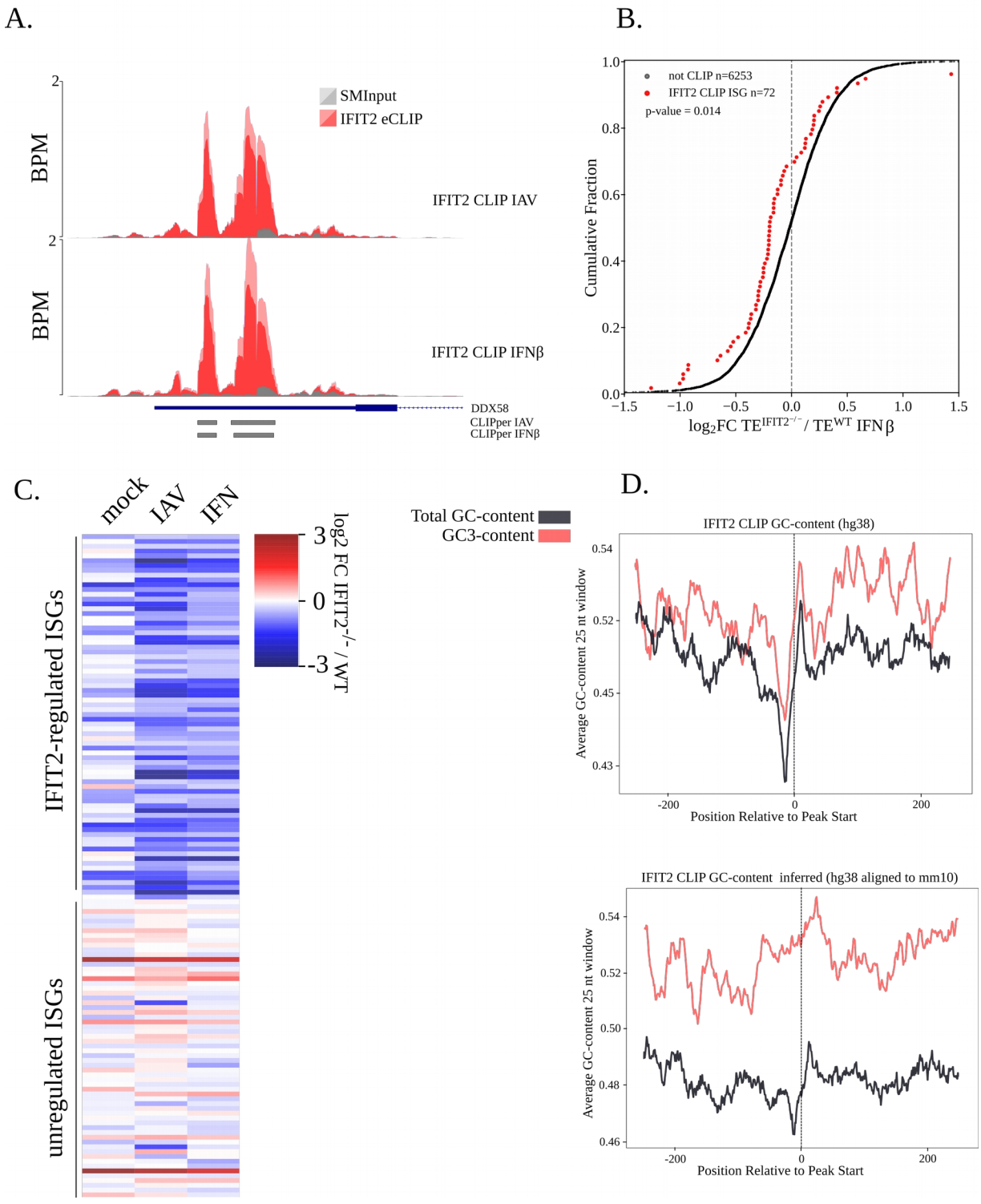

Figure 1. IFIT2 post-transcriptionally regulates type I interferon responses. (A) Read coverage in bins per million (BPM) over the DDX58 (RIG-I) 3'-UTR from IFIT2 eCLIP libraries of A549s infected with influenza (m.o.i.=0.02, 24h) or treated with IFNβ (250 U/mL, 8h) relative to SMInput. CLIPper-called peaks denoted under coverage track. Solid colors represent mean and shaded represent standard deviation of (n=2) biological replicates. (B) Cumulative distribution curves of $\log_2$ changes in translation

efficiency between IFIT2 knockout and wildtype A549s treated with 250 U/mL IFNβ for 8h. Translation efficiency was calculated by normalizing ribosome-profiling reads to mRNA abundance in mRNA-sequencing libraries. Red dots denote IFIT2-bound interferon-stimulated genes (ISGs), black represent all other transcripts. P-value calculated with Mann-Whitney U test. (C) Log_2 fold changes in gene expression as measured by mRNA-seq between IFIT2 knockout and wildtype cells mock treated, infected with influenza (m.o.i.=0.02, 24h) or treated with IFNβ (250 U/mL, 8h). Genes separated by IFIT2-regulated ISGs (top) with log_2 fold change < -0.58 in both influenza and IFNβ conditions or a subsample of unregulated ISGs (bottom). (D) Human (hg38) coding sequences with IFIT2 CLIP peaks were aligned to orthologous sequences in mice (mm10) and both GC-content and GC3-content (wobble base GC-content) were calculated in 25 nt windows and plotted relative to the center of the CLIP peak in humans (top) or the orthologous IFIT2-bound region in mice (bottom). Low GC3-content around CLIP peaks not preserved in mice.

Dimerization effectively buries the majority of the RNA-binding interface, possibly preventing RNA recognition. Thus, dimerization of IFIT2 may regulate its ability to associate with RNA, and future studies are needed to determine the role and regulation of homodimers in IFIT2 function.

Despite their evolutionary relatedness, paralogues and orthologues of IFIT proteins recognize discrete moieties in RNA to regulate RNA-binding[12,14,30]. For example, human IFIT1B and its paralogue murine Ifit1 bind and independently recognize different cap structures to mediate disparate antiviral specificities. In contrast, our data suggest that both IFIT2 and murine Ifit2 positively regulate influenza virus gene expression. Unlike IFIT1B proteins, this observation may indicate that IFIT2 paralogues retain similar functionality, despite ~60% sequence identity. To test this, we aligned the human mRNA sequences of IFIT2 CLIP peaks localized within coding sequences to their corresponding murine coding sequences. IFIT2 peaks demonstrate AU-rich preferences in both the total sequence (GC) and the GC-content of the wobble base (GC3), suggesting that IFIT2-binds coding sequences with AU-rich codons (Fig. 1D, top). Human CLIP peaks transposed onto murine Ifit2 sequences demonstrate AU-rich preferences in the total sequence, indicative of amino acid conservation. In contrast, this preference is lost in the wobble base, indicating that selection for AU-rich codons at locations of IFIT2-binding in humans is absent in mice (Fig. 1D, bottom). This observation could be a result of the recognition of different mRNAs or unique sequence preferences of IFIT2 paralogues. Regardless, these data suggest that IFIT2 paralogues likely enhance influenza virus gene expression independently, and that their sequence and binding preferences mirror their percent sequence identity.

1.4 Roles for IFIT complexes and mRNA gene networks

Not only does IFIT2 homodimerize, but IFIT2 and IFIT3 also associate and are predicted to form a similar domain-swapped dimer architecture[18,28]. While IFIT2 can stimulate apoptosis when expressed in isolation, IFIT3 is known to abrogate this phenotype. Our data suggest that RNA-binding is important for IFIT2-dependent apoptosis. Together, these observations encourage a model where the RNA-binding activities of IFIT2 are regulated by dimerization with IFIT3. As part of larger superstructures, IFIT2 and IFIT3 can also associate with IFIT1[18,28,32]. IFIT1 was demonstrated to play no role in restricting influenza virus, but we interestingly identified IFIT1 as a top pro-viral hit in our CRISPR-based screen[33]. Because the screen leveraged cell death as a selection mechanism, it is possible that IFIT1 acts with IFIT2 and IFIT3 to promote influenza virus-induced cell death. It is tempting to speculate on the functional role of IFIT heterocomplexes in regulating RNA, but direct experiments in cells lacking specific IFIT proteins are needed in order to disambiguate the combined roles of RNA-binding by IFITs.

To address the separate and combined roles of IFIT proteins, future studies can utilize pre-existing knockout clones of IFIT genes to build a human cell line that lacks all four IFIT proteins. Reintroduction of IFIT proteins into a genetically clean background would allow for the evaluation of the role for single or combined IFIT proteins in regulating known IFIT-mediated phenomenon. In addition, development of eCLIP-seq spike-in strategies in Chapter 3 could be used to quantitatively assess the binding of IFIT proteins to host or viral RNAs in heterocomplexes. The IFIT1:IFIT3 interface could act as a convenient control for these experiments, where the C-terminus of IFIT3 regulates the cap0-binding affinity of IFIT1[34].

As an mRNA-binding protein, IFIT2 also indirectly interacts with a network of proteins

regulating mRNA translation, localization, and turnover[35–38]. IFIT2 functions during translation by binding and recognizing AU-rich elements in mRNAs, a common motif in regulating RNA stability and half-life[27,39]. mRNAs with these AU-rich sequences are regulated by mRNA binding proteins like AU-rich element RNA-binding protein 1 (AUF1) or K-homology splicing regulatory protein (KSRP), which destabilize mRNAs and promote their decay[40–42]. Competition for AU-rich elements at baseline is an intriguing mechanism for the tight control of the expression of IFIT2-bound ISGs, where ISG mRNAs are hypothetically degraded unless high levels of IFIT2 effectively compete for the same pool of targets. In sum, IFIT2 is one member of a much larger network of hundreds of mRNA-binding proteins, and the degeneracy by which mRNA-binding proteins recognize their targets suggest that multiple overlapping regulatory networks influence gene expression in type I interferon responses[39,43–45].

1.5 Co-option of IFIT2:

Understanding the cellular role for IFIT2 provides insight into influenza's co-option of this antiviral factor. Viruses are subject to the immediate host environment in which they replicate, and in the case of acute infections like those of influenza virus, it is almost always an antiviral state[1,46,47]. When viruses co-opt host factors, they are naive to our superficial categorization of host proteins as broadly pro- or antiviral. IFIT2 plays a role in positively regulating translation of ISG mRNAs to globally enhance the antiviral state. This same process represents a convenient target during infection for influenza virus usurp to enhance expression of its own gene product. Thus, whether proteins are "proviral" or "antiviral" is contextual, dependent on the virus, the cell and the host background.

2.1 NP innate-immune antagonism

Nucleoproteins are indispensable to viral replication cycles of negative-strand RNA viruses, where they oligomerize on viral RNA in a sequence agnostic fashion[48–51]. Viruses express high levels of nucleoproteins to facilitate genome replication. These levels far exceed the quantity present in RNPs and thus hint at the existence of additional roles for nucleoproteins[52–54]. Here, we unbiasedly profiled the RNAs bound by influenza virus NP during infection. Contrary to a non-specific aggregation model, NP associates with specific classes of non-coding RNAs during infection. These RNAs are functionally diverse, and represent small non-coding RNAs that play roles in splicing, ribosome biogenesis, transcription, translation, and other minor cellular tasks. Infection differentially induces the immunogenecity of these RNA species, suggesting that they are dynamically regulated during infection. Accordingly, these short RNAs are also actively surveyed by the pattern recognition receptor, RIG-I. These data develop a model whereby sequence-independent associations between NP and host RNAs facilitate the disruption of RIG-I's normal activity in monitoring the RNA landscape in cells.

2.2 RIG-I sensing of host non-coding RNAs

As a PRR, RIG-I is responsible for surveying the cell for RNAs for viruses or other pathogens[4,55]. To accomplish this task, RIG-I specifically searches for PAMPs that are characteristic of RNA viruses. The PAMP sensed by RIG-I resembles the ends of negative-strand RNA virus genomes, where base-pairing between the 5'- and 3'-ends creates a short double-stranded RNA duplex adorned by a 5'-triphosphate[56,57]. The C-terminal domain (CTD) of RIG-I differentially binds and discriminates 5'-triphosphates from 5'-monophosphates to mediate the loading of a helicase domain onto the blunt-ended substrate, subsequently releasing the N-terminal CARDs from an autoinhibited state[4,58,59]. ATP-hydrolysis then promotes the

translocation of RIG-I away from the 5’-end of RNA, re-exposing the PAMP and allowing another RIG-I molecule to potentially bind[60–62].

Oligomerization of RIG-I onto substrate RNAs likely represents the biologically relevant active form of the PRR. Multimerization of at least four adjacent molecules allows RIG-I to signal through MAVS to promote induction of innate immunity[63,64]. RIG-I has a footprint of 8-10 nucleotides of dsRNA which encourages a model where RIG-I substrates must be at least ~65 nucleotides in length in order to efficiently signal[60]. Indeed, it was found that increasing the length of dsRNA substrate from ~50 nucleotides to ~200 nucleotides can result in >10,000-fold differences in the immunogenicity of short RNAs[65]. Activation of MAVS via RIG-I with RNAs shorter than 50 nucleotides is thought to occur as the result of TRIM25 mediated ubiquitination and bundling of CARDS from RIG-I molecules bound to separate PAMP RNAs[64,66,67]. This mechanism allows for RIG-I to still perform its function in recognizing very short PAMP RNAs, albeit at a much lower efficiency relative to slightly longer RNA substrates.

The biochemical kinetics of RIG-I association with RNAs directly influence its functional role in RNA surveillance. The CTD of RIG-I binds RNA with an association constant that approaches the theoretical diffusion limit, thus bounding the association between a discrete RIG-I molecule and RNA only by the concentration of the RNA ligand itself, assuming that RIG-I is the limiting component[60]. Dissociation of RIG-I from immunogenic 5’-triphosphylated RNA versus silent 5´monophosphorylated RNA is then regulated by dissociation constants that differ by only two-fold. Specificity for 5’-triphosphate ends is further regulated by the rates of helicase loading and ATP-hydrolysis/translocation, which occur faster and slower respectively dependent upon the presence of 5’-triphosphates. This model allows for the accumulation of RIG-I molecules on PAMP RNAs, but also necessitates and suggests the presence of a recycling

mechanism, where RIG-I aberrantly bound to host RNAs can translocate and eject itself off of host non-coding RNAs prior to oligomerization to prevent signaling[60–62,65]. Reliance upon oligomerization for activation leaves RIG-I vulnerable to disruptions of this proofreading activity.

Our quantitative eCLIP of RIG-I at baseline or during influenza virus infection fit well with previous biochemical and *in vivo* studies of RIG-I function. We define a small pool of host-non coding RNAs that are bound and monitored by RIG-I. This includes U6 snRNAs, Y RNAs, vault RNAs, and tRNAs. All of these RNAs are highly expressed and stable throughout infection, and the expansive size of this pool (YRNAs can be present at >1,000,000 copies per cell) in combination with biochemical information suggest that discrete RIG-I molecules are likely always contacting host non-coding RNAs, performing their normal function in surveying the RNA landscape of cells[68,69]. This mechanism not only allows for the normal function of RIG-I, but also host regulation of the RIG-I pathway via modulation of non-coding RNA 5'-ends.

2.3 Regulation of RNA ends and RNA localization

Our data indicate that non-coding RNA 5'-ends are specifically regulated during infection to alter their immunogenicity. NP-bound non-coding RNA purified from uninfected cells failed to initiate RIG-I sensing, while those same RNAs isolated from infected cells potently activated innate immune responses. Of the RNAs surveyed by RIG-I, all are transcribed by RNA pol III, suggesting that all exist with a 5'-triphosphate at least transiently[70]. RNA pol III transcribed RNAs are regulated by enzymes that catalyze the removal or modification of 5'-triphosphate moieties. This step in the processing of ncRNAs has been implicated in the RIG-I-mediated induction of innate immunity to viruses that do not ordinarily produce RIG-I ligands[71,72].

Dual-specificity phosphatase 11 (DUSP11) has been connected to the regulation of innate immunity via trimming of 5’-triphosphates to 5’-monophosphates. This activity has been shown to regulate innate immunity in the tumor microenvironment via regulation of vesicle-enclosed 7SL RNAs, influence reactivation of KSHV via stimulation of RIG-I with 5’-triphosphate vaultRNAs, and similarly promote the restriction of HIV via differential regulation of the 5’-ends of Y RNAs[71–74]. Thus, our observations of differential immunogenicity of non-coding RNAs during infection may be mediated by regulation of DUSP11 during influenza virus infection.

Some RNA pol III transcribed RNAs like tRNAs are post-transcriptionally processed to remove their 5’-end, thus making them unlikely agonists of RIG-I. Other RNA pol III transcribed RNAs such as U6 snRNA and 7SK RNA are post-transcriptionally capped by MEPCE to yield a γ-methyltriphosphate moiety[75]. While it is unlikely that RIG-I can discriminate between 5’-triphosphates and 5’- γ-methyltriphosphates based on structural predictions, γ-methyltriphosphates are resistant to CIP-mediate dephosphorylation, and may similarly prevent γ-methyltriphosphate RNAs from being regulated by DUSP11[76]. How RIG-I avoids oligomerizing upon U6 snRNAs is not understood, but other RNAs such as m7G-capped RNAs represent poor substrates for RIG-I recognition because of 2’O-methylation of the first and second ribose sugars of mRNAs[77]. This process of 2’O-methylation can be regulated during interferon responses where cap 2’O-methyl transferase is responsible for the methylation of specific ISG mRNAs and subsequent relief of IFIT1-mediated translational repression[78]. U6 snRNAs are heavily decorated with post-transcriptional modifications including 2’O-methylation[79]. Thus, it is possible that other enzymatic modifiers play a role in the infection-specific regulation of 5’-ends of non-coding RNAs, thereby regulating the intrinsic ability of these RNAs to stimulate RIG-I.

Other RNAs with 5’-triphosphate ends are shielded from recognition by RIG-I by RNA-binding partners. During HSV-1 infection, a 5S rRNA pseudogene is released from its ribosomal protein binding partners and translocates to the cytosol to stimulate RIG-I[80]. We similarly identified that some 5S rRNA pseudogenes bind to RIG-I, but these are dwarfed in quantity compare to other non-coding RNA partners. RIG-I is a primarily cytoplasmic protein, and thus the nuclear-cytoplasmic localization of RNAs undoubtedly plays a role in making substrates available to RIG-I in the cytosol. We identify U6 snRNAs as RIG-I interactors, which function in pre-mRNA splicing in the nucleus. Spliceosomal snRNAs are assembled into their respective snRNPs in the cytosol before import back into the nucleus as precursors to active spliceosomes[79,81]. The cytoplasmic localization of U6 is known to be transient relative to other snRNAs, and thus supports a mechanism where RIG-I constantly samples a transient pool of U6 snRNAs searching for infection-specific induction of immunogenicity. A similar mechanism could be at play for ncRNAs that are not characterized as thoroughly, such as vtRNAs and Y RNAs. Thus, multiple mechanisms likely converge to regulate the endogenous pool of RNAs monitored by RIG-I to mediate the infection-specific change in immunogenicity that we observe.

Our data suggest that differential 5’-regulation may regulate the immunogenicity of host RNAs. To address this open question, it will be necessary to directly define the regulation of DUSP11 phosphatase activity during IAV infection. If DUSP11 plays a major role in preventing innate immune activation, we would expect that DUSP11-deficient cells produce immunogenic RNAs independent of infection. RNAs from DUSP11-deficient and IAV-infected cells would be 5’-triphosphorylated at levels greater than that of mock cells. However, RNA and peptide levels of DUSP11 are stable during IAV infection relative to mock conditions (data not show). Thus, it is possible that DUSP11 is being regulated in other ways to abrogate phosphatase activity. To

assay the activity of DUSP11 directly, we will purify DUSP11 from mock-infected or IAV-infected cells and query the ability of the native enzyme to decap 5'-triphosphorylated substrates. DUSP11 is regulated by phosphorylation, and further experiments would examine the post-translational regulation of DUSP11 activity[82]. Finally, if the 5'-phosphate status is determined to be stable during infection and independent of DUSP11, RNA mass spectrometry could be used to unbiasedly identify the RNA modifications on purifed samples of non-coding RNAs[83]. Similar to RIG-I discrimination of cap0/cap1, this could link changes in RNA modifications or processing intermediates to the activation of RIG-I.

2.4 Regulation of NP localization and role in innate sensing

Context-specific NP eCLIP revealed unique RNA-binding patterns of NP that may reflect subcellular localizations dynamically regulated throughout infection. NP contains both a nuclear import signal and a nucleolar localization signal that regulate the nuclear import of NP early during infection[84,85]. Late in infection, NP globally shifts to the cytosol with the assembly of RNPs into virions, but this global migration includes unencapsidated NP molecules[86,87]. Early studies indicated that the nuclear-cytoplasmic localization of NP is probably regulated by phosphorylation, and more recent work suggests that phosphorylation regulates a free pool of NP that exists outside of RNPs[88,89]. Thus, phosphorylation of NP may regulate the diverse RNA-binding patterns that we recognized. Post-translational cleavage of NP could also play a role in this phenomenon. Influenza A NP contains a caspase cleaveage motif (EXD/X) centered around amino acid D16[90]. This site is cleaved by caspases during infection of mammalian cells, and results in the loss of 16 amino acids from the N-terminus of NP. Coincidentally, this is also the nuclear-localization signal, and thus caspase-mediated changes in the nuclear-cytoplasmic localization of NP could play a role in regulating the RNAs bound by NP during infection. More

work is needed to understand the discrete factors that regulate the shuttling of free NP within different nuclear compartments and the cytosol in infected cells.

Our work establishes a new role for the RNA-binding capabilities of NP, and suggests that the cytoplasmic binding of host RNAs interferes with the ability for RIG-I to kinetically survey the host RNA landscape. In this model, NP binds single-stranded regions of non-coding RNAs to effectively prevent RIG-I from translocating and ejecting itself from non-coding RNAs. The change in immunogenicity observed in these non-coding RNAs may even serve as “bait”, whereby the short size of these RNAs coupled with the oligomerization properties of NP may result in an inability of RIG-I to form tetramers on immunogenic host RNAs. While NS1 still plays the predominant role in antagonizing RIG-I-dependent innate immunity, our data with NP suggest that multiple viral factors are likely at work, and that this could be a potentially ubiquitous mechanism by which negative-strand RNA viruses embed auxiliary functions in the non-specific RNA-binding of their nucleocapsids.

2.5 Additional roles for NP in regulation of other RNA processes

While the majority of host reads bound by NP were from non-coding RNAs, we also identified more than 900 bound protein-coding RNAs. These binding regions are located near the transcription start site of mRNAs and cross canonical intron/exon boundaries, suggesting that NP binds pre-mRNAs (Fig. 2A). To test if this phenomenon is occurring globally, SMInput-normalized NP CLIP read coverage was compared across the gene body of all expressed human mRNAs (Fig. 2B). Strikingly, NP is often enriched on the 5’-end of genes and absent on the 3’-end of genes. This binding pattern is reminiscent of RNA pol II ChIP-seq binding profiles, and suggests wide-spread associations with the 5’-end of nascent transcripts[91].

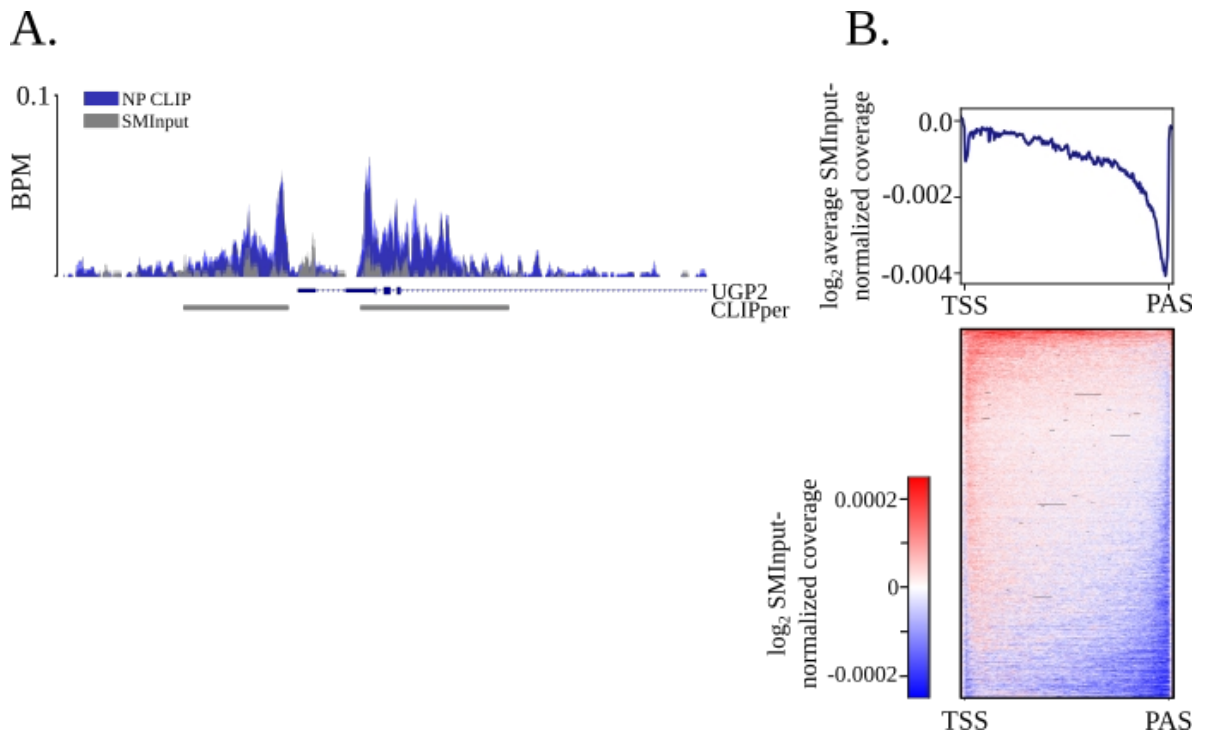

Figure 2. NP binds nascent RNAs near transcription start sites. (A) Read coverage in bins per million (BPM) over the UGP2 transcription start site in NP eCLIP libraries from A549s infected with influenza (m.o.i.=0.02, 24h) relative to SMInput. CLIPper-called peaks denoted under coverage track. Solid colors represent mean and shaded represent standard deviation of (n=2) biological replicates. CLIPper peak and read density upstream of UGP2 represent NP binding to antisense transcription product. (B) Log_2 average of SMInput-normalized NP eCLIP plotted from transcription start site (TSS) to polyA site (PAS) (top). Log_2 SMInput-normalized coverage across individual genes (bottom). NP-binding is enriched downstream of TSS.

Influenza viruses disrupt RNA pol II elongation via several mechanisms. Some strains of influenza NS1 can bind CPSF30 to prevent mRNA maturation and cause RNA pol II run on defects[92]. It has also been suggested that influenza virus exerts additional pressures on transcriptional machinery to inhibit elongation[93–95]. NP associates with several non-coding RNAs that it could be using to exert this phenomenon. U4, U5, and U6 snRNAs are assembled into the Lsm8 snRNP to mediate the final step in splicing[96]. The recruitment of the spliceosome to the first intron of pre-mRNAs facilitates the passage of RNA pol II through an initiation checkpoint allowing for rapid transcription through the gene body[97]. NP also binds 7SK RNA, the defining member of the 7SK snRNP. This complex is involved in transcription elongation, where release of positive transcription elongation factor (P-TEFb) from 7SK allows for P-TEFb to phosphorylate the RNA pol II C-terminal domain and promote transcription elongation[98]. RNAs from both of these complexes appear to associate readily with NP, and thus these could be mechanisms by which influenza virus disrupts proper RNA pol II elongation. Direct studies assaying splicing and RNA pol II elongation in infection and NP induction will be needed to elucidate the effect of NP:RNA complexes with U4/U5/U6 and 7SK RNA, respectively. These data highlight the complex nature of the role of ncRNAs in maintaining cellular homeostasis and suggest that the plastic nature by which NP engages RNAs could affect many cellular processes involving RNA.

3.1 Final Remarks

RNA-binding proteins play pivotal roles in the viral lifecycle and the innate immune response to viral pathogens. In Chapter 2 of this thesis, we describe the co-option of a normally antiviral RNA-binding protein by influenza virus to promote translation of viral mRNAs. In Chapter 3 of this thesis, we characterize the interplay between the RNA-binding activity of a

viral nucleocapsid with RNA-sensors of viral infection. Collectively, these data emphasize the ubiquitous nature of RNA-binding protein/RNA interactions in host/virus relationships. Recently, it was predicted that the human genome encodes >1700 RNA-binding proteins, of which at least 55 are involved in the innate response to pathogens[44,99]. How these 55 proteins work in concert with the RNA-binding proteins and RNA landscape of cells while also interacting with RNA and RNA-binding proteins from viruses presents an exciting frontier in virology research enabled by improved tools to characterize and study RNA-binding proteins. This work establishes just two examples of the many complex regulatory interactions that likely exist at the nexus of virology and RNA biology.

References

1. Long, J. S., Mistry, B., Haslam, S. M. & Barclay, W. S. Host and viral determinants of influenza A virus species specificity. *Nat. Rev. Microbiol.* **17**, 67–81 (2019).
2. Kirui, J., Tran, V. & Mehle, A. Host factors regulating the influenza virus replication machinery. in *Influ Curr Res.* 77–100 (2016).
3. King, C. R. & Mehle, A. The later stages of viral infection: An undiscovered country of host dependency factors. *PLoS Pathog.* **16**, 1–7 (2020).
4. Rehwinkel, J. & Gack, M. U. RIG-I-like receptors: their regulation and roles in RNA sensing. *Nat. Rev. Immunol.* **20**, 537–551 (2020).
5. Diamond, M. S. & Farzan, M. The broad-spectrum antiviral functions of IFIT and IFITM proteins. *Nat. Rev. Immunol.* **13**, 46–57 (2012).
6. Van Nostrand, E. L. *et al.* Robust transcriptome-wide discovery of RNA-binding protein binding sites with enhanced CLIP (eCLIP). *Nat. Methods* **13**, 508–514 (2016).
7. Wheeler, E. C., Van Nostrand, E. L. & Yeo, G. W. Advances and challenges in the detection of transcriptome-wide protein–RNA interactions. *Wiley Interdiscip. Rev. RNA* **9**, 1–11 (2018).
8. Fensterl, V. *et al.* Interferon-Induced Ifit2 / ISG54 Protects Mice from Lethal VSV Neuropathogenesis. **8**, (2012).
9. Wetzel, J. L., Fensterl, V. & Sen, G. C. Sendai Virus Pathogenesis in Mice Is Prevented by Ifit2 and Exacerbated by Interferon. *J. Virol.* **88**, 13593–13601 (2014).
10. Cho, H., Shrestha, B., Sen, G. C. & Diamond, M. S. A Role for Ifit2 in Restricting West Nile Virus Infection in the Brain. *J. Virol.* **87**, 8363–8371 (2013).
11. Pei, R. *et al.* Interferon-Induced Proteins with Tetratricopeptide Repeats 1 and 2 Are Cellular Factors That Limit Hepatitis B Virus Replication. *J. Innate Immun.* **6**, 182–191 (2014).
12. Daugherty, M. D., Schaller, A. M., Geballe, A. P. & Malik, H. S. Evolution-guided functional analyses reveal diverse antiviral specificities encoded by IFIT1 genes in mammals. 1–22 (2016) doi:10.7554/eLife.14228.
13. Liu, Y., Zhang, Y., Liu, T. & Gui, J. Lineage-Specific Expansion of IFIT Gene Family : An Insight into Coevolution with IFN Gene Family. **8**, (2013).
14. Mears, H. V. & Sweeney, T. R. Mouse Ifit1b is a cap1-RNA–binding protein that inhibits mouse coronavirus translation and is regulated by complexing with Ifit1c. *J. Biol. Chem.* **295**, 17781–17801 (2020).

15. Abbas, Y. M. *et al.* Structure of human IFIT1 with capped RNA reveals adaptable mRNA binding and mechanisms for sensing N1 and N2 ribose 2′-O methylations. *Proc. Natl. Acad. Sci.* **114**, E2106–E2115 (2017).

16. Terenzi, F., Hui, D. J., Merrick, W. C. & Sen, G. C. Distinct Induction Patterns and Functions of Two Closely Related Interferon-inducible Human Genes , ISG54 and ISG56 *. **281**, 34064–34071 (2006).

17. Yang, Z. *et al.* Crystal structure of ISG54 reveals a novel RNA binding structure and potential functional mechanisms. *Cell Res.* **22**, 1328–1338 (2012).

18. Fleith, R. C. *et al.* IFIT3 and IFIT2/3 promote IFIT1-mediated translation inhibition by enhancing binding to non-self RNA. *Nucleic Acids Res.* **46**, 5269–5285 (2018).

19. Collart, M. A. & Weiss, B. Ribosome pausing, a dangerous necessity for co-translational events. *Nucleic Acids Res.* **48**, 1043–1055 (2021).

20. Gebauer, F. & Hentze, M. W. Molecular mechanisms of translational control. *Nat. Rev. Mol. Cell Biol.* **5**, 827–835 (2004).

21. Ikeuchi, K., Izawa, T. & Inada, T. Recent progress on the molecular mechanism of quality controls induced by ribosome stalling. *Front. Genet.* **10**, 1–7 (2019).

22. Doma, M. K. & Parker, R. Endonucleolytic cleavage of eukaryotic mRNAs with stalls in translation elongation. *Nature* **440**, 561–564 (2006).

23. Juszkiewicz, S. & Hegde, R. S. Initiation of Quality Control during Poly(A) Translation Requires Site-Specific Ribosome Ubiquitination. *Mol. Cell* **65**, 743-750.e4 (2017).

24. Sinha, N. K. *et al.* EDF1 coordinates cellular responses to ribosome collisions. *Elife* **9**, 1–84 (2020).

25. Pevzner. 乳鼠心肌提取 HHS Public Access. *Physiol. Behav.* **176**, 139–148 (2017).

26. Sundaramoorthy, E. *et al.* ZNF598 and RACK1 Regulate Mammalian Ribosome-Associated Quality Control Function by Mediating Regulatory 40S Ribosomal Ubiquitylation. *Mol. Cell* **65**, 751-760.e4 (2017).

27. Savan, R. Post-transcriptional regulation of interferons and their signaling pathways. *J. Interf. Cytokine Res.* **34**, 318–329 (2014).

28. Stawowczyk, M., Van Scoy, S., Kumar, K. P. & Reich, N. C. The Interferon Stimulated Gene 54 Promotes Apoptosis. *J. Biol. Chem.* **286**, 7257–7266 (2011).

29. Chen, L. *et al.* Inhibition of Proteasome Activity Induces Aggregation of IFIT2 in the Centrosome and Enhances IFIT2-Induced Cell Apoptosis. *Int. J. Biol. Sci.* **13**, 383–390 (2017).

30. Katibah, G. E. *et al.* Broad and adaptable RNA structure recognition by the human interferon-induced tetratricopeptide repeat protein IFIT5. *Proc. Natl. Acad. Sci. U. S. A.* **111**, 12025–30 (2014).

31. Abbas, Y. M., Theres, B., Martínez-montero, S., Cencic, R. & Habjan, M. Structure of human IFIT1 with capped RNA reveals adaptable mRNA binding and mechanisms for. (2017) doi:10.1073/pnas.1612444114.

32. Mears, H. V. & Sweeney, T. R. Better together: The role of IFIT protein-protein interactions in the antiviral response. *J. Gen. Virol.* **99**, 1463–1477 (2018).

33. Pinto, A. K. *et al.* Human and Murine IFIT1 Proteins Do Not Restrict Infection of Negative-Sense RNA Viruses of the Orthomyxoviridae, Bunyaviridae, and Filoviridae Families. *J. Virol.* **89**, 9465–9476 (2015).

34. Johnson, B. *et al.* Human IFIT3 Modulates IFIT1 RNA Binding Specificity and Protein Stability. *Immunity* **48**, 487-499.e5 (2018).

35. Hocine, S., Singer, R. H. & Grünwald, D. RNA processing and export. *Cold Spring Harb. Perspect. Biol.* **2**, 1–20 (2010).

36. Gale, M., Tan, S.-L. & Katze, M. G. Translational Control of Viral Gene Expression in Eukaryotes. *Microbiol. Mol. Biol. Rev.* **64**, 239–280 (2000).

37. Garneau, N. L., Wilusz, J. & Wilusz, C. J. The highways and byways of mRNA decay. *Nat. Rev. Mol. Cell Biol.* **8**, 113–126 (2007).

38. Di Liegro, C. M., Schiera, G. & Di Liegro, I. Regulation of mRNA transport, localizationand translation in the nervous system of mammals (Review). *Int. J. Mol. Med.* **33**, 747–762 (2014).

39. Stumpo, D. J., Lai, W. S. & Blackshear, P. J. Inflammation: cytokines and RNA-based regulation. *Wiley Interdiscip. Rev. RNA* **1**, 60–80 (2010).

40. Sarkar, B., Xi, Q., He, C. & Schneider, R. J. Selective Degradation of AU-Rich mRNAs Promoted by the p37 AUF1 Protein Isoform. *Mol. Cell. Biol.* **23**, 6685–6693 (2003).

41. Winzen, R. *et al.* Functional Analysis of KSRP Interaction with the AU-Rich Element of Interleukin-8 and Identification of Inflammatory mRNA Targets. *Mol. Cell. Biol.* **27**, 8388–8400 (2007).

42. Lal, A. *et al.* Concurrent versus individual binding of HuR and AUF1 to common labile target mRNAs. *EMBO J.* **23**, 3092–3102 (2004).

43. Khabar, K. S. A. Post-transcriptional control during chronic inflammation and cancer: A focus on AU-rich elements. *Cell. Mol. Life Sci.* **67**, 2937–2955 (2010).

44. Hentze, M. W., Castello, A., Schwarzl, T. & Preiss, T. A brave new world of RNA-binding proteins. *Nat. Rev. Mol. Cell Biol.* **19**, 327–341 (2018).

45. Dominguez, D. *et al.* Sequence, Structure, and Context Preferences of Human RNA Binding Proteins. *Mol. Cell* **70**, 854–867 (2018).

46. Schoggins, J. W. & Rice, C. M. Interferon-stimulated genes and their antiviral effector functions. *Curr. Opin. Virol.* **1**, 519–25 (2011).

47. Schoggins, J. W. Interferon-Stimulated Genes: What Do They All Do? *Annu. Rev. Virol.* **6**, 567–584 (2019).

48. Ortín, J. & Martín-Benito, J. The RNA synthesis machinery of negative-stranded RNA viruses. *Virology* **479**–**480**, 532–544 (2015).

49. Ye, Q., Krug, R. M. & Tao, Y. J. The mechanism by which influenza A virus nucleoprotein forms oligomers and binds RNA. *Nature* **444**, 1078–1082 (2006).

50. Luo, M., Terrell, J. R. & Mcmanus, S. A. Nucleocapsid Structure of Negative Strand RNA Virus. *Viruses* **12**, (2020).

51. Ruigrok, R. W. H., Crépin, T. & Kolakofsky, D. Nucleoproteins and nucleocapsids of negative-strand RNA viruses. *Curr. Opin. Microbiol.* **14**, 504–510 (2011).

52. Curran, J., Marq, J. B. & Kolakofsky, D. An N-terminal domain of the Sendai paramyxovirus P protein acts as a chaperone for the NP protein during the nascent chain assembly step of genome replication. *J. Virol.* **69**, 849–855 (1995).

53. Chenavas, S. *et al.* Monomeric Nucleoprotein of Influenza A Virus. *PLoS Pathog.* **9**, (2013).

54. Mullin, A. E., Dalton, R. M., Joao Amorim, M., Elton, D. & Digard, P. Increased amounts of the influenza virus nucleoprotein do not promote higher levels of viral genome replication. *J. Gen. Virol.* **85**, 3689–3698 (2004).

55. Hansen, J. D., Vojtech, L. N. & Laing, K. J. Sensing disease and danger: A survey of vertebrate PRRs and their origins. *Dev. Comp. Immunol.* **35**, 886–897 (2011).

56. te Velthuis, A. J. W. *et al.* Mini viral RNAs act as innate immune agonists during influenza virus infection. *Nat. Microbiol.* **3**, 1234–1242 (2018).

57. Barik, S. What really rigs up RIG-I? *J. Innate Immun.* **8**, 429–436 (2016).

58. Jiang, F. *et al.* Structural basis of RNA recognition and activation by innate immune receptor RIG-I. *Nature* **479**, 423–427 (2011).

59. Kowalinski, E. *et al.* Structural basis for the activation of innate immune pattern-recognition receptor RIG-I by viral RNA. *Cell* **147**, 423–435 (2011).

60. Devarkar, S. C., Schweibenz, B., Wang, C., Marcotrigiano, J. & Patel, S. S. RIG-I Uses an ATPase-Powered Translocation-Throttling Mechanism for Kinetic Proofreading of RNAs and Oligomerization. *Mol. Cell* **72**, 355-368.e4 (2018).

61. Louber, J., Brunel, J., Uchikawa, E., Cusack, S. & Gerlier, D. Kinetic discrimination of self/non-self RNA by the ATPase activity of RIG-I and MDA5. *BMC Biol.* **13**, 11–14 (2015).

62. Lässig, C. *et al.* ATP hydrolysis by the viral RNA sensor RIG-I prevents unintentional recognition of self-RNA. *Elife* **4**, 1–20 (2015).

63. Zhu, S., Jackson, R. & Flavell, R. A. The lock-washer: A reconciliation of the RIG-I activation models. *Cell Res.* **24**, 645–646 (2014).

64. Peisley, A., Wu, B., Xu, H., Chen, Z. J. & Hur, S. Structural basis for ubiquitin-mediated antiviral signal activation by RIG-I. *Nature* **508**, 110–114 (2014).

65. Patel, J. R. *et al.* ATPase-driven oligomerization of RIG-I on RNA allows optimal activation of type-I interferon. *EMBO Rep.* **14**, 780–787 (2013).

66. Gack, M. U. *et al.* TRIM25 RING-finger E3 ubiquitin ligase is essential for RIG-I-mediated antiviral activity. *Nature* **446**, 916–920 (2007).

67. Jiang, X. *et al.* Ubiquitin-Induced Oligomerization of the RNA Sensors RIG-I and MDA5 Activates Antiviral Innate Immune Response. *Immunity* **36**, 959–973 (2012).

68. Palazzo, A. F. & Lee, E. S. Non-coding RNA: What is functional and what is junk? *Front. Genet.* **5**, 1–11 (2015).

69. Kheir, E. & Krude, T. Non-coding Y RNAs associate with early replicating euchromatin in concordance with the origin recognition complex. *J. Cell Sci.* **130**, 1239–1250 (2017).

70. Busch, H., Ramachandra, R., Rothblum, L. & YC, C. SnRNAs, SnRNPs, and RNA processing. *Annu. Rev. Biochem.* (1982).

71. Vabret, N. *et al.* Y-RNAs lead an endogenous program of RIG-I agonism mobilized upon RNA virus infection and targeted by HIV. *bioRxiv* (2019) doi:10.1101/773820.

72. Zhao, Y., Ye, X., Dunker, W., Song, Y. & Karijolich, J. RIG-I like receptor sensing of host RNAs facilitates the cell-intrinsic immune response to KSHV infection. *Nat. Commun.* **9**, 1–14 (2018).

73. Choi, J. H. *et al.* DUSP11-mediated control of 5′-triphosphate RNA regulates RIG-I sensitivity. *Genes Dev.* **34**, 1697–1712 (2020).

74. Nabet, B. Y. *et al.* Exosome RNA Unshielding Couples Stromal Activation to Pattern Recognition Receptor Signaling in Cancer. *Cell* **170**, 352-366.e13 (2017).

75. Jeronimo, C. *et al.* Systematic Analysis of the Protein Interaction Network for the Human Transcription Machinery Reveals the Identity of the 7SK Capping Enzyme. *Mol. Cell* **27**, 262–274 (2007).

76. Yan, B., Tzertzinis, G., Schildkraut, I. & Ettwiller, L. Comprehensive determination of transcription start sites derived from all RNA polymerases using ReCappable-seq. *Genome Res.* **32**, 162–174 (2022).

77. Devarkar, S. C. *et al.* Structural basis for m7G recognition and 2′-O-methyl discrimination in capped RNAs by the innate immune receptor RIG-I. *Proc. Natl. Acad. Sci. U. S. A.* **113**, 596–601 (2016).

78. Williams, G. D., Gokhale, N. S. & Snider, D. L. The mRNA Cap 2=-O-Methyltransferase CMTR1 Regulates the Expression of Certain Interferon-Stimulated Genes. *mSphere* **5**, 1–13 (2020).

79. Will, C. L. & Lührmann, R. Spliceosomal UsnRNP biogenesis, structure and function. *Curr. Opin. Cell Biol.* **13**, 290–301 (2001).

80. Chiang, J. J. *et al.* Viral unmasking of cellular 5S rRNA pseudogene transcripts induces RIG-I-mediated immunity article. *Nat. Immunol.* **19**, 53–62 (2018).

81. Mourão, A. *et al.* Structural basis for the recognition of spliceosomal SmN/B/B' proteins by the RBM5 OCRE domain in splicing regulation. *Elife* **5**, 1–26 (2016).

82. Lang, R. & Raffi, F. A. M. Dual-specificity phosphatases in immunity and infection: An update. *Int. J. Mol. Sci.* **20**, (2019).

83. Wein, S. *et al.* A computational platform for high-throughput analysis of RNA sequences and modifications by mass spectrometry. *Nat. Commun.* **11**, 1–12 (2020).

84. Ozawa, M. *et al.* Contributions of Two Nuclear Localization Signals of Influenza A Virus Nucleoprotein to Viral Replication. *J. Virol.* **81**, 30–41 (2007).

85. Neumann, G., Castrucci, M. R. & Kawaoka, Y. Nuclear import and export of influenza virus nucleoprotein. *J. Virol.* **71**, 9690–9700 (1997).

86. Digard, P., Elton, D., Simpson-Holley, M. & Medcalf, E. Interaction of the influenza virus nucleoprotein with F-actin. *Int. Congr. Ser.* **1219**, 503–512 (2001).

87. Li, J., Yu, M., Zheng, W. & Liu, W. Nucleocytoplasmic shuttling of influenza a virus proteins. *Viruses* **7**, 2668–2682 (2015).

88. Mondal, A., Potts, G. K., Dawson, A. R., Coon, J. J. & Mehle, A. Phosphorylation at the Homotypic Interface Regulates Nucleoprotein Oligomerization and Assembly of the Influenza Virus Replication Machinery. *PLoS Pathog.* **11**, 1–24 (2015).

89. Bui, M., Myers, J. E. & Whittaker, G. R. Nucleo-cytoplasmic localization of influenza virus nucleoprotein depends on cell density and phosphorylation. *Virus Res.* **84**, 37–44 (2002).

90. Zhirnov, O. P., Konakova, T. Y., Garten, W. & Klenk, H. D. Characterization of influenza virus nucleocapsid protein NP proteolytic cleavage in infected cells. *Vopr. Virusol.* **44**, 275–279 (1999).

91. Zaborowska, J., Egloff, S. & Murphy, S. The pol II CTD: New twists in the tail. *Nat. Struct. Mol. Biol.* **23**, 771–777 (2016).

92. Nemeroff, M. E., Barabino, S. M. L., Li, Y., Keller, W. & Krug, R. M. Influenza virus NS1 protein interacts with the cellular 30 kDa subunit of CPSF and inhibits 3′ end formation of cellular pre-mRNAs. *Mol. Cell* **1**, 991–1000 (1998).

93. Walker, A. P. & Fodor, E. Interplay between Influenza Virus and the Host RNA Polymerase II Transcriptional Machinery. *Trends Microbiol.* **27**, 398–407 (2019).

94. Bauer, D. L. V. *et al.* Influenza Virus Mounts a Two-Pronged Attack on Host RNA Polymerase II Transcription. *Cell Rep.* **23**, 2119-2129.e3 (2018).

95. Chan, A. Y., Vreede, F. T., Smith, M., Engelhardt, O. G. & Fodor, E. Influenza virus inhibits RNA polymerase II elongation. *Virology* **351**, 210–217 (2006).

96. Matera, A. G. & Wang, Z. A day in the life of the spliceosome. *Nat. Rev. Mol. Cell Biol.* **15**, 108–121 (2014).

97. Chathoth, K. T., Barrass, J. D., Webb, S. & Beggs, J. D. A Splicing-Dependent Transcriptional Checkpoint Associated with Prespliceosome Formation. *Mol. Cell* **53**, 779–790 (2014).

98. Peterlin, B. M., Brogie, J. E. & Price, D. H. 7SK snRNA: A noncoding RNA that plays a major role in regulating eukaryotic transcription. *Wiley Interdiscip. Rev. RNA* **3**, 92–103 (2012).

99. Schoggins, J. W. *et al.* A diverse range of gene products are effectors of the type i interferon antiviral response. *Nature* **472**, 481–485 (2011).

Appendix

Contribution published as:

Baker SF, Ledwith MP, Mehle A. Differential Splicing of ANP32A in Birds Alters Its Ability to Stimulate RNA Synthesis by Restricted Influenza Polymerase. Cell Reports. 2018;24(10):2581-2588.e4. doi:10.1016/j.celrep.2018.08.012

Abstract:

Adaptation of viruses to their hosts can result in specialization and a restricted host range. Species specific polymorphisms in the influenza virus polymerase restrict its host range during transmission from birds to mammals. ANP32A was recently identified as a cellular co-factor affecting polymerase adaption and activity. Avian influenza polymerases require ANP32A containing an insertion resulting from an exon duplication uniquely encoded in birds. Here we find that natural splice variants surrounding this exon create avian ANP32A proteins with distinct effects on polymerase activity. We demonstrate species-independent direct interactions between all ANP32A variants and the PB2 polymerase subunit. This interaction is enhanced in the presence of viral genomic RNA. In contrast, only avian ANP32A restored ribonucleoprotein complex assembly for a restricted polymerase by enhancing RNA synthesis. Our data suggest that ANP32A splicing variation among birds differentially affects viral replication, polymerase adaption, and the potential of avian hosts to be reservoirs.

Contribution: Helped design the computational workflow for the identification of splicing isoforms of ANP32A in birds.

Contribution available as a preprint:

Baker SF, Meistermann H, Tzouros M, Baker A, Golling S, Siebourg Polster J, Ledwith MP, Gitter A, Augustin A, Javanbakht H, Mehle A. Alternative splicing liberates a cryptic cytoplasmic isoform of mitochondrial MECR that antagonizes influenza virus. bioRxiv 2020.11.09.355982; doi: https://doi.org/10.1101/2020.11.09.355982

Abstract:

Viruses must balance their reliance on host cell machinery for replication while avoiding host defense. They often exploit conserved essential host genes whose critical role for the cell limits mutational escape. Conversely, host antiviral genes are often nonessential and can undergo mutation or regulated expression to thwart infection and limit self damage. Influenza A viruses are zoonotic agents that frequently switch hosts, causing localized outbreaks with the potential for larger pandemics. The host range of influenza virus is limited by the need for successful interactions between the virus and cellular partners. Here we used immuno-competitive capturemass spectrometry to identify cellular proteins that interact with human- and avian-style viral polymerases. We focused on the pro-viral activity of heterogenous nuclear ribonuclear protein U-like 1 (hnRNP UL1) and the anti-viral activity of mitochondrial enoyl CoA-reductase (MECR). MECR is localized to mitochondria where it functions in mitochondrial fatty acid synthesis (mtFAS). While a small fraction of the polymerase subunit PB2 localizes to the mitochondria, we could not confirm interactions with full-length MECR. By contrast, RNA-seq revealed a minor splice variant that creates cytoplasmic MECR (cMECR). cMECR engages the viral polymerase and suppresses viral replication. MECR ablation through genome editing or drug treatment is detrimental for cell health, creating a generic block virus replication. Using the yeast homolog Etr1 to supply the metabolic functions of MECR, we showed that specific antiviral activity is independent of mtFAS and lies solely within cMECR. Thus, a cryptic antiviral activity is embedded within a key metabolic enzyme, possibly protecting it from viral countermeasures.

Contribution: Prepared RNA-seq data from A549 cells infected with influenza virus that aided in the identification of the alternatively-spliced cMECR.